Propagation of a hydraulic fracture with tortuosity: Linear and hyperbolic crack laws

Mankabo Rahab Reshoketswe Kgatle,

A thesis submitted to the Faculty of Science, University of the Witwatersrand, Johannesburg, South Africa, in fulfilment of the requirements for the degree of Doctor of Philosophy.

Declaration

I declare that this thesis is my own unaided work. It is being submitted for the degree of Doctor of Philosophy at the University of the Witwatersrand, Johannesburg. It has not been submitted before for any degree or examination at any other university.

Mankabo Rahab Reshoketswe Kgatle

08 July 2015

Abstract

The propagation of hydraulic fractures with tortuosity is investigated. Tortuosity is the complicated fracture geometry that results from asperities at the fluid-rock interface and, if present, from contact regions. A tortuous hydraulic fracture can either be open without contact regions or partially open with contact regions. We replace the tortuous hydraulic fracture by a two-dimensional symmetric model fracture that accounts for tortuosity. A modified Reynolds flow law is used to model the tortuosity in the flow due to surface roughness at the fracture walls. In order to close the model, the linear and hyperbolic crack laws which describe the presence of contact regions in a partially open fracture are used. The Perkins-Kern-Nordgren approximation in which the normal stress at the crack walls is proportional to the half-width of the symmetric model fracture is used. A Lie point symmetry analysis of the resulting governing partial differential equations with their corresponding boundary conditions is applied in order to derive group invariant solutions for the half-width, volume and length of the fracture. For the linear hydraulic fracture, three exact analytical solutions are derived. The operating conditions of two of the exact analytical solutions are identified by two conservation laws. The exact analytical solutions describe fractures propagating with constant speed, with constant volume and with fluid extracted at the fracture entry. The latter solution is the limiting solution of fluid extraction solutions. During the fluid extraction process, fluid flows in two directions, one towards the fracture entry and the other towards the fracture tip. It is found that for fluid injection the width averaged fluid velocity increases approximately linearly along the length of the fracture. This leads to the derivation of approximate analytical

solutions for fluid injection working conditions. Numerical solutions for fluid injection and extraction are computed. The hyperbolic hydraulic fracture is found to admit only one working condition of fluid injected at the fracture entry at a constant pressure. The solution is obtained numerically. Approximate analytical solutions that agree well with numerical results are derived. The constant pressure solutions of the linear and hyperbolic hydraulic fracture are compared. While the hyperbolic hydraulic fracture model is generally considered to be a more realistic model of a partially open fracture, it does not give information about fluid extraction. The linear hydraulic fracture model gives various solutions for different working conditions at the fracture entry including fluid extraction.

In memory of my father

Johannes Ramabule Kgatle

1951 - 1999

Acknowledgements

Firstly, I would like to thank God for giving me the strength to work hard and complete this PhD thesis.

Secondly, my gratitude goes to Professor David P. Mason for his academic support. His patience and positive outlook to every challenge has encouraged me throughout my studies. He showed me how to approach a problem in research and to knowledgably allow findings to guide me rather than expectations. I am also grateful for all the time and hard work he always put in our work sessions.

I would like to thank all Professors in the School of Computer Science and Applied Mathematics for all the encouragement they have provided in the duration of my studies and for arranging seminars that have always added more insight with regards to my work. The informal discussions with higher degree students in the School of Computer Science and Applied Mathematics are also appreciated.

My gratitude goes to NRF for the continuous financial support in the duration of my studies.

Lastly, I would like to thank my loving family: Thokozani Maseko, my mother and siblings for the continuous encouragement and support that they have provided me with throughout my studies, it is highly and dearly appreciated.

Contents

List of Figures

List of Tables

Chapter 1

INTRODUCTION

1.1 Introduction

The process in which a fracture in a continuous medium, such as a rock mass, is propagated by viscous fluid, such as water, oil, fluidized sand or magma, is known as hydraulic fracturing. A hydraulic fracture can either propagate from a point source of fluid or, in the case of a pre-existing fracture, from a non-zero initial length.

In this work we will investigate the propagation of a tortuous hydraulic fracture. Tortuosity is the complicated geometry caused by roughness on the upper and lower surfaces of the fracture and, if present, by contact regions, that leads to fluid flowing in complex ways in the fracture. A tortuous hydraulic fracture can either be open, when the fluid pressure is sufficient to support the normal stresses at the fracture walls, or partially open, when the fluid pressure is insufficient to support the normal stresses at the fracture walls which leads to the formation of contact regions [1]. It therefore follows that in a partially open fracture, the normal stresses are supported by both the fluid pressure and the contact regions. We will discuss open fractures although the main focus will be on partially open fractures. For partially open fractures, we will consider the linear and the hyperbolic crack laws that describe the presence of contact regions.

In order to model the tortuosity, we will replace the tortuous hydraulic fracture by a two-dimensional symmetric model fracture that accounts for surface roughness and, in a partially open fracture, for contacts regions.

1.2 Background to hydraulic fracturing

There are two types of hydraulic fractures, natural and man-made hydraulic fractures. Examples of the former type of fracture include magma-driven fractures [2–6]. Man-made hydraulic fracturing is used mostly in the petroleum industry whereby the aim is to extract oil or gas from shale [7–9], without using methods such as rock explosion which generate dust and small particles harmful to miners as discussed in [10, 11]. A typical procedure of how man-made hydraulic fractures can be created and how oil or gas is extracted from shale is illustrated in Figure 1.1. The method may be outlined as follows [9, 12]: A viscous solution, usually containing sand and other particles that increase permeability in the fracture, is added to water to increase the viscosity of the water. A vertical well of the order of a thousand metres deep below ground is drilled. The well is insulated with steel and then with cement to affirm that there is no leakage of chemicals from the well to the water table that lies a few metres below ground. When the insulated well is in the shale, its direction is changed to be horizontal. Small initial fractures in the insulated well that lies within the shale are made with controlled gun charges. Then the highly viscous solution is injected into the well at an ultra high pressure. The solution reaches the initial fractures, travels inside them, then creates even more fractures which are maintained opened by the particles in the solution. Then the oil or gas is extracted. Examples of man-made hydraulic fractures include fractures used to enhance the fluid flow in geothermal energy reservoirs [1] and fractures propagated to break rock in mining [10, 11]. The study of hydraulic fractures in different materials can also play a significant role in the energy industry where a mixture of low level liquid nuclear waste and cement is injected into shale beds before it sets, disposing the radioactive waste, [13].

While research in natural fractures was motivated by attempts to understand natural

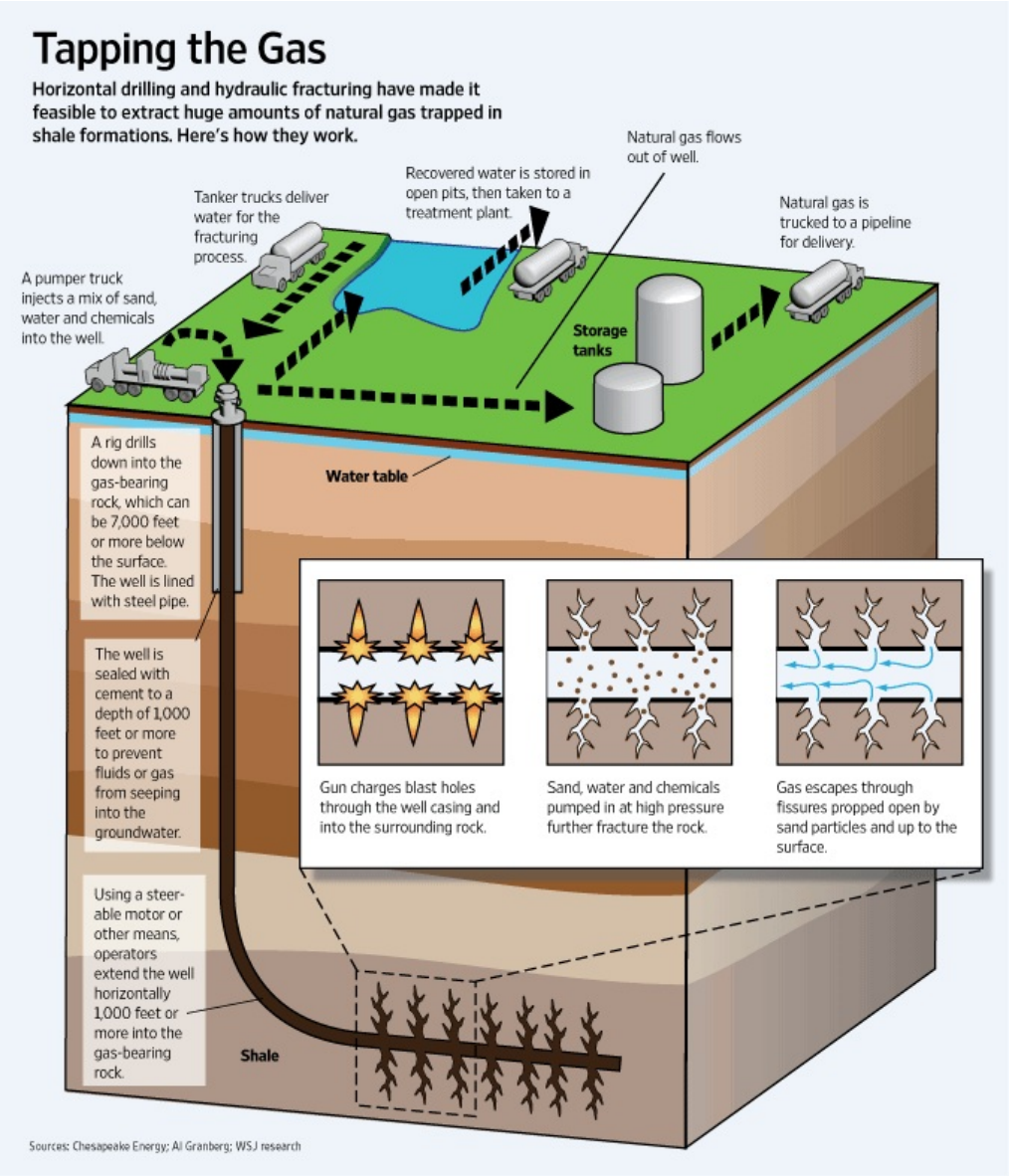

Figure 1.1: Oil/Gas field [9].

phenomena, such as rivers that form from previously solid planes of land and processes that take place underground moments before a volcano erupts, investigations of man-made fractures were motivated by physical problems that could be related to work done on natural fractures. The field of hydraulic fractures has grown greatly since its origins nearly half a century ago with various authors contributing to the development of research in man-made hydraulic fracturing, [1, 10, 11, 14]. While other methods of fracturing, such as stress-corrosion cracking, have been investigated and compared with hydraulic

fracturing to deduce which is more efficient [2], hydraulic fracturing remains the more popular and viable method.

Several models have been formulated and investigated for the process of hydraulic fracturing and some of the most popular ones are:

- The two-dimensional or KGD model which was developed by Khristianovic and Zheltov [15]. This model assumes that the fracture in Figure 1.2 is two-dimensional. The assumption implies that the shape of the fracture at any $y > 0$ is exactly the same as the shape of the fracture when $y = 0$.

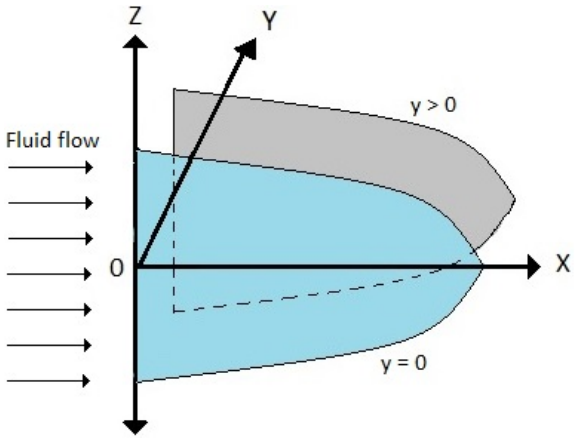

Figure 1.2: 2-D model.

- The PKN model developed by Perkins and Kern [16] and Nordgren [17] assumes that the cross-sectional area of the fracture is elliptic with a constant height H and a decreasing width w as the fracture tip is approached.

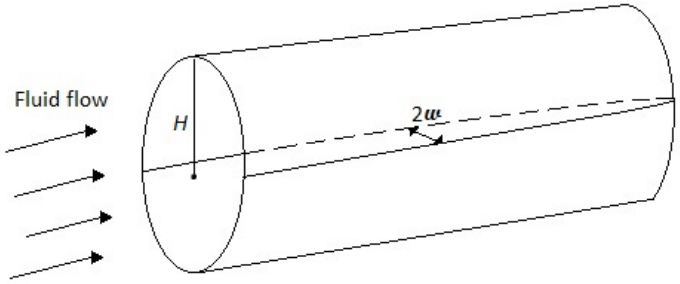

Figure 1.3: PKN Model.

- The penny-shaped crack model assumes that the fracture propagates from a point source axisymmetrically [18]. This assumption implies that the fracture is propagated from a point source and grows outwards radially as illustrated in Figure 1.4.

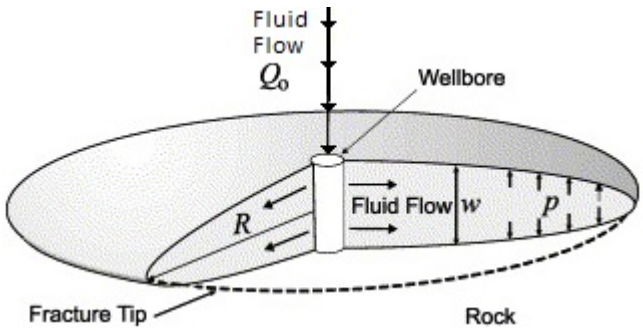

Figure 1.4: A penny shaped hydraulic fracture [12].

- Complex fluid flow in a tortuous hydraulic fracture due to roughness of the fluid-rock interface is modelled by replacing h^3 in the cubic flow law equation by $a_n h^n$ [1]. A tortuous hydraulic fracture is illustrated in Figure 1.5.

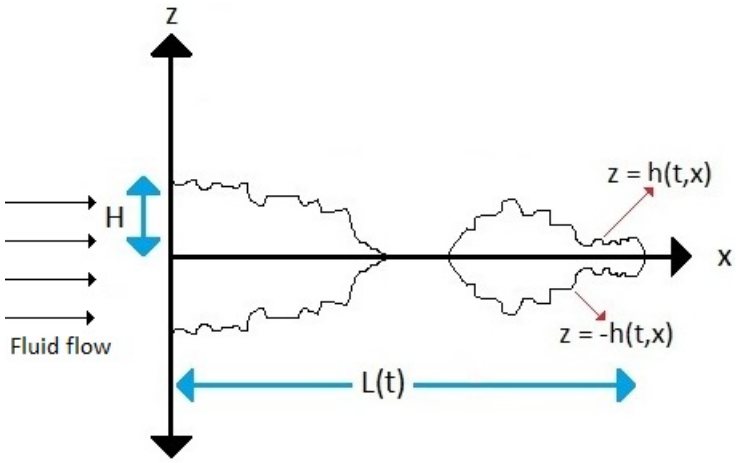

Figure 1.5: Tortuous hydraulic fracture with contact areas due to touching asperities on opposite fracture walls.

1.3 Literature review

Over the years, many authors have contributed extensively to the field of hydraulic fractures and they have built significant models and derived laws that assist in understanding the general behavior of fracture propagation. One such law is the cubic flow law which states that: "*The volume rate of fluid flow across a section in a smooth parallel surfaced fracture is proportional to the applied pressure gradient and the cube of the separation distance*". Its significant implication is that fluid flow may be fully characterized by the separation distance (aperture) although velocity varies across that distance [19]. This law applies well in a fracture that has a smooth fluid-rock interface and no contact between the upper and lower surfaces of the fracture. The flow law results in the nonlinear diffusion equation

$$\frac{\partial h}{\partial t} = \frac{1}{3}\frac{\partial}{\partial x}\Big(h^3\frac{\partial p}{\partial x}\Big), \tag{1.3.1}$$

which describes Reynolds flow that was investigated in [10] and [11], where h is the fracture half-width, p is the fluid pressure and t, x are the time and spatial variables, respectively.

Now, many fractures that arise in practice are not smooth but possess many irregularities and the flow is tortuous due to the asperities on the fluid-rock interface and the areas of contact between the upper and lower surfaces. Several authors such as [1, 19–23] have questioned the validity of the cubic flow law in a tortuous fracture. After investigation most authors agreed that while the cubic flow law would still be applicable in a moderately tortuous fracture with small asperities and without contact regions, it is not advisable to use the cubic flow law in modelling a very tortuous fracture that has large asperities and contact regions because it gives theoretical results with large errors when compared with experiments. Due to this limitation, various authors have proposed different models that account for very tortuous fractures and in this work, we will use one of those models which is the general flow law that accounts for asperities in a fracture. This general flow law, which was used by Fitt et al [1], requires that we replace the cubic term h^3 in equation (1.3.1) by $a_n h^n$ where a_n is a dimensional constant with dimensions L^{3-n} and the parameter n is a constant greater than zero. The constants n and a_n are determined experimentally [1]. For wide fractures the value of n is much larger than 3

while for narrow fractures n is less than 3, for instance $n = 1$ and $n = 2$. The value $n = 1$ is referred to as the linear flow law [1]. A more detailed discussion about flow laws derived by analysing and fitting experimental data is given by Cook [23].

For an open fracture the effective stress must vanish and for a partially open fracture, the effective stress must be negative, where the effective stress is defined as the sum of the fluid pressure and the normal stresses at the fracture walls. The Perkins and Kern [16] and Nordgren [17] approximation will be made in which the normal stress at the crack walls is proportional to the half-width of the symmetric model fracture. Adachi and Pierce [24] have shown that the PKN approximation is a good approximation far from the fracture tip. The linear crack law [25] and the hyperbolic crack law [26–28] which satisfy the negative effective stress condition will be used to mathematically describe the different ways in which contact regions can be formed in a partially open fracture.

1.4 Research work outline

In this thesis, we will investigate the effect of tortuosity due to asperities and contact regions on the propagation of a pre-existing hydraulic fracture. We will discuss both an open and a partially open fracture though the main focus will be on the latter.

In Chapter 2, we will discuss and present rigorous derivations of the governing equations for an open tortuous hydraulic fracture, a partially open tortuous hydraulic fracture with contact regions modelled by the linear crack law and a partially open tortuous hydraulic fracture with contact regions modelled by the hyperbolic crack law. It becomes clear in this chapter that an open hydraulic fracture and a partially open linear hydraulic fracture share the same governing equations with the difference contained in the diffusion constant. The main aim of Chapter 2 will be to replace the actual tortuous fractures by two-dimensional symmetric model fractures that take the effect of asperities at the fluid-rock interface and, if present, also contact regions in the fractures into account. Firstly, we will analyse the general flow law that accounts for the presence of asperities at the fluid-rock interface, then we will close the model by considering crack laws that describe

whether there are contact regions or not in the fracture.

In Chapter 3, we will discuss the methods of solution that will be used in solving the governing equations for an open fracture and partially open fractures with contact regions modelled by the linear and hyperbolic crack laws respectively. We will discuss how Lie group analysis can be used in order to solve the governing equations. We will also discuss three methods of deriving conservation laws for the governing partial differential equations: the direct, the multiplier and the partial Lagrangian methods.

Chapters 4 and 6 present derivations of conservation laws for partial differential equations describing a linear hydraulic fracture and a hyperbolic hydraulic fracture.

Since an open fracture and a partially open linear hydraulic fracture share the same governing equations, with the difference contained in the diffusion constant, we will analyse both fractures in Chapter 5. We will first present derivations of the group invariant solution for the half-width, volume and length of the fracture. We will then investigate if the conserved vectors derived in Chapter 4 and the Lie point symmetries of the governing partial differential equation are associated. By Sjöberg's double reduction theorem [29], analysis of association may lead to derivations of analytical solutions. We will then explore different working conditions at the fracture entry. For operating conditions whose governing equations we cannot solve analytically, we will compute numerical solutions. We will analyse both analytical and numerical solutions for different working conditions at the fracture entry. In Chapter 5, we will also analyse the width averaged fluid velocity and the fluid flux in the fracture in order to understand the resulting fluid flow for different working conditions at the fracture entry. Analysis of the width averaged fluid velocity for fluid injection working conditions leads to the derivation of approximate analytical solutions of the kind introduced by Fareo [30]. All the fluid-injection work discussed in Chapter 5 is based on the paper *"Propagation of a linear hydraulic fracture with tortuosity"* [31].

In Chapter 7 we will analyse the governing equations describing a hyperbolic hydraulic fracture. The hyperbolic crack law is generally considered to be a more realistic mathematical formulation describing contact regions in a fracture [1]. This motivates our investigation of a tortuous hydraulic fracture with contact regions modelled by the hyperbolic crack law. As in Chapter 5, we will use Lie point symmetries in order to derive the

group invariant solution for the half-width, volume and length of the fracture. We will investigate if the Lie point symmetries of the governing partial differential equation and the conserved vectors derived in Chapter 6 are associated. This will lead to the investigation of analytical solutions as done in Chapter 5. Numerical solutions of the hyperbolic hydraulic fracture will also be computed. We will then compare solution of the linear hydraulic fracture and solutions of the hyperbolic hydraulic fracture.

Chapter 8 summarizes all of the findings in this work and highlights significant results we have obtained.

Chapter 2

MODEL FORMULATION

2.1 Introduction

In this chapter, we investigate a hydraulic fracture that has asperities or surface roughness on the fluid-rock interface. The fracture that will be investigated can be open (a fracture with no contact regions) or partially open (a fracture with contact regions). In a partially open fracture contact regions due to touching asperities, which are formed by high compressive stresses on the fracture, are present. The fluid flow in a tortuous fracture will be investigated. For an open fracture, the PKN approximation will be sufficient to close the respective model. For a partially open fracture, both the crack law model that affirms the existence of contact regions and the PKN approximation will be sufficient to close the model. In partially open fractures, we will investigate two types of crack laws that describe the different ways in which the contact regions are formed, the linear and the hyperbolic crack laws.

2.2 Problem description

Hydraulic fracturing occurs in a wide range of materials. In this work, we will consider the medium in which the hydraulic fracturing process occurs to be rock. The methods and concepts used to describe hydraulic fracturing in rock also apply to other materials in principle. The properties of other materials will be the difference between that analysis and the analysis given in this work. The surrounding rock is impermeable and the fluid injected at the fracture entry is incompressible.

The fracture investigated has asperities at the fluid-rock interface. This results from

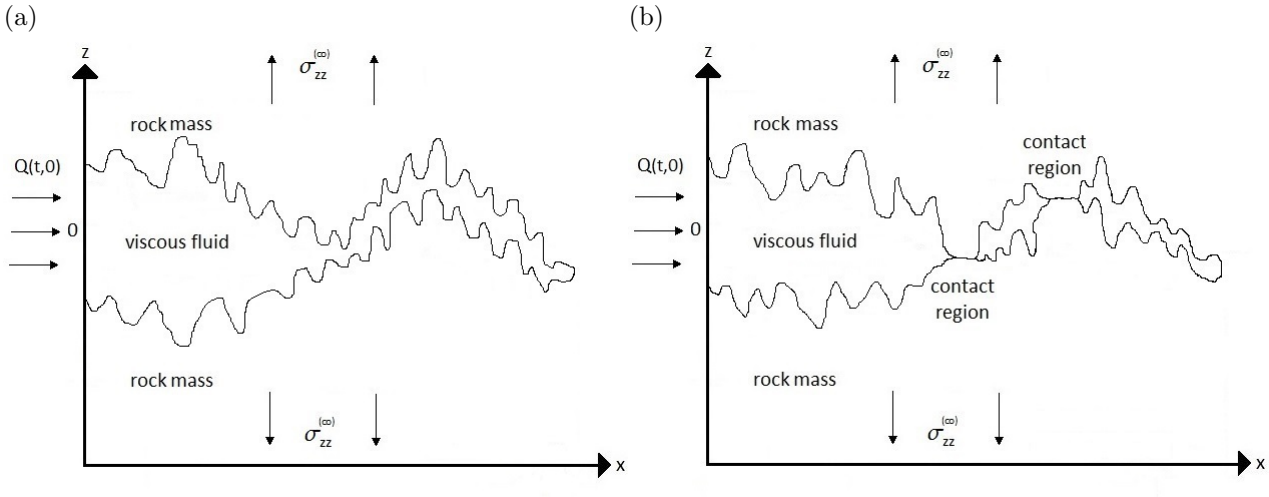

Figure 2.1: Hydraulic fractures with asperities on the crack walls: (a) an open hydraulic fracture without contact regions, (b) a partially open hydraulic fracture with contact regions.

the non-uniform manner in which fractures usually occur in nature. To draw such a fracture is difficult given that the fracture changes shape and asperities evolve as time increases. Therefore schematic diagrams (Figure 2.1a) for an open fracure and (Figure 2.1b) for a partially open fracture only illustrate how asperities and contact regions may form in a fracture. Figure 2.1 does not present the exact profiles of the actual fractures. The relation between the half-width of the fracture and the stresses in the surrounding rock will be discussed later in this chapter.

To model the fluid flow in a fracture with asperities at the fluid-rock interface, we re-

place the tortuous fractures (Figure 2.1) by a two-dimensional symmetric model hydraulic fracture (Figure 2.2) but with a modified flow law that accounts for asperities at the fluid-rock interface and, for a partially open fracture, also a modified crack law that accounts for the presence of contact regions in the fracture. The $x-axis$ is along the length of

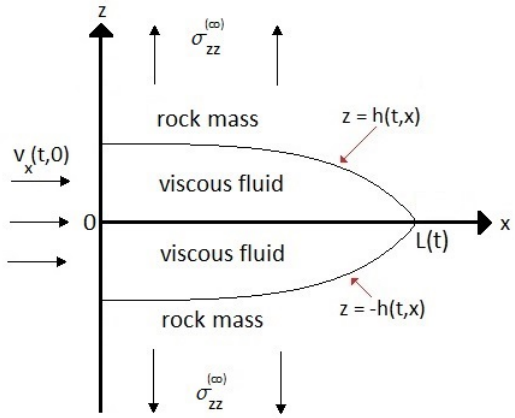

Figure 2.2: A two-dimensional symmetric model of a hydraulic fracture without asperities and contact regions.

the fracture, the $z-axis$ is along the half-width of the fracture and the $y-axis$ is along the breadth of the fracture as shown in Figure 2.2. The fracture entry is at $x=0$ and all quantities are independent of y. The fluid velocity components and the fluid pressure are defined as follows:

$$v_x = v_x(t,x,z), \qquad v_y = 0, \qquad v_z = v_z(t,x,z), \qquad p = p(t,x,z), \tag{2.2.1}$$

where t, x, z are the time and spatial variables, respectively. To close the tortuous flow model for the partially open fracture, the linear and hyperbolic crack laws will be considered. For a tortuous open fracture, only the PKN approximation will be used to close the flow model.

2.3 General assumptions

The following general assumptions apply to all the fracture models that will be considered:

- The fracture is two-dimensional.
- The fluid is a Newtonian fluid.
- The body force due to gravity is neglected.
- The rock mass is a linearly elastic material.
- The rock mass is an impermeable medium.
- The fracture propagates in the positive x-direction and its half-width $h(t, x)$ is perfectly symmetric about the positive x-axis.
- The length of the fracture is $L(t)$ and is a function of time because the fracture propagates over time.
- The fracture is pre-existing with a non-zero initial length $L(0)$.
- Lubrication theory is applied:

$$Re\Big(\frac{H}{L}\Big)^2 << 1, \qquad\qquad \frac{H}{L} << 1,$$

  where Re is the Reynolds number of the flow.
- The tortuosity in the flow due to the asperities on the fluid-rock interface is modelled by replacing h^3 by $a_n h^n$ in the nonlinear diffusion equation for the half-width h, where a_n and n are constants determined experimentally.

2.4 Governing equations

In order to develop a hydraulic fracture model for the described problem, we consider the behaviour of the fluid flow within the rock and the behaviour of the surrounding elastic rock. We investigate the manner in which the two are intertwined resulting in a hydraulic fracture model.

2.4.1 Flow law models

It is necessary to first consider the simpler case of Reynolds type flow where the fluid-rock interface is fairly smooth and there are no contact regions. The procedure will then be to modify the resulting flow model (cubic flow law) in order to incorporate the presence of asperities at the fluid-rock interface.

The Navier-Stokes equation with zero body force and the continuity equation for an incompressible fluid are given by

$$\frac{\partial \underline{v}}{\partial t} + (\underline{v}.\underline{\nabla})\underline{v} = -\frac{1}{\rho}\nabla p + \nu\nabla^2\underline{v}, \tag{2.4.1}$$

$$\frac{\partial v_x}{\partial x} + \frac{\partial v_z}{\partial z} = 0, \tag{2.4.2}$$

where ρ is the fluid density and $\nu = \mu/\rho$ is the kinematic viscosity of the fluid with μ the dynamic viscosity. The resulting x and z components of the Navier-Stokes equation are

$$\rho\left[\frac{\partial v_x}{\partial t} + v_x\frac{\partial v_x}{\partial x} + v_z\frac{\partial v_x}{\partial z}\right] = -\frac{\partial p}{\partial x} + \mu\left[\frac{\partial^2 v_x}{\partial x^2} + \frac{\partial^2 v_x}{\partial z^2}\right], \tag{2.4.3}$$

$$\rho\left[\frac{\partial v_z}{\partial t} + v_x\frac{\partial v_z}{\partial x} + v_z\frac{\partial v_z}{\partial z}\right] = -\frac{\partial p}{\partial z} + \mu\left[\frac{\partial^2 v_z}{\partial x^2} + \frac{\partial^2 v_z}{\partial z^2}\right]. \tag{2.4.4}$$

We introduce the dimensionless variables

$$x^* = \frac{x}{L}, \quad z^* = \frac{z}{H}, \quad v_x^* = \frac{v_x}{U}, \quad v_z^* = \frac{v_z L}{UH}, \quad p^* = \frac{H^2 p}{UL\mu}, \quad t^* = \frac{Ut}{L}, \tag{2.4.5}$$

where L is the characteristic fracture length chosen to be the initial length of the pre-existing fracture, H and U, both of which will be specified later, are the characteristic half-width and fluid velocity in the x-direction respectively,

$$V = \frac{H}{L}U, \tag{2.4.6}$$

is the characteristic velocity in the z-direction, which is obtained by balancing the two terms in the continuity equation,

$$P = \frac{UL\mu}{H^2} \tag{2.4.7}$$

is the characteristic fluid pressure for the lubrication approximation [32] which is obtained by balancing the pressure gradient in the x-direction with the viscous force in the x-direction and

$$T = \frac{L}{U} \tag{2.4.8}$$

is the characteristic time. Non-dimensionalising the partial differential equations (2.4.2) to (2.4.4) using the dimensionless variables, (2.4.5), reduces equations (2.4.3) and (2.4.4) to

$$Re\Big(\frac{H}{L}\Big)^2\left[\frac{\partial v_x^*}{\partial t^*} + v_x^*\frac{\partial v_x^*}{\partial x^*} + v_z^*\frac{\partial v_x^*}{\partial z^*}\right] = -\frac{\partial p^*}{\partial x^*} + \Big(\frac{H}{L}\Big)^2\frac{\partial^2 v_x^*}{\partial x^{*^2}} + \frac{\partial^2 v_x^*}{\partial z^{*^2}}, \tag{2.4.9}$$

$$Re\Big(\frac{H}{L}\Big)^4\left[\frac{\partial v_z^*}{\partial t^*} + v_x^*\frac{\partial v_z^*}{\partial x^*} + v_z^*\frac{\partial v_z^*}{\partial z^*}\right] = -\frac{\partial p^*}{\partial z^*} + \Big(\frac{H}{L}\Big)^4\frac{\partial^2 v_z^*}{\partial x^{*^2}} + \Big(\frac{H}{L}\Big)^2\frac{\partial^2 v_z^*}{\partial z^{*^2}}, \tag{2.4.10}$$

and leaves equation (2.4.2) invariant under the transformations (2.4.5). Since the half-width of the fracture is very small compared to the length of the fracture, we make the lubrication approximation:

$$Re\Big(\frac{H}{L}\Big)^2 << 1, \qquad \frac{H}{L} << 1, \tag{2.4.11}$$

where Re is the Reynolds number

$$Re = \frac{UL}{\nu}. \tag{2.4.12}$$

In the lubrication approximation, the x and z components of the Navier-Stokes equation, (2.4.9) and (2.4.10), and the continuity equation, (2.4.2), reduce in dimensional form to

$$\frac{\partial p}{\partial x} = \mu\frac{\partial^2 v_x}{\partial z^2}, \tag{2.4.13}$$

$$\frac{\partial p}{\partial z} = 0, \tag{2.4.14}$$

$$\frac{\partial v_x}{\partial x} + \frac{\partial v_z}{\partial z} = 0. \tag{2.4.15}$$

The corresponding boundary conditions at the fracture walls, $z = \pm h(t,x)$, are

$$z = h(t,x): \qquad v_x(t,x,h) = 0, \tag{2.4.16}$$

$$v_z(t,x,h) = \frac{\partial h}{\partial t}, \tag{2.4.17}$$

$$z = -h(t,x): \qquad v_x(t,x,-h) = 0, \tag{2.4.18}$$

$$v_z(t,x,-h) = -\frac{\partial h}{\partial t}. \tag{2.4.19}$$

The no slip boundary conditions, (2.4.16) and (2.4.18), describe the fact that the fluid at the fracture walls does not slip but sticks to the fracture walls. The no leak-off boundary conditions, (2.4.17) and (2.4.19), obtained with the aid of the no slip boundary conditions, (2.4.16) and (2.4.18), describe the fact that the surrounding rock mass encasing the fracture is impermeable.

Now, using the Leibnitz rule for differentiation under the integral sign [33], it can be shown that integrating the continuity equation (2.4.15) across the fracture width from $-h(t,x)$ to $h(t,x)$ and imposing the no leak-off boundary conditions, (2.4.17) and (2.4.19), on the result gives

$$\frac{\partial h}{\partial t} + \frac{1}{2}\frac{\partial Q}{\partial x} = 0, \tag{2.4.20}$$

where

$$Q(t,x) = \int_{-h(t,x)}^{h(t,x)} v_x(t,x,z)dz \tag{2.4.21}$$

is the volume flux of fluid across a fracture per unit breadth. But since (2.4.14) implies that pressure is only dependent on time t and the spacial variable x, integrating (2.4.13) twice with respect to the spatial variable z and imposing the no slip boundary conditions, (2.4.16) and (2.4.18), gives the fluid velocity in the x direction:

$$v_x(t,x,z) = -\frac{1}{2\mu}(h^2 - z^2)\frac{\partial p}{\partial x}. \tag{2.4.22}$$

It follows that equation (2.4.21) becomes

$$Q(t,x) = -\frac{2}{3\mu}h^3\frac{\partial p}{\partial x} \tag{2.4.23}$$

and substituting (2.4.23) into (2.4.20) gives the partial differential equation relating $p(t,x)$ and $h(t,x)$:

$$\frac{\partial h}{\partial t} = \frac{1}{3\mu}\frac{\partial}{\partial x}\Big(h^3\frac{\partial p}{\partial x}\Big). \tag{2.4.24}$$

Equation (2.4.24) is the resulting Reynolds flow law. For later analysis on the behaviour of the fluid flow in the fracture, it will be more meaningfuly to use the width averaged fluid velocity

$$\overline{v}_x(t,x) = \frac{1}{2h(t,x)}\int_{-h(t,x)}^{h(t,x)} v_x(t,x,z)dz = \frac{Q(t,x)}{2h(t,x)} = -\frac{h^2}{3\mu}\frac{\partial p}{\partial x}, \tag{2.4.25}$$

as opposed to the fluid velocity (2.4.22) given that the half-width of the fracture is much less than the length of the fracture.

Now, it is necessary to investigate a flow law that takes into account the assumption that the fluid-rock interface of the hydraulic fracture has asperities. Two different types of tortuous fractures will be considered, open and partially open fractures. The former type of fracture has asperities but no contact regions while the latter type of fracture has asperities some of which are big enough to touch forming contact regions. The two types of fracture (either open or partially open) will be discussed in more detail later in this Chapter. As discussed in Chapter 1, Section 1.3, a flow model where h^3 is replaced by $a_n h^n$, in order to account for the presence of asperities at the fracture walls, is used. The volume flux per unit breadth therefore becomes

$$Q(t,x) = -\frac{2}{3\mu} a_n h^n \frac{\partial p}{\partial x}. \tag{2.4.26}$$

From (2.4.26) it is clear that (2.4.24) reduces to a flow law that accounts for asperities present at the fluid-rock interface:

$$\frac{\partial h}{\partial t} = \frac{a_n}{3\mu} \frac{\partial}{\partial x}\Big(h^n \frac{\partial p}{\partial x}\Big). \tag{2.4.27}$$

The Reynolds flow (2.4.24) can be deduced from (2.4.27) provided $n = 3$ and $a_3 = 1$ while the linear flow, discussed by Fitt et al [1] in more detail, can be deduced from (2.4.27) provided $n = 1$. In this work, we will consider parameter values of n in the range $0 < n \leq 3$. This will allow comparison of Reynolds type flow when $n = 3$ and tortuous type flow when $0 < n < 3$. Where necessary, we will then consider values of $n > 3$.

The corresponding width averaged fluid velocity (2.4.25) reduces to

$$\overline{v}_x(t,x) = -\frac{a_n}{3\mu} h^{n-1} \frac{\partial p}{\partial x}. \tag{2.4.28}$$

2.4.2 Crack law models

It is of importance to now consider the behaviour of the surrounding rock encasing the fracture. A tortuous fracture can be an open fracture without contact regions or a partially open fracture with contact regions formed by touching asperities. Contact regions

are one of the features that adds to the tortuous behaviour of fluid flow in a tortuous fracture [23]. For a partially open fracture it is therefore necessary to investigate crack laws that satisfy the presence of contact regions. For an open fracture, it is necessary to investigate the condition that make it possible for the fracture to stay open.

In order to understand whether a fracture is open or partially open, we need to investigate the stresses that occur in the rock neighbouring the fluid-rock interface. The existence of the contact regions within a fracture is determined by whether or not the pressure at the fluid-rock interface exerted by the fluid is sufficient to support the normal stress along the fracture walls.

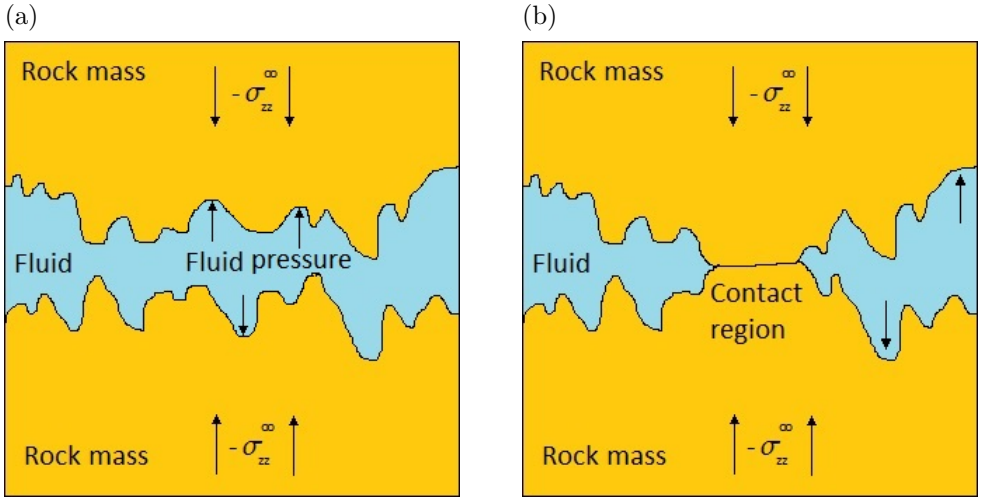

Figure 2.3: (a) Fluid pressure $p(t,x)$ is sufficient to support the normal stress $\sigma_{zz}(t,x)$ along the fluid-rock interface, (b) Fluid pressure $p(t,x)$ is insufficient to support the normal stress $\sigma_{zz}(t,x)$ along the fluid-rock interface.

Figure 2.3 (a) illustrates a fracture with asperities and no contact regions. In this fracture, since the fluid pressure is sufficient to support the normal stress along the fluid-rock interface, the equation that relates the fluid pressure to the normal stress is

$$p(t,x) = -\sigma_{zz}(t,x), \tag{2.4.29}$$

where $\sigma_{zz}(t,x) < 0$. For an open fracture the effective stress in the fracture therefore vanishes:

$$p(t,x) + \sigma_{zz}(t,x) = 0. \tag{2.4.30}$$

The zero effective stress condition (2.4.30) is very important and must be satisfied in order to affirm that the fracture is open.

Figure 2.3 (b) illustrates a partially open fracture that has both asperities and contact regions. In such a fracture, the fluid pressure is insufficient to support the normal stress along the fluid-rock interface and therefore

$$p(t,x) < -\sigma_{zz}(t,x), \tag{2.4.31}$$

where $\sigma_{zz}(t,x) < 0$. For a partially open fracture the effective stress in the fracture is therefore negative:

$$p(t,x) + \sigma_{zz}(t,x) < 0. \tag{2.4.32}$$

The negative effective stress condition (2.4.32) is very important and must be satisfied in order to affirm that the fracture has contact regions and is therefore partially open.

Two crack laws that satisfy the negative effective stress condition (2.4.32), the linear and the hyperbolic crack laws, are investigated. These crack laws affirm the presence of contact regions in the fracture.

The maximum crack height is h_{max} and h_{min} is the minimum crack height. For $h \geq h_{max}$, the crack is considered to be fully open as illustrated in Figure 2.3 (a) and for $h_{min} \leq h < h_{max}$, the crack is partially open as illustrated in Figure 2.3 (b). These definitions of the half-width of the fracture will be used in the analyses of the linear and the hyperbolic crack laws. It is found that the minimum crack height never vanishes, $h_{min} \neq 0$, even under high compressive stresses, that is, when $-\sigma_{zz}(t,x)$ is very large [1].

Linear crack law model

In this work, we use the piecewise linear crack law proposed by Pine and Cundall [25] which gives a linear relation between the half-width of the fracture, $h(t,x)$, and the effective stress, $\sigma_{zz}(t,x) + p(t,x)$:

$$h(t,x) = \begin{cases} h_{max} - \left(\frac{\sigma_{zz}(t,x)+p(t,x)}{\sigma_R}\right)(h_{max} - h_{min}), & \sigma_R < \sigma_{zz}(t,x) + p(t,x) < 0 \\ h_{min}, & \sigma_{zz}(t,x) + p(t,x) \leq \sigma_R, \end{cases} \tag{2.4.33}$$

where $\sigma_R < 0$, referred to as the reference stress, is the least effective stress. Considering the case where $h_{max} >> h_{min}$, it is reasonable to make the approximation that $h_{min} = 0$. The linear crack law (2.4.33) reduces to

$$h(t,x) = \begin{cases} h_{max}\left(1 - \frac{(\sigma_{zz}(t,x)+p(t,x))}{\sigma_R}\right), & 0 < \frac{\sigma_{zz}(t,x)+p(t,x)}{\sigma_R} < 1 \\ 0, & \frac{\sigma_{zz}(t,x)+p(t,x)}{\sigma_R} \geq 1. \end{cases} \tag{2.4.34}$$

It is clear that (2.4.34) can be written as

$$p(t,x) + p_1(t,x) = -\sigma_{zz}(t,x), \tag{2.4.35}$$

where

$$p_1(t,x) = -\sigma_R\left(1 - \frac{h(t,x)}{h_{max}}\right) > 0. \tag{2.4.36}$$

For a partially open fracture, it is clear that equation (2.4.35) satisfies the negative effective stress condition, (2.4.32). From (2.4.35) it also clear that in a partially open fracture, the compressive normal stress, $-\sigma_{zz}(t,x)$, is supported by both the fluid pressure, $p(t,x)$, and the pressure due to contact regions $p_1(t,x)$ defined in (2.4.36). For an open fracture, equation (2.4.35) satisfies the zero effective stress condition, (2.4.30), provided the contribution from contact regions is zero, that is, provided $p_1(t,x) = 0$ and therefore $\sigma_R = 0$.

Hyperbolic crack law model

The hyperbolic crack law gives a hyperbolic relation between the half-width of the fracture, $h(t,x)$, and the effective stress, $\sigma_{zz}(t,x) + p(t,x)$. This model is considered to be a more realistic deformation model for joints in partial contact (that is, for partially open fractures) [1]. It was first proposed by Goodman [26] and further discussed by Bandis et al [27] and Murphy et al [28] and is given by:

$$h(t,x) = \left(\frac{1 + \left(\frac{\sigma_{zz}(t,x)+p(t,x)}{k}\right)\frac{h_{min}}{h_{max}}}{1 + \left(\frac{\sigma_{zz}(t,x)+p(t,x)}{k}\right)}\right)h_{max} \tag{2.4.37}$$

where $k < 0$ and is a constant. The dimensions of k are the dimensions of stress. This parameter is determined experimentally. For example for a fracture which is 2 km deep, $k = -10^7\, Pa$.

Now, similarly as in the linear crack law model, we assume that the minimum crack height is much smaller than the maximum crack height, $h_{min} << h_{max}$. The half-width of the fracture, (2.4.37), therefore reduces to

$$h(t,x) = \left(\frac{1}{1 + \left(\frac{\sigma_{zz}(t,x)+p(t,x)}{k}\right)} \right) h_{max}. \tag{2.4.38}$$

It is clear that (2.4.38) can be written as

$$p(t,x) + p_2(t,x) = -\sigma_{zz}(t,x), \tag{2.4.39}$$

where

$$p_2(t,x) = -k\left(\frac{h_{max}}{h(t,x)} - 1 \right) > 0. \tag{2.4.40}$$

For a partially open fracture, (2.4.39) satisfies the negative effective stress condition, (2.4.32), such that the compressive normal stress, $-\sigma_{zz}(t,x)$, at the fracture walls is supported by both the fluid pressure, $p(t,x)$, and the pressure due to contact regions, (2.4.40). Note that for partially open fractures, $k < 0$. For an open fracture, it is clear that (2.4.39) satisfies the zero effective stress condition (2.4.30) provided the pressure contribution due to contact regions is zero, that is, provided $p_2(t,x) = 0$ and therefore $k = 0$.

2.4.3 PKN approximation

Now lastly in the modelling process, it is necessary to define a relation between the half-width of the fracture, $h(t,x)$, and the normal stress, $\sigma_{zz}(t,x)$. By applying the theory of plane strain to the surrounding rock mass, the normal stress at the fracture walls can be expressed as a Cauchy principal value integral in terms of the spatial gradient of the half-width of the fracture [34]:

$$\sigma_{zz}(t,x) = \sigma_{zz}^{(\infty)} + \frac{G}{2\pi(1-\nu)} \barint_{-\infty}^{\infty} \frac{\partial h}{\partial s}(t,s) \frac{ds}{(s-x)}, \tag{2.4.41}$$

where the bar on the integral sign denotes the Cauchy principal value, $\sigma_{zz}^{(\infty)}$ is the normal stress at infinity in the rock mass and G and ν are the shear modulus and Poisson ratio of the rock mass respectively. A similarity solution can be obtained for the integro-differential

equation for the half-width but the resulting boundary value problem is difficult to solve [1, 2, 5, 6, 34]. In this work instead of using (2.4.41), we use the Perkins-Kern-Nordgren (PKN) approximation [16, 17] widely used in the oil and gas industry:

$$\sigma_{zz}(t,x) = \sigma_{zz}^{\infty} - \Lambda h(t,x), \tag{2.4.42}$$

where

$$\Lambda = \frac{E}{(1-\nu^2)B}, \tag{2.4.43}$$

and E is the Young's modulus of the surrounding rock while B is the breadth of the fracture. Adachi and Peirce [24] have shown that the PKN approximation is a good approximation in the outer region away from the fracture tip and that the small correction term involves the second spatial derivative of the fracture's half-width.

2.4.4 Closure for tortuosity models

For a partially open fracture with the contact regions governed by the linear crack law, using the PKN approximation, (2.4.42), it can be verified that (2.4.35) reduces to

$$p(t,x) = -\sigma_{zz}^{(\infty)} + \Lambda h(t,x) + \sigma_R\Big(1 - \frac{h(t,x)}{h_{max}}\Big), \tag{2.4.44}$$

where $\sigma_R < 0$. From differentiating (2.4.44), the spatial gradient of the fluid pressure is therefore given by

$$\frac{\partial p}{\partial x} = \left(\Lambda - \frac{\sigma_R}{h_{max}}\right)\frac{\partial h}{\partial x}. \tag{2.4.45}$$

For a partially open fracture with contact regions governed by the hyperbolic crack law, using the PKN approximation, (2.4.42), it is clear that (2.4.39) reduces to

$$p(t,x) = -\sigma_{zz}^{(\infty)} + \Lambda h(t,x) + k\Big(\frac{h_{max}}{h(t,x)} - 1\Big), \tag{2.4.46}$$

where $k < 0$. The derivative of (2.4.46) is therefore given by

$$\frac{\partial p}{\partial x} = \left(\Lambda - \frac{k h_{max}}{h^2(t,x)}\right)\frac{\partial h}{\partial x}. \tag{2.4.47}$$

Note that for an open fracture, the fluid pressure equations, (2.4.44) and (2.4.46), satisfy the zero effective stress condition, (2.4.30), provided $\sigma_R = 0$ and $k = 0$ respectively. Equations (2.4.44) and (2.4.46) therefore reduce to

$$p(t,x) = -\sigma_{zz}^{(\infty)} + \Lambda h(t,x), \tag{2.4.48}$$

which is the fluid pressure sufficient to support the normal stress in an open fracture. The derivative of (2.4.48) with respect to x therefore gives the spatial gradient of the fluid pressure in an open fracture:

$$\frac{\partial p}{\partial x} = \Lambda \frac{\partial h}{\partial x}, \tag{2.4.49}$$

which can also be derived from (2.4.45) and (2.4.47) by setting $\sigma_R = 0$ and $k = 0$ respectively.

Now, to close the model for a partially open fracture with contact regions governed by the linear crack law, we substitute (2.4.45) into (2.4.26) to (2.4.28) to obtain

$$Q(t,x) = -\frac{2a_n\Lambda}{3\mu}\left(1 - \frac{\sigma_R}{\Lambda h_{max}}\right)h^n \frac{\partial h}{\partial x}, \tag{2.4.50}$$

$$\frac{\partial h}{\partial t} = \frac{a_n\Lambda}{3\mu}\left(1 - \frac{\sigma_R}{\Lambda h_{max}}\right)\frac{\partial}{\partial x}\left(h^n \frac{\partial h}{\partial x}\right), \tag{2.4.51}$$

$$\overline{v}_x(t,x) = -\frac{a_n\Lambda}{3\mu}\left(1 - \frac{\sigma_R}{\Lambda h_{max}}\right)h^{n-1} \frac{\partial h}{\partial x}, \tag{2.4.52}$$

where $\sigma_R < 0$. Substituting (2.4.47) into (2.4.26) to (2.4.28) gives equations describing a partially open fracture with contact regions governed by the hyperbolic crack law:

$$Q(t,x) = -\frac{2a_n\Lambda}{3\mu}\left(h^n - \frac{kh_{max}}{\Lambda}h^{n-2}\right)\frac{\partial h}{\partial x}, \tag{2.4.53}$$

$$\frac{\partial h}{\partial t} = \frac{a_n\Lambda}{3\mu}\frac{\partial}{\partial x}\left(h^n - \frac{kh_{max}}{\Lambda}h^{n-2}\right)\frac{\partial h}{\partial x}, \tag{2.4.54}$$

$$\overline{v}_x(t,x) = -\frac{a_n\Lambda}{3\mu}\left(h^{n-1} - \frac{kh_{max}}{\Lambda}h^{n-3}\right)\frac{\partial h}{\partial x}, \tag{2.4.55}$$

where $k < 0$. For an open fracture without contact regions we set $\sigma_R = 0$ and $k = 0$, respectively, and therefore equations (2.4.50) to (2.4.52) and (2.4.53) to (2.4.55) reduce to

$$Q(t,x) = -\frac{2a_n\Lambda}{3\mu}h^n\frac{\partial h}{\partial x}, \tag{2.4.56}$$

$$\frac{\partial h}{\partial t} = \frac{a_n\Lambda}{3\mu}\frac{\partial}{\partial x}\Big(h^n\frac{\partial h}{\partial x}\Big), \tag{2.4.57}$$

$$\overline{v}_x(t,x) = -\frac{a_n\Lambda}{3\mu}h^{n-1}\frac{\partial h}{\partial x}. \tag{2.4.58}$$

Boundary conditions

We now consider the boundary conditions for the nonlinear diffusion equations (2.4.51), (2.4.54) and (2.4.57). For all the governing partial differential equations, the half-width at the fracture tip vanishes, therefore:

$$h(t, L(t)) = 0, \tag{2.4.59}$$

where $L(t)$ is the length of the fracture. This boundary condition is a moving boundary condition given that the length of the fracture $L(t)$ keeps increasing as the fracture propagates [35]. At the fracture tip there is no fluid flux out of the fracture, therefore the solution to the partial differential equations (2.4.51), (2.4.54) and (2.4.57) must satisfy the zero flux condition:

$$Q(t, L(t)) = 0. \tag{2.4.60}$$

From (2.4.50), for a partially open fracture with contact regions modelled by the linear crack law, the zero flux condition (2.4.60) is satisfied provided

$$h^n(t, L(t))\frac{\partial h}{\partial x}(t, L(t)) = 0. \tag{2.4.61}$$

From (2.4.56), it is clear that for an open fracture the zero flux condition (2.4.60) is satisfied provided the same condition (2.4.61) is satisfied. For a partially open fracture with contact regions modelled by the hyperbolic crack law, from (2.4.53) the zero flux condition (2.4.60) is satisfied provided

$$\frac{kh_{max}}{\Lambda}h^{n-2}(t, L(t))\frac{\partial h}{\partial x}(t, L(t)) - h^n(t, L(t))\frac{\partial h}{\partial x}(t, L(t)) = 0. \tag{2.4.62}$$

Now, for the boundary condition at the fracture entry, it is important to note that since the surrounding rock encasing the fracture is impermeable, the flux of fluid at the fracture entry is equal to the rate of change of the volume of the fracture:

$$Q(t,0) = \frac{dV}{dt} \tag{2.4.63}$$

where $V(t)$ is the volume of the fracture per unit breadth:

$$V(t) = 2\int_0^{L(t)} h(t,x)dx. \tag{2.4.64}$$

For a partially open fracture with contact regions modelled by the linear crack law, from (2.4.50) the boundary condition (2.4.63) becomes

$$-\frac{2a_n\Lambda}{3\mu}\left(1 - \frac{\sigma_R}{\Lambda h_{max}}\right)h^n(t,0)\frac{\partial h}{\partial x}(t,0) = \frac{dV}{dt}, \tag{2.4.65}$$

where $\sigma_R < 0$ and $V(t)$ is given by (2.4.64). For a partially open fracture with contact regions modelled by the hyperbolic crack law, from (2.4.53) the boundary condition (2.4.63) becomes

$$\frac{2a_n\Lambda}{3\mu}\left[\frac{kh_{max}}{\Lambda}h^{n-2}(t,0)\frac{\partial h}{\partial x}(t,0) - h^n(t,0)\frac{\partial h}{\partial x}(t,0)\right] = \frac{dV}{dt}, \tag{2.4.66}$$

where $k < 0$ and $V(t)$ is given by (2.4.64). By setting $\sigma_R = 0$ and $k = 0$ in (2.4.65) and (2.4.66) respectively, it is clear that the second boundary condition for an open fracture without contact regions is

$$-\frac{2a_n\Lambda}{3\mu}h^n(t,0)\frac{\partial h}{\partial x}(t,0) = \frac{dV}{dt}, \tag{2.4.67}$$

where $V(t)$ is given by (2.4.64).

Dimensionless equations and boundary conditions

It now remains to non-dimensionalise the governing equations and the corresponding boundary conditions such that we do not need to work with units. It is necessary to specify the characteristic quantities, the length, half-width and fluid velocity along the length of the fracture. For both types of fracture, open and partially open, we choose the characteristic length of the fracture to be the initial length of the fracture:

$$L = L(0) = L_0 \tag{2.4.68}$$

and the characteristic half-width of the fracture is chosen to be the maximum half-width of the fracture:

$$H = h_{max}. \tag{2.4.69}$$

For a partially open fracture with contact regions modelled by the linear crack law, from (2.4.44) it follows that a suitable characteristic pressure, P, is

$$P = -\sigma_{zz}^{(\infty)} + \Lambda h_{max}. \tag{2.4.70}$$

Equating (2.4.70) with the characteristic fluid pressure for the lubrication approximation, (2.4.7), gives the characteristic fluid velocity along the length of a partially open fracture with contact regions modelled by the linear crack law:

$$U = \frac{\Lambda h_{max}^3}{\mu L_0}\left(1 - \frac{\sigma_{zz}^{(\infty)}}{\Lambda h_{max}}\right). \tag{2.4.71}$$

Now, using the following dimensionless variables:

$$\begin{aligned} &x^* = \frac{x}{L_0}, \quad h^* = \frac{h}{h_{max}}, \quad t^* = \frac{Ut}{L_0}, \quad L^* = \frac{L}{L_0}, \\ &V^* = \frac{V}{h_{max}L_0}, \quad \overline{v}_x^* = \frac{\overline{v}_x}{U}, \quad Q^* = \frac{Q}{h_{max}U}, \quad p^* = \frac{p}{P}, \end{aligned} \tag{2.4.72}$$

it can be verified that for a partially open fracture with contact regions modelled by the linear crack law, the problem is to solve the nonlinear diffusion equation

$$\frac{\partial h^*}{\partial t^*} = K_n \frac{\partial}{\partial x^*}\left(h^{*n}\frac{\partial h^*}{\partial x^*}\right), \tag{2.4.73}$$

subject to the boundary conditions

$$h^*(t^*, L^*(t^*)) = 0, \tag{2.4.74}$$

$$-2K_n h^{*n}(t^*, 0)\frac{\partial h^*}{\partial x^*}(t^*, 0) = \frac{dV^*}{dt^*}, \tag{2.4.75}$$

where

$$V^*(t^*) = 2\int_0^{L^*(t^*)} h^*(t^*, x^*)dx^* \tag{2.4.76}$$

is the volume of the fracture and the diffusion constant, K_n, is

$$K_n = \frac{a_n h_{max}^{n-3}}{3}\left(\frac{1 - \frac{\sigma_R}{\Lambda h_{max}}}{1 - \frac{\sigma_{zz}^{(\infty)}}{\Lambda h_{max}}}\right). \tag{2.4.77}$$

The volume flux, the width averaged fluid velocity and the fluid pressure are

$$Q^*(t^*, x^*) = -2K_n h^{*n} \frac{\partial h^*}{\partial x^*}, \tag{2.4.78}$$

$$\overline{v}_x^*(t^*, x^*) = -K_n h^{*n-1} \frac{\partial h^*}{\partial x^*}, \tag{2.4.79}$$

$$p^*(t^*, x^*) = \left(\frac{1 - \frac{\sigma_R}{\Lambda h_{max}}}{1 - \frac{\sigma_{zz}^{(\infty)}}{\Lambda h_{max}}} \right) h^*(t^*, x^*) + \left(\frac{\sigma_R - \sigma_{zz}^{(\infty)}}{\Lambda h_{max} - \sigma_{zz}^{(\infty)}} \right), \tag{2.4.80}$$

respectively, with $\sigma_R < 0$. The solution must identically satisfy the zero flux condition at the fracture tip:

$$h^{*n}(t^*, L^*(t^*)) \frac{\partial h^*}{\partial x^*}(t^*, L^*(t^*)) = 0. \tag{2.4.81}$$

The condition (2.4.81) is always satisfied provided $\partial h^*/\partial x^*$ is bounded at the fracture tip, $x = L(t)$. However we will later find that for $n > 1$, $\partial h^*/\partial x^*$ is unbounded. Therefore the zero flux condition at the fracture tip, (2.4.81), serves as a check for the model when $n > 1$.

For a partially open fracture with contact regions modelled by the hyperbolic crack law, from (2.4.46) we again choose the characteristic pressure P to be given by (2.4.70) and using (2.4.7) the characteristic fluid velocity U is again given by (2.4.71). Now, using the dimensionless variables (2.4.72), it can be verified that for a partially open fracture with contact regions modelled by the hyperbolic crack law, the problem is to solve the partial differential equation

$$\frac{\partial h^*}{\partial t^*} = K_n \frac{\partial}{\partial x^*} \left(h^{*n} \frac{\partial h^*}{\partial x^*} + \phi h^{*n-2} \frac{\partial h^*}{\partial x^*} \right), \tag{2.4.82}$$

subject to the boundary conditions

$$h^*(t^*, L^*(t^*)) = 0, \tag{2.4.83}$$

$$-2K_n \left[h^{*n}(t^*, 0) \frac{\partial h^*}{\partial x^*}(t^*, 0) + \phi h^{*n-2}(t^*, 0) \frac{\partial h^*}{\partial x^*}(t^*, 0) \right] = \frac{dV^*}{dt^*}, \tag{2.4.84}$$

where the volume of the fracture, $V^*(t^*)$, is given by (2.4.76), the diffusion constant K_n is

$$K_n = \frac{a_n h_{max}^{n-3}}{3} \left(\frac{1}{1 - \frac{\sigma_{zz}^{(\infty)}}{\Lambda h_{max}}} \right) \tag{2.4.85}$$

and

$$\phi = -\frac{k}{\Lambda h_{max}}, \tag{2.4.86}$$

with $k < 0$. The volume flux per unit breadth, the width averaged fluid velocity and the fluid pressure are

$$Q^*(t^*, x^*) = -2K_n\left(h^{*n}\frac{\partial h^*}{\partial x^*} + \phi h^{*n-2}\frac{\partial h^*}{\partial x^*}\right), \tag{2.4.87}$$

$$\overline{v}_x^*(t^*, x^*) = -K_n\left(h^{*n-1}\frac{\partial h^*}{\partial x^*} + \phi h^{*n-3}\frac{\partial h^*}{\partial x^*}\right), \tag{2.4.88}$$

$$p^*(t^*, x^*) = \left(\frac{1 - \frac{\phi}{h^{*2}(t^*, x^*)}}{1 - \frac{\sigma_{zz}^{(\infty)}}{\Lambda h_{max}}}\right)h^*(t^*, x^*) - \left(\frac{k + \sigma_{zz}^{(\infty)}}{\Lambda h_{max} - \sigma_{zz}^{(\infty)}}\right). \tag{2.4.89}$$

It is necessary that the obtained solution for a partially open fracture with contact regions modelled by the hyperbolic crack law satisfy the zero flux condition at the fracture tip:

$$h^{*n}(t^*, L^*(t^*))\frac{\partial h^*}{\partial x^*}(t^*, L^*(t^*)) + \phi h^{*n-2}(t^*, L^*(t^*))\frac{\partial h^*}{\partial x^*}(t^*, L^*(t^*)) = 0. \tag{2.4.90}$$

The condition (2.4.90) is always satisfied provided $\partial h^*/\partial x^*$ is bounded at the fracture tip, $x = L(t)$. However we will later find that for $n > 3$, $\partial h^*/\partial x^*$ is unbounded. Therefore the zero flux condition at the fracture tip, (2.4.90), serves as a check for the model when $n > 3$.

For an open fracture with no contact regions, from (2.4.48) and (2.4.7) it can be shown that the characteristic fluid velocity along an open fracture is also given by (2.4.71). In fact it can be verified that governing equations (2.4.73) to (2.4.81) are valid for an open fracture with $\sigma_R = 0$.

2.5 Conclusions

In this chapter three models were formulated, two for a partially open fracture and one for an open fracture. For a partially open fracture with contact regions modelled by the linear crack law, the half-width of the fracture is directly proportional to the effective stress. For a partially open fracture with contact regions modelled by the hyperbolic crack law, the

half-width of the fracture is inversely proportional to the effective stress. The latter model is considered to be a more realistic deformation model for contact regions [1].

It is important to note that in dimensionless form, the boundary value problems for an open fracture and for a partially open fracture with contact regions modelled by the linear crack law are the same. The two problems are mathematically distinguished by the fact that for an open fracture the least effective stress is zero, that is σ_R=0, since for an open fracture the effective stress must always vanish, while for a partially open fracture with contact regions modelled by the linear crack law the least effective stress is negative, that is $\sigma_R < 0$, given that the negative effective stress condition must always hold for a partially open fracture.

In this Chapter dimensionless quantities are denoted by a star (*). In subsequent Chapters the star (*) will be suppressed, it being understood that dimensionless quantities are used unless otherwise stated.

Chapter 3

METHODS OF SOLUTION

3.1 Introduction

In this section we consider methods of solution that will be used to solve the governing equations derived in Chapter 2. The methods of solving partial differential equations used by Spence and Sharp [34] in analysing the propagation of a hydraulic fracture and by Huppert [36] in analysing the propagation of viscous gravity currents will not be used in this work. This is because both the hydraulic fracture considered by Spence and Sharp and the gravity currents considered by Huppert propagate from a line source of fluid while the hydraulic fracture considered in this work is pre-existing and therefore has an initially non-zero length. We therefore use the more powerful method of Lie group analysis in order to solve the governing partial differential equations, [11, 14, 31, 37, 38]. It follows that Lie point symmetries will be derived and used to solve the governing partial differential equations.

In this section, we will also outline different methods of deriving conservation laws for partial differential equations, namely: the direct method, the multiplier method and the partial Lagrangian method.

3.2 Lie point symmetry approach

A symmetry is a transformation that when applied to an object leaves that object unchanged. The notion of symmetry can be easily observed when patterns in nature repeat themselves. Different shapes in nature have a different number of symmetries, such as quadrilaterals that have a finite number of symmetries and circles that have an infinite number of symmetries. And although the concept of symmetry may seem to come intuitively from analysis of the geometry of shapes, it was in fact an outcome of the analysis of solutions to higher order (higher than quartic) algebraic equations, Galois (1811 - 1832). The concept of Lie point symmetries was introduced by Sophus Lie (1842 - 1899). It is a systematic method that allows one to either derive an exact analytical solution of a differential equation or reduce the order of a differential equation from $k+1$ to k, where $k \in \mathbb{Z}^+$, or to reduce a partial differential equation to an ordinary differential equation as will be done in this work. This method has been used by several authors in order to solve various differential equations, [11, 14, 31, 37, 38]. In this work, we will use the Lie point symmetry approach in order to reduce the governing partial differential equations derived in Chapter 2 to ordinary differential equations and therefore find the corresponding group invariant solutions of the governing partial differential equations.

Consider the second order PDE for $h(t,x)$

$$F(t,x,h,h_t,h_x,h_{tt},h_{tx},h_{xx}) = 0, \tag{3.2.1}$$

where the subscripts t *and* x *denote partial differentiation with respect to* t *and* x*. Then*

$$X = \xi^1(t,x,h)\frac{\partial}{\partial t} + \xi^2(t,x,h)\frac{\partial}{\partial x} + \eta(t,x,h)\frac{\partial}{\partial h}, \tag{3.2.2}$$

is a Lie point symmetry of the PDE (3.2.1) *provided*

$$X^{[2]}(F)\Big|_{F=0} = 0, \tag{3.2.3}$$

where

$$X^{[2]} = X + \zeta_1\frac{\partial}{\partial h_t} + \zeta_2\frac{\partial}{\partial h_x} + \zeta_{11}\frac{\partial}{\partial h_{tt}} + \zeta_{12}\frac{\partial}{\partial h_{tx}} + \zeta_{22}\frac{\partial}{\partial h_{xx}} \tag{3.2.4}$$

is the second prolongation of the generator X with [39]

$$\zeta_i = D_i(\eta) - h_k D_i(\xi^k), \qquad i = 1, 2, \tag{3.2.5}$$

$$\zeta_{ij} = D_j(\zeta_i) - h_{ik} D_j(\xi^k), \qquad i, j = 1, 2. \tag{3.2.6}$$

In equations (3.2.5) and (3.2.6), there is summation over the repeated index k from 1 to 2 and

$$D_1 = D_t = \frac{\partial}{\partial t} + h_t \frac{\partial}{\partial h} + h_{tt} \frac{\partial}{\partial h_t} + h_{xt} \frac{\partial}{\partial h_x} + \dots \tag{3.2.7}$$

$$D_2 = D_x = \frac{\partial}{\partial x} + h_x \frac{\partial}{\partial h} + h_{tx} \frac{\partial}{\partial h_t} + h_{xx} \frac{\partial}{\partial h_x} + \dots \tag{3.2.8}$$

are the total derivatives.

In the determining equation (3.2.3), t, x, h and all the partial derivatives of h are regarded as independent variables. When t, x, h and partial derivatives of h are regarded as independent, partial differentiation is denoted by a subscript.

The group invariant solution $h = \Psi(t, x)$ generated by the Lie point symmetry X, (3.2.2), of the PDE (3.2.1) satisfies

$$X(h - \Psi(t, x))\Big|_{h=\Psi} = 0. \tag{3.2.9}$$

Substituting the group invariant solution into the PDE (3.2.1) reduces it to an ordinary differential equation (ODE).

3.3 Conservation laws

In this work we will also investigate conservation laws for the governing partial differential equations which were derived in Chapter 2. A conservation law for the partial differential equation (PDE) (3.2.1) is defined as

$$D_1 T^1 + D_2 T^2\Big|_{F=0} = 0, \tag{3.3.1}$$

where D_1 and D_2 are the total derivatives given by (3.2.7) and (3.2.8). The vector $\mathbf{T} = \left(T^1, T^2\right)$ is called a conserved vector. We will derive conservation laws for the governing PDEs using three methods: the direct method, the multiplier method and the partial Lagrangian method. These methods and various other methods of obtaining conservation laws for partial differential equations have been reviewed by Naz et al [40]. The conserved vectors can easily be deduced from the conservation laws. We will investigate if there exist any other conserved vectors besides the ones derived using these three methods. This will be done by investigating if new conserved vectors can be generated from known conserved vectors by applying the following theorem of Kara and Mahomed [41, 42]:
If X given by (3.2.2) *is a Lie point symmetry of the PDE* (3.2.1) *and* $\mathbf{T} = \left(T^1, T^2\right)$ *is a conserved vector for the PDE then*

$$T^i_* = X(T^i) + T^i D_k(\xi^k) - T^k D_k(\xi^i), \qquad i = 1, 2, \tag{3.3.2}$$

are the components of a conserved vector for the PDE.
The generated conserved vector (3.3.2) may be a new conserved vector of the PDE or simply a linear combination of the known conserved vectors or zero.

3.3.1 Direct method

Of all methods that are used to derive conservation laws for a partial differential equation, the direct method has the most straight forward calculations. It is a well established method that was introduced by Laplace [43].

Firstly, an assumption has to be made on which variables the components T^1 and T^2 of the conserved vector $\mathbf{T}$ depend. For example, the components of the conserved vector could have the form $T^1 = T^1(t, x, h, h_t)$ and $T^2 = T^2(t, x, h, h_x, h_{xx})$. The components of the conserved vector $\mathbf{T}$ are then substituted into (3.3.1) which is expanded using definitions (3.2.7) and (3.2.8) of the total derivatives. Equation (3.3.1) is the determining equation for the components T^1 and T^2 of the conserved vector $\mathbf{T}$. The size of the determining equation will depend on which variables the components of the conserved vector are assumed to depend. The determining equation is then evaluated on the governing partial

differential equation (PDE) (3.2.1), generally by replacing one of the partial derivatives. The remaining variables in the determining equation are then independent. The determining equation is first separated by powers and products of the variables which do not appear in T^1 or T^2. The equations obtained are further separated until a solution for T^1 and T^2 is obtained. The components T^1 and T^2 in general contain constants and give a linear combination of conserved vectors.

Some of the conserved vectors obtained may be trivial. A conserved vector $\mathbf{T} = (T^1, T^2)$ is trivial if

$$D_1 T^1 + D_2 T^2 = 0 \tag{3.3.3}$$

without evaluating (3.3.3) on the PDE.

3.3.2 Multiplier method

The multiplier method is used to obtain conservation laws and therefore conserved vectors for partial differential equations (PDEs) and has been widely used in the literature by various authors, [40, 44, 45]. We will describe the multiplier method for the derivation of conservation laws for the second order PDE (3.2.1) for $h(t, x)$. The variables t, x, h, h_t, h_x and all higher order partial derivatives of h are treated as independent variables.

Firstly an assumption has to be made on which variables the multiplier Λ depends. The more variables included, the larger the range of conserved vectors that may be derived but the length of the calculation will be greater. We may choose $\Lambda = \Lambda(t, x, h, h_t, h_x)$ or include higher order partial derivatives of h. A multiplier Λ of the PDE (3.2.1) has the property that

$$\Lambda(F) = D_1 T^1 + D_2 T^2 \tag{3.3.4}$$

for all functions $h(t, x)$ and not only solutions of the PDE (3.2.1). The right-hand side of (3.3.4) is a divergence expression and T^1 and T^2 are the components of a conserved vector $\mathbf{T} = (T^1, T^2)$. The next step is to apply to (3.3.4) the Euler operator

$$E_h = \frac{\delta}{\delta h} = \frac{\partial}{\partial h} - D_t \frac{\partial}{\partial h_t} - D_x \frac{\partial}{\partial h_x} + D_t^2 \frac{\partial}{\partial h_{tt}} + D_x D_t \frac{\partial}{\partial h_{xt}} + D_x^2 \frac{\partial}{\partial h_{xx}} - ..., \tag{3.3.5}$$

which annihilates divergence expressions. Equation (3.3.4) becomes

$$E_h\Big[\Lambda(F)\Big] = 0, \tag{3.3.6}$$

which is the determining equation for the multiplier Λ. Now, (3.3.6) must be satisfied by all functions of $h(t, x)$. Equation (3.3.6) is therefore separated by powers and products of the partial derivatives of h which do not occur in Λ. The equations derived are further separated until Λ is obtained.

Lastly, we substitute the expression obtained for the multiplier Λ into the left-hand side of (3.3.4) and use elementary mathematical manipulations to express the left-hand side of (3.3.4) in the form $D_1T^1 + D_2T^2$ for arbitrary functions $h(t, x)$. When $h(t, x)$ is a solution of the PDE (3.2.1), then

$$D_1T^1 + D_2T^2 = 0 \tag{3.3.7}$$

which gives the required conservation laws and therefore conserved vectors for the PDE (3.2.1). The multiplier Λ generally depends on several constants and (3.3.7) consists of a linear combination of conservation laws, one for each constant in Λ.

3.3.3 Partial Lagrange method

A differential function L is a Lagrangian of the partial differential equation (3.2.1) if the PDE is equivalent to the Euler-Lagrange differential equation

$$E_hL = \frac{\delta L}{\delta h} = 0, \tag{3.3.8}$$

where E_h is the Euler operator defined in equation (3.3.5). By Noether's theorem [46], the Lagrangian L of a partial differential equation can be used to derive conservation laws.

Now it is either difficult or impossible to derive Lagrangians for some partial differential equations such as the heat equation. For this reason Kara and Mahomed [47] introduced the idea of the partial Lagrangian for a PDE and developed the partial Lagrangian method for the derivation of conservation laws for a PDE.

A differential function L is a partial Lagrangian of the partial differential equation

$$F = F^0 + F^1 = 0 \tag{3.3.9}$$

if the PDE can be expressed as the Euler-Lagrange type differential equation

$$E_h L = \frac{\delta L}{\delta h} = f F^1 \tag{3.3.10}$$

where f is a non-zero function.

Note that $F^1 \neq 0$. If $F^1 = 0$, then instead of a partial Lagrangian, we would have a Lagrangian of the partial differential equation. The partial Lagrangians L in this thesis will have highest derivative order one. The partial Lagrangian method is quite general however in this thesis, we will consider the definition of the partial Lagrangian method for a partial differential equation with only two independent variables and one dependent variable.

A Lie Bäcklund operator $\mathbf{X}$ *defined in* (3.2.2) *is a partial Noether symmetry generator corresponding to the partial Lagrangian L if there exists gauge functions B^1 and B^2 such that*

$$X^{[1]}(L) + L(D_1\xi^1 + D_2\xi^2) = (D_1 B^1 + D_2 B^2) + (\eta - \xi^1 h_t - \xi^2 h_x) E_h L, \tag{3.3.11}$$

where $X^{[1]}$ is the first prolongation of (3.2.2)*:*

$$X^{[1]} = X + \zeta_1 \frac{\partial}{\partial h_t} + \zeta_2 \frac{\partial}{\partial h_x} \tag{3.3.12}$$

and ζ_1, ζ_2 are given by equation (3.2.5)*.*

Solving the determining equation (3.3.11) for the gauge functions, B^1 and B^2, and the symmetries, ξ^1, ξ^2 and η, allows us to derive components

$$T^1 = B^1 - \xi^1 L - (\eta - \xi^1 h_t - \xi^2 h_x) \frac{\partial L}{\partial h_t}, \tag{3.3.13}$$

$$T^2 = B^2 - \xi^2 L - (\eta - \xi^1 h_t - \xi^2 h_x) \frac{\partial L}{\partial h_x}, \tag{3.3.14}$$

of the conserved vector(s) $\mathbf{T}$ for the partial differential equation (3.3.9). In general the gauge functions and the symmetry generator contain constants and (3.3.13) and (3.3.14) form a linear combination of conserved vectors.

3.4 Conclusions

In this Section the Lie point symmetry approach to solving partial differential equations was briefly outlined. All the required steps from deriving the Lie point symmetry generator to obtaining the group invariant solution of the partial differential equation were described. It is a systematic method that can be used to solve a large range of nonlinear partial differential equations. It must also be possible to express the boundary conditions in the group invariant form to solve the problem.

Conservation laws will be used to analyse the partial differential equations in this thesis. Three methods of deriving conservation laws; the direct; the multiplier and the partial Lagrangian methods will be used in case one method does not give all the results. We will investigate if the three methods give different conserved vectors or the same conserved vectors. We will associate Lie point symmetries with conservation laws and investigate if this leads to new analytical solutions.

Chapter 4

CONSERVATION LAWS OF THE LINEAR HYDRAULIC FRACTURE WITH TORTUOSITY

4.1 Introduction

From Chapter 2, it is clear that a partially open fracture with contact regions modelled by the linear crack law and an open fracture without contact regions are governed by the same nonlinear diffusion equation

$$\frac{\partial h}{\partial t} = K_n \frac{\partial}{\partial x}\left(h^n \frac{\partial h}{\partial x} \right), \tag{4.1.1}$$

where the diffusion constant K_n is different for the two types of fracture. As discussed in Chapter 2, we will always consider parameter values of n that satisfy the condition $n > 0$. In this Chapter conservation laws for the governing nonlinear diffusion equation (4.1.1) are rigorously derived using the three methods outlined in Chapter 3, the direct; the multiplier and the partial Lagrangian methods.

For all calculations regarding conservation laws, we consider all variables, t, x, h and

the partial derivatives of h to be independent variables. The subscript notation for partial derivatives will therefore be used. It is therefore necessary to re-express equation (4.1.1) in the form

$$G = h_t - K_n n h^{n-1} h_x^2 - K_n h^n h_{xx} = 0. \tag{4.1.2}$$

When t and x are regarded as the only independent variables, the standard notation for partial derivatives will be used.

4.2 Direct method

In order to investigate the conservation laws for the partial differential equation (4.1.1) we consider the form (3.3.1). Now the elementary conserved vector, from (4.1.1), is

$$T^1 = h, \quad T^2 = -K_n h^n h_x, \tag{4.2.1}$$

which does not depend on h_t. We investigate if there are other conserved vectors which are independent of h_t and look for conserved vectors of the form

$$T^1 = T^1(t, x, h, h_x), \quad T^2 = T^2(t, x, h, h_x). \tag{4.2.2}$$

The resulting determining equation (3.3.1) is

$$\left(\frac{\partial T^1}{\partial t} + \frac{\partial T^1}{\partial h} h_t + \frac{\partial T^1}{\partial h_x} h_{xt} + \frac{\partial T^2}{\partial x} + \frac{\partial T^2}{\partial h} h_x + \frac{\partial T^2}{\partial h_x} h_{xx} \right) \Bigg|_{(4.1.1)} = 0. \tag{4.2.3}$$

Substituting h_t from equation (4.1.2) into the determining equation (4.2.3) reduces it to

$$\frac{\partial T^1}{\partial t} + \frac{\partial T^2}{\partial x} + \left(K_n h^n \frac{\partial T^1}{\partial h} + \frac{\partial T^2}{\partial h_x} \right) h_{xx} + \frac{\partial T^1}{\partial h_x} h_{xt} + K_n n h^{n-1} \frac{\partial T^1}{\partial h} h_x^2 + \frac{\partial T^2}{\partial h} h_x = 0. \tag{4.2.4}$$

Now, separating equation (4.2.4) in the variables on which the components T^1 and T^2 do not depend gives the following results:

$$h_{xt} : \frac{\partial T^1}{\partial h_x} = 0, \tag{4.2.5}$$

which implies that

$$T^1 = T^1(t, x, h) \tag{4.2.6}$$

and

$$h_{xx} : K_n h^n \frac{\partial T^1}{\partial h} + \frac{\partial T^2}{\partial h_x} = 0, \tag{4.2.7}$$

which when integrated with respect to h_x, noting equation (4.2.6), gives

$$T^2 = -K_n h^n \frac{\partial T^1}{\partial h} h_x + A(t, x, h). \tag{4.2.8}$$

The remaining terms in (4.2.4) after the separating procedure are

$$Remainder : \frac{\partial T^1}{\partial t} + \frac{\partial T^2}{\partial x} + K_n n h^{n-1} \frac{\partial T^1}{\partial h} h_x^2 + \frac{\partial T^2}{\partial h} h_x = 0. \tag{4.2.9}$$

Now, substituting the expression for T^2 given by (4.2.8) into (4.2.9) gives

$$\frac{\partial T^1}{\partial t} + \frac{\partial A}{\partial x} + \left(\frac{\partial A}{\partial h} - K_n h^n \frac{\partial^2 T^1}{\partial x \partial h} \right) h_x - K_n h^n \frac{\partial^2 T^1}{\partial h^2} h_x^2 = 0. \tag{4.2.10}$$

Separating equation (4.2.10) in powers of h_x gives the following results:

$$h_x^2 : \frac{\partial^2 T^1}{\partial h^2} = 0, \tag{4.2.11}$$

which when integrated twice with respect to h, noting equation (4.2.6), gives

$$T^1(t, x, h) = B(t, x)h + C(t, x); \tag{4.2.12}$$

$$h_x : \frac{\partial A}{\partial h} - K_n h^n \frac{\partial^2 T^1}{\partial x \partial h} = 0, \tag{4.2.13}$$

in which when using (4.2.12) for T^1 and integrating with respect to h gives

$$A(t, x, h) = K_n \frac{h^{n+1}}{(n+1)} \frac{\partial B}{\partial x} + D(t, x), \tag{4.2.14}$$

where $n > 0$, and the remainder

$$remainder : \frac{\partial T^1}{\partial t} + \frac{\partial A}{\partial x} = 0. \tag{4.2.15}$$

Now, substituting (4.2.12) for T^1 and (4.2.14) for A into equation (4.2.15) gives

$$\frac{\partial B}{\partial t} h + \frac{\partial C}{\partial t} + K_n \frac{h^{n+1}}{(n+1)} \frac{\partial^2 B}{\partial x^2} + \frac{\partial D}{\partial x} = 0. \tag{4.2.16}$$

Separating (4.2.16) in powers of h gives the following results:

$$h : \frac{\partial B}{\partial t} = 0 \tag{4.2.17}$$

which implies that

$$B = B(x); \tag{4.2.18}$$

$$h^{n+1} : \frac{d^2B}{dx^2} = 0, \tag{4.2.19}$$

which when integrated twice with respect to x gives

$$B = ax + b, \tag{4.2.20}$$

where a and b are constants and the remaining terms

$$remainder : \frac{\partial C}{\partial t} + \frac{\partial D}{\partial x} = 0. \tag{4.2.21}$$

Now, using equations (4.2.8), (4.2.12), (4.2.14) and (4.2.20) gives

$$\mathbf{T} = \left((ax+b)h + C(t,x), \quad K_n \left[\frac{h^{n+1}}{(n+1)} a - h^n (ax+b) h_x \right] + D(t,x) \right). \tag{4.2.22}$$

Now

$$\mathbf{T} = [C(t,x), \quad D(t,x)] \tag{4.2.23}$$

is a trivial conserved vector because, by (4.2.21), equation (3.3.1) is identically satisfied without imposing the PDE (4.1.2). We therefore set $C(t,x) = 0$ and $D(t,x) = 0$. The remaining terms in (4.2.22) consist of a linear combination of two conserved vectors. Setting $a = 0$ and $b = 1$ gives the elementary conserved vector

$$\mathbf{T}_{(1)} = (h, -K_n h^n h_x), \tag{4.2.24}$$

while setting $a = 1$ and $b = 0$ in (4.2.22) gives a second conserved vector

$$\mathbf{T}_{(2)} = \left(xh, -K_n \left[xh^n h_x - \frac{h^{n+1}}{n+1} \right] \right). \tag{4.2.25}$$

There are therefore two non-trivial conserved vectors for the PDE (4.1.1) of the form (4.2.2).

4.3 Multiplier method

We first consider a multiplier Λ of the form

$$\Lambda = \Lambda(t, x, h). \tag{4.3.1}$$

The multiplier (4.3.1) has the property

$$\Lambda(t,x,h)\Big(h_t - K_n n h^{n-1} h_x^2 - K_n h^n h_{xx}\Big) = D_1 T^1 + D_2 T^2, \tag{4.3.2}$$

where D_1 and D_2 are the total derivatives given by equations (3.2.7) and (3.2.8). Now applying the Euler operator E_h, (3.3.5), on (4.3.2) gives

$$E_h\left[\Lambda(t,x,h)\Big(h_t - K_n n h^{n-1} h_x^2 - K_n h^n h_{xx}\Big)\right] = 0, \tag{4.3.3}$$

since the Euler operator annihilates divergence expressions. Expanding equation (4.3.3) and simplifying the result gives

$$2K_n h^n \frac{\partial \Lambda}{\partial h} h_{xx} + K_n h^{n-1}\left(n\frac{\partial \Lambda}{\partial h} + h\frac{\partial^2 \Lambda}{\partial h^2}\right) h_x^2 + 2K_n h^n \frac{\partial^2 \Lambda}{\partial x \partial h} h_x + K_n h^n \frac{\partial^2 \Lambda}{\partial x^2} + \frac{\partial \Lambda}{\partial t} = 0. \tag{4.3.4}$$

Since the multiplier Λ is independent of derivatives of h, (4.3.1), it follows that equation (4.3.4) can be separated by powers and products of the derivatives of h to give the following results:

$$h_{xx} : \frac{\partial \Lambda}{\partial h} = 0, \tag{4.3.5}$$

which implies that

$$\Lambda = \Lambda(t,x); \tag{4.3.6}$$

$$h_x^2 : h\frac{\partial^2 \Lambda}{\partial h^2} + n\frac{\partial \Lambda}{\partial h} = 0, \tag{4.3.7}$$

and

$$h_x : \frac{\partial^2 \Lambda}{\partial x \partial h} = 0, \tag{4.3.8}$$

which are identically satisfied and the remaining terms

$$Remainder : K_n h^n \frac{\partial^2 \Lambda}{\partial x^2} + \frac{\partial \Lambda}{\partial t} = 0, \tag{4.3.9}$$

where $n > 0$. Separating the remainder (4.3.9) in powers of h gives the following results:

$$h^0 : \frac{\partial \Lambda}{\partial t} = 0, \tag{4.3.10}$$

which implies that

$$\Lambda = \Lambda(x) \tag{4.3.11}$$

and

$$h^n : \frac{d^2\Lambda}{dx^2} = 0, \tag{4.3.12}$$

which when integrated with respect to x gives the multiplier

$$\Lambda = ax + b, \tag{4.3.13}$$

where a and b are constants. So far, $h(t, x)$ has been arbitrary. Suppose now that $h(t, x)$ is a solution of the PDE (4.1.2). Then applying the multiplier, (4.3.13), to the PDE (4.1.2) gives

$$(ax + b)(h_t - K_n n h^{n-1} h_x^2 - K_n h^n h_{xx}) = 0 \tag{4.3.14}$$

which when written in canonical form (that is, taking $a = 0$, $b = 1$ and $a = 1$, $b = 0$) yields the two equations

$$h_t - K_n n h^{n-1} h_x^2 - K_n h^n h_{xx} = 0, \tag{4.3.15}$$

$$x(h_t - K_n n h^{n-1} h_x^2 - K_n h^n h_{xx}) = 0. \tag{4.3.16}$$

The two equations (4.3.15) and (4.3.16) can be written as

$$D_1 T^1 + D_2 T^2 = 0 \tag{4.3.17}$$

using elementary mathematical manipulations. Firstly, we observe that the first term in equation (4.3.15) can be expressed as

$$h_t = D_1(h), \tag{4.3.18}$$

which implies that

$$T^1 = h. \tag{4.3.19}$$

The second and third terms of equation (4.3.15) can be written as

$$-K_n(n h^{n-1} h_x^2 + h^n h_{xx}) = D_2(-K_n h^n h_x), \tag{4.3.20}$$

which implies that

$$T^2 = -K_n h^n h_x. \tag{4.3.21}$$

Equations (4.3.19) and (4.3.21) are the components of the elementary conserved vector for the partial differential equation (4.1.2) denoted as

$$\begin{aligned}\mathbf{T_{(1)}} &= (T^1, T^2) \\ &= (h, -K_n h^n h_x).\end{aligned} \tag{4.3.22}$$

Similarly, we use elementary manipulations to express (4.3.16) in the form (4.3.17). The first term in (4.3.16) can be expressed as

$$xh_t = D_1(xh), \tag{4.3.23}$$

which implies that

$$T^1 = xh. \tag{4.3.24}$$

The second and third terms in (4.3.16) can be expressed as

$$-K_n(xnh^{n-1}h_x^2 + xh^n h_{xx}) = D_2\left(- K_n\left[xh^n h_x - \frac{h^{n+1}}{(n+1)}\right]\right), \tag{4.3.25}$$

which implies that

$$T^2 = -K_n\left[xh^n h_x - \frac{h^{n+1}}{(n+1)}\right]. \tag{4.3.26}$$

Equations (4.3.24) and (4.3.26) are the components of the second conserved vector for the partial differential equation (4.1.2) denoted as

$$\begin{aligned}\mathbf{T_{(2)}} &= (T^1, T^2) \\ &= \left(xh, -K_n\left[xh^n h_x - \frac{h^{n+1}}{(n+1)}\right]\right).\end{aligned} \tag{4.3.27}$$

We observe that the conserved vectors obtained by the multiplier method, (4.3.22) and (4.3.27), are the same as those obtained by the direct method, (4.2.24) and (4.2.25).

We now investigate if there exists other conserved vectors besides the elementary conserved vector (4.3.22) and the second conserved vector (4.3.27) already derived. Consider a multiplier that depends also on the first order partial derivatives of h of the form

$$\Lambda = \Lambda(t, x, h, h_t, h_x). \tag{4.3.28}$$

Now a multiplier of the PDE (4.1.2) has the property

$$\Lambda(t,x,h,h_t,h_x)\Big(h_t - K_n n h^{n-1}h_x^2 - K_n h^n h_{xx}\Big) = D_1T^1 + D_2T^2. \tag{4.3.29}$$

Since the Euler operator annihilates divergence expressions such as the one on the right hand side of (4.3.29), we apply the Euler operator (3.3.5) to (4.3.29) to obtain

$$E_h\left[\Lambda(t,x,h,h_t,h_x)\Big(h_t - K_n n h^{n-1}h_x^2 - K_n h^n h_{xx}\Big)\right] = 0. \tag{4.3.30}$$

Now, expanding equation (4.3.30) gives

$$\begin{aligned}
&\frac{\partial\Lambda}{\partial h}(h_t - K_n n h^{n-1}h_x^2 - K_n h^n h_{xx}) - \Lambda K_n(n(n-1)h^{n-2}h_x^2 + nh^{n-1}h_{xx})\\
&- D_2\left(\frac{\partial\Lambda}{\partial h_x}h_t - K_n\frac{\partial\Lambda}{\partial h_x}(nh^{n-1}h_x^2 + h^n h_{xx})\right) + D_2(2\Lambda K_n n h^{n-1}h_x)\\
&- D_1\left(\frac{\partial\Lambda}{\partial h_t}h_t - K_n\frac{\partial\Lambda}{\partial h_t}(nh^{n-1}h_x^2 + h^n h_{xx})\right) - D_1(\Lambda) - D_2^2(\Lambda K_n h^n) = 0.
\end{aligned} \tag{4.3.31}$$

Equation (4.3.31) can be expanded further, however given that the multiplier (4.3.28) also depends on first order partial derivatives of h, it follows that expanding (4.3.31) further will give a very long equation. In order to simplify the calculation, we first investigate if the coefficients of the highest order partial derivatives of h, which are third order in this calculation, can give information about the independent variables of the multiplier (4.3.28) and we then proceed successively to lower order partial derivatives. The highest order partial derivatives in this calculation are third order derivatives which result from the third, fifth and last terms of equation (4.3.31). The remaining terms in (4.3.31) are independent of third order partial derivatives of h and depend only on lower order partial derivatives. In (4.3.31), the third term gives

$$-D_2\left(\frac{\partial\Lambda}{\partial h_x}h_t - K_n\frac{\partial\Lambda}{\partial h_x}(nh^{n-1}h_x^2 + h^n h_{xx})\right) = K_n h^n\frac{\partial\Lambda}{\partial h_x}h_{xxx} + \textit{terms independent of third order derivatives of } h; \tag{4.3.32}$$

the fifth terms gives

$$-D_1\left(\frac{\partial\Lambda}{\partial h_t}h_t - K_n\frac{\partial\Lambda}{\partial h_t}(nh^{n-1}h_x^2 + h^n h_{xx})\right) = K_n h^n\frac{\partial\Lambda}{\partial h_t}h_{xxt} + \textit{terms independent of third order derivatives of } h \tag{4.3.33}$$

and the last term gives

$$-D_2^2(\Lambda K_n h^n) = -K_n\left(h^n\frac{\partial\Lambda}{\partial h_x}h_{xxx} + h^n\frac{\partial\Lambda}{\partial h_t}h_{xxt}\right) + \textit{terms independent of third order derivatives of } h. \tag{4.3.34}$$

It is clear that the sum of the third order partial derivative terms in equations (4.3.32), (4.3.33) and (4.3.34) is zero. It therefore follows that the coefficients of third order partial derivatives of h do not give any useful information that may lead to the derivation of the multiplier (4.3.28). We now need to consider analysing the coefficients of terms with second order partial derivatives of h. Expanding (4.3.31) gives

$$\begin{aligned}
&-2\frac{\partial\Lambda}{\partial h_t}h_{tt} - 2\left(K_n h^n\frac{\partial^2\Lambda}{\partial x\partial h_t} + \frac{\partial\Lambda}{\partial h_x}\right)h_{tx} + K_n h^n\left(\frac{\partial^2\Lambda}{\partial t\partial h_t} - \frac{\partial^2\Lambda}{\partial x\partial h_x} - 2\frac{\partial\Lambda}{\partial h}\right)h_{xx}\\
&+\left(K_n h^n\frac{\partial^2\Lambda}{\partial h\partial h_t} + K_n n h^{n-1}\frac{\partial\Lambda}{\partial h_t} - \frac{\partial^2\Lambda}{\partial h_x^2}\right)h_{xx}h_t - \frac{\partial^2\Lambda}{\partial h_t^2}h_{tt}h_t + K_n h^n\frac{\partial^2\Lambda}{\partial h_t^2}h_{tt}h_{xx}\\
&- K_n h^n\frac{\partial^2\Lambda}{\partial h_t^2}h_{tx}^2 + K_n h^{n-1}\left(3n\frac{\partial\Lambda}{\partial h_x} - h\frac{\partial^2\Lambda}{\partial h\partial h_x}\right)h_{xx}h_x + K_n n h^{n-1}\frac{\partial^2\Lambda}{\partial h_x^2}h_{xx}h_x^2\\
&- 2\frac{\partial^2\Lambda}{\partial h_t\partial h_x}h_{tx}h_t + 2K_n n h^{n-1}\frac{\partial^2\Lambda}{\partial h_t\partial h_x}h_{tx}h_x^2 + K_n n h^{n-1}\frac{\partial^2\Lambda}{\partial h_t^2}h_{tt}h_x^2\\
&+ 2K_n\left(nh^{n-1}\frac{\partial\Lambda}{\partial h_t} - h^n\frac{\partial^2\Lambda}{\partial h\partial h_t}\right)h_{tx}h_x\\
&+ \textit{terms independent of second order partial derivatives of } h.
\end{aligned} \tag{4.3.35}$$

Since Λ is independent of the second order partial derivatives of h, we therefore can separate (4.3.35) by the second order partial derivatives of h. Firstly, we separate (4.3.35) by h_{tt} to obtain

$$h_{tt} : \frac{\partial\Lambda}{\partial h_t} = 0, \tag{4.3.36}$$

which implies that

$$\Lambda = \Lambda(t, x, h, h_x); \tag{4.3.37}$$

then we separate (4.3.35) by h_{tx} to obtain

$$h_{tx} : \frac{\partial \Lambda}{\partial h_x} + K_n h^n \frac{\partial^2 \Lambda}{\partial x \partial h_t} = 0. \tag{4.3.38}$$

But from (4.3.37), it follows that (4.3.38) reduces to

$$\frac{\partial \Lambda}{\partial h_x} = 0, \tag{4.3.39}$$

which implies that

$$\Lambda = \Lambda(t, x, h). \tag{4.3.40}$$

From (4.3.40) it is clear that the multiplier Λ is independent of first order partial derivatives of h and therefore yields the same conserved vectors, (4.3.22) and (4.3.27). It follows that multipliers of the form (4.3.28) do not lead to new conserved vectors.

4.4 Partial Lagrangian method

We consider the partial Lagrangian

$$L = \frac{K_n}{2} h^n h_x^2 \tag{4.4.1}$$

of the partial differential equation (4.1.2). The partial differential equation (4.1.2) can be re-expressed as

$$h_{xx} = \frac{1}{K_n h^n} h_t - \frac{n}{h} h_x^2. \tag{4.4.2}$$

Now, applying the Euler operator E_h given by equation (3.3.5) to the partial Lagrangian (4.4.1) and evaluating the result on the partial differential equation (4.4.2) gives

$$E_h\left(\frac{K_n}{2} h^n h_x^2\right)\Big|_{(4.4.2)} = \frac{K_n}{2} n h^{n-1} h_x^2 - h_t. \tag{4.4.3}$$

The determining equation for the partial Noether operator

$$X = \xi^1(t, x, h)\frac{\partial}{\partial t} + \xi^2(t, x, h)\frac{\partial}{\partial x} + \eta(t, x, h)\frac{\partial}{\partial h} \tag{4.4.4}$$

and the gauge functions B^1 and B^2 is

$$X^{[1]}L + L(D_1\xi^1 + D_2\xi^2) = D_1B^1 + D_2B^2 + (\eta - \xi^1 h_t - \xi^2 h_x)\Big(E_h L\Big|_{(4.4.2)}\Big), \qquad (4.4.5)$$

where D_1 and D_2 are the total derivatives, (3.2.7) and (3.2.8), with respect to t and x respectively. We consider gauge functions of the form

$$B^1 = B^1(t, x, h), \quad B^2 = B^2(t, x, h). \qquad (4.4.6)$$

The operator $X^{[1]}$ is the first prolongation

$$X^{[1]} = X + \zeta_2 \frac{\partial}{\partial h_x}, \qquad (4.4.7)$$

of the partial Noether operator where ζ_2 is defined by equation (3.2.5).

Now, substituting (4.4.1), (4.4.3), (4.4.6) and (4.4.7) into (4.4.5) gives

$$\begin{aligned}
&\left(K_n h^n \frac{\partial \eta}{\partial x} - \frac{\partial B^2}{\partial h}\right) h_x + \left(\frac{K_n}{2} h^n \frac{\partial \xi^1}{\partial t} - \frac{K_n}{2} h^n \frac{\partial \xi^2}{\partial x} + K_n h^n \frac{\partial \eta}{\partial h}\right) h_x^2 \\
&- \left(K_n h^n \frac{\partial \xi^1}{\partial x} + \xi^2\right) h_x h_t + \left(\frac{K_n}{2} n h^{n-1} \xi^1 - \frac{K_n}{2} h^n \frac{\partial \xi^1}{\partial h}\right) h_x^2 h_t \\
&+ \left(\frac{K_n}{2} n h^{n-1} \xi^2 - \frac{K_n}{2} h^n \frac{\partial \xi^2}{\partial h}\right) h_x^3 + \left(\eta - \frac{\partial B^1}{\partial h}\right) h_t - \xi^1 h_t^2 \\
&- \left(\frac{\partial B^1}{\partial t} + \frac{\partial B^2}{\partial x}\right) = 0. \qquad (4.4.8)
\end{aligned}$$

Since the unknown functions ξ^1, ξ^2, η, B^1 and B^2 are independent of the partial derivatives of h, we separate (4.4.8) by powers and products of the partial derivatives of h. Firstly, we separate (4.4.8) by h_t^2 to obtain

$$h_t^2 : \xi^1 = 0, \qquad (4.4.9)$$

then separating (4.4.8) by $h_x h_t$ gives

$$h_x h_t : K_n h^n \frac{\partial \xi^1}{\partial x} + \xi^2 = 0, \qquad (4.4.10)$$

which reduces to

$$\xi^2 = 0. \qquad (4.4.11)$$

Separating (4.4.8) by h_x^3 and $h_x^2 h_t$ gives no new information while further separating (4.4.8) by h_x^2 gives

$$h_x^2 : K_n h^n \frac{\partial \eta}{\partial h} + \frac{K_n}{2} h^n \frac{\partial \xi^1}{\partial t} - \frac{K_n}{2} h^n \frac{\partial \xi^2}{\partial x} = 0, \tag{4.4.12}$$

which, by equations (4.4.9) and (4.4.11), reduces to

$$\frac{\partial \eta}{\partial h} = 0, \tag{4.4.13}$$

which implies that

$$\eta = \eta(t, x). \tag{4.4.14}$$

Separating (4.4.8) by h_t gives

$$h_t : \eta - \frac{\partial B^1}{\partial h} = 0, \tag{4.4.15}$$

and since $\eta = \eta(t, x)$, (4.4.15) can be integrated with respect to h to give

$$B^1(t, x, h) = h\eta(t, x) + M(t, x). \tag{4.4.16}$$

Separating (4.4.8) by h_x gives

$$h_x : K_n h^n \frac{\partial \eta}{\partial x} - \frac{\partial B^2}{\partial h} = 0, \tag{4.4.17}$$

which when integrated with respect to h gives

$$B^2(t, x, h) = \frac{K_n}{(n+1)} h^{n+1} \frac{\partial \eta}{\partial x} + N(t, x). \tag{4.4.18}$$

After separating equation (4.4.8) with respect to the partial derivatives of h, the remaining terms are

$$Remainder : \frac{\partial B^1}{\partial t} + \frac{\partial B^2}{\partial x} = 0. \tag{4.4.19}$$

Now, substituting equation (4.4.16) for $B^1(t, x, h)$ and equation (4.4.18) for $B^2(t, x, h)$ into equation (4.4.19) gives

$$h\frac{\partial \eta}{\partial t} + \frac{\partial M}{\partial t} + \frac{K_n}{(n+1)} h^{n+1} \frac{\partial^2 \eta}{\partial x^2} + \frac{\partial N}{\partial x} = 0, \tag{4.4.20}$$

where we always consider $n > 0$. Separating (4.4.20) in powers of h gives the following results:

$$h : \frac{\partial \eta}{\partial t} = 0, \tag{4.4.21}$$

which implies that

$$\eta = \eta(x); \tag{4.4.22}$$

$$h^{n+1} : \frac{d^2\eta}{dx^2} = 0, \tag{4.4.23}$$

which when integrated with respect to x twice gives

$$\eta = ax + b, \tag{4.4.24}$$

where a and b are constants. The remaining terms independent of h are

$$\frac{\partial M}{\partial t} + \frac{\partial N}{\partial x} = 0. \tag{4.4.25}$$

From equation (4.4.24), it follows that the gauge functions (4.4.16) and (4.4.18) reduce to

$$B^1(t, x, h) = (ax + b)h + M(t, x), \tag{4.4.26}$$

$$B^2(t, x, h) = \frac{aK_n}{(n+1)}h^{n+1} + N(t, x). \tag{4.4.27}$$

Now, from (3.3.13) and (3.3.14) the components of the conserved vector corresponding to the partial Noether symmetry of the partial differential equation and gauge functions are

$$T^1 = B^1 - \xi^1 L - (\eta - \xi^1 h_t - \xi^2 h_x)\frac{\partial L}{\partial h_t}, \tag{4.4.28}$$

$$T^2 = B^2 - \xi^2 L - (\eta - \xi^1 h_t - \xi^2 h_x)\frac{\partial L}{\partial h_x}. \tag{4.4.29}$$

Substituting the gauge functions, (4.4.26) and (4.4.27), the symmetry: (4.4.9); (4.4.11) and (4.4.24), and the partial Lagrangian, (4.4.1), into equations (4.4.28) and (4.4.29) gives the conserved vector

$$T^1 = (ax + b)h + M(t, x), \tag{4.4.30}$$

$$T^2 = \frac{aK_n}{(n+1)}h^{n+1} - K_n(ax + b)h^n h_x + N(t, x). \tag{4.4.31}$$

But $T = [M(t, x),\ \ N(t, x)]$ is a trivial conserved vector because equation (3.3.1) is identically satisfied by (4.4.25) without imposing the PDE (4.1.2). We therefore set $M = 0$ and $N = 0$. The remaining terms in (4.4.30) and (4.4.31) consist of a linear combination

of two conserved vectors. Expressing equations (4.4.30) and (4.4.31) in canonical form, by setting $a = 0$, $b = 1$ and $a = 1$, $b = 0$, gives respectively the elementary conserved vector

$$\mathbf{T_{(1)}} = (h, -K_n h^n h_x), \tag{4.4.32}$$

and the second conserved vector

$$\mathbf{T_{(2)}} = \left(xh, -K_n \left[xh^n h_x - \frac{h^{n+1}}{(n+1)} \right] \right). \tag{4.4.33}$$

The conserved vectors (4.4.32) and (4.4.33) are the same as those derived by the direct method, (4.2.24) and (4.2.25), and by the multiplier method, (4.3.22) and (4.3.27).

4.5 Generation of new conserved vectors from known conserved vectors

In this Section we investigate if the partial differential equation (4.1.1) has other conserved vectors besides the elementary conserved vector, (4.4.32), and the second conserved vector, (4.4.33), derived in Sections 4.2, 4.3 and 4.4. We consider the method of generating conserved vectors from known conserved vectors that was introduced by Kara and Mahomed [42]. We will use the elementary conserved vector, (4.4.32), and the second conserved vector, (4.4.33), to generate other conserved vectors. The generated conserved vectors may either be new conserved vectors of the partial differential equation (4.1.1) or they may only be linear combinations of the known conserved vectors or they may be zero.

If

$$X = \xi^1(t, x, h)\frac{\partial}{\partial t} + \xi^2(t, x, h)\frac{\partial}{\partial x} + \eta(t, x, h)\frac{\partial}{\partial h}, \tag{4.5.1}$$

is a Lie point symmetry generator of a PDE in two independent variables and (T^1, T^2) is a conserved vector for the same PDE, then Kara and Mahomed have shown that

$$T^i_* = X(T^i) + T^i D_k(\xi^k) - T^k D_k(\xi^i), \quad i = 1, 2 \tag{4.5.2}$$

are the components of a conserved vector for the PDE. The expanded form of (4.5.2) can be written as

$$T^1_* = X(T^1) + T^1 D_2(\xi^2) - T^2 D_2(\xi^1), \tag{4.5.3}$$

$$T^2_* = X(T^2) + T^2 D_1(\xi^1) - T^1 D_1(\xi^2), \tag{4.5.4}$$

where D_1 and D_2 are total derivatives given by (3.2.7) and (3.2.8). In (4.5.2), X is prolongated to as many derivatives as required, depending on which partial derivatives are contained in the components of the conserved vector.

For the partial differential equation (4.1.1), the Lie point symmetry generator X, which is derived in Appendix A, is

$$\mathbf{X} = (c_1 + c_2 t)\frac{\partial}{\partial t} + (c_3 + c_4 x)\frac{\partial}{\partial x} + \frac{1}{n}(2c_4 - c_2)h\frac{\partial}{\partial h}. \tag{4.5.5}$$

The first prolongation $X^{[1]}$ of the operator (4.5.5) is, using the formula (3.3.12),

$$X^{[1]} = (c_1 + c_2 t)\frac{\partial}{\partial t} + (c_3 + c_4 x)\frac{\partial}{\partial x} + \frac{1}{n}(2c_4 - c_2)h\frac{\partial}{\partial h} + \frac{1}{n}\Big((2-n)c_4 - c_2\Big)h_x\frac{\partial}{\partial h_x}. \tag{4.5.6}$$

Consider first the elementary conserved vector (4.4.32). Using (4.5.3) to (4.5.6), it can be verified that

$$T^1_* = \frac{1}{n}[(n+2)c_4 - c_2]T^1_{(1)}, \quad T^2_* = \frac{1}{n}[(n+2)c_4 - c_2]T^2_{(1)} \tag{4.5.7}$$

and therefore

$$\mathbf{T}^*_{(\mathbf{1})} = \frac{1}{n}\left[(n+2)c_4 - c_2\right]\mathbf{T}_{(\mathbf{1})}. \tag{4.5.8}$$

Similarly, for the second conserved vector (4.4.33),

$$\begin{aligned} T^1_* &= c_3 T^1_{(1)} + \frac{1}{n}[2(n+1)c_4 - c_2]T^1_{(2)}, \\ T^2_* &= c_3 T^2_{(1)} + \frac{1}{n}[2(n+1)c_4 - c_2]T^2_{(2)} \end{aligned} \tag{4.5.9}$$

and hence

$$\mathbf{T}^*_{(\mathbf{2})} = c_3\mathbf{T}_{(\mathbf{1})} + \frac{1}{n}[2(n+1)c_4 - c_2]\mathbf{T}_{(\mathbf{2})}. \tag{4.5.10}$$

The conserved vector $\mathbf{T}^*_{(\mathbf{1})}$ is a constant multiple of the elementary conserved vector $\mathbf{T}_{(\mathbf{1})}$, (4.4.32). The conserved vector $\mathbf{T}^*_{(\mathbf{2})}$ is a linear combination of the elementary conserved vector $\mathbf{T}_{(\mathbf{1})}$, (4.4.32), and the second conserved vector $\mathbf{T}_{(\mathbf{2})}$, (4.4.33). The conserved vectors $\mathbf{T}^*_{(\mathbf{1})}$ and $\mathbf{T}^*_{(\mathbf{2})}$ are therefore not new conserved vectors.

4.6 Conclusions

In this Chapter, we investigated conserved vectors for the partial differential equation (4.1.1). We used three methods: the direct, the multiplier and the partial Lagrangian methods to investigate conservation laws for the partial differential equation (4.1.1) in case one method would not give all conserved vectors for the PDE (4.1.1). The three methods considered gave the same result of two independent conserved vectors, the elementary and the second conserved vectors. Each method can be extended to take a step further in investigating if more conserved vectors for the PDE exist. The direct method can be extended by considering components, T^1 and T^2, which depend on more partial derivatives of h. The multiplier method can be extended by considering multipliers which depend on more variables. We saw that by including first order partial derivatives of h no new conserved vectors were obtained. The partial Lagrangian method can be extended by considering gauge functions which depend on more variables. In all cases the inclusion of more variables in the form of partial derivatives of h will lead to larger calculations. The assistance of computer programs, such as MAPLE, to perform the calculations will eventually be required.

The direct method is the easiest to use and understand because it does not require additional theory. The multiplier method requires one final step to calculate the conserved vector after the multiplier has been derived. Although the mathematical manipulations are elementary in this final step, it requires experience to know how to perform them. The partial Lagrangian method is a powerful method which applies to PDEs which do not have a Lagrangian. It gives an explicit formula for the conserved vector at the end of the calculation. However, unlike the direct method, it depends on background theory which needs to be studied in order to understand the method fully.

In investigating if the PDE (4.1.1) has other conserved vectors besides the ones identified by the direct, multiplier and partial Lagrangian methods, we generated other conserved vectors from the known conserved vectors. However this method did not yield any new conserved vectors either. The generated conserved vectors were only a linear combination of the known elementary and second conserved vectors. We will further investigate the elementary and second conserved vectors in Chapter 5.

Chapter 5

LINEAR HYDRAULIC FRACTURE WITH TORTUOSITY

5.1 Introduction

In this Chapter, we analyse the following partial differential equation describing a tortuous fracture either with contact areas modelled by the linear crack law or without contact areas:

$$\frac{\partial h}{\partial t} = K_n \frac{\partial}{\partial x}\Big(h^n \frac{\partial h}{\partial x}\Big), \tag{5.1.1}$$

where the diffusion constant K_n is

$$K_n = \frac{a_n h_{max}^{n-3}}{3}\left(\frac{1-\frac{\sigma_R}{\Lambda h_{max}}}{1-\frac{\sigma_{zz}^{(\infty)}}{\Lambda h_{max}}}\right). \tag{5.1.2}$$

In (5.1.2) for a partially open fracture, with contact regions modelled by the linear crack law, $\sigma_R < 0$ while for an open fracture $\sigma_R = 0$.

The effects of tortuosity due to surface roughness on the fluid-rock interface and, in a partially open fracture, due to contact regions on the length, volume and half-width of the fracture will be investigated. The Lie point symmetries of (5.1.1), the calculations of which are outlined in Appendix A, are necessary for deriving the group invariant solution

for the problem. Section 5.2 outlines the derivation of the group invariant solution which transforms the governing nonlinear diffusion equation (5.1.1) to an ordinary differential equation. Important fracture properties such as the fracture length and volume are obtained in the process of expressing the boundary conditions for the nonlinear diffusion equation (5.1.1) in terms of the group invariant solution. This method of solution that was introduced by Fitt et al [11], has been extended to obtain solutions for a hydraulic fracture in a permeable rock mass and solutions for a non-Newtonian fluid driven fracture by Fareo and Mason [14, 38] and also to obtain solutions for a turbulent fluid fracture by Anthonyrajah et al [37]. In Section 5.3, we rescale the boundary value problem including important fracture properties. Section 5.4 focusses on the association of Lie point symmetries of (5.1.1) with the conserved vectors for (5.1.1) obtained in Chapter 4. Section 5.5 discusses the operating conditions considered at the fracture entry. In Section 5.6, the asymptotic solution at the fracture tip for the governing ordinary differential equation is obtained. Section 5.7 outlines the derivation of the exact analytical solutions for a fracture with constant volume and a fracture propagating at constant speed. A third exact analytical solution, generated by the Lie point symmetry associated with the second conserved vector, is derived. This analytical solution is discussed and the flux of fluid along the fracture is investigated to give more insight into the nature of the analytical solution. Section 5.8 discusses numerical methods used to solve the problem while Section 5.9 investigates the change of the width averaged fluid velocity along the fracture. For fluid injection, the approximate analytical solution is investigated in Section 5.10. Further analysis of the third exact analytical solution and some of the numerical solutions is made in Section 5.11. Section 5.12 summarises the main results obtained in this Chapter. All the work regarding fluid injection discussed in this Chapter is based on the paper [31].

5.2 Group invariant solution

In order to obtain the group invariant solution for the partial differential equation (5.1.1), it is necessary to consider the Lie point symmetry of (5.1.1), the calculation of which is

rigorously outlined in Appendix A,

$$X = (c_1 + c_2 t)\frac{\partial}{\partial t} + (c_3 + c_4 x)\frac{\partial}{\partial x} + \frac{1}{n}(2c_4 - c_2)h\frac{\partial}{\partial h}. \tag{5.2.1}$$

where c_1, c_2, c_3 and c_4 are constants. Equation (5.1.1) therefore has four Lie point symmetries.

The group invariant solution $h = \Psi(t, x)$ of (5.1.1) satisfies

$$X(h - \Psi)\Big|_{h=\Psi} = 0, \tag{5.2.2}$$

where X is given by (5.2.1). Equation (5.2.2) gives the first order linear partial differential equation,

$$(c_1 + c_2 t)\frac{\partial \Psi}{\partial t} + (c_3 + c_4 x)\frac{\partial \Psi}{\partial x} = \frac{1}{n}(2c_4 - c_2)\Psi. \tag{5.2.3}$$

We assume that $c_2 \neq 0$. If $c_2 = 0$ then the fracture would not evolve with time. We first consider the general case in which $c_4/c_2 \neq 1/2$. Then the differential equations of the characteristic curves of (5.2.3) are

$$\frac{dt}{(c_1 + c_2 t)} = \frac{dx}{(c_3 + c_4 x)} = \frac{d\Psi}{\left[\frac{1}{n}(2c_4 - c_2)\Psi\right]}. \tag{5.2.4}$$

The first pair of terms in (5.2.4) give

$$\frac{c_3 + c_4 x}{(c_1 + c_2 t)^{\frac{c_4}{c_2}}} = a_1, \tag{5.2.5}$$

where a_1 is a constant. The first and last terms in (5.2.4) give

$$\frac{\Psi}{(c_1 + c_2 t)^{\frac{2}{n}\left(\frac{c_4}{c_2} - \frac{1}{2}\right)}} = a_2, \tag{5.2.6}$$

where a_2 is a constant. The general solution of the first order PDE (5.2.3) is

$$a_2 = F(a_1), \tag{5.2.7}$$

where F is an arbitrary function. Since $\Psi = h(t, x)$, the group invariant solution of the half-width of the fracture is

$$h(t, x) = (c_1 + c_2 t)^{\frac{2}{n}\left(\alpha - \frac{1}{2}\right)} F(\xi), \tag{5.2.8}$$

where the similarity variable, given by equation (5.2.5), is

$$\xi = \frac{c_3 + c_4 x}{(c_1 + c_2 t)^{\alpha}}, \tag{5.2.9}$$

and

$$\alpha = \frac{c_4}{c_2}. \tag{5.2.10}$$

For the special case $c_4/c_2 = 1/2$, the differential equations of the characteristic curves of (5.2.3) reduce to

$$\frac{dt}{(c_1 + c_2 t)} = \frac{dx}{\left(c_3 + \frac{1}{2}c_2 x\right)} = \frac{d\Psi}{0}. \tag{5.2.11}$$

Two first integrals are

$$\frac{c_3 + \frac{1}{2}c_2 x}{(c_1 + c_2 t)^{\frac{1}{2}}} = a_1, \quad \Psi = a_2, \tag{5.2.12}$$

where a_1 and a_2 are constants. Since $\Psi = h(t, x)$, the general solution is

$$h(t, x) = F(\xi), \quad \xi = \frac{c_3 + \frac{1}{2}c_2 x}{(c_1 + c_2 t)^{\frac{1}{2}}}, \tag{5.2.13}$$

which is the same as (5.2.8) with $\alpha = 1/2$.

It is now necessary to express the nonlinear diffusion equation (5.1.1), the corresponding boundary conditions, the volume of the fracture, the width averaged fluid velocity and the fluid flux per unit breadth in terms of the group invariant solution (5.2.8).

In order to express the partial differential equation (5.1.1) in terms of the group invariant solution (5.2.8), we need the derivatives of the similarity variable (5.2.9):

$$\frac{\partial \xi}{\partial t} = -\frac{c_4 \xi}{c_1 + c_2 t}, \quad \frac{\partial \xi}{\partial x} = \frac{c_4}{(c_1 + c_2 t)^{\alpha}}. \tag{5.2.14}$$

Subsituting (5.2.8), with the aid of (5.2.14), into (5.1.1) transforms the partial differential equatiation (5.1.1) to the ordinary differential equation:

$$c_4 K_n \frac{d}{d\xi}\left(F^n \frac{dF}{d\xi}\right) + \frac{d}{d\xi}(\xi F) + \frac{1}{n}\left(\frac{1}{\alpha} - (n+2)\right)F = 0. \tag{5.2.15}$$

Since the constant c_3 does not feature anywhere in the ordinary differential equation (5.2.15) we choose $c_3 = 0$ so that $\xi = 0$ when $x = 0$.

The boundary condition at the fracture tip, $x = L(t)$, is

$$h(t, L(t)) = 0. \tag{5.2.16}$$

Imposing the boundary condition (5.2.16) on the half-width $h(t,x)$, given by (5.2.8), gives

$$(c_1+c_2t)^{\frac{2}{n}(\alpha-\frac{1}{2})}F\left(\frac{c_4L(t)}{(c_1+c_2t)^{\alpha}}\right)=0, \tag{5.2.17}$$

which implies that, [37],

$$F(A(t))=0, \tag{5.2.18}$$

where

$$A(t)=\frac{c_4L(t)}{(c_1+c_2t)^{\alpha}}. \tag{5.2.19}$$

Differentiating (5.2.18) with respect to t gives

$$\frac{dF}{dA}\frac{dA}{dt}=0. \tag{5.2.20}$$

Since

$$\frac{dF}{dA}\neq 0, \tag{5.2.21}$$

because F is not a constant function, it follows that

$$\frac{dA}{dt}=0. \tag{5.2.22}$$

This implies that

$$A(t)=\frac{c_4L(t)}{(c_1+c_2t)^{\alpha}}=k, \tag{5.2.23}$$

where k is a constant and therefore

$$L(t)=\frac{kc_1^{\alpha}}{c_4}\left(1+\frac{c_2}{c_1}t\right)^{\alpha}. \tag{5.2.24}$$

Now, the characteristic length of the fracture, L, was chosen to be the initial length of the fracture, $L(0)$, as discussed in Chapter 2. Therefore the dimensionless fracture length is

$$L^*(t)=\frac{L(t)}{L}=\frac{L(t)}{L(0)},\quad L^*(0)=1. \tag{5.2.25}$$

Imposing (5.2.25) to the dimensionless fracture length (5.2.24) gives

$$\frac{kc_1^{\alpha}}{c_4}=1 \tag{5.2.26}$$

and therefore the dimensionless length of the fracture is

$$L(t) = \left(1 + \frac{c_2}{c_1}t\right)^{\alpha}, \tag{5.2.27}$$

where the star denoting dimensionless variables is suppressed in (5.2.27). The boundary condition at the fracture tip, (5.2.18), becomes

$$F\left(\frac{c_4}{c_1^{\alpha}}\right) = 0. \tag{5.2.28}$$

The second boundary condition, (2.4.75), derived in Chapter 2 by balancing the fluid flux into the fracture at the fracture entry with the rate of change of the volume of the fracture, given that the rock is impermeable, is

$$-2K_n h^n(t,0)\frac{\partial h}{\partial x}(t,0) = \frac{dV}{dt}, \tag{5.2.29}$$

where the volume of the fracture V, (2.4.76), is

$$V(t) = 2\int_0^{L(t)} h(t,x)dx. \tag{5.2.30}$$

Substituting the group invariant solution of the half-width of the fracture (5.2.8) into (5.2.30) gives

$$V(t) = V_o\Big(1 + \frac{c_2}{c_1}t\Big)^{\frac{n+2}{n}\left(\alpha - \frac{1}{n+2}\right)}, \tag{5.2.31}$$

where

$$V_o = \frac{2}{c_4}c_1^{\frac{n+2}{n}\left(\alpha - \frac{1}{n+2}\right)}\int_0^{\frac{c_4}{c_1^{\alpha}}} F(\xi)d\xi. \tag{5.2.32}$$

Differentiating (5.2.31) gives

$$\frac{dV}{dt} = V_o\Big(\frac{c_2}{c_1}\Big)\frac{(n+2)}{n}\left(\alpha - \frac{1}{n+2}\right)\left(1 + \frac{c_2}{c_1}t\right)^{\frac{n+2}{n}\left(\alpha - \frac{n+1}{n+2}\right)}, \tag{5.2.33}$$

which when substituted, both with $h(t,x)$ given by (5.2.8), into (5.2.29) gives the second boundary condition at the fracture entry in terms of the group invariant solution:

$$c_4 K_n F^n(0)\frac{dF}{d\xi}(0) = \frac{1}{n}\left(\frac{1}{\alpha} - (n+2)\right)\int_0^{\frac{c_4}{c_1^{\alpha}}} F(\xi)d\xi. \tag{5.2.34}$$

The zero flux condition at the fracture tip, (2.4.81), expressed in terms of the group invariant solution is

$$F^n\Big(\frac{c_4}{c_1^\alpha}\Big)\frac{dF}{d\xi}\Big(\frac{c_4}{c_1^\alpha}\Big) = 0. \tag{5.2.35}$$

As discussed in the modelling process in Chapter 2, the zero flux condition at the fracture tip (5.2.35) provides a check on the model for $n > 1$.

The volume flux of fluid per unit breadth, (2.4.78), and the width averaged fluid velocity, (2.4.79), given in Chapter 2 are

$$Q(t,x) = -2K_n h^n \frac{\partial h}{\partial x}, \tag{5.2.36}$$

$$\overline{v}_x(t,x) = -K_n h^{n-1}\frac{\partial h}{\partial x}. \tag{5.2.37}$$

Substituting (5.2.8), with the aid of (5.2.14), into equations (5.2.36) and (5.2.37) gives

$$Q(t,x) = -2K_n c_4 (c_1 + c_2 t)^{\frac{n+2}{n}\left(\alpha - \frac{n+1}{n+2}\right)} F^n \frac{dF}{d\xi}, \tag{5.2.38}$$

$$\overline{v}_x(t,x) = -K_n c_4 (c_1 + c_2 t)^{\alpha-1} F^{n-1}\frac{dF}{d\xi}. \tag{5.2.39}$$

5.3 Scaling of the governing equations

In this Section, we simplify the equations for the boundary value problem (5.2.15), (5.2.28) and (5.2.34), the constant V_o, (5.2.32), the fluid flux, (5.2.38), and the width averaged fluid velocity, (5.2.39), by making the transformation variables,

$$u = \frac{x}{L(t)}, \quad \xi = \frac{c_4}{c_1^\alpha}u, \quad F(\xi) = Bf(u), \qquad 0 \le u \le 1, \tag{5.3.1}$$

where B is a constant to be chosen. It is clear that the equations for the length, (5.2.27), and the volume, (5.2.31), of the fracture are not affected by the transformation variables, (5.3.1), because ξ and $F(\xi)$ are not contained in them. However the constant, V_o, (5.2.32), contained in the volume of the fracture will be changed by the transformation variables. Firstly, rescaling the ordinary differential equation (5.2.15) with the transformation vari-

ables (5.3.1) gives

$$\frac{K_n B^n c_1^{2\alpha}}{c_4}\frac{d}{du}\left(f^n\frac{df}{du}\right)+\frac{d}{du}(uf)+\frac{1}{n}\left(\frac{1}{\alpha}-(n+2)\right)f=0. \tag{5.3.2}$$

We then choose

$$\frac{K_n B^n c_1^{2\alpha}}{c_4}=1 \tag{5.3.3}$$

and therefore

$$B=\left(\frac{c_4}{K_n c_1^{2\alpha}}\right)^{\frac{1}{n}}. \tag{5.3.4}$$

We consider the ordinary differential equation (5.3.2) and rescale the boundary conditions (5.2.28) and (5.2.34) in order to obtain the boundary value problem:

$$\frac{d}{du}\left(f^n\frac{df}{du}\right)+\frac{d}{du}(uf)+\frac{1}{n}\left(\frac{1}{\alpha}-(n+2)\right)f=0, \tag{5.3.5}$$

$$f(1)=0, \tag{5.3.6}$$

$$f^n(0)\frac{df}{du}(0)=\frac{1}{n}\left(\frac{1}{\alpha}-(n+2)\right)\int_0^1 f(u)du. \tag{5.3.7}$$

It can be verified that rescaling the remaining equations and summarising equations that are unaffected by the transformation variables (5.3.1) give the following equations of the half-width, length and volume of the fracture:

$$h(t,u)=\left(\frac{c_4}{K_n c_1}\right)^{\frac{1}{n}}\left(1+\frac{c_2}{c_1}t\right)^{\frac{2}{n}\left(\alpha-\frac{1}{2}\right)}f(u), \tag{5.3.8}$$

$$L(t)=\left(1+\frac{c_2}{c_1}t\right)^{\alpha}, \tag{5.3.9}$$

$$V(t)=V_0\left(1+\frac{c_2}{c_1}t\right)^{\frac{n+2}{n}\left(\alpha-\frac{1}{n+2}\right)}, \tag{5.3.10}$$

with

$$V_0=2\left(\frac{c_4}{K_n c_1}\right)^{\frac{1}{n}}\int_0^1 f(u)du, \tag{5.3.11}$$

while the volume flux per unit breadth and the width averaged fluid velocity reduce to

$$Q(t,u) = -2K_n\left(\frac{c_4}{K_n c_1}\right)^{\frac{n+1}{n}}\left(1+\frac{c_2}{c_1}t\right)^{\frac{n+2}{n}\left(\alpha-\frac{n+1}{n+2}\right)} f^n(u)\frac{df}{du}, \tag{5.3.12}$$

$$\overline{v}_x(t,u) = -\frac{c_4}{c_1}\left(1+\frac{c_2}{c_1}t\right)^{\alpha-1} f^{n-1}(u)\frac{df}{du}. \tag{5.3.13}$$

The solution must satisfy the zero flux condition (5.2.35) which when simplified using (5.3.1) and (5.3.4) gives

$$f^n(1)\frac{df}{du}(1) = 0. \tag{5.3.14}$$

It is important to emphasize that the system of equations (5.3.5) to (5.3.14) describes an open fracture without contact regions and a partially open fracture with contact regions modelled by the linear crack law. The distinction between the two types of fracture is that for an open fracture the diffusion constant K_n is defined by (5.1.2) with $\sigma_R = 0$ while for a partially open fracture with contact regions modelled by the linear crack law the diffusion constant K_n is defined by (5.1.2) with $\sigma_R < 0$. The parameter α is chosen according to the operating condition at the fracture entry and will be discussed later in this Chapter. The diffusion constant K_n is obtained through experiments. It now remains to obtain the ratios c_4/c_1 and c_2/c_1.

From Chapter 2, using the fact that the characteristic half-width of the fracture is chosen to be the maximum half-width, $H = h_{max}$, we have

$$h^*(t^*,u^*) = \frac{h(t,u)}{H} = \frac{h(t,u)}{h_{max}}, \tag{5.3.15}$$

where $h^*(t^*,u^*)$ is the dimensionless half-width of the fracture. Equations (5.3.5) to (5.3.14) are dimensionless although the star notation representing dimensionless variables is suppressed. We define the constant β by

$$\beta = h^*(0,u_{max}). \tag{5.3.16}$$

Because of the form of $h(t,u)$, given by (5.3.8), $f(u)$ does not contribute to the evolution of the half-width of the fracture, h, with time and therefore u_{max}, unlike x_{max}, is independent of time. From the discussion of the crack laws, in Section 2.4.2 of Chapter 2, it was

established that a partially open fracture results when $h_{min} \leq h(t,x) < h_{max}$ and an open fracture results when $h(t,x) \geq h_{max}$, where we approximated $h_{min} = 0$ since $h_{min} << h_{max}$. From that analysis and equations (5.3.15) and (5.3.16) it follows that for a partially open fracture $0 \leq \beta < 1$ while for an open fracture $\beta \geq 1$. Imposing condition (5.3.16) on the dimensionless half-width of the fracture, (5.3.8), gives

$$\frac{c_4}{c_1} = K_n \left(\frac{\beta}{f_{max}} \right)^n, \tag{5.3.17}$$

where

$$f_{max} = f(u_{max}). \tag{5.3.18}$$

It follows that

$$\frac{c_2}{c_1} = \frac{c_2}{c_4}\frac{c_4}{c_1} = \frac{1}{\alpha}\frac{c_4}{c_1} = \frac{K_n}{\alpha}\left(\frac{\beta}{f_{max}} \right)^n. \tag{5.3.19}$$

Substituting the ratios c_4/c_1 and c_2/c_1 into (5.3.8) to (5.3.13) gives:

$$h(t,u) = \beta \left[1 + \frac{1}{\alpha}\left(\frac{\beta}{f_{max}} \right)^n K_n t \right]^{\frac{2}{n}\left(\alpha - \frac{1}{2}\right)} \frac{f(u)}{f_{max}}, \tag{5.3.20}$$

$$L(t) = \left[1 + \frac{1}{\alpha}\left(\frac{\beta}{f_{max}} \right)^n K_n t \right]^{\alpha}, \tag{5.3.21}$$

$$V(t) = V_o \left[1 + \frac{1}{\alpha}\left(\frac{\beta}{f_{max}} \right)^n K_n t \right]^{\frac{n+2}{n}\left(\alpha - \frac{1}{n+2}\right)}, \tag{5.3.22}$$

where

$$V_o = 2\beta \int_0^1 \frac{f(u)}{f_{max}} du, \tag{5.3.23}$$

$$Q(t,u) = -2K_n \left(\frac{\beta}{f_{max}} \right)^{n+1} \left[1 + \frac{1}{\alpha}\left(\frac{\beta}{f_{max}} \right)^n K_n t \right]^{\frac{n+2}{n}\left(\alpha - \frac{n+1}{n+2}\right)} f^n(u)\frac{df}{du}, \tag{5.3.24}$$

$$\overline{v}_x(t,u) = -K_n \left(\frac{\beta}{f_{max}} \right)^{n} \left[1 + \frac{1}{\alpha}\left(\frac{\beta}{f_{max}} \right)^n K_n t \right]^{\alpha - 1} f^{n-1}(u)\frac{df}{du}. \tag{5.3.25}$$

with

$$\frac{c_4}{c_1} = K_n \left(\frac{\beta}{f_{max}} \right)^n, \quad \frac{c_2}{c_1} = \frac{c_2}{c_4}\frac{c_4}{c_1} = \frac{K_n}{\alpha}\left(\frac{\beta}{f_{max}} \right)^n. \tag{5.3.26}$$

It is clear that the problem is to solve the boundary value problem (5.3.5) to (5.3.7) where the properties of the fracture are given by equations (5.3.20) to (5.3.23) and the equations for the fluid flux and the width averaged fluid velocity in the fracture are given by (5.3.24) and (5.3.25).

There are three parameters in equations (5.3.20) to (5.3.26), α, β and K_n. The value of α is obtained from the working condition at the fracture entry. The value of β depends on the pre-existing model fracture and whether it is open or partially open. The diffusion constant K_n is defined by (5.1.2). It depends on experimental results and on whether the fracture is open or partially open.

Equations (5.3.20) to (5.3.26) apply for both fluid injection and fluid extraction at the fracture entry. From (5.3.22) the total volume of the fracture $V(t)$ will remain constant when $\alpha = 1/(n+2)$. For fluid injection $V(t)$ will increase and $\alpha > 1/(n+2)$ while for fluid extraction $V(t)$ will decrease and $\alpha < 1/(n+2)$. For fluid injection, it is found that $u_{max} = 0$ and therefore $f_{max} = f(0)$ while for fluid extraction $0 < u_{max} < 1$ and therefore $f_{max} = f(u_{max}) \neq f(0)$.

5.4 Association of a Lie point symmetry with a conserved vector

In this Section we will investigate if the Lie point symmetry (5.2.1) of the PDE (5.1.1) is associated with the conserved vectors (4.4.32) and (4.4.33) of the same PDE (5.1.1).

A Lie point symmetry

$$X = \xi^1(t,x,h)\frac{\partial}{\partial t} + \xi^2(t,x,h)\frac{\partial}{\partial x} + \eta(t,x,h)\frac{\partial}{\partial h} \tag{5.4.1}$$

of a PDE is said to be associated with a conserved vector $\mathbf{T}$ *of the same PDE if* $\mathbf{T}^* = \mathbf{0}$*, that is, if* [41, 42]

$$X(T^i) + T^i D_k(\xi^k) - T^k D_k(\xi^i) = 0, \quad i = 1, 2. \tag{5.4.2}$$

This investigation is motivated by Sjöberg's double reduction Theorem [29]. According to this Theorem, the association of a Lie point symmetry of a PDE with a conserved vector of the same PDE leads to a reduction of the PDE to an ODE which can be integrated at

least once and this may lead to an invariant solution of the PDE if further integration of the ODE is possible. In this Section, we therefore investigate if the Lie point symmetry of the PDE (5.1.1) is associated with the conserved vector of the PDE (5.1.1) for some ratio of the constants c_1, c_2, c_3 and c_4. If the association exists, by Sjöberg's double reduction Theorem, it may be possible to derive an invariant analytical solution of the PDE (5.1.1).

From Chapter 4, the conserved vector $\mathbf{T}^*_{(\mathbf{1})}$ generated from the elementary conserved vector (4.4.32) and the Lie point symmetry (5.2.1) is given by

$$\mathbf{T}^*_{(\mathbf{1})} = \frac{1}{n}\Big[(n+2)c_4 - c_2\Big]\mathbf{T}_{(\mathbf{1})}. \tag{5.4.3}$$

The Lie point symmetry (5.2.1) is associated with the elementary conserved vector (4.4.32) provided

$$\mathbf{T}^*_{(\mathbf{1})} = \frac{1}{n}\Big[(n+2)c_4 - c_2\Big]\mathbf{T}_{(\mathbf{1})} = 0, \tag{5.4.4}$$

that is provided

$$\alpha = \frac{1}{n+2}, \tag{5.4.5}$$

where $\alpha = c_4/c_2$. The result (5.4.5) is satisfied for all values of the constant c_3. For simplicity as done in Section 5.2 of this Chapter, we set $c_3 = 0$. By dividing (5.2.1) by $c_4 = c_2/(n+2)$, the associated Lie point symmetry can be written as

$$X = (n+2)\Big(\frac{c_1}{c_2} + t\Big)\frac{\partial}{\partial t} + x\frac{\partial}{\partial x} - h\frac{\partial}{\partial h}. \tag{5.4.6}$$

Substituting (5.4.5) into (5.3.22) gives

$$V(t) = V_o, \tag{5.4.7}$$

where V_o is a constant given by (5.3.23). From (5.4.7), it is clear that the condition (5.4.5) deduced from the association of the elementary conserved vector (4.4.32) with the Lie point symmetry generator (5.2.1) represents a fracture evolving with constant volume and therefore a fracture without fluid injection or extraction at the fracture entry.

Now, the conserved vector $\mathbf{T}^*_{(\mathbf{2})}$ generated from the second conserved vector (4.4.33) and the Lie point symmetry generator (5.2.1) is given by

$$\mathbf{T}^*_{(\mathbf{2})} = c_3\mathbf{T}_{(\mathbf{1})} + \frac{1}{n}\Big[2(n+1)c_4 - c_2\Big]\mathbf{T}_{(\mathbf{2})}. \tag{5.4.8}$$

The Lie point symmetry (5.2.1) is associated with the second conserved vector (4.4.33) provided

$$\mathbf{T}^{*}_{(\mathbf{2})} = c_3\mathbf{T}_{(\mathbf{1})} + \frac{1}{n}\Big[2(n+1)c_4 - c_2\Big]\mathbf{T}_{(\mathbf{2})} = 0, \tag{5.4.9}$$

that is provided

$$\alpha = \frac{1}{2(n+1)} \quad \text{and} \quad c_3 = 0, \tag{5.4.10}$$

where $\alpha = c_4/c_2$. Unlike with the elementary conserved vector, it is necessary that $c_3 = 0$ in order for the Lie point symmetry (5.2.1) to be associated with the second conserved vector (4.4.33). Dividing (5.2.1) by $c_4 = c_2/[2(n+1)]$ the associated Lie point symmetry can be expressed as

$$X = 2(n+1)\Big(\frac{c_1}{c_2} + t\Big)\frac{\partial}{\partial t} + x\frac{\partial}{\partial x} - 2h\frac{\partial}{\partial h}. \tag{5.4.11}$$

The rate of change of the volume of the fracture with time, obtained by differentiating (5.3.22) with respect to t when $\alpha = 1/[2(n+1)]$ is

$$\frac{dV}{dt} = -V_o K_n \left(\frac{\beta}{f_{max}}\right)^n \left[1 + 2(n+1)\left(\frac{\beta}{f_{max}}\right)^n K_n t\right]^{-\frac{(2n+3)}{2(n+1)}} < 0. \tag{5.4.12}$$

Thus, since there is no fluid leak-off at the fluid-rock interface, the working condition $\alpha = 1/[2(n+1)]$ describes fluid extraction from the fracture at the fracture entry. This phenomena will be investigated further in the subsequent Sections.

In the Lie point symmetries (5.4.6) and (5.4.11), c_1/c_2 is given by the reciprocal of c_2/c_1 in (5.3.26).

If the Lie point symmetry (5.2.1) had not been derived, it would still be possible to obtain the associated Lie point symmetry by solving two determining equations which are the two components of (5.4.2) for ξ^1, ξ^2 and η.

5.5 Operating conditions at the fracture entry

In this Section, we consider the different operating conditions at the fracture entry by investigating parameter values for α using equations (5.3.20) to (5.3.26). Table 5.1 shows

operating conditions with the corresponding values of the parameter α. The working condition $1/[2(n+1)]$ was obtained in Section 5.4 from association of the Lie point symmetry of the PDE (5.1.1) with the second conserved vector of the PDE. The time derivative of the volume of the fracture given by (5.4.12) showed that this working condition describes fluid extraction at the fracture entry. At this point it is not clear what other physical significance this working condition has in the problem. When the volume of the fracture is constant due to no fluid injection or extraction at the fracture entry, it follows from (5.3.22) that $\alpha = 1/(n+2)$. This working condition was also derived from the association of the Lie point symmetry of the PDE (5.1.1) with the elementary conserved vector of the PDE in Section 5.4.

Operating conditions at the fracture entry	α
Constant speed of propagation	1
Constant rate of fluid injection	$\frac{n+1}{n+2}$
Constant pressure	$\frac{1}{2}$
Constant volume (No fluid injection or extraction)	$\frac{1}{n+2}$
Special fluid extraction working condition	$\frac{1}{2(n+1)}$

Table 5.1: Operating conditions at the fracture entry and corresponding values of α.

When the pressure at which the fluid is being pumped into the fracture at the entry is constant, then from the PKN approximation and equation (2.4.80) it is clear that the half-width of the fracture must also be constant and therefore from (5.3.20), $\alpha = 1/2$. It is clear from (5.2.33) that when the rate at which the fluid is being pumped into the fracture at the entry, dV/dt, is constant then $\alpha = (n+1)/(n+2)$. This parameter value can also be obtained from the flux, (5.3.24), given that the rock encasing the fracture is impermeable and therefore $Q(t,0) = dV/dt$. The parameter value $\alpha = 1$ is obtained from the derivative of the length $L(t)$, (5.3.21), when the speed at which the fracture propagates is constant. This condition is a mathematical limit as opposed to an operating condition at the fracture entry given that it is not clear how one can attain it in practice. Though not definitive, one way to implement this working condition may be to inject fluid at the fracture entry at a constant rate, then to slowly increase the rate at which the fluid is pumped into the

fracture until the desired outcome is reached.

Operating conditions greater than the constant volume working condition, $\alpha > 1/(n+2)$, define fractures with fluid injected at the fracture entry while operating conditions less than the constant volume working condition, $\alpha < 1/(n+2)$, define fractures with fluid extracted at the fracture entry.

Analytical solutions to the governing equations, (5.3.5) to (5.3.7) and (5.3.20) to (5.3.26), for a fracture with constant volume, $\alpha = 1/(n+2)$, for a fracture propagating with constant speed, $\alpha = 1$, and for a fracture with fluid extracted at the fracture entry, $\alpha = 1/[2(n+1)]$, will be investigated in this Chapter. Numerical solutions for the remaining working conditions in Table 5.1 will be explored.

5.6 Asymptotic solution at the fracture tip

Before considering exact analytical solutions and numerical solutions, it is necessary to investigate the asymptotic solution at the fracture tip of the ODE (5.3.5) that is valid for all working conditions. The asymptotic solution is taken to assume the form

$$f(u) \sim A(1-u)^p, \qquad as \quad u \to 1, \tag{5.6.1}$$

where A and p are constants to be determined. It is clear that (5.6.1) satisfies the boundary condition (5.3.6) at the fracture tip which is required. However it is not expected that (5.6.1) should satisfy the boundary condition (5.3.7) at the fracture entry. Substituting (5.6.1) into the ordinary differential equation (5.3.5) gives

$$A^{n+1}p[(n+1)p-1](1-u)^{(n+1)p-2} - Ap(1-u)^{p-1} + A\left[p+1+\frac{1}{n}\left(\frac{1}{\alpha}-(n+2)\right)\right](1-u)^p = 0. \tag{5.6.2}$$

The first two terms of (5.6.2) cancel each other provided the exponents are the same and the coefficients are the same. This gives

$$p = \frac{1}{n}, \quad A = n^{\frac{1}{n}}. \tag{5.6.3}$$

The remaining term (the third term of (5.6.2)) tends to zero as $u \to 1$. The asymptotic solution is

$$f(u) \sim n^{\frac{1}{n}}(1-u)^{\frac{1}{n}}, \qquad as \quad u \to 1. \tag{5.6.4}$$

The asymptotic solution is valid for all values of α and all $n > 0$ and hence for all operating conditions at the fracture entry.

It follows from (5.6.4) that

$$f^n(u)\frac{df}{du}(u) \sim -n^{\frac{1}{n}}(1-u)^{\frac{1}{n}}, \qquad as \quad u \to 1, \tag{5.6.5}$$

and therefore the zero flux condition at the fracture tip, (5.3.14), is satisfied for all α and all $n > 0$. Also from equations (5.3.20) and (5.6.4), where $u = x/L(t)$, it is clear that

$$h(t,x) \sim \frac{\beta}{f_{max}} L(t)^{\frac{2}{n}\left(1-\frac{1}{2\alpha}\right)} n^{\frac{1}{n}} \left[1 - \frac{x}{L(t)}\right]^{\frac{1}{n}}, \quad as \quad x \to L(t) \tag{5.6.6}$$

and therefore

$$\frac{\partial h}{\partial x}(t,x) \sim -\frac{\beta}{f_{max}} L(t)^{\frac{(2-n)}{n}\left(1-\frac{1}{(2-n)\alpha}\right)} n^{\frac{1-n}{n}} \left[1 - \frac{x}{L(t)}\right]^{\frac{1-n}{n}}, \quad as \quad x \to L(t). \tag{5.6.7}$$

Hence

$$\frac{\partial h}{\partial x}(t, L(t)) = \begin{cases} -\infty, & n > 1, \\ -\dfrac{\beta}{f_{max}} L(t)^{1-\frac{1}{\alpha}}, & n = 1, \\ 0, & 0 < n < 1. \end{cases} \tag{5.6.8}$$

For all operating conditions at the fracture entry, the lubrication approximation breaks down at the fracture tip when $n > 1$ because the spatial gradient of the half-width at $x = L(t)$ is singular for $n > 1$. For all working conditions the spatial gradient of the half-width at $x = L(t)$ is finite and non-zero for $n = 1$ and zero for $0 < n < 1$. Therefore the lubrication approximation applies when $0 < n \leq 1$.

5.7 Exact analytical solutions

In this Section, we investigate the exact analytical solutions of the partial differential equation (5.1.1). This is done by obtaining the analytical solution $f(u)$ to the boundary value

problem (5.3.5) to (5.3.7) and substituting the result into the half-width, length and volume equations given by (5.3.20) to (5.3.23). For fluid injection, $u_{max} = 0$ and therefore $f_{max} = f(0)$ while for fluid extraction $0 < u_{max} < 1$ and therefore $f_{max} = f(u_{max}) \neq f(0)$.

5.7.1 Constant volume $[\alpha = 1/(n+2)]$

We first consider the special case in which the total volume of the fracture remains constant, $\alpha = 1/(n+2)$. Note that this working condition was obtained through analysis of the equation for the volume of the fracture, (5.3.22), and also from the association of the Lie point symmetry of the PDE, (5.1.1), with the elementary conserved vector, (4.4.32), of the PDE. In this solution there is no injection or extraction of fluid at the fracture entry. The exact analytical solution for a fracture with constant volume and no asperities at the fluid-rock interface was derived by Fitt et al [11].

When $\alpha = 1/(n+2)$, the boundary value problem (5.3.5) to (5.3.7) reduces to

$$\frac{d}{du}\left(f^n \frac{df}{du}\right) + \frac{d}{du}(uf) = 0, \tag{5.7.1}$$

$$f(1) = 0, \tag{5.7.2}$$

$$f^n(0)\frac{df}{du}(0) = 0. \tag{5.7.3}$$

Integrating (5.7.1) once gives

$$f^n \frac{df}{du} + uf = A, \tag{5.7.4}$$

where A is a constant. Imposing the boundary condition (5.7.3) on (5.7.4) gives $A = 0$. It therefore follows that (5.7.4) is a variables separable ordinary differential equation which when integrated gives

$$\frac{f^n}{n} = B - \frac{u^2}{2}, \tag{5.7.5}$$

where B is a constant. Imposing the boundary condition (5.7.2) onto (5.7.5) gives $B = 1/2$. It is therefore clear that for constant volume, the solution (5.7.5) to the boundary value problem (5.7.1) to (5.7.3) is

$$f(u) = \left(\frac{n}{2}\right)^{\frac{1}{n}}(1-u^2)^{\frac{1}{n}}. \tag{5.7.6}$$

In expanded form, equation (5.7.6) can be re-expressed as

$$f(u) = n^{\frac{1}{n}} 2^{-\frac{1}{n}} (1+u)^{\frac{1}{n}} (1-u)^{\frac{1}{n}}, \tag{5.7.7}$$

which clearly satisfies the asymptotic solution (5.6.4) as $u \to 1$. It is readily checked that the constant volume solution (5.7.7) satisfies the zero flux condition at the fracture tip, (5.3.14). The length $L(t)$, (5.3.21), volume $V(t)$, (5.3.22), and half-width $h(t,x)$, (5.3.20), of the fracture with $f(u)$ defined by (5.7.6) are

$$L(t) = \left[1 + \frac{2(n+2)}{n} \beta^n K_n t\right]^{\frac{1}{n+2}}, \tag{5.7.8}$$

$$V(t) = V_o = 2\beta \int_0^1 (1-u^2)^{\frac{1}{n}} du, \tag{5.7.9}$$

$$h(t,x) = \beta \left[1 + \frac{2(n+2)}{n} \beta^n K_n t\right]^{-\frac{1}{n+2}} \left(1 - \left(\frac{x}{L(t)}\right)^2\right)^{\frac{1}{n}}, \tag{5.7.10}$$

where $u = x/L(t)$. When there is no fluid injection or extraction at the fracture entry the length of the fracture, (5.7.8), continues to grow as the half-width of the fracture, (5.7.10), decreases in order to keep the total volume of the fracture constant, (5.7.9). This is shown in Figures 5.1 and 5.2. From differentiating (5.7.10), it is found that the spatial gradient of the half-width of the fracture is

$$\frac{\partial h}{\partial x}(t,x) = -\frac{2\beta x}{n L^3(t)} \left(1 - \frac{x^2}{L^2(t)}\right)^{\frac{1-n}{n}} \tag{5.7.11}$$

and therefore

$$\frac{\partial h}{\partial x}(t, L(t)) = \begin{cases} -\infty, & n > 1, \\ -\dfrac{2\beta}{L^2(t)}, & n = 1, \\ 0, & 0 < n < 1. \end{cases} \tag{5.7.12}$$

When $n > 1$, there is a singularity at the fracture tip due to the infinite spatial gradient of the half-width at the fracture tip and therefore the lubrication approximation $H/L << 1$ breaks down in the neighbourhood of the fracture tip as shown in Figures 5.1 (a) and 5.2 (a). However for $0 < n \leq 1$, the lubrication approximation is satisfied. When $n = 1$, the spatial gradient of the half-width at the fracture tip is finite, (Figures 5.1 (b) and 5.2 (b)), while $0 < n < 1$ gives a zero spatial gradient of the half-width at the fracture tip as shown

in Figures 5.1 (c) and 5.2 (c). It can be verified that the slope at the fracture tip, (5.7.12), satisfies the asymptotic spatial gradient of the half-width of the fracture, (5.6.8), provided $u \to 1$.

For a fracture with constant volume, it is found that an initially partially open fracture remains partially open for all scaled time $K_n t$. This is clearly shown in Figure 5.1 where $\beta = 0.75$. An initially open fracture always has partially open regions in the neighbourhood of the fracture tip. However, given that for such a fracture most of the fracture is open, we consider it an open fracture. An initially open fracture with constant volume remains open only until $h(t,0) = 1$ ($h(t,0) = h_{max}$ in dimensional form), that is, only until the scaled transition time

$$K_n t_\tau = \frac{n(\beta^{n+2} - 1)}{2(n+2)\beta^n} \tag{5.7.13}$$

after which it becomes partially open. Before the scaled time (5.7.13) the fracture is open but after the scaled transition time (5.7.13) asperities in the fracture begin to touch all along the fracture forming a partially open fracture. The diffusion constant K_n in (5.7.13) is defined by (5.1.2) where $\sigma_R = 0$ for an open fracture.

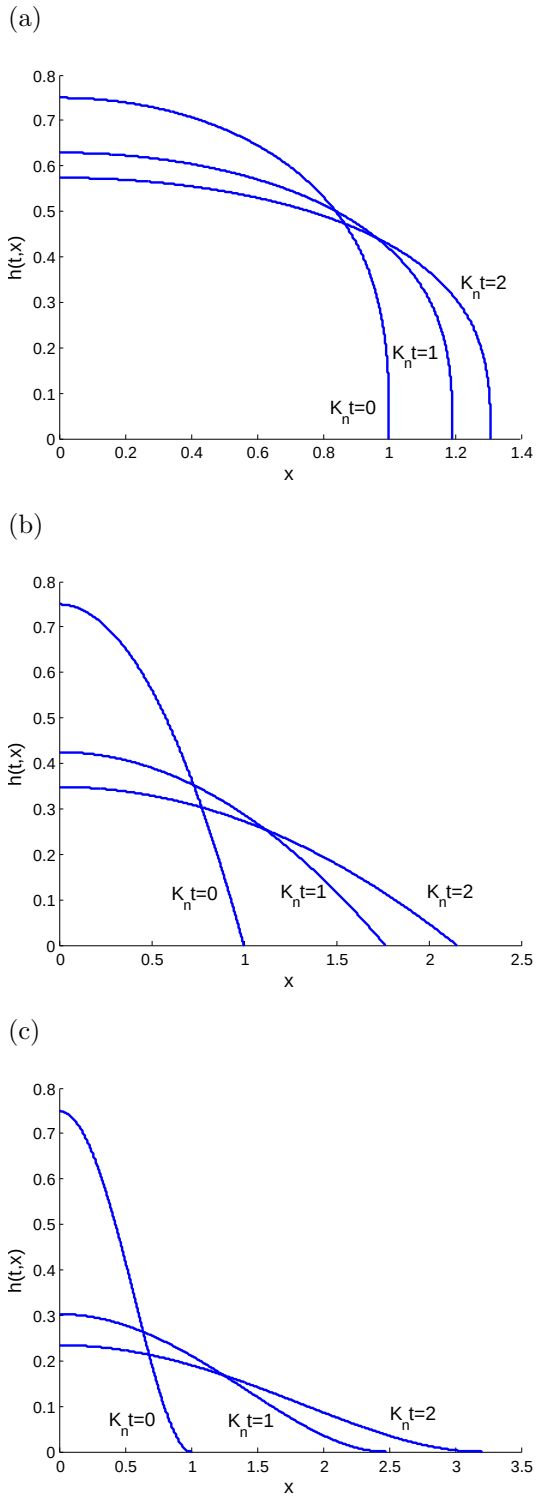

Figure 5.1: Partially open fracture of constant volume with $\beta = 0.75$ and $\alpha = \frac{1}{n+2}$. The analytical solution (5.7.10) for the half-width $h(t, x)$ plotted against x for increasing values of the scaled time $K_n t$ and (a) $n = 3$, (b) $n = 1$, (c) $n = 0.5$.

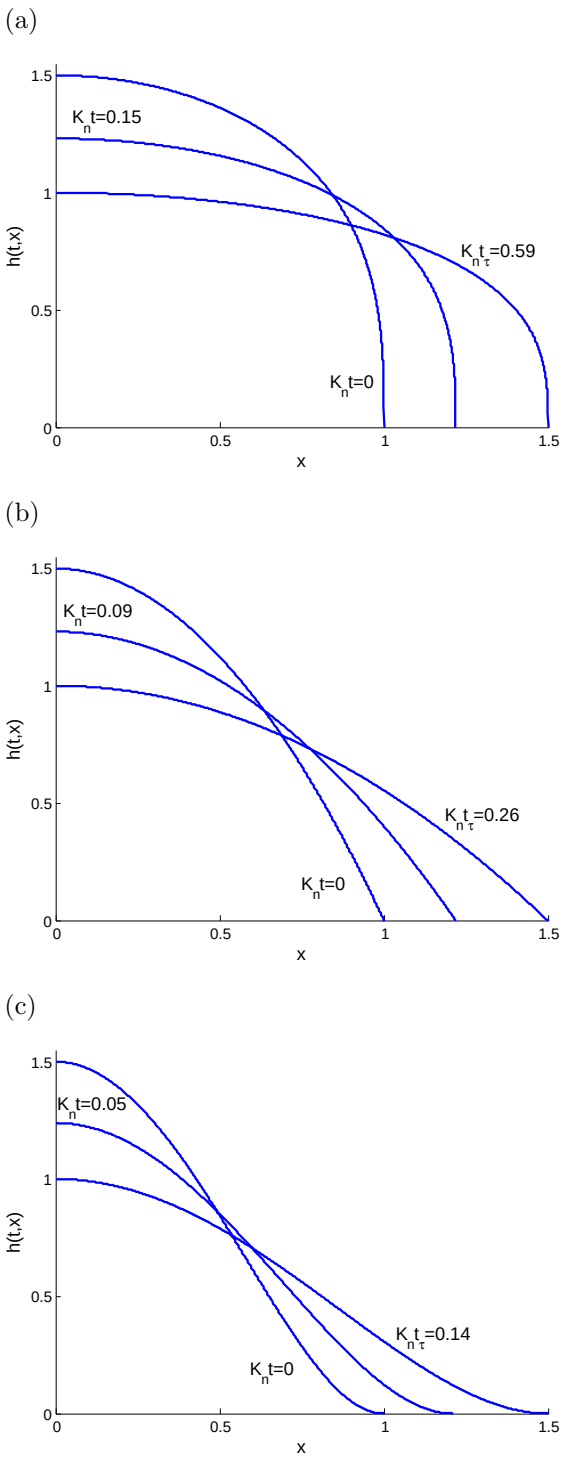

Figure 5.2: Open fracture of constant volume with $\beta = 1.5$ and $\alpha = \frac{1}{n+2}$. The analytical solution (5.7.10) for the half-width $h(t, x)$ plotted against x for increasing values of the scaled time $K_n t$ and (a) $n = 3$, (b) $n = 1$, (c) $n = 0.5$.

5.7.2 Constant speed of propagation $[\alpha = 1]$

In order to investigate if there exists another exact analytical solution, we consider a solution of the form

$$f(u) = A(1-u)^p, \tag{5.7.14}$$

where A and p are constants to be determined. This form of solution was first investigated for a pre-existing fluid driven fracture in impermeable rock [11]. Substituting (5.7.14) into the ordinary differential equation (5.3.5) gives

$$A^{n+1}p[(n+1)p-1](1-u)^{(n+1)p-2} - Ap(1-u)^{p-1} + A\left[p+1+\frac{1}{n}\left(\frac{1}{\alpha}-(n+2)\right)\right](1-u)^p = 0. \tag{5.7.15}$$

It is clear that (5.7.15) is the same as (5.6.2) due to the fact that the processes of investigating this exact solution and obtaining the asymptotic solution are the same except for one detail. For the asymptotic solution, we consider the solution as $u \to 1$ but for the analytical solution, we consider the solution that is valid everywhere along $0 \leq u \leq 1$. For the asymptotic solution the third term in (5.7.15) vanishes for all values of α as $u \to 1$ while for the analytical solution it vanishes only for the special value of α. The first and second terms in (5.7.15), as previously, give

$$A = n^{\frac{1}{n}}, \quad p = \frac{1}{n} \tag{5.7.16}$$

and therefore (5.7.14) becomes

$$f(u) = n^{\frac{1}{n}}(1-u)^{\frac{1}{n}}. \tag{5.7.17}$$

The remaining third term in (5.7.15) with p defined by (5.7.16) vanishes provided

$$\alpha = 1. \tag{5.7.18}$$

It is readily observed that the solution (5.7.17) satisfies the first boundary condition (5.3.6). Substituting the solution (5.7.17) into the left hand side of the second boundary condition (5.3.7) gives

$$f^n(0)\frac{df}{du}(0) = -n^{\frac{1}{n}} \tag{5.7.19}$$

and substituting the solution (5.7.17) into the right hand side of the second boundary condition (5.3.7) gives the same result, (5.7.19). It is therefore verified that when $\alpha = 1$, the solution (5.7.17) of the ODE (5.3.5) satisfies both of the boundary conditions (5.3.6) and (5.3.7) and therefore (5.7.17) is another exact analytical solution to the boundary value problem (5.3.5) to (5.3.7). It is clear that the exact analytical solution (5.7.17) identically satisfies the asymptotic condition (5.6.4) as $u \to 1$. It can be verified that (5.7.17) also satisfies the zero flux condition at the fracture tip, (5.3.14).

The length, volume and half-width for the model fracture are therefore

$$L(t) = 1 + \frac{\beta^n}{n} K_n t, \tag{5.7.20}$$

$$V(t) = \frac{2\beta n}{(n+1)} \left[1 + \frac{\beta^n}{n} K_n t \right]^{\frac{n+1}{n}}, \tag{5.7.21}$$

$$h(t,x) = \beta \left[1 + \frac{\beta^n}{n} K_n t \right]^{\frac{1}{n}} \left(1 - \frac{x}{L(t)} \right)^{\frac{1}{n}}, \tag{5.7.22}$$

where $u = x/L(t)$. The length, (5.7.20), volume, (5.7.21), and half-width, (5.7.22), of the fracture all increase with increasing scaled time $K_n t$ as shown in Figures 5.3 and 5.4. The condition $\alpha = 1$, (5.7.18), corresponds to the case whereby the speed at which the fracture propagates, dL/dt, is constant. In dimensional form, dL/dt is

$$\frac{dL}{dt} = \frac{\beta^n \Lambda a_n h_{max}^n}{3\mu n L_o} \left(1 - \frac{\sigma_R}{\Lambda h_{max}} \right) \tag{5.7.23}$$

which clearly depends on the flow law through a_n and n and on the crack law through σ_R. For an open fracture $\sigma_R = 0$ while for a partially open fracture $\sigma_R < 0$.

From (5.7.20) and (5.7.22), the spatial gradient of the half-width is

$$\frac{\partial h}{\partial x}(t,x) = -\frac{\beta}{n} L(t)^{\frac{1-n}{n}} \left(1 - \frac{x}{L(t)} \right)^{\frac{1-n}{n}}, \tag{5.7.24}$$

and therefore

$$\frac{\partial h}{\partial x}(t, L(t)) = \begin{cases} -\infty, & n > 1, \\ -\beta, & n = 1, \\ 0, & 0 < n < 1. \end{cases} \tag{5.7.25}$$

It is important to note that (5.7.25) satisfies the asymptotic solution (5.6.8) as $u \to 1$. For $n > 1$, there is singularity at the fracture tip as shown in Figures 5.3 (a) and 5.4 (a) due to the infinite spatial gradient of the half-width at the fracture tip. For $0 < n \leq 1$, tortuosity removes the singularity at the fracture tip. The parameter $n = 1$, (Figures 5.3 (b) and 5.4 (b)), yields a finite spatial gradient of the half-width of the fracture at the fracture tip and for the case $0 < n < 1$, (Figures 5.3 (c) and 5.4 (c)), the spatial gradient of the half-width of the fracture at the fracture tip vanishes. Another observation from Figures 5.3 and 5.4 is that the parameter n has an effect on the nature in which the fracture grows. For small n, $0 < n < 1$, the half-width of the fracture grows more rapidly than the length of the fracture while for large n, $n > 1$, the length of the fracture grows more rapidly than the half-width of the fracture. The parameter $n = 1$ is the dividing case and the fracture length and half-width grow at the same rate.

A fracture propagating with constant speed keeps on growing in both length and half-width, therefore if such a fracture is initially open ($\beta = 1.5$) it will continue to be open for all scaled time $K_n t$. For a fracture propagating at constant speed that is initially partially open, the half-width increases steadily with time and when $h(t, 0) = 1$ ($h(t, 0) = h_{max}$ in dimensional variables) the contact regions begin to move apart forming an open fracture. This will occur at the scaled transition time

$$K_n t_\tau = \frac{n}{\beta^n}\left[\left(\frac{1}{\beta}\right)^n - 1\right]. \tag{5.7.26}$$

The diffusion constant K_n in (5.7.26) is defined by (5.1.2) where $\sigma_R = 0$ for an open fracture.

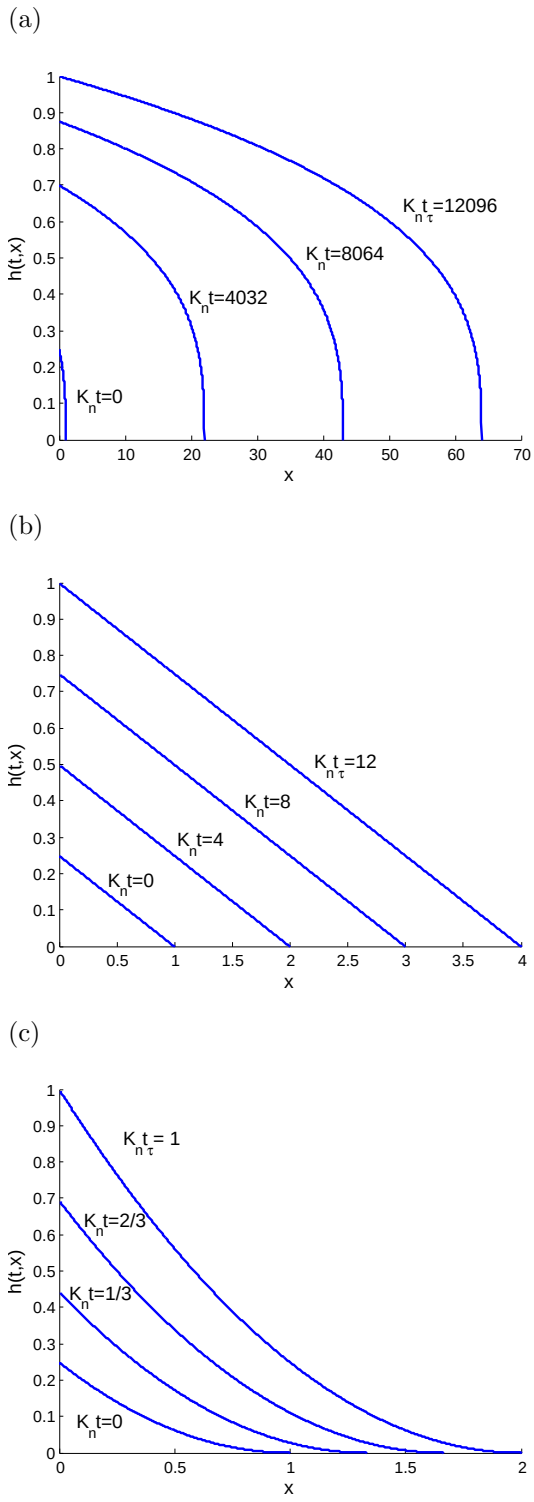

Figure 5.3: Partially open fracture ($\beta = 0.25$) propagating with constant speed ($\alpha = 1$). The analytical solution (5.7.22) for the half-width $h(t, x)$ plotted against x for increasing values of the scaled time $K_n t$ and (a) $n = 3$, (b) $n = 1$, (c) $n = 0.5$.

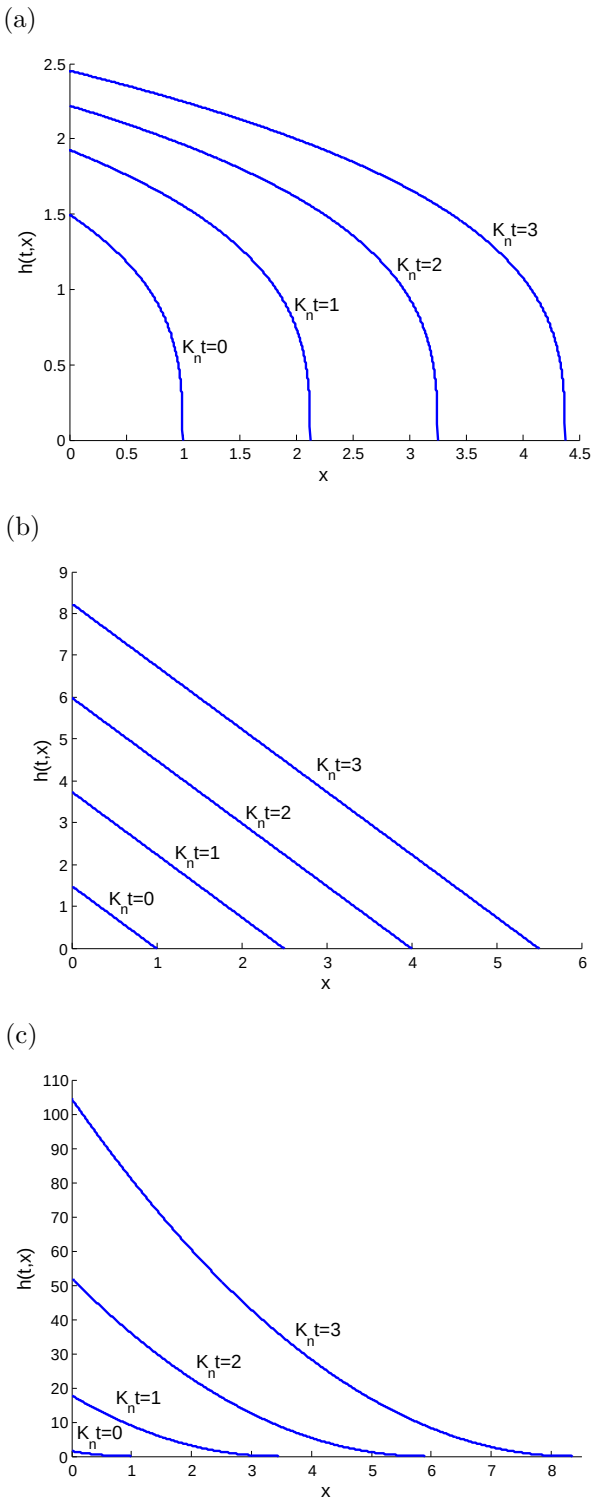

Figure 5.4: Open fracture ($\beta = 1.5$) propagating with constant speed ($\alpha = 1$). The analytical solution (5.7.22) for the half-width $h(t, x)$ plotted against x for increasing values of the scaled time $K_n t$ and (a) $n = 3$, (b) $n = 1$, (c) $n = 0.5$.

5.7.3 Limiting extraction condition $[\alpha = 1/[2(n+1)]]$

The working condition $\alpha = 1/[2(n+1)]$ is obtained from association of the Lie point symmetry of the nonlinear diffusion equation (5.1.1) with the second conserved vector, (4.4.33), of the PDE. When $\alpha = 1/[2(n+1)]$, the boundary value problem (5.3.5) to (5.3.7) becomes

$$\frac{d}{du}\left(f^n \frac{df}{du}\right) + \frac{d}{du}\Big(uf\Big) + f = 0, \tag{5.7.27}$$

$$f(1) = 0, \tag{5.7.28}$$

$$f^n(0)\frac{df}{du}(0) = \int_0^1 f(u)du. \tag{5.7.29}$$

Expanding the second term in (5.7.27) rewrites equation (5.7.27) as

$$\frac{d}{du}\left(f^n \frac{df}{du}\right) + u\frac{df}{du} + 2f = 0. \tag{5.7.30}$$

Multiplying (5.7.30) by u and simplifying the result gives

$$\frac{d}{du}\left(uf^n \frac{df}{du}\right) + \frac{d}{du}(u^2 f) - \frac{1}{(n+1)}\frac{d}{du}(f^{n+1}) = 0. \tag{5.7.31}$$

Integrating (5.7.31) with respect to u subject to the boundary condition (5.7.28) and the zero flux condition at the fracture tip (5.3.14), which is always satisfied by the asymptotic solution, gives

$$uf^n \frac{df}{du} + u^2 f - \frac{1}{(n+1)} f^{n+1} = 0. \tag{5.7.32}$$

Dividing (5.7.32) by uf and simplifying the result gives

$$\frac{d}{du}(f^n) - \Big(\frac{n}{n+1}\Big)\frac{1}{u} f^n = -nu, \tag{5.7.33}$$

which is a first order linear ODE for $f^n(u)$. Multiplying (5.7.33) by the integrating factor

$$I = u^{-\frac{n}{n+1}} \tag{5.7.34}$$

and using the product rule on the result reduces equation (5.7.33) to

$$\frac{d}{du}\Big(u^{-\frac{n}{n+1}} f^n\Big) = -nu^{\frac{1}{n+1}}. \tag{5.7.35}$$

Integrating (5.7.35) subject to the boundary condition (5.7.28) yields:

$$f(u) = \left(\frac{n(n+1)}{n+2}\right)^{\frac{1}{n}} \left[1 - u^{\frac{n+2}{n+1}}\right]^{\frac{1}{n}} u^{\frac{1}{n+1}}. \tag{5.7.36}$$

The second boundary condition (5.7.29) was not used in the derivation of (5.7.36). Substituting (5.7.36) into the left hand side of the second boundary condition (5.7.29) gives

$$f^n(0)\frac{df}{du}(0) = \left(\frac{n}{n+2}\right)^{\frac{n+1}{n}} (n+1)^{\frac{1}{n}} \tag{5.7.37}$$

and substituting (5.7.36) into the right hand side of (5.7.29) gives the same result, (5.7.37). It is therefore verified that (5.7.36) satisfies the derivative boundary condition (5.7.29).

From (5.7.36), it is clear that for $\alpha = 1/[2(n+1)]$, $f(0) = 0$ and therefore $f_{max} \neq f(0)$. The maximum function value f_{max} for the limiting case $\alpha = 1/[2(n+1)]$ can be obtained by first differentiating (5.7.36) with respect to u to obtain

$$\frac{df}{du} = \left(\frac{n}{n+2}\right)^{\frac{1}{n}} (n+1)^{\frac{1-n}{n}} \left(1 - u^{\frac{n+2}{n+1}}\right)^{\frac{1}{n}} u^{-\frac{n}{n+1}} - \left[\frac{n(n+1)}{n+2}\right]^{\frac{1-n}{n}} \left(1 - u^{\frac{n+2}{n+1}}\right)^{\frac{1-n}{n}} u^{\frac{2}{n+1}}, \tag{5.7.38}$$

which when set to zero and simplified gives

$$u_{max} = \left(\frac{n}{2(n+1)}\right)^{\frac{n+1}{n+2}}, \tag{5.7.39}$$

then substituting the result, (5.7.39), into equation (5.7.36) to obtain

$$f_{max} = f(u_{max}) = \left(\frac{n}{2}\right)^{\frac{2(n+1)}{n(n+2)}} \left(\frac{1}{n+1}\right)^{\frac{1}{n+2}}. \tag{5.7.40}$$

From (5.3.21), (5.3.22), (5.3.23) and (5.3.20) the length, volume and half-width of the fracture for $\alpha = 1/[2(n+1)]$ are

$$L(t) = \left[1 + 2\left(\frac{2(n+1)}{n}\right)^{\frac{2(n+1)}{n+2}} \beta^n K_n t\right]^{\frac{1}{2(n+1)}}, \tag{5.7.41}$$

$$V(t) = V_o\left[1 + 2\left(\frac{2(n+1)}{n}\right)^{\frac{2(n+1)}{n+2}} \beta^n K_n t\right]^{-\frac{1}{2(n+1)}} = \frac{V_o}{L(t)}, \tag{5.7.42}$$

where

$$V_o = 2\beta\left[\frac{2(n+1)n^{\frac{n}{2}}}{(n+2)^{\frac{n+2}{2}}}\right]^{\frac{2(n+1)}{n(n+2)}}, \tag{5.7.43}$$

and

$$h(t,x) = \frac{(n+2)}{2n}\frac{V_o}{L^2(t)}\left(\frac{x}{L(t)}\right)^{\frac{1}{n+1}}\left[1-\left(\frac{x}{L(t)}\right)^{\frac{n+2}{n+1}}\right]^{\frac{1}{n}}, \tag{5.7.44}$$

where $u = x/L(t)$. The behaviour of the fracture at the fracture tip can be assessed by differentiating (5.7.44) and evaluating the result at the fracture tip, as $x \to L(t)$, for different values of $n > 0$. The spatial gradient of the half-width of the fracture, (5.7.44), is

$$\begin{aligned}\frac{\partial h}{\partial x}(t,x) =& \frac{(n+2)}{2n(n+1)}\frac{V_o}{L^3(t)}\left(\frac{x}{L(t)}\right)^{\frac{-n}{n+1}}\left[1-\left(\frac{x}{L(t)}\right)^{\frac{n+2}{n+1}}\right]^{\frac{1}{n}} \\ &- \frac{(n+2)^2}{2n^2(n+1)}\frac{V_o}{L^3(t)}\left(\frac{x}{L(t)}\right)^{\frac{2}{n+1}}\left[1-\left(\frac{x}{L(t)}\right)^{\frac{n+2}{n+1}}\right]^{\frac{1-n}{n}}.\end{aligned} \tag{5.7.45}$$

Evaluating (5.7.45) as $x \to L(t)$ gives

$$\frac{\partial h}{\partial x}(t,L(t)) = \begin{cases} -\infty, & n > 1, \\ -\dfrac{2^{\frac{5}{3}}\beta}{L^3(t)}, & n = 1, \\ 0, & 0 < n < 1, \end{cases} \tag{5.7.46}$$

which agrees with the result obtained from the asymptotic solution, (5.6.8), that the spacial gradient of the half-width at the fracture tip is negative infinity for $n > 1$, is finite for $n = 1$ and is zero for $0 < n < 1$. This is shown in Figures 5.5 and 5.6 for $n = 3, 1$ and 0.5. The removal of the singularity at the fracture tip with increasing tortuosity (divergence from the Reynolds flow, $n = 3$) was also observed in Figures 5.1 and 5.2 for constant volume and Figures 5.3 and 5.4 for a fracture propagating with constant speed.

The half-width of the fracture at the fracture entry is always zero ($h(t,0) = 0$) for all scaled time $K_n t$ which is clearly shown in Figures 5.5 and 5.6. This is a result of the assumption made earlier for mathematical simplification that $h_{min} = 0$ since $h_{min} << h_{max}$. The volume of the fracture, (5.7.42), decreases with increasing scaled time $K_n t$. This implies that although the half-width at the fracture entry vanishes ($h(t,0) = 0$), due to the assumption $h_{min} = 0$, fluid is extracted at the fracture entry. Later in this Section we will investigate the flux of fluid along the fracture in order to understand and further explain the decrease in the total volume when the half-width at the fracture entry vanishes ($h(t,0) = 0$ for $t \geq 0$) and when there is no fluid leak-off at the fluid-rock interface.

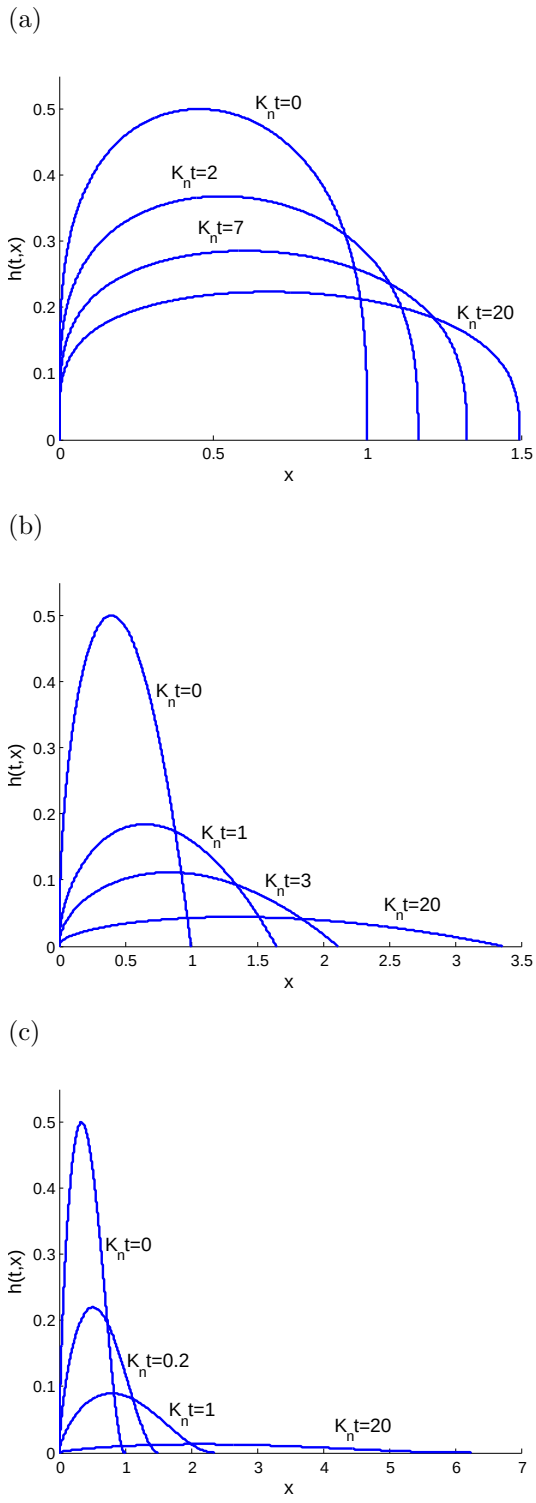

Figure 5.5: Partially open fracture ($\beta = 0.5$) propagating with $\alpha = \frac{1}{2(n+1)}$. The analytical solution (5.7.44) for the half-width $h(t,x)$ plotted against x for increasing values of the scaled time $K_n t$ and (a) $n = 3$, (b) $n = 1$, (c) $n = 0.5$.

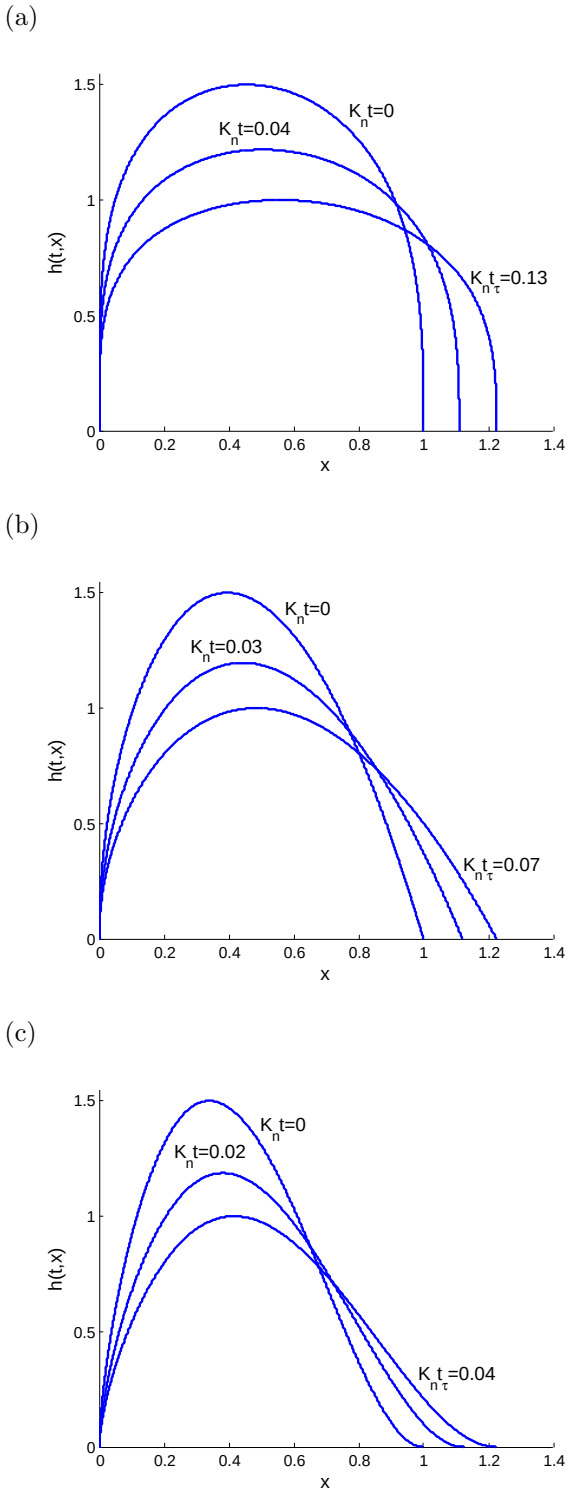

Figure 5.6: Open fracture ($\beta = 1.5$) propagating with $\alpha = \frac{1}{2(n+1)}$. The analytical solution (5.7.44) for the half-width $h(t,x)$ plotted against x for increasing values of the scaled time $K_n t$ and (a) $n = 3$, (b) $n = 1$, (c) $n = 0.5$.

Also

$$\frac{\partial h}{\partial x}(t,x) \propto x^{\frac{-n}{n+1}}, \quad \text{as} \quad x \to 0. \tag{5.7.47}$$

The spatial gradient of the half-width at the fracture entry is therefore infinite and further it is positive. The working condition $\alpha = 1/[2(n+1)]$ gives the limiting solution for fluid extraction from the fracture.

As we have observed the length of the fracture, given by (5.7.41), increases steadily as the scaled time $K_n t$ increases. From (5.7.44) the half-width of the fracture vanishes at the fracture entry, $x = 0$, and at the fracture tip, $x = L(t)$, and it decreases steadily with time for $0 < x < L(t)$. An initially partially open fracture with $0 < \beta < 1$ will therefore remain partially open for all values of $K_n t$. An initially open fracture with $\beta \geq 1$ will become partially open as $K_n t$ increases when

$$h(t, u_{max}) = 1. \tag{5.7.48}$$

By using (5.7.39) for u_{max} we find that

$$h(t, u_{max}) = \beta \left[1 + 2 \left(\frac{2(n+1)}{n} \right)^{\frac{2(n+1)}{n+2}} \beta^n K_n t \right]^{-\frac{1}{n+1}} \tag{5.7.49}$$

and hence an open fracture will become partially open at the scaled transition time

$$K_n t_\tau = \frac{1}{2\beta^n} \left[\frac{n}{2(n+1)} \right]^{\frac{2(n+1)}{n+2}} (\beta^{n+1} - 1). \tag{5.7.50}$$

For times greater (5.7.50), the model for an open fracture ceases to exist and the asperities on opposite walls touch along the length of the fracture forming contact regions that define a partially open fracture.

It was verified from analysis of the volume of the fracture, (5.7.42), that the limiting working condition $\alpha = 1/[2(n+1)]$ gives a solution that describes the process of fluid being extracted from the fracture at the fracture entry. In order to investigate this fluid flow behaviour further, we analyse the fluid flux in the fracture.

The volume flux per unit breadth is given by equation (5.3.24). Using (5.7.40) for f_{max} and (5.7.36) for $f(u)$, the volume flux (5.3.24), when $\alpha = 1/[2(n+1)]$, becomes

$$Q(t,x) = -\frac{2K_n\beta^{n+1}}{L(t)^{2n+3}}\left(\frac{2^{\frac{2(n+1)^2}{n(n+2)}}(n+1)^{\frac{n^2+2n+2}{n(n+2)}}}{n^{\frac{n+1}{n+2}}(n+2)^{\frac{n+1}{n}}}\right)\left[1-\frac{2(n+1)}{n}\Big(\frac{x}{L(t)}\Big)^{\frac{n+2}{n+1}}\right]\left[1-\Big(\frac{x}{L(t)}\Big)^{\frac{n+2}{n+1}}\right]^{\frac{1}{n}}, \tag{5.7.51}$$

where $L(t)$ is given by (5.7.41) and $u = x/L(t)$. In order to plot curves of the fluid flux one would need to specify the diffusion constant K_n. In order to keep the analysis general, we therefore consider instead the fluid flux ratio

$$\frac{Q(t,x)}{|Q(0,0)|} = -\frac{1}{L(t)^{2n+3}}\left[1-\frac{2(n+1)}{n}\left(\frac{x}{L(t)}\right)^{\frac{n+2}{n+1}}\right]\left[1-\left(\frac{x}{L(t)}\right)^{\frac{n+2}{n+1}}\right]^{\frac{1}{n}}. \tag{5.7.52}$$

At the fracture tip, $x = L(t)$,

$$Q(t,L(t)) = 0, \qquad t \geq 0. \tag{5.7.53}$$

This implies that there is no fluid leaking at the fracture tip and therefore the zero flux condition at the fracture tip (5.3.14) is satisfied. At the fracture entry, $x = 0$,

$$\frac{Q(t,0)}{|Q(0,0)|} = -\frac{1}{L(t)^{2n+3}}, \qquad t \geq 0. \tag{5.7.54}$$

Thus fluid flows out of the fracture at the fracture entry. This agrees with the result obtained earlier in this Section that when $\alpha = 1/[2(n+1)]$ the volume of the fracture steadily decreases and tends to zero as t tends to infinity. This is clearly shown in Figures 5.7 and 5.8. For an initially open fracture (Figure 5.8), the fluid is extracted from the fracture fairly quickly until the transition scale time $K_n t_\tau$, (5.7.50). In a partially open fracture (Figure 5.7), it takes more time for the fluid to be extracted from the fracture. For the working condition $\alpha = 1/[2(n+1)]$, we observed that $h(t,x) = h_{min}$ at the fracture entry and at the fracture tip. As explained earlier, the half-width of the fracture vanishes at the fracture entry and at the fracture tip because of the approximation we made that $h_{min} = 0$. But in practice, h_{min} is never equal to zero however small it may be due to the large compressive stresses [1]. For $0 \leq x < L(t)$, when $h(t,x) = h_{min}$ the flux of fluid is non-zero and tends to the finite non-zero value given by (5.7.51) as $h_{min} \to 0$. At the fracture entry (5.7.51) reduces to a finite non-zero flux that can be deduced from (5.7.54). This is because the flux at the fracture entry is $2h(t,0)\overline{v}_x(t,0)$ and as $h(t,0) \to 0$, the width averaged fluid velocity $\overline{v}_x(t,0) \to -\infty$ such that the product is finite and non-zero, (5.7.54).

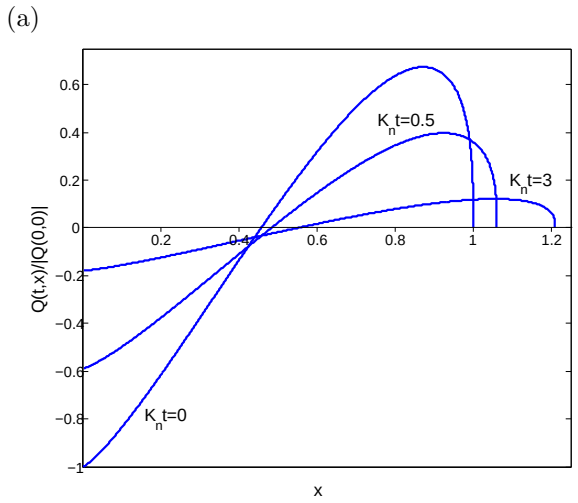

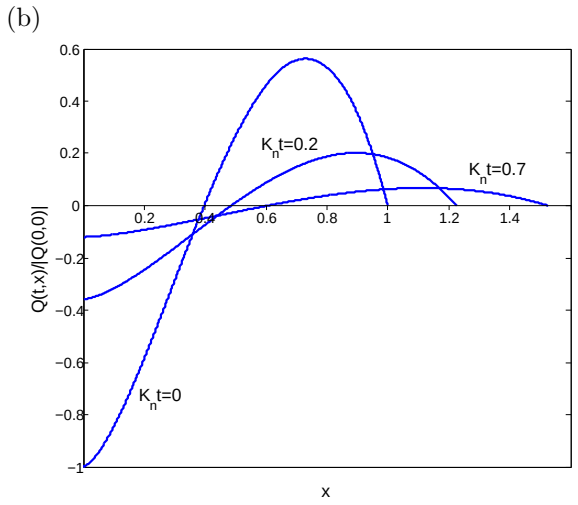

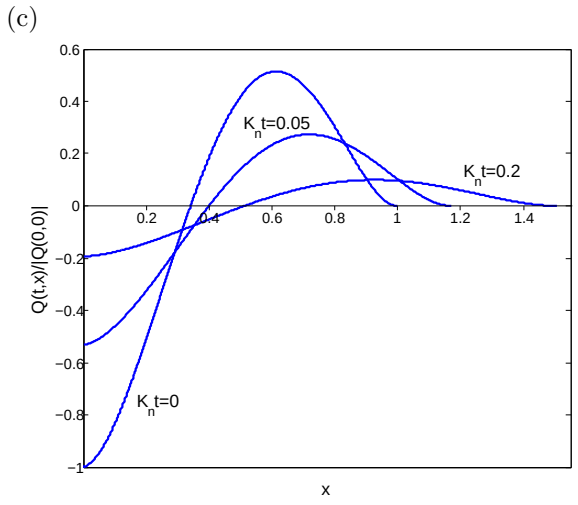

Figure 5.7: Partially open fracture ($\beta = 0.5$) propagating with $\alpha = \frac{1}{2(n+1)}$. The flux (5.7.52) plotted against x for increasing values of the scaled time $K_n t$ and (a) $n = 3$, (b) $n = 1$, (c) $n = 0.5$.

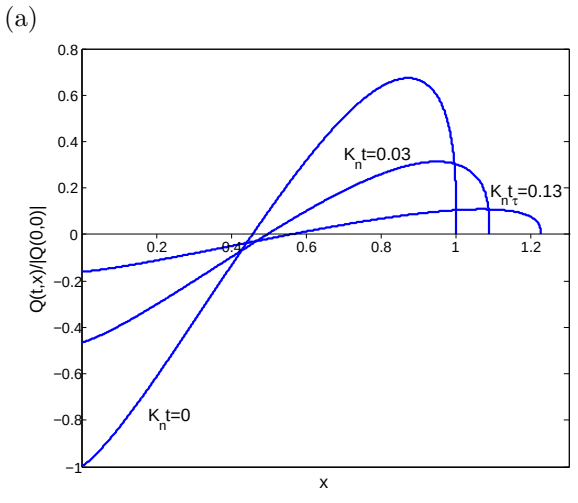

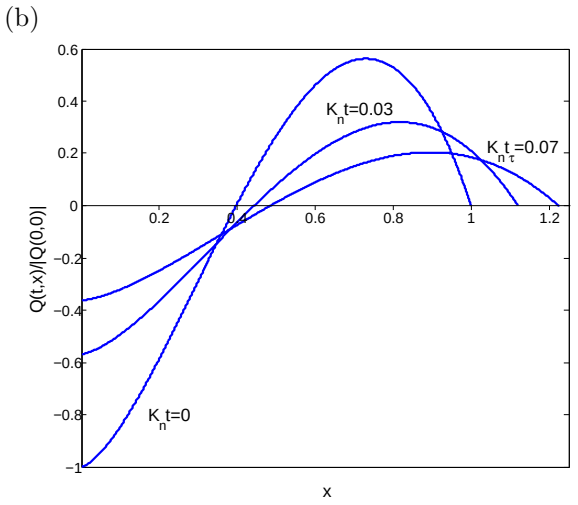

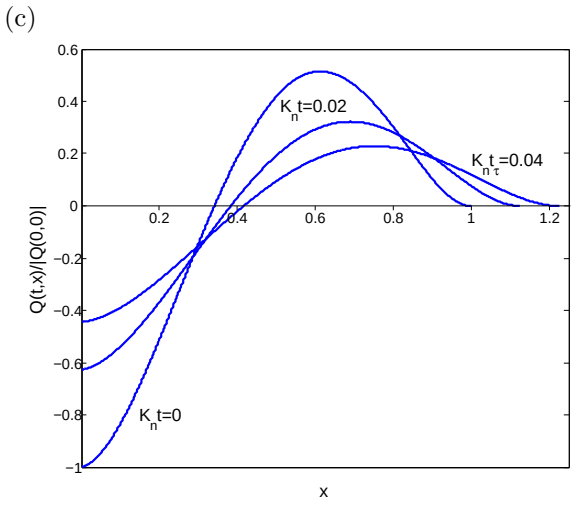

Figure 5.8: Open fracture ($\beta = 1.5$) propagating with $\alpha = \frac{1}{2(n+1)}$. The fluid flux (5.7.52) plotted against x for increasing values of the scaled time $K_n t$ and (a) $n = 3$, (b) $n = 1$, (c) $n = 0.5$.

A more interesting result that comes from the fluid flux analysis is the manner in which the fluid extraction process occurs which is shown in Figures 5.7 and 5.8. As some of the fluid flows out of the fracture, ,$Q(t,x)$¡0 for $0 < x < x_{max}$, at the same time some of the fluid relaxes further into the fracture, $Q(t,x)$¿0 for $x_{max} < x < L(t)$. This explains the steady increase in the length of the fracture, (5.7.41), with increasing scaled time $K_n t$ during the fluid extraction process.

Figure 5.9 illustrates the concept of fluid extraction as deduced from the fluid flux

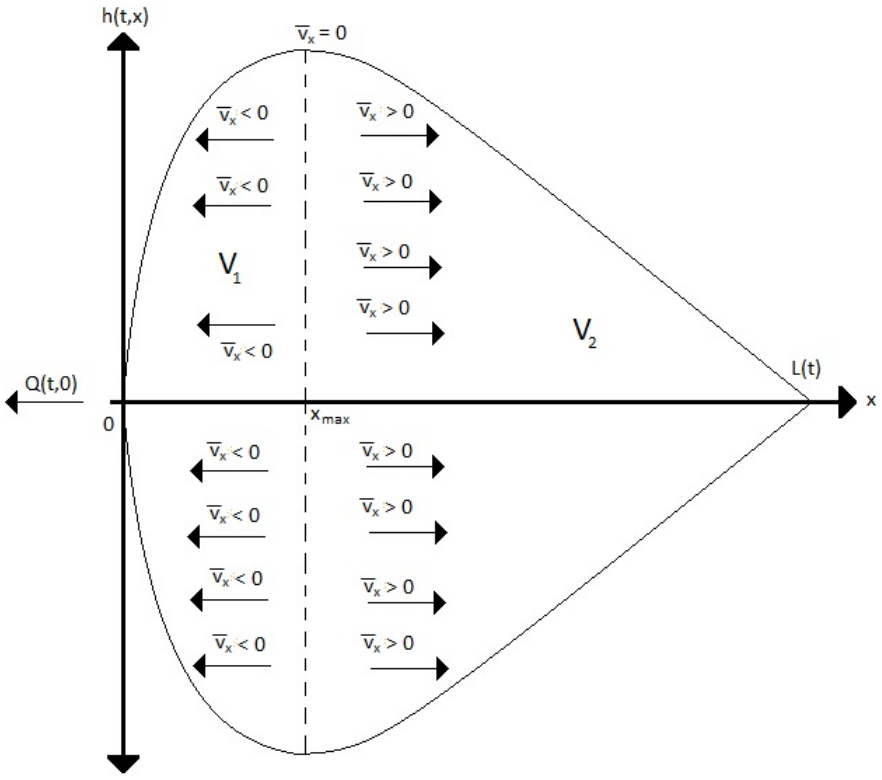

Figure 5.9: Illustration of the process of fluid extraction (for n=1).

analysis. The dotted line in Figure 5.9 denotes the cross-section on which the fluid elements are not moving and therefore the width averaged fluid velocity $\overline{v}_x(t,x)$ is zero. Since

$$Q(t,x) = 2h(t,x)\overline{v}_x(t,x), \tag{5.7.55}$$

this occurs when $Q = 0$, and therefore when the flux of fluid, (5.7.51), is equated to zero to give

$$u = \frac{x}{L(t)} = \left[\frac{n}{2(n+1)}\right]^{\frac{n+1}{n+2}}. \tag{5.7.56}$$

But from (5.7.39),

$$u_{max} = \frac{x_{max}}{L(t)} = \left[\frac{n}{2(n+1)}\right]^{\frac{n+1}{n+2}}. \tag{5.7.57}$$

Thus $\overline{v}_x(t,x)$ vanishes at the position of the maximum half-width of the fracture. The fluid in the region $0 < x < x_{max}$ flows out of the fracture while the fluid in the region $x_{max} < x < L(t)$ flows towards the fracture tip. We have

$$x_{max} = \left[\frac{n}{2(n+1)}\right]^{\frac{n+1}{n+2}} L(t), \tag{5.7.58}$$

where $L(t)$ is given by (5.7.41). Thus x_{max} increases with time and moves into the fracture in the direction of the fracture tip. In comparison, u_{max} is constant in time. Thus the cross-section on which $\overline{v}_x(t,x) = 0$ when scaled with $L(t)$ is a fixed point in the fracture.

In order to investigate fluid extraction further, we consider the volumes of the two regions of the fracture formed by the transition cross-section (dotted line) in Figure 5.9. We denote the volume per unit breadth of the first region of the fracture adjacent to the fracture entry by V_1 and the volume of the second region that contains the fracture tip by V_2. Then

$$V_1(t) = 2\int_0^{x_{max}} h(t,x)dx, \tag{5.7.59}$$

$$V_2(t) = 2\int_{x_{max}}^{L(t)} h(t,x)dx. \tag{5.7.60}$$

By using (5.7.44) for $h(t,x)$ we obtain

$$V_1(t) = \frac{V_o}{L(t)}\left[1 - \left(\frac{n+2}{2(n+1)}\right)^{\frac{n+1}{n}}\right], \tag{5.7.61}$$

$$V_2(t) = \frac{V_o}{L(t)}\left[\frac{n+2}{2(n+1)}\right]^{\frac{n+1}{n}}, \tag{5.7.62}$$

where V_o is the initial volume of the fracture given by (5.7.43) and L(t) is the length of the fracture given by (5.7.41). We see that

$$V_1(t) + V_2(t) = \frac{V_o}{L(t)} = V(t) \tag{5.7.63}$$

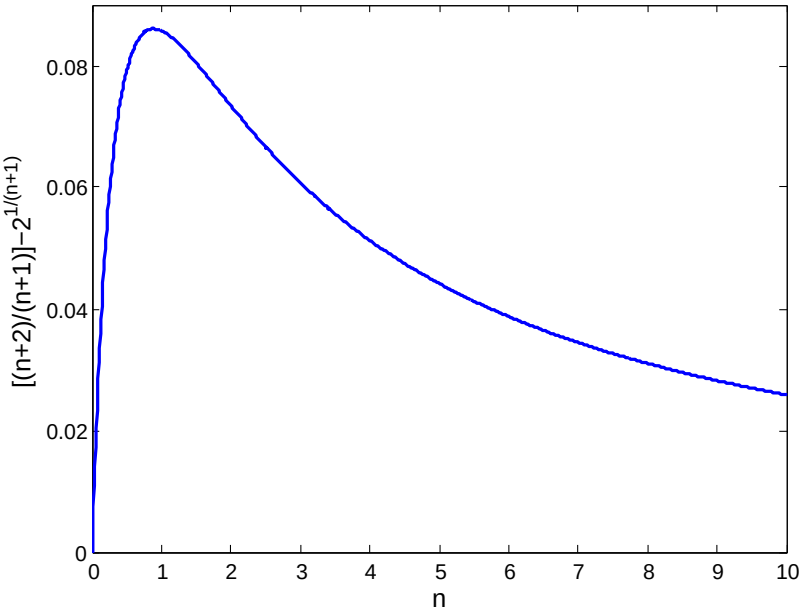

Figure 5.10: Condition for V_2 to be greater than V_1

by (5.7.42). Since $L(t) \to \infty$ as $t \to \infty$ it follows that $V_1(t) \to 0$ and $V_2(t) \to 0$ as $t \to \infty$ which is consistent with fluid extraction from the fracture. Also $V_2 > V_1$ provided

$$\frac{n+2}{n+1} - 2^{\frac{1}{n+1}} > 0. \tag{5.7.64}$$

Figure 5.10 shows that the condition (5.7.64) is satisfied for all $n > 0$. Therefore V_2 is always greater than V_1 since $n > 0$. Now

$$\frac{V_1}{V_2} = \left[\frac{2(n+1)}{(n+2)}\right]^{\frac{n+1}{n}} - 1. \tag{5.7.65}$$

Although $V_1(t)$ and $V_2(t)$ separately depend on time, the ratio V_1/V_2 is independent of time. It can be verified analytically that

$$\lim_{n\to\infty} \frac{V_1}{V_2} = 1, \qquad \lim_{n\to 0} \frac{V_1}{V_2} = \exp\left(\frac{1}{2}\right) - 1 \approx 0.6487 \tag{5.7.66}$$

and therefore

$$\lim_{n\to\infty} \frac{V_2}{V_1} = 1, \qquad \lim_{n\to 0} \frac{V_2}{V_1} \approx 1.5415. \tag{5.7.67}$$

Graphs of the ratios V_1/V_2 and V_2/V_1 against n are shown in Figure 5.11. We see from the graphs that V_1/V_2 increases monotonically with n and V_2/V_1 decreases monotonically

with n to the limiting value of one. Since $V_2 > V_1$ therefore the ratio $\frac{V_1}{V_2}$, which is between zero and one, is monotonically increasing while the ratio $\frac{V_2}{V_1}$, which is greater than one, is monotonically decreasing. Both ratios tend towards the limit $V_2/V_1 = V_1/V_2 = 1$. This is clearly shown in Figure 5.11.

Consider now the graphs of the working conditions α against n plotted in Figure 5.12.

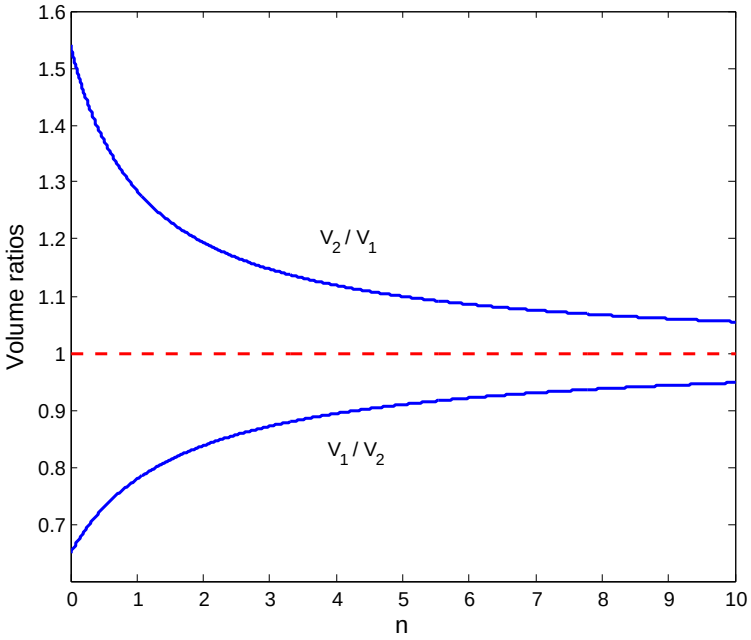

Figure 5.11: Ratio of volumes curves

Values of α above the curve $\alpha = 1/(n+2)$, which describes a fracture evolving with constant volume, yield solutions of fluid injection at the fracture entry. Working conditions in the range $1/[2(n+1)] \leq \alpha < 1/(n+2)$, yield solutions of fluid extraction at the fracture entry. The association of the Lie point symmetry of the governing PDE, (5.1.1), with the conserved vectors for the PDE, analysed in Section 5.4, lead to the constant volume working condition, $\alpha = 1/(n+2)$, and the limiting fluid extraction working condition, $\alpha = 1/[2(n+1)]$. Both cases were solved analytically. Furthermore, we observe that these two working conditions serve as boundaries of the fluid extraction region. We have taken the upper boundary of the fluid injection region to be $\alpha = 1$ which describes a fracture propagating with constant speed. Fluid injection solutions exist for $\alpha > 1$ but they may not be physical because their speed of propagation would always be accelerating. The

lower boundary for fluid injection is the constant volume working condition. We observe that the working conditions representing the boundaries of the fluid injection problem are also solved analytically. In Figure 5.12, values of α in the purple shaded area yield

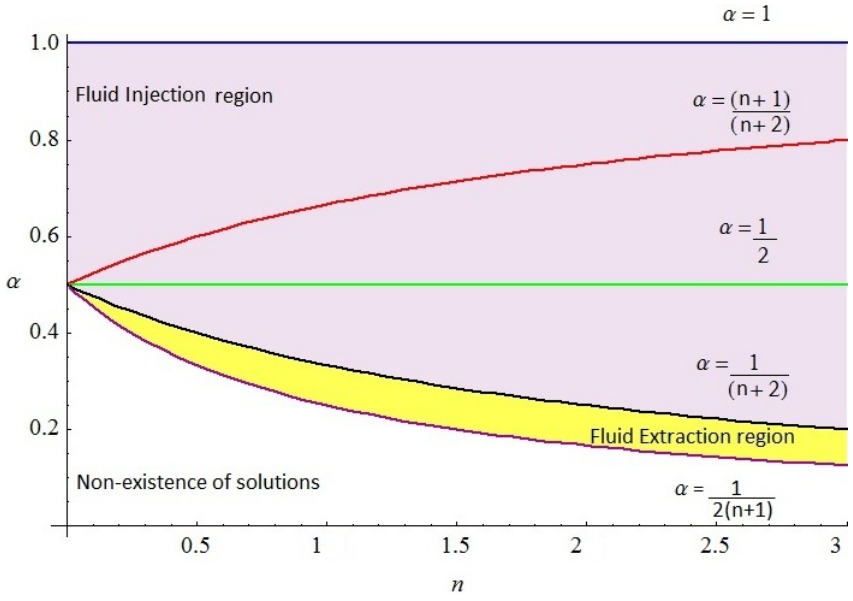

Figure 5.12: Working conditions in the fracture

solutions of fluid injection at the fracture entry and therefore the purple area represents the fluid injection region while values of α in the yellow shaded area lead to solutions of fluid extraction at the fracture entry and therefore the yellow area represents the fluid extraction region. For values of α in the white unshaded area, solutions do not exist because the limiting solution, corresponding to $\alpha = 1/[2(n+1)]$, describes a fracture that is closed at the fracture entry.

While the working conditions defined by boundaries for the fluid injection and extraction regions yield analytical solutions, solutions for working conditions within the fluid injection and extraction regions in Figure 5.12 cannot be solved analytically. They will therefore be investigated numerically in the next Section.

5.8 Numerical solution

In Section 5.7 we investigated and discussed three exact analytical solutions: for a fracture propagating with constant volume, $\alpha = 1/(n+2)$; for a fracture propagating with constant speed, $\alpha = 1$, and for a fracture with fluid extracted at the fracture entry, $\alpha = 1/[2(n+1)]$. These working conditions were found to be boundaries of the fluid injection region, $1/(n+2) < \alpha \leq 1$, and the fluid extraction region, $1/[2(n+1)] \leq \alpha < 1/(n+2)$. We were not able to find analytical solution for working conditions within the ranges $1/(n+2) < \alpha < 1$ and $1/[2(n+1)] < \alpha < 1/(n+2)$, hence numerical solution for values of α within these two regions will be investigated.

For fluid injection, the working conditions that will be investigated numerically are $\alpha = (n+1)/(n+2)$ for a fracture that propagates with a constant rate of fluid injection at the fracture entry and $\alpha = 1/2$ for a fracture that propagates with a constant fluid pressure of injection at the fracture entry. These conditions were discussed earlier in this Chapter and are listed in Table 5.1. For fluid extraction, the working conditions that will be numerically investigated will be discussed and specified later in this Section. The numerical method used in this Section is that of transforming a boundary value problem into two initial value problems that are easier to solve. Solving the pair of initial value problems is equivalent to solving the original boundary value problem. The method has been used in the literature to solve Blasius-type boundary value problems and will be discussed in detail in this Section prior to deriving the numerical solutions.

5.8.1 Transformation of BVP to two IVPs

Attempting to numerically solve the boundary value problem, (5.3.5) to (5.3.7), as it stands, is difficult because of the nonlinearity in the ordinary differential equation (5.3.5) and the complicated boundary condition, (5.3.7), that has an integral function. The method of solution considered in this thesis requires transforming the boundary value problem, (5.3.5) to (5.3.7), into two initial value problems which are easier to solve. Solv-

ing the two initial value problems is equivalent to solving the original boundary value problem.

This method of transforming a boundary value problem into a pair of initial value problems was first used to solve the Blasius boundary value problem for steady two-dimensional flow of an incompressible fluid past a flat plate placed edgewise to the stream [48, 49]. Ames [50] showed that if an ordinary differential equation and boundary conditions are invariant under a scaling transformation, then the boundary value problem can be transformed into two initial value problems. Klamkin [49] considers an ordinary differential equation with a homogeneous boundary condition at the left end on an infinite interval. Na [51, 52] extends the method and shows it can also be used in finite intervals. Klamkin [53] further shows that the same method of solution can be used when the left end boundary condition is not homogeneous.

We first consider a scaling transformation of the variables of the form

$$\overline{u} = \lambda^a u, \quad \overline{f} = \lambda^b f, \tag{5.8.1}$$

where a and b are constants to be determined. Substituting the transformation (5.8.1) into the ordinary differential equation (5.3.5) gives

$$\lambda^{2a-nb}\frac{d}{d\overline{u}}\left(\overline{f}^n\frac{d\overline{f}}{d\overline{u}}\right) + \frac{d}{d\overline{u}}(\overline{u}\overline{f}) + \frac{1}{n}\left(\frac{1}{\alpha} - (n+2)\right)\overline{f} = 0. \tag{5.8.2}$$

The ordinary differential equation (5.3.5) is invariant under the scaling transformation (5.8.1) provided

$$b = \frac{2}{n}a. \tag{5.8.3}$$

Now, we take $a = 1$. The ODE (5.3.5) is therefore invariant under the scaling transformation

$$\overline{u} = \lambda u, \tag{5.8.4}$$

$$\overline{f}(\overline{u}) = \lambda^{\frac{2}{n}} f(u). \tag{5.8.5}$$

The method of Lie group analysis can be used to give an alternative derivation of this scaling transformation, [12]. The transformation, (5.8.4) and (5.8.5), will now be used to transform the boundary value problem, (5.3.5) to (5.3.7), into two initial value problems.

The transformation, (5.8.4) and (5.8.5), is substituted into the boundary value problem, (5.3.5) to (5.3.7). We choose $\overline{f}(0) = 1$ which then gives

$$f(0) = \lambda^{-\frac{2}{n}} \tag{5.8.6}$$

that is used in the second initial value problem. The parameter λ is found from the condition $\overline{f}(\lambda) = 0$ which is derived from the boundary condition $f(1) = 0$. The first initial value problem is:

Initial value problem I (IVP I)

$$\frac{d}{d\overline{u}}\left(\overline{f}^n \frac{d\overline{f}}{d\overline{u}}\right) + \frac{d}{d\overline{u}}(\overline{u}\overline{f}) + \frac{1}{n}\left(\frac{1}{\alpha} - (n+2)\right)\overline{f} = 0, \tag{5.8.7}$$

$$\overline{f}(0) = 1, \tag{5.8.8}$$

$$\frac{d\overline{f}}{d\overline{u}}(0) = \frac{1}{n}\left(\frac{1}{\alpha} - (n+2)\right)\int_0^{\lambda} \overline{f}(\overline{u})d\overline{u}, \tag{5.8.9}$$

where $0 \leq \overline{u} \leq \lambda$ and λ satisfies

$$\overline{f}(\lambda) = 0. \tag{5.8.10}$$

Substituting the scaling transformation, (5.8.4) and (5.8.5), into the first initial value problem, (5.8.7) to (5.8.9), gives

$$\frac{d}{du}\left(f^n \frac{df}{du}\right) + \frac{d}{du}(uf) + \frac{1}{n}\left(\frac{1}{\alpha} - (n+2)\right)f = 0, \tag{5.8.11}$$

$$f(0) = \lambda^{-\frac{2}{n}}, \tag{5.8.12}$$

$$\frac{df}{du}(0) = \frac{\lambda^2}{n}\left(\frac{1}{\alpha} - (n+2)\right)\int_0^1 f(u)du. \tag{5.8.13}$$

The condition (5.8.10) is satisfied in the second initial value problem through the parameter λ featured in equations (5.8.11) to (5.8.13). Now, instead of using equation (5.8.13) for the derivative boundary condition, we consider the simpler alternative obtained by

differentiating (5.8.5) with respect to u and evaluating the result at $u = 0$. This gives the second initial value problem:

Initial value problem II (IVP II)

$$\frac{d}{du}\left(f^n \frac{df}{du}\right) + \frac{d}{du}(uf) + \frac{1}{n}\left(\frac{1}{\alpha} - (n+2)\right) f = 0, \tag{5.8.14}$$

$$f(0) = \lambda^{-\frac{2}{n}}, \tag{5.8.15}$$

$$\frac{df}{du}(0) = \lambda^{\frac{n-2}{n}} \frac{d\overline{f}}{d\overline{u}}(0), \tag{5.8.16}$$

where $0 \leq u \leq 1$ and λ and $\frac{d\overline{f}}{d\overline{u}}(0)$ are obtained from IVP I.

The first initial value problem, (5.8.7) to (5.8.9), is used to calculate the value of the parameter λ using the condition (5.8.10). The second initial value problem (5.8.14) to (5.8.16) is used to calculate the solution of $f(u)$ using the values of the parameter λ and $\frac{d\overline{f}(0)}{d\overline{u}}$ obtained from the first initial value problem.

The initial value problems (5.8.7) to (5.8.9) and (5.8.14) to (5.8.16) are solved using the built-in MATLAB ode45 solver which solves the problems using variable stepsize Runge Kutta methods of order 4 and 5 [54]. For IVP I the MATLAB ode45 solver is combined with the shooting method in the backward direction. We use the asymptotic solution

$$\overline{f}(\overline{u}) \sim \lambda^{\frac{1}{n}} n^{\frac{1}{n}} (\lambda - \overline{u})^{\frac{1}{n}}, \quad \text{as} \quad \overline{u} \to \lambda, \tag{5.8.17}$$

obtained by applying the transformation, (5.8.4) and (5.8.5), to the asymptotic solution (5.6.4) for $f(u)$. Differentiating (5.8.17) by $\overline{u}$ gives

$$\frac{d\overline{f}}{d\overline{u}}(\overline{u}) \sim -\lambda^{\frac{1}{n}} n^{\frac{1-n}{n}} (\lambda - \overline{u})^{\frac{1-n}{n}}, \quad \text{as} \quad \overline{u} \to \lambda. \tag{5.8.18}$$

For the first initial value problem in the first iteration, a solution obtained by ode45 is shot to the $\overline{f}$-axis from the chosen estimate of the root λ, with the slope at that point, $d\overline{f}/d\overline{u}$, (5.8.18). A solution for the first initial value problem is accepted provided both initial

conditions, (5.8.8) and (5.8.9), are satisfied within an error tolerance of 10^{-10}. If the two initial conditions are not satisfied, the procedure is repeated in the second and subsequent iterations until the initial conditions are satisfied. Parameter values of λ and derivative function values at λ for the subsequent iterations are obtained from the previous iteration. The parameter λ is improved at each iteration by the bisection algorithm.

Prior to solving the two initial value problems for the working conditions for fluid extraction, $1/[2(n+1)] < \alpha < 1/(n+2)$, and fluid injection, $1/(n+2) < \alpha < 1$, it is necessary to first check the accuracy of the numerical method. This can be done by solving the two initial value problems, (5.8.7) to (5.8.9) and (5.8.14) to (5.8.16), numerically for the cases $\alpha = 1$ and $\alpha = 1/(n+2)$ and comparing them with the exact analytical solutions for the same working conditions obtained in Section 5.7. The accuracy of the numerical method cannot be checked using the fluid extraction working condition $\alpha = 1/[2(n+1)]$ because this is a special case that does not satisfy the condition (5.8.8) but instead satisfies the condition $\overline{f}(0) = 0$. For constant volume, $\alpha = 1/(n+2)$, it is readily verified that the first initial value problem when analytically solved gives

$$\overline{f}(\overline{u}) = \left(\frac{n}{2}\right)^{\frac{1}{n}} \left(\frac{2}{n} - \overline{u}^2\right)^{\frac{1}{n}}, \quad \lambda = \left(\frac{2}{n}\right)^{\frac{1}{2}}, \quad \frac{d\overline{f}}{d\overline{u}}(0) = 0. \tag{5.8.19}$$

The second initial value problem for constant volume when analytically solved gives the solution (5.7.6) for $f(u)$. For constant speed of propagation, $\alpha = 1$, the first initial value problem gives

$$\overline{f}(\overline{u}) = n^{\frac{1}{2n}} \left(\frac{1}{\sqrt{n}} - \overline{u}\right)^{\frac{1}{n}}, \quad \lambda = \frac{1}{\sqrt{n}}, \quad \frac{d\overline{f}}{d\overline{u}}(0) = -\frac{1}{\sqrt{n}}, \tag{5.8.20}$$

while the second initial value problem for a fracture propagating at constant speed when analytically solved gives the solution (5.7.17) for $f(u)$. It is therefore verified that solving the two initial value problems is the same as solving the boundary value problem. For both constant volume and constant speed, while the analytical solutions (5.7.6) and (5.7.17) serve as a check for the second initial value problem, the analytical solutions (5.8.19) and (5.8.20) serve as a check for the first initial value problem. For constant volume and constant speed, it remains to solve the two initial value problems numerically and check if the results correspond with the exact analytical results given in (5.7.6), (5.7.17), (5.8.19)

and (5.8.20). We have verified that numerically solving IVP I for constant volume and constant speed working conditions gives values of the parameter λ and the derivative $\frac{d\bar{f}}{d\bar{u}}(0)$ that are at least correct to 3 decimal places when compared to (5.8.19) and (5.8.20). We have also found that the order of accuracy of λ and $\frac{d\bar{f}}{d\bar{u}}(0)$ obtained from IVP I is sufficient to give numerical solutions for $f(u)$ that agree very well with the analytical solution for $f(u)$, (5.7.6) and (5.7.17). The solutions for $h(t,x)$ obtained numerically overlap the half-width curves obtained analytically and shown in Figures 5.1, 5.2, 5.3 and 5.4. The numerical method performed very well for the two test problems. We therefore expect it to perform satisfactorily for the initial value problems corresponding to the working conditions $1/[2(n+1)] < \alpha < 1$. For values of α close to the fluid extraction limit, $1/[2(n+1)]$, we can expect that the numerical solution will not be too different from the analytical solution for $\alpha = 1/[2(n+1)]$ which will provide another test for the method.

5.8.2 Fluid injection $[1/(n+2) < \alpha < 1]$

Now consider solutions for two working conditions defined within the fluid injection region, $\alpha = 1/2$ and $\alpha = (n+1)/(n+2)$. Figures 5.13 and 5.14 show the solution for the half-width of the fracture propagating over time when fluid is injected at the fracture entry with constant pressure, $\alpha = 1/2$, and Figures 5.15 and 5.16 show the solution of the half-width of the fracture propagating over time when fluid is injected into the fracture at the fracture entry at a constant rate, $\alpha = (n+1)/(n+2)$. The parameter n has the same effect on these problems as it did for the analytical solutions discussed earlier, that is for $n > 1$ the lubrication approximation breaks down at the fracture tip because of the infinite spatial gradient of the half-width of the fracture at the fracture tip, and more interestingly, for $0 < n \leq 1$, the singularity is removed at the fracture tip.

From equation (5.3.20), where $f_{max} = f(0)$ for fluid injection, the half-width of the fracture at the fracture entry, where $K_n t_\tau$ is the scaled transition time from an initially partially open fracture to an open fracture or from an initially open fracture to a partially

open fracture, is given by

$$h(t_\tau, 0) = \beta\left(1 + \frac{1}{\alpha}\Big(\frac{\beta}{f(0)}\Big)^n K_n t_\tau\right)^{\frac{2}{n}\left(\alpha-\frac{1}{2}\right)}. \tag{5.8.21}$$

We first consider the constant pressure working condition, $\alpha = 1/2$. Then (5.8.21) reduces to

$$h(t_\tau, 0) = \beta, \quad t \geq 0. \tag{5.8.22}$$

From (5.8.22), it is clear that for the constant pressure working condition the scaled transition time $K_n t_\tau$ does not exist since the parameter β is a constant independent of time. This implies that for $\alpha = 1/2$, an initially partially open fracture ($0 < \beta < 1$) stays partially open for all scaled time $K_n t$ and an initially open fracture ($\beta \geq 1$) stays open for all scaled time $K_n t$.

We then consider $\alpha \neq 1/2$. In order to obtain the scaled transition time, $K_n t_\tau$, when either an initially partially open fracture becomes an open fracture or an initially open fracture becomes a partially open fracture, it is neccessary to set the half-width of the fracture at the fracture entry equal to one. Thus from (5.8.21),

$$\beta\left(1 + \frac{1}{\alpha}\Big(\frac{\beta}{f(0)}\Big)^n K_n t_\tau\right)^{\frac{2}{n}\left(\alpha-\frac{1}{2}\right)} = 1, \tag{5.8.23}$$

and solving for $K_n t_\tau$ gives

$$K_n t_\tau = \alpha\Big(\frac{f(0)}{\beta}\Big)^n \left[\Big(\frac{1}{\beta}\Big)^{\frac{n}{2\alpha-1}} - 1\right]. \tag{5.8.24}$$

We consider $\alpha > 1/2$. If a fracture is initially open, then $\beta > 1$ and $K_n t_\tau < 0$, which is not physical since a time scale has to be positive. Thus an initially open fracture remains open for all scaled time $K_n t$. This is in agreement with Figure 5.4 for the analytical solution for $\alpha = 1$ and Figure 5.16 for the numerical solution for $\alpha = (n+1)/(n+2)$. If a fracture is initially partially open, then $0 < \beta < 1$ and $K_n t_\tau > 0$. Therefore an initially partially open fracture will become an open fracture at the scaled transition time $K_n t_\tau$ given by (5.8.24). The contact regions will all have moved apart. We then consider $0 < \alpha < 1/2$. Then it helps with physical interpretation to write (5.8.24) as

$$K_n t_\tau = \alpha\Big(\frac{f(0)}{\beta}\Big)^n \Big[\beta^{\frac{n}{1-2\alpha}} - 1\Big]. \tag{5.8.25}$$

If the fracture is initially open then $\beta > 1$ and $K_n t_\tau > 0$. After the scaled transition

time (5.8.25), all the asperities at the fluid-rock interface touch forming contact regions that classify the fracture as partially open. If the fracture is initially partially open the $0 < \beta < 1$ and $K_n t_\tau < 0$, which is not physical since a time scale has to be positive. Therefore an initially partially open fracture remains partially open for all scaled time $K_n t$. This is in agreement with the analytical solution for $\alpha = 1/(n+2)$, shown in Figure 5.1.

For $\alpha = 1/2$ in Figures 5.13 and 5.14, the length of the fracture grows with increasing scaled time $K_n t$ while the half-width of the fracture at the fracture entry is the same for all scaled time $K_n t$. This occurs because, through the PKN approximation, fluid pressure is directly proportional to the half-width of the fracture, therefore when the fluid pressure at the fracture entry is constant, so is the half-width of the fracture at the fracture entry. For $\alpha = (n+1)/(n+2)$ in Figures 5.15 and 5.16, the length of the model fracture grows more rapidly than the half-width of the model fracture for increasing scaled time $K_n t$.

The lengths, (5.3.21), of partially open fractures, $\beta = 0.5$, for different working conditions listed in Table 5.1 are investigated in Figure 5.17. The fracture lengths are plotted against increasing scaled time $K_n t$ and compared for $n = 3$, 1 and 0.5. The touching asperities forming contact regions first move apart forming an open fracture for the constant speed of propagation working condition, $\alpha = 1$. This occurs at $K_n t_\tau = 168$ for $n = 3$, at $K_n t_\tau = 2$ for $n = 1$ and at $K_n t_\tau = 0.29$ for $n = 0.5$. The lengths in Figure 5.17 (a) for all working conditions investigated in the fluid injection region are plotted up to the scaled transition time $K_n t_\tau = 168$ for $\alpha = 1$. In Figure 5.17 (b) and (c) the remaining lengths are plotted up to the scaled transition times for an initially partially open fracture with constant rate-of-fluid injection to form an open fracture. For such a fracture $K_n t_\tau = 577.67$ for $n = 3$, $K_n t_\tau = 8.26$ for $n = 1$ and $K_n t_\tau = 1.58$ for $n = 0.5$. The two initially partially open fractures, with working conditions of constant pressure and constant volume, remain partially open for all scaled time $K_n t$. From Figure 5.17, it is clear that in a partially open fracture the length of the fracture becomes less dependent on the operating conditions at the fracture entry as n decreases and the flow becomes more tortuous. This is consistent with Table 5.1 where α, the exponent in (5.3.21) for $L(t)$ for both fluid injection and extraction, tends to the constant pressure value, $\alpha = 1/2$, as $n \to 0$.

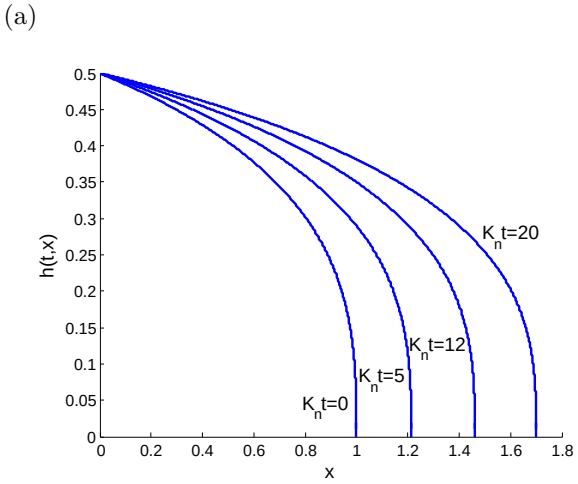

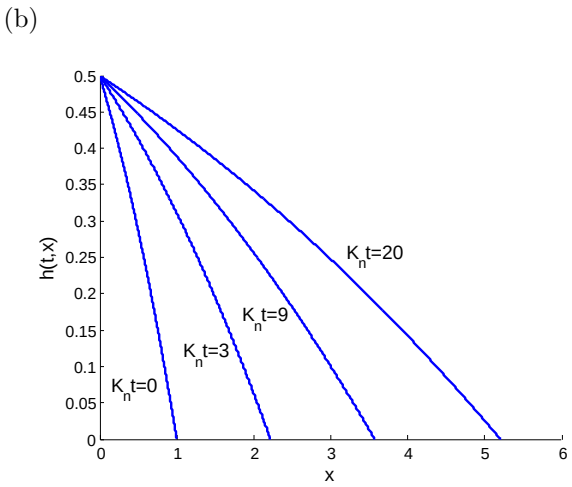

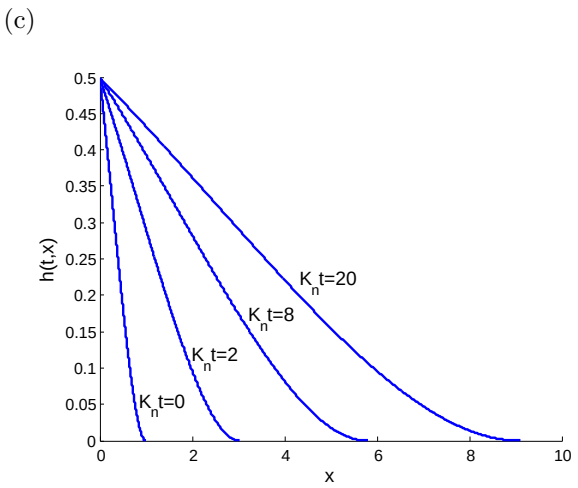

Figure 5.13: Partially open fracture ($\beta = 0.5$) propagating with $\alpha = 1/2$. The numerical solution (5.3.20) for the half-width $h(t, x)$ plotted against x for increasing values of the scaled time $K_n t$ and (a) $n = 3$, (b) $n = 1$, (c) $n = 0.5$.

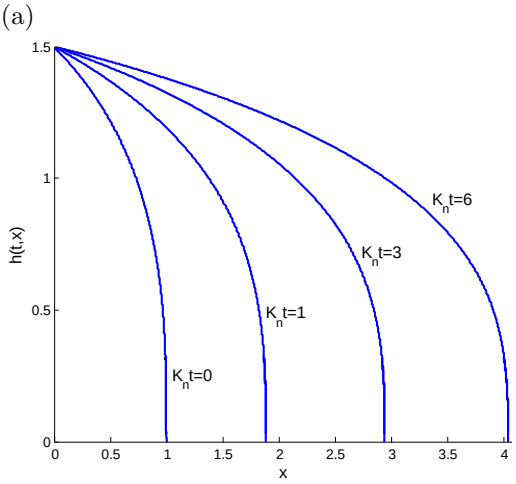

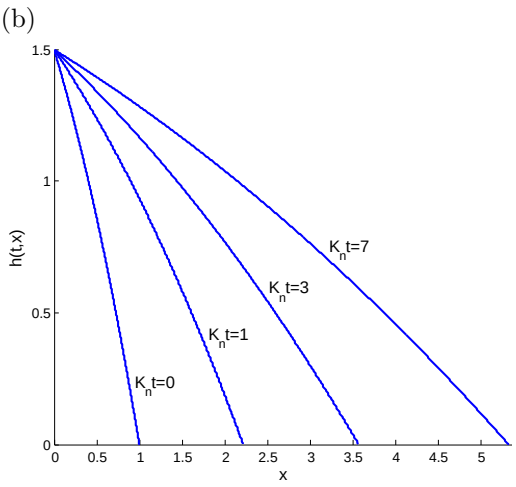

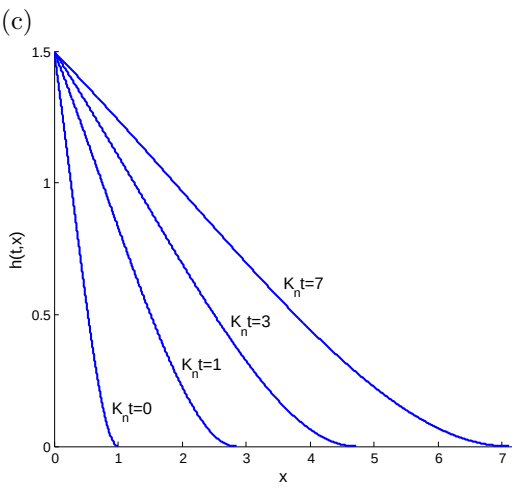

Figure 5.14: Open fracture ($\beta = 1.5$) propagating with $\alpha = 1/2$. The numerical solution (5.3.20) for the half-width $h(t, x)$ plotted against x for increasing values of the scaled time $K_n t$ and (a) $n = 3$, (b) $n = 1$, (c) $n = 0.5$.

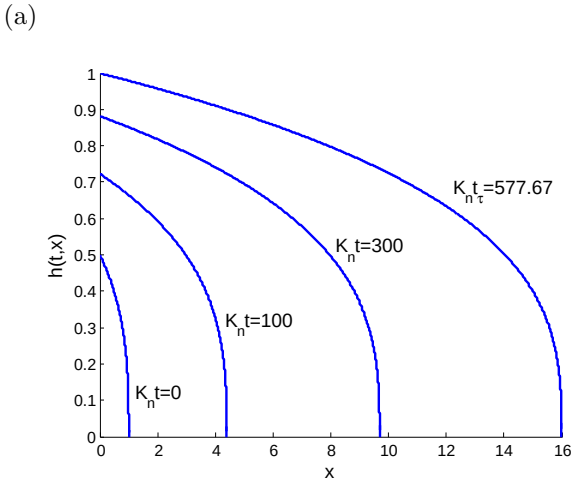

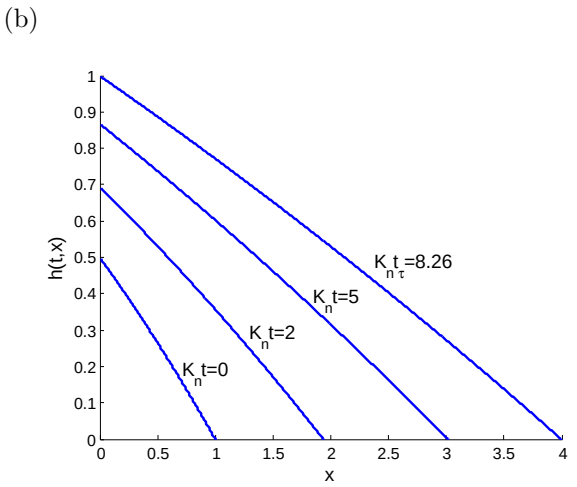

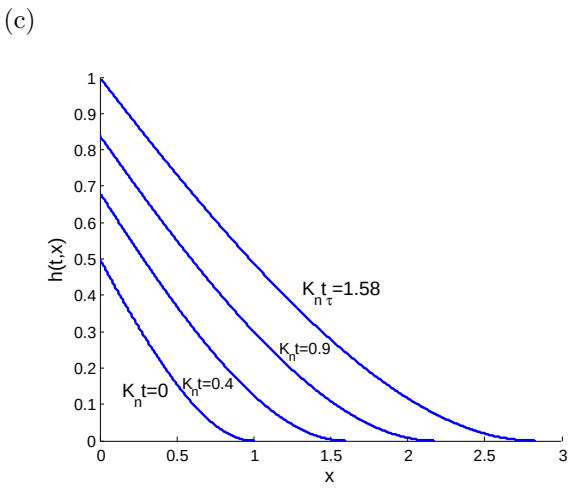

Figure 5.15: Partially open fracture ($\beta = 0.5$) propagating with $\alpha = \frac{n+1}{n+2}$. The numerical solution (5.3.20) for the half-width $h(t, x)$ plotted against x for increasing values of the scaled time $K_n t$ and (a) $n = 3$, (b) $n = 1$, (c) $n = 0.5$.

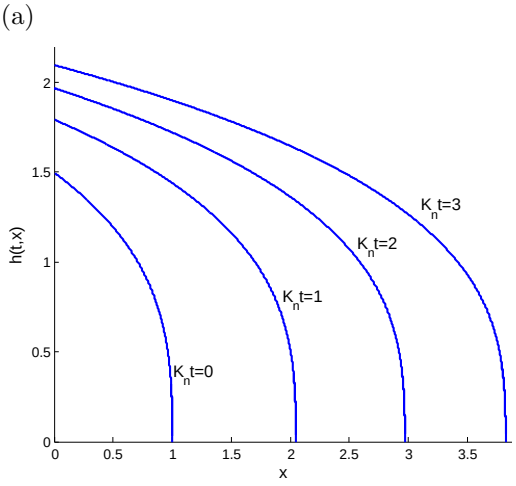

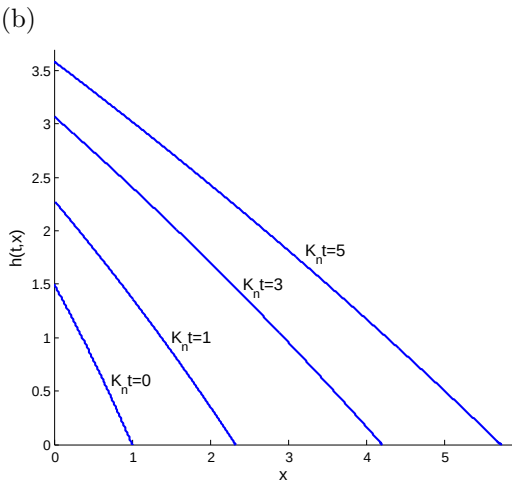

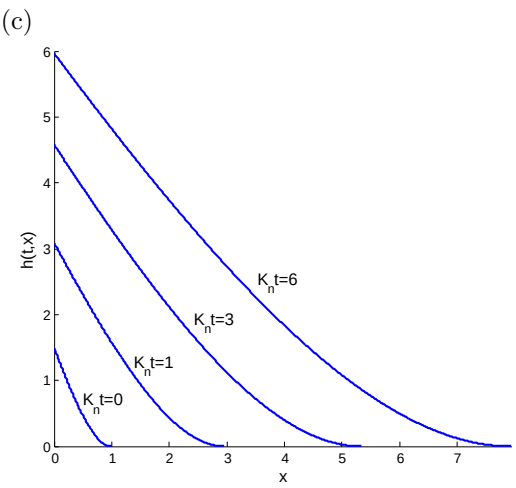

Figure 5.16: Open fracture ($\beta = 1.5$) propagating with $\alpha = \frac{n+1}{n+2}$. The numerical solution (5.3.20) for the half-width $h(t, x)$ plotted against x for increasing values of the scaled time $K_n t$ and (a) $n = 3$, (b) $n = 1$, (c) $n = 0.5$.

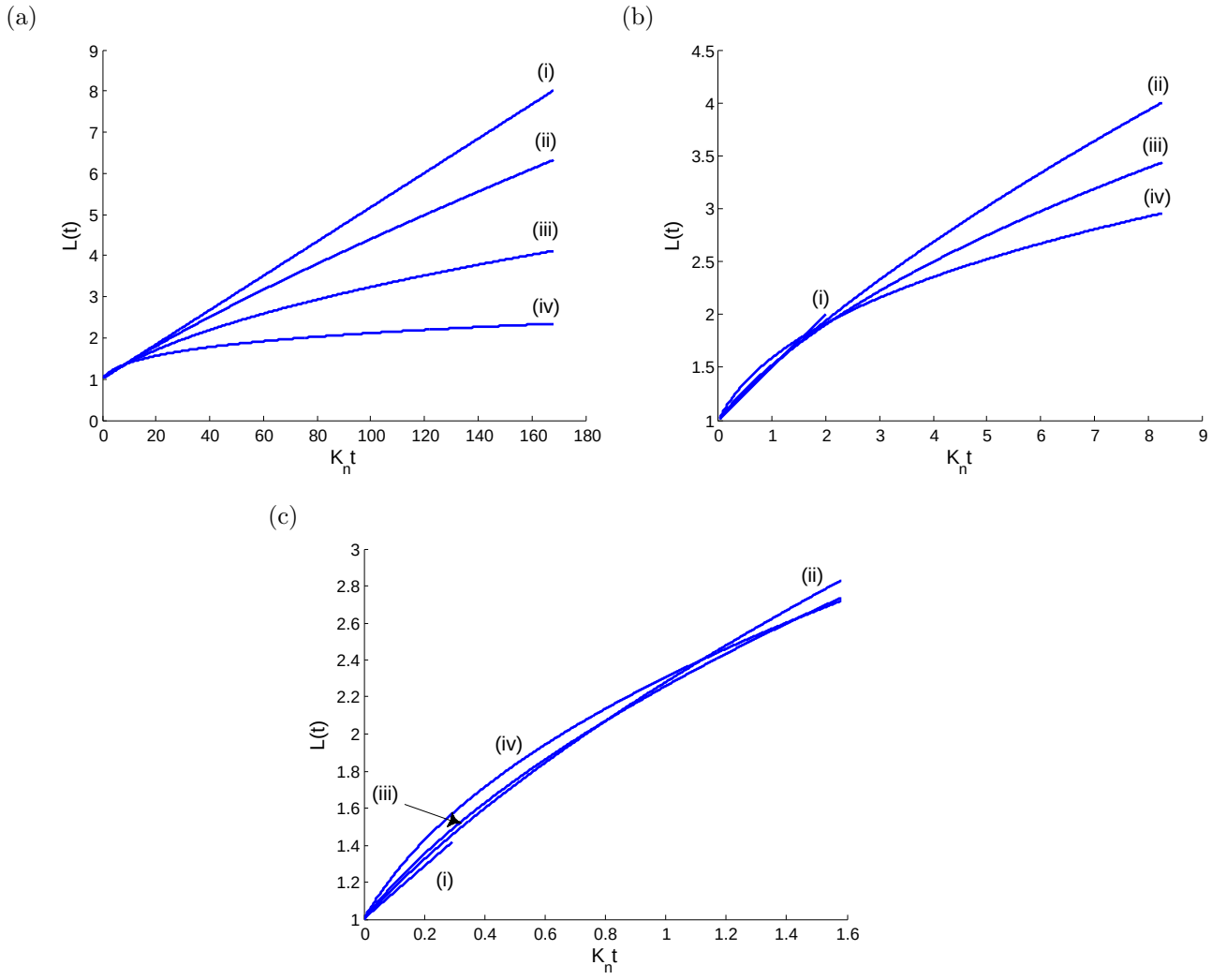

Figure 5.17: The length $L(t)$ of a partially open fracture with $\beta = 0.5$ plotted against the scaled time $K_n t$ for (a) $n = 3$, (b) $n = 1$, (c) $n = 0.5$ and for working conditions (i) constant speed of propagation, (ii) constant rate of fluid injection, (iii) constant pressure at the fracture entry and (iv) constant volume. In (a) lengths are plotted until the transition time for (i) to form an open fracture while in (b) and (c) until the transition time for (ii) to form an open fracture.

The limit analysis from Table 5.1 further suggests that the lengths of all working conditions dependent on n, both in the fluid injection and extraction regions, tend to behave like the length of the constant pressure working condition when $n \to 0$ and the fluid flow becomes more tortuous. This result is verified for fluid injection, in Figure 5.17, but still remains to be verified for fluid extraction.

5.8.3 Fluid extraction $[1/[2(n+1)] < \alpha < 1/(n+2)]$

We now investigate solutions of the boundary value problem and therefore the group invariant solution of the half-width of the fracture corresponding to working conditions within the fluid extraction region. This implies that we consider values of α that are in the range $1/[2(n+1)] < \alpha < 1/(n+2)$. We define a working condition within the fluid extraction region as

$$\alpha = \frac{1}{\gamma n + 2}, \qquad 1 < \gamma < 2. \tag{5.8.26}$$

Note that when $\gamma = 1$, (5.8.26) reduces to the constant volume working condition, $\alpha = 1/(n+2)$, and when $\gamma = 2$, (5.8.26) reduces to the limiting fluid extraction working condition, $\alpha = 1/[2(n+1)]$, both working conditions that are boundaries of the fluid extraction region. For all $n > 0$, we consider two values of α within the fluid extraction domain. We choose $\gamma = 4/3$ that reduces (5.8.26) to $\alpha = 3/[2(2n+3)]$ and $\gamma = 5/3$ that reduces (5.8.26) to $\alpha = 3/(5n+6)$. Figures 5.18 and 5.19 show the numerical solution of the half-width of the fracture plotted against x for a range of scaled times $K_n t$ when $\alpha = 3/[2(2n+3)]$ and Figures 5.20 and 5.21 show similar plots of the numerical solutions for the half-width of the fracture when $\alpha = 3/(5n+6)$. All values of α defined within the fluid extraction region, $1/[2(n+1)] \leq \alpha < 1/(n+2)$, are less than $1/2$. It follows that if a fracture is initially open then $\beta > 1$ and $K_n t_\tau > 0$. After the scaled transition time

$$K_n t_\tau = \alpha \left(\frac{f_{max}}{\beta} \right)^n (\beta^{\frac{n}{1-2\alpha}} - 1), \tag{5.8.27}$$

where $f_{max} \neq f(0)$, all the asperities at the fluid-rock interface touch forming contact regions and therefore transforming an open fracture to a partially open fracture. If the fracture is initially partially open then $0 < \beta < 1$ and $K_n t_\tau < 0$, which is not physical since a time scale has to be positive. Therefore an initially partially open fracture remains partially open for all scaled time $K_n t$. This is in agreement with the analytical solutions for $\alpha = 1/(n+2)$, shown in Figure 5.1, and for $\alpha = 1/[2(n+1)]$, shown in Figure 5.5. This is also in agreement with the numerical solutions for $\alpha = 3/[2(2n+3)]$, shown in Figure 5.18, and for $\alpha = 3/(5n+6)$, shown in Figure 5.20.

We see from Figures 5.18 to 5.21 that the tortuosity parameter n has a similar effect on

the fracture tips for working conditions defined in the fluid extraction region as in the fluid injection region, that is, for $n > 1$ there a is singularity at the fracture tip and therefore the lubrication approximation breaks down while for $0 < n \leq 1$ the spatial derivative of the half-width of the fracture at the fracture tip is finite and therefore the lubrication approximation is satisfied: for $n = 1$ the spatial gradient at the fracture tip is non-zero while for $0 < n < 1$ it is zero. This agrees with the asymptotic solution at the fracture tip, (5.6.8).

Figures 5.18 to 5.21 show a positive slope in the neighbourhood of the fracture entry. This occurs until the analytical solution for $\alpha = 1/[2(n+1)]$, the limiting solution of fluid extraction (shown in Figures 5.5 and 5.6), is satisfied. For this solution the fracture entry is closed, $h(t, 0) = 0$. For fluid injection the slope of the half-width of the fracture in the neighbourhood of the fracture entry is negative, for constant volume the slope in the neighbourhood of the fracture entry is zero and for fluid extraction the slope of the half-width of the fracture in the neighbourhood of the fracture entry is positive. The limiting fluid extraction solution for the half-width of the fracture has an infinite positive slope at the fracture entry. Unlike in the fluid injection region, decreasing the value of α in the fluid extraction region results in decreasing the half-width of the fracture at the fracture entry, as seen in Figures 5.18 to 5.21. The gradual closing of the half-width of the fracture at the fracture entry will be investigated later in Section 5.8.4.

It is now necessary to investigate the manner in which the fluid flows out of the fracture at the fracture entry within the extraction region. For the limiting fluid extraction working condition, $\alpha = 1/[2(n + 1)]$, analysed in Section 5.7, it was found that during the fluid extraction process, as some fluid flows out of the fracture at the fracture entry, some other fluid relaxes further into the fracture causing the length of the fracture to continuously increase. This process was found to continue with increasing scaled time until in the limit $t \to \infty$, all the fluid was extracted from the fracture. It remains to investigate if the process of fluid extraction within the fluid extraction region behaves in the same way as that for the limiting fluid extraction solution.

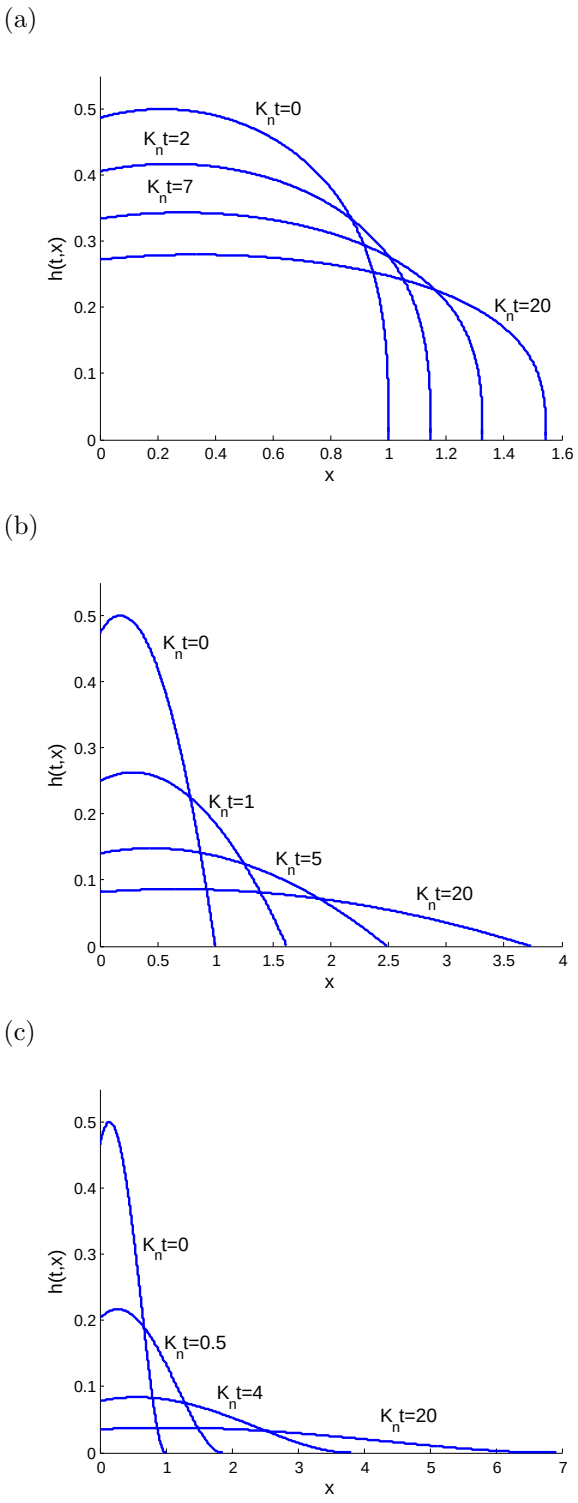

Figure 5.18: Partially open fracture ($\beta = 0.5$) propagating with $\alpha = \frac{3}{2(2n+3)}$. The numerical solution (5.3.20) for the half-width $h(t,x)$ plotted against x for increasing values of the scaled time $K_n t$ and (a) $n = 3$, (b) $n = 1$, (c) $n = 0.5$.

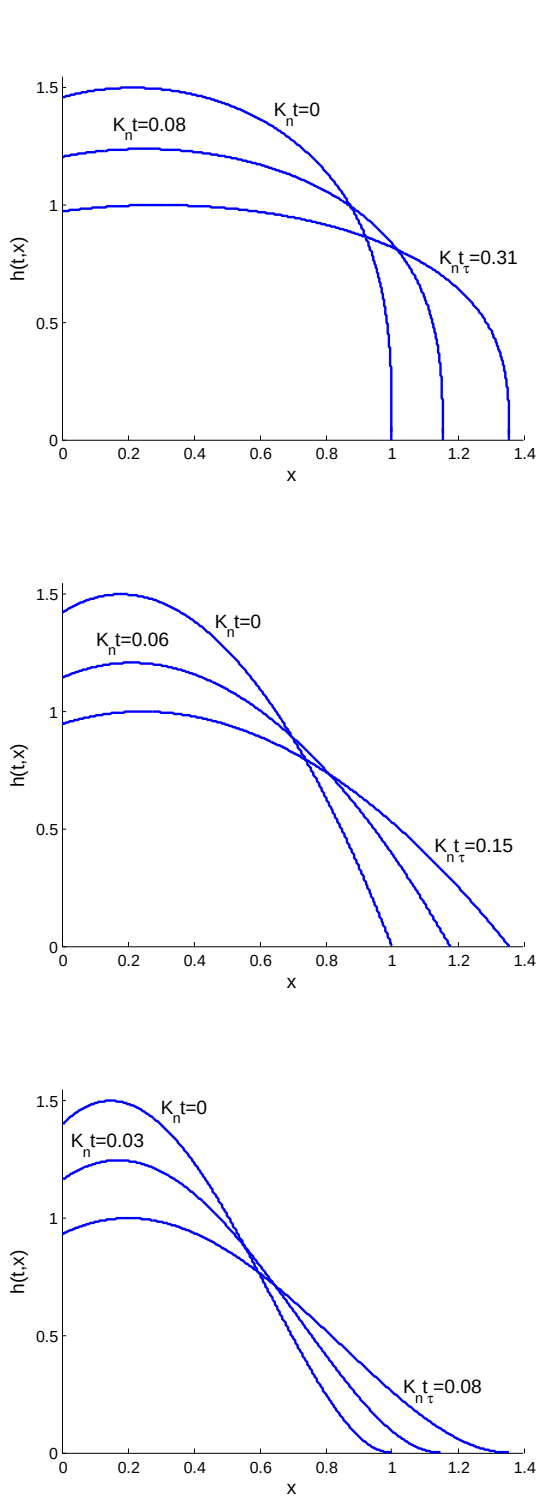

Figure 5.19: Open fracture ($\beta = 1.5$) propagating with $\alpha = \frac{3}{2(2n+3)}$. The numerical solution (5.3.20) for the half-width $h(t,x)$ plotted against x for increasing values of the scaled time $K_n t$ and (a) $n = 3$, (b) $n = 1$, (c) $n = 0.5$.

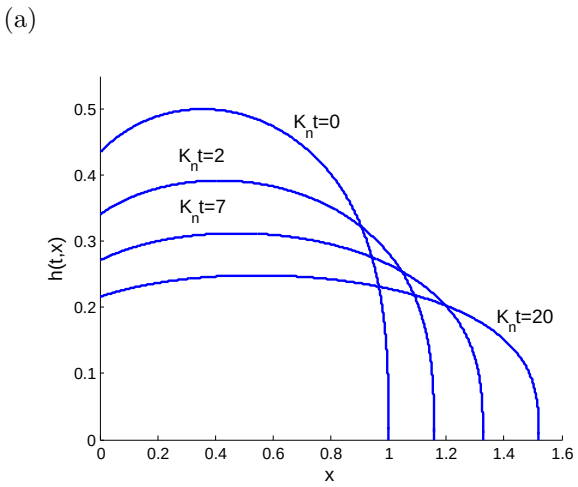

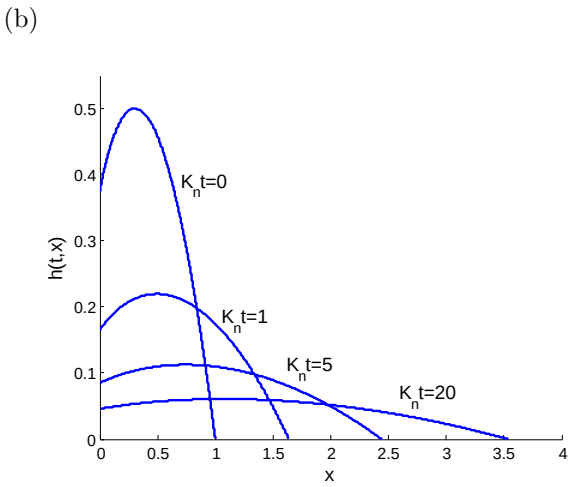

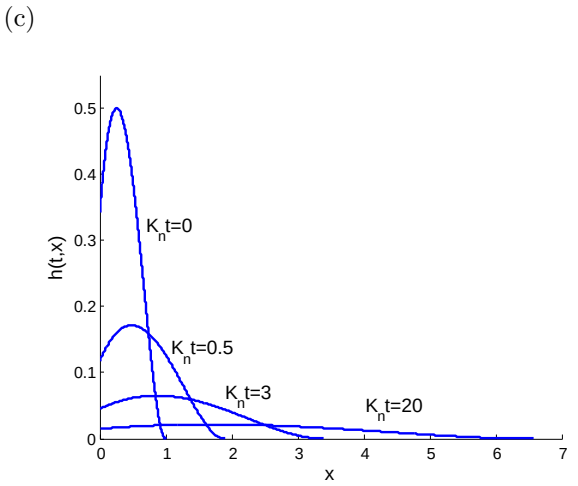

Figure 5.20: Partially open fracture ($\beta = 0.5$) propagating with $\alpha = \frac{3}{(5n+6)}$. The numerical solution (5.3.20) for the half-width $h(t,x)$ plotted against x for increasing values of the scaled time $K_n t$ and (a) $n = 3$, (b) $n = 1$, (c) $n = 0.5$.

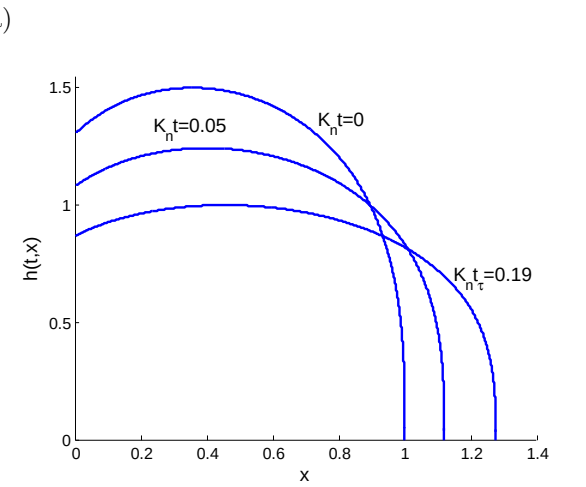

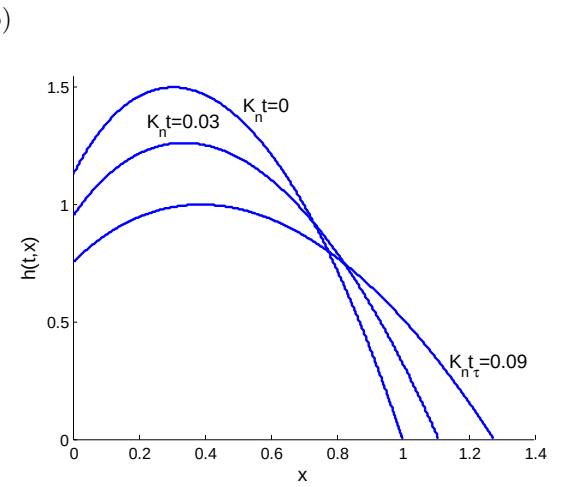

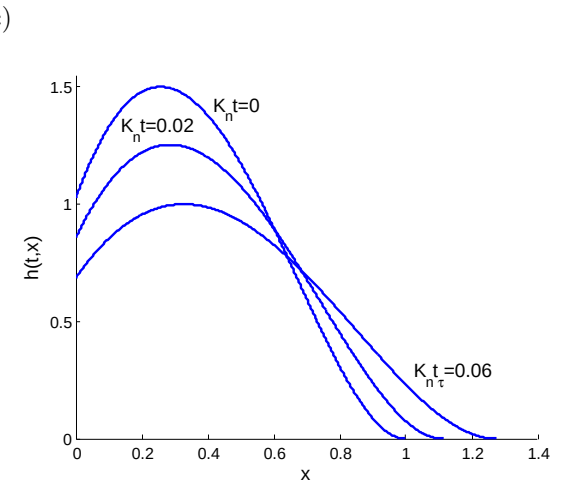

Figure 5.21: Open fracture ($\beta = 1.5$) propagating with $\alpha = \frac{3}{(5n+6)}$. The numerical solution (5.3.20) for the half-width $h(t,x)$ plotted against x for increasing values of the scaled time $K_n t$ and (a) $n = 3$, (b) $n = 1$, (c) $n = 0.5$.

In order to investigate the behaviour of fluid extraction for the working conditions $\alpha = 3/[2(2n+3)]$ and $\alpha = 3/(5n+6)$ defined within the fluid extraction region, it is necessary to analyse the fluid flux in the fracture, which is defined by equation (5.3.24). Although values of the diffusion constant K_n can be obtained through experiments for different values of n, these values are not readily available. We also want to keep the investigation general and not applicable to only some values of the physical quantities. Therefore when plotting, we consider the flux ratio

$$\frac{Q(t,x)}{|Q(0,0)|} = -\left[1 + \frac{1}{\alpha}\left(\frac{\beta}{f_{max}}\right)^n K_n t\right]^{\frac{n+2}{n}\left(\alpha - \frac{n+1}{n+2}\right)} \left(\frac{f(u)}{f(0)}\right)^n \left[\frac{df}{du} \Big/ \frac{df}{du}(0)\right], \qquad (5.8.28)$$

where both $Q(t,x)$ and $|Q(0,0)|$ are obtained from the general equation of fluid flux given by (5.3.24) with $u = x/L(t)$. The graphs of (5.8.28) against x at $t = 0$ for different values of n all start at the point $(0,-1)$ which is a useful property when comparing the fluid flux for a range of values of n. From (5.8.28) it is clear that the exponent of the flux ratio is always negative for any working condition chosen within the fluid extraction region. It therefore follows that $Q(t,x) \to 0$ as $t \to \infty$ for $0 \leq x \leq L(t)$. This result implies that for any chosen working condition within the fluid extraction region, all the fluid in the fracture has flowed out of the fracture at the fracture entry as $t \to \infty$.

Plotting (5.8.28) for working conditions $\alpha = 3/[2(2n+3)]$ and $\alpha = 3/(5n+6)$, corresponding to $\gamma = 4/3$ and $\gamma = 5/3$ respectively, and for $\beta = 0.5$ gives Figures 5.22 and 5.23. It is clear from these Figures that for working conditions within the fluid extraction region, as some of the fluid flows out of the fracture, some of the fluid relaxes further into the fracture increasing the length of the fracture. This occurs with increasing scaled time $K_n t$ until all of the fluid is extracted from the fracture as $t \to \infty$.

We now compare different values of α within the fluid extraction range, $1/[2(n+1)] \leq \alpha < 1/(n+2)$, for a chosen value of n in order to investigate which working condition yields the maximum rate of fluid extraction. In this analysis, we cannot use the fluid flux ratio, (5.8.28), because both $f(0)$ and $\frac{df}{du}(0)$ contained in $|Q(0,0)|$ depend on the parameter α and we cannot use $Q(t,x)$, given by (5.3.24), because K_n is not readily available.

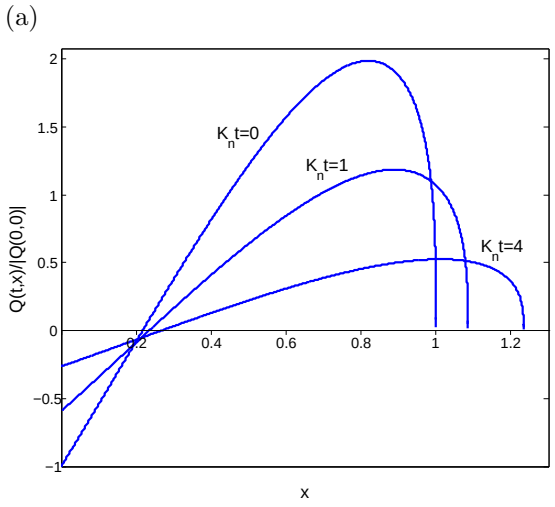

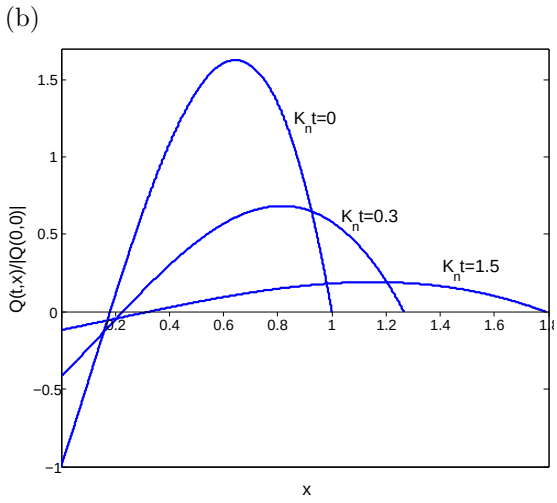

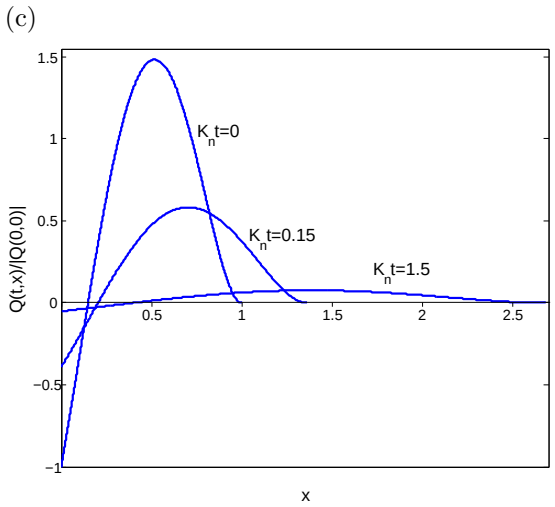

Figure 5.22: Fluid flux, (5.8.28), in a partially open fracture ($\beta = 0.5$) propagating with $\alpha = \frac{3}{2(2n+3)}$ plotted against x for increasing values of the scaled time $K_n t$ and for (a) $n = 3$, (b) $n = 1$, (c) $n = 0.5$.

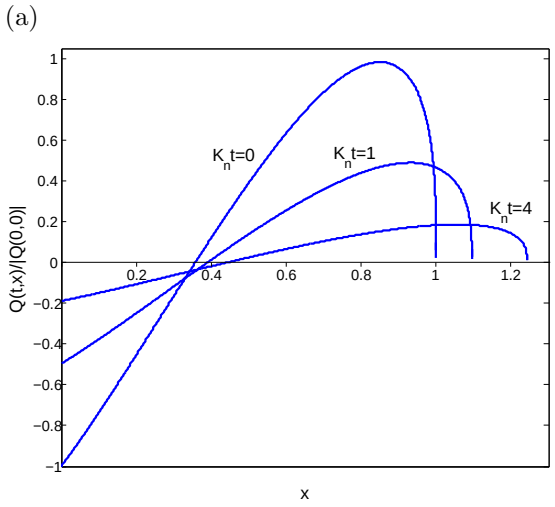

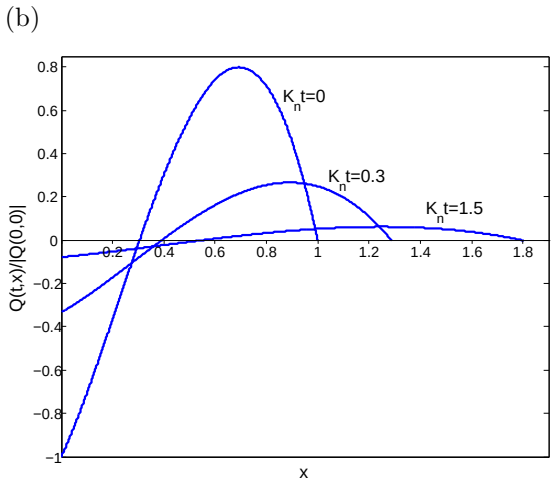

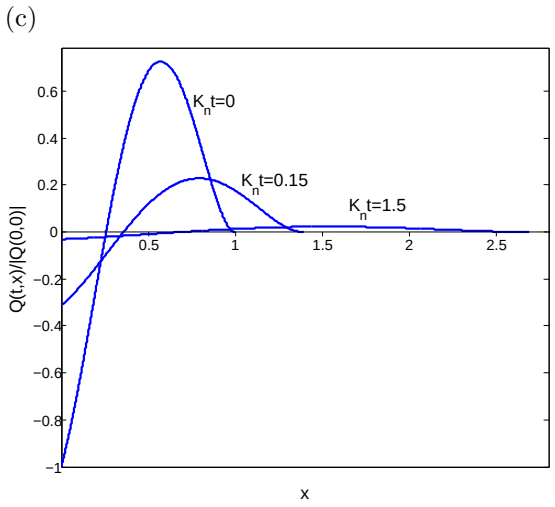

Figure 5.23: Fluid flux, (5.8.28), in a partially open fracture ($\beta = 0.5$) propagating with $\alpha = \frac{3}{(5n+6)}$ plotted against x for increasing values of the scaled time $K_n t$ and for (a) $n = 3$, (b) $n = 1$, (c) $n = 0.5$.

We therefore consider a different fluid flux ratio

$$\frac{Q(t,x)}{|Q(0,0)|_{\gamma=2}} = -\left(\frac{n^{\frac{n+1}{n+2}}(n+2)^{\frac{n+1}{n}}}{2^{\frac{2(n+1)^2}{n(n+2)}}(n+1)^{\frac{n^2+2n+2}{n(n+2)}}f_{max}^{n+1}}\right)\left[1+\frac{1}{\alpha}\left(\frac{\beta}{f_{max}}\right)^n K_n t\right]^{\frac{n+2}{n}\left(\alpha-\frac{n+1}{n+2}\right)} f^n(u)\frac{df}{du}, \tag{5.8.29}$$

where

$$|Q(0,0)|_{\gamma=2} = 2K_n\beta^{n+1}\left(\frac{2^{\frac{2(n+1)^2}{n(n+2)}}(n+1)^{\frac{n^2+2n+2}{n(n+2)}}}{n^{\frac{n+1}{n+2}}(n+2)^{\frac{n+1}{n}}}\right) \tag{5.8.30}$$

is the fluid flux derived from the limiting fluid extraction condition of $\gamma = 2$, $\alpha = 1/[2(n+1)]$, when $t = 0$ and $x = 0$. Since $|Q(0,0)|_{\gamma=2}$ depends only on $\alpha = 1/[2(n+1)]$, we can compare the fluid flow behaviour of different working conditions within the fluid extraction region for a chosen parameter n using (5.8.29). Figure 5.24 shows different fluid flow behaviour in the fracture for $n = 3$ and for (a) $\alpha = 1/[2(n+1)]$, (b) $\alpha = 3/(5n+6)$ and (c) $\alpha = 3/[2(2n+3)]$. From the negative fluid flux in Figure 5.24, it is clear that less fluid flows out of the fracture at the fracture entry ($x = 0$) for $t \geq 0$ when α is closer to the constant volume working condition, $1/(n+2)$, and more fluid flows out of the fracture at the fracture entry ($x = 0$) for $t \geq 0$ when α is closer to the limiting fluid extraction condition, $1/2(n+2)$. Furthermore, we see that the limiting fluid extraction condition gives the maximum rate of fluid extraction from the fracture. This is because $Q(t,0)$ is the most negative for $\alpha = 1/[2(n+1)]$ and $Q(t,0) = dV/dt$. We have verified that the same conclusion is drawn for $n = 1$ and for $n = 0.5$. This result will be further investigated later in this Chapter.

The length of the fracture for working conditions within the fluid extraction region are plotted in Figure 5.25. As $n \to 0$ and the flow becomes more tortuous, the length of the fracture becomes less dependent on the working conditions at the fracture entry and the graphs cluster around the solution for the limiting value $\alpha = 1/2$ in Figure 5.25. The exception is the limiting fracture for fluid extraction which propagates at a slower speed and its graph does not cluster with the other graphs in Figure 5.25. It was also found for fluid injection in Figure 5.17 that the length of the fracture becomes less depedent on the working conditions at the fracture entry as the flow becomes more tortuous.

(a)

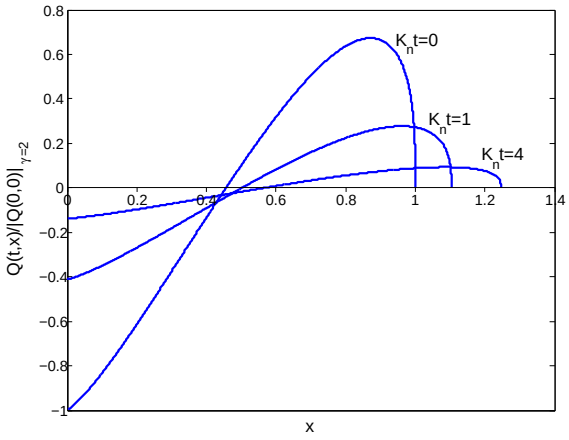

(b)

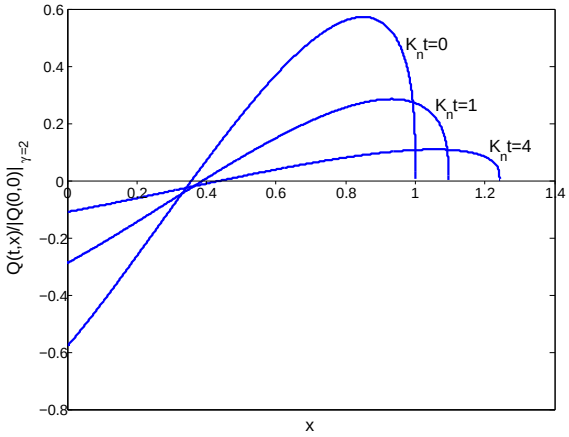

(c)

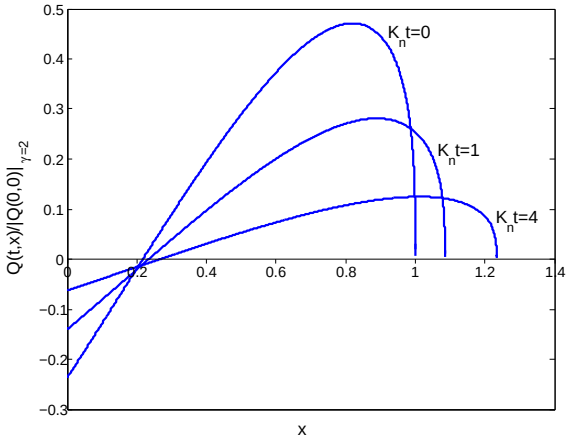

Figure 5.24: Fluid flux ratio $Q(t,x)/|Q(0,0)|_{\gamma=2}$ in a partially open fracture ($\beta = 0.5$) plotted against x with $n = 3$ and for the scaled times $K_n t = 0, 1$ and 4 and for working conditions (a) $1/[2(n+1)]$, (b) $3/(5n+6)$ and (c) $3/[2(2n+3)]$.

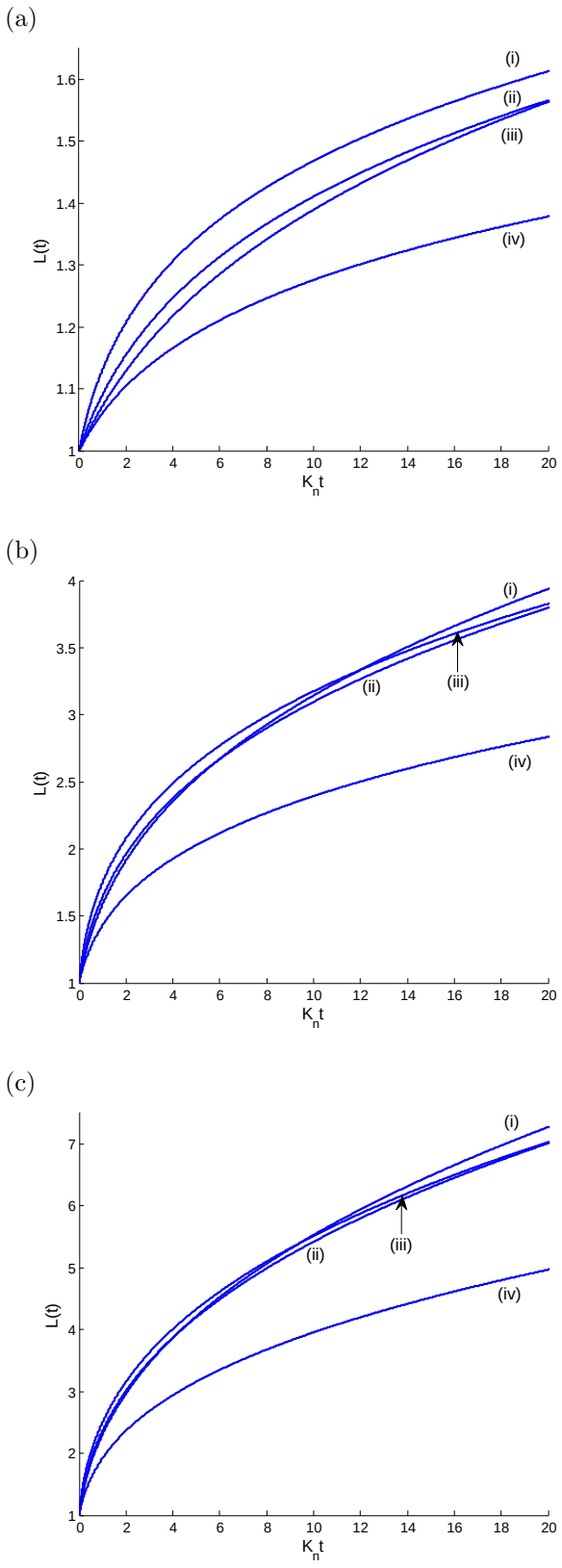

Figure 5.25: The length $L(t)$ of a partially open fracture with $\beta = 0.5$ plotted against the scaled time $K_n t$ for (a) $n = 3$, (b) $n = 1$, (c) $n = 0.5$ and for working conditions (i) $\alpha = 1/(n+2)$, (ii) $\alpha = 3/[2(2n+3)]$, (iii) $\alpha = 3/(5n+6)$ and (iv) $\alpha = 1/[2(n+1)]$.

5.8.4 Half-width at the fracture entry

In order to investigate the behaviour of the half-width at the fracture entry for different working conditions, we plot the half-width of the fracture, (5.3.20), against x at time $t = 0$ for $0 \leq x \leq 1$ and for different working conditions. The same conclusion that will be obtained in this analysis can be drawn when considering higher scaled times $K_n t$.

Figure 5.26 shows the initial half-width for different fluid injection working conditions and for the constant volume working condition. Figure 5.27 shows the initial half-width when fluid is extracted and when the volume of the fracture is constant. Figures 5.26 and 5.27 are plotted separately for clarity. From Figure 5.26 it is clear that all working conditions for fluid injection are characterized by a negative slope of the half-width at the fracture entry. The half-width at the fracture entry is the same for all working conditions with fluid injection and the same value of β. This is due to the fact that for fluid injection, the maximum half-width of the fracture is at the fracture entry. The constant volume working condition shown in both Figures 5.26 and 5.27 is characterized by the zero slope of the half-width at the fracture entry. Furthermore, the half-width at the fracture entry for a fracture with constant volume is the maximum half-width of the fracture. From Figure 5.27 it is clear that fluid extraction is characterized by a positive slope of the half-width at the fracture entry. Since the maximum half-width for any fluid extraction working condition is not at the fracture entry but at some distance x_{max} along the fracture, where x_{max} increases as α decreases, it follows that the half-width at the fracture entry decreases as α decreases. It starts to decrease after the constant volume working condition, $\alpha < 1/(n+2)$, and continues to decrease until the limiting fluid extraction working condition, $\alpha = 1/[2(n+1)]$, at which the minimum half-width at the fracture entry of zero is achieved. The limiting fluid extraction working condition shown in Figure 5.27 is characterized by a half-width at the fracture entry that has a positive and infinite spatial gradient which is the largest gradient at the fracture entry.

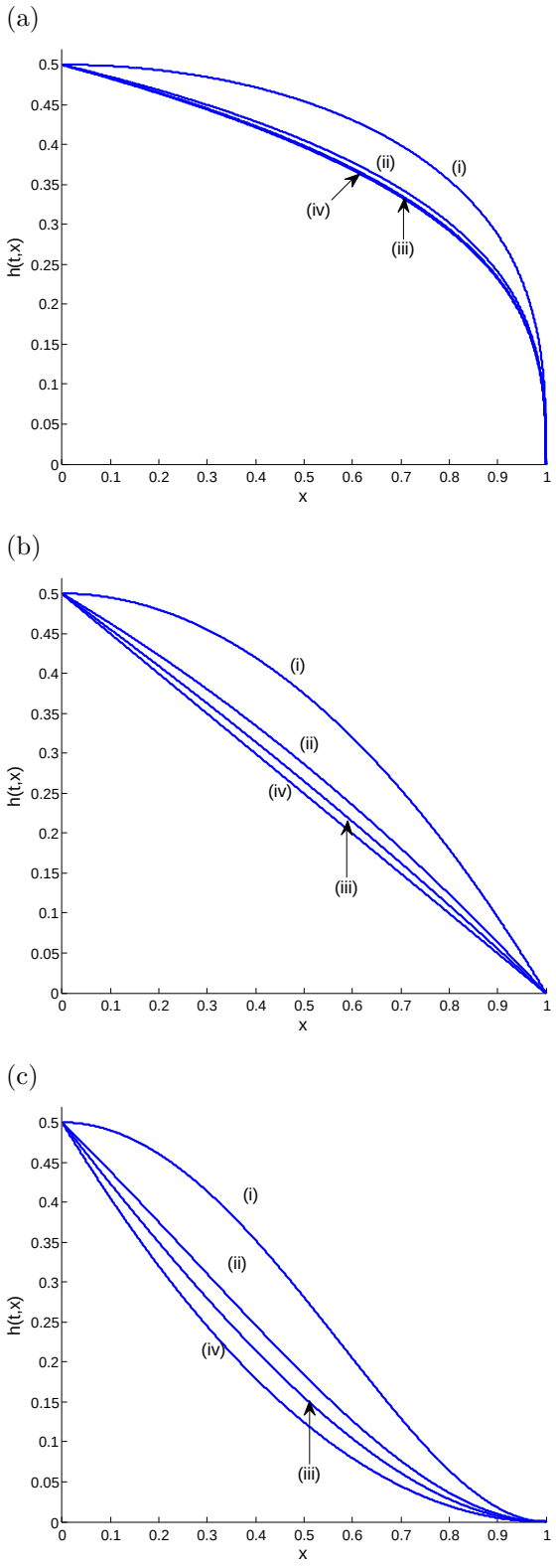

Figure 5.26: Partially open fractures, $\beta = 0.5$, for time $t = 0$. The half-width of the fracture plotted against x for working conditions (i) constant volume (ii) constant pressure (iii) constant rate of fluid injection (iv) constant speed of propagation and for (a) $n = 3$, (b) $n = 1$, (c) $n = 0.5$.

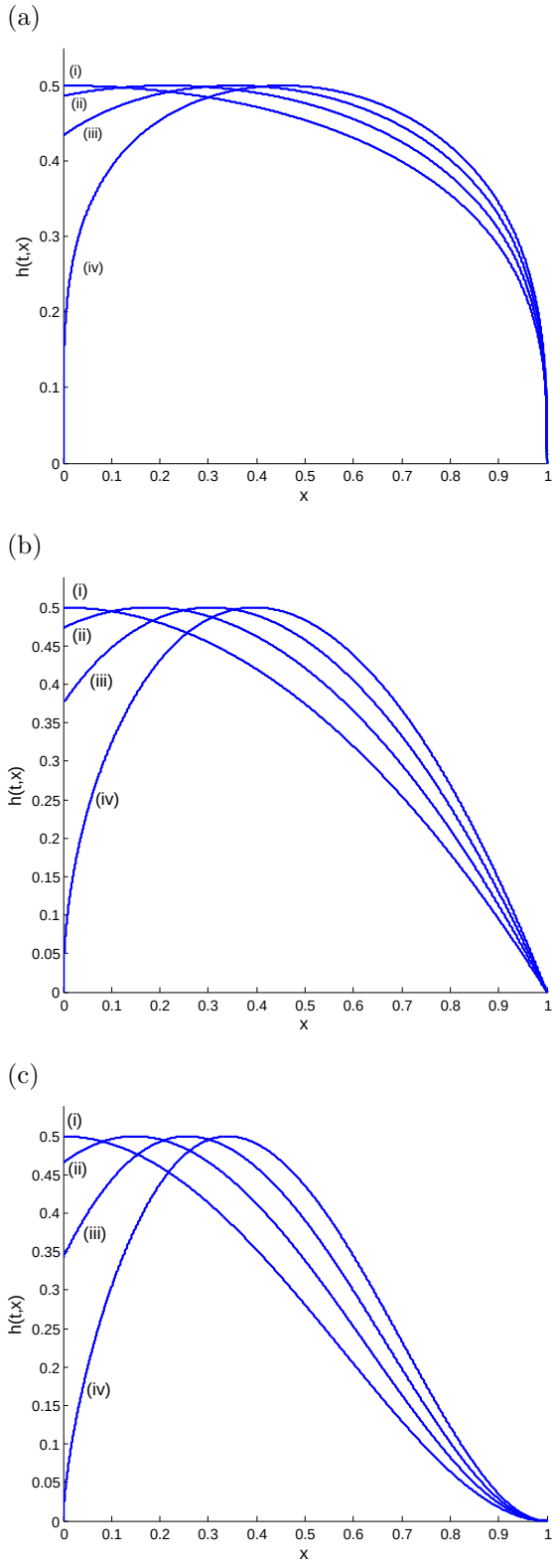

Figure 5.27: Partially open fractures ($\beta = 0.5$) for time $t = 0$. The half-width of the fracture plotted against x for working conditions (i) $\alpha = 1/(n+2)$ (ii) $\alpha = 3/[2(2n+3)]$ (iii) $\alpha = 3/(5n+6)$ (iv) $\alpha = 1/[2(n+1)]$ and for (a) $n = 3$, (b) $n = 1$, (c) $n = 0.5$.

5.9 Width averaged fluid velocity

In this Section, we analyse the width averaged fluid velocity because it is a good measure to investigate the behaviour of the fluid flow in the fracture given the very thin nature of the fracture. This is done by considering the ratio of the width averaged fluid velocity, (5.3.25), and the velocity at which the fracture propagates, dL/dt, obtained by differentiating the length of the fracture, (5.3.21):

$$\frac{\overline{v}_x}{\frac{dL(t)}{dt}} = -f^{n-1}(u)\frac{df}{du}, \quad 0 \leq u \leq 1. \tag{5.9.1}$$

The average is taken over the model fracture which replaces the actual fracture. The velocity ratio was investigated by Anthonyrajah et al. [37] for a fracture with turbulent fluid flow and by Fareo [30] for a fracture driven by a power law fluid. Since we have obtained analytical solutions for $f(u)$ and for the working conditions $\alpha = 1$, $\alpha = 1/(n+2)$ and $\alpha = 1/[2(n+1)]$, we can derive analytical expressions for the velocity ratio (5.9.1) for these working conditions.

For $\alpha = 1$, the analytical solution for $f(u)$ is (5.7.17) while the derivative of $f(u)$ is

$$\frac{df}{du} = -n^{\frac{1-n}{n}}(1-u)^{\frac{1-n}{n}}. \tag{5.9.2}$$

Substituting (5.7.17) and (5.9.2) into (5.9.1) gives the velocity ratio for the case when the rate of propagation of the fracture is kept constant:

$$\frac{\overline{v}_x}{\frac{dL(t)}{dt}} = 1. \tag{5.9.3}$$

From (5.9.3) it is clear that when the speed of propagation of the fracture is constant, the velocity ratio is constant everywhere along the length of the fracture.

For $\alpha = 1/(n+2)$, the analytical solution for $f(u)$ is given by (5.7.6) and the derivative of $f(u)$ is

$$\frac{df}{du} = -\left(\frac{n}{2}\right)^{\frac{1-n}{n}}(1-u^2)^{\frac{1-n}{n}}u. \tag{5.9.4}$$

Substituting (5.7.6) and (5.9.4) into (5.9.1) gives the velocity ratio for the case when the volume of the fracture is kept constant:

$$\frac{\overline{v}_x}{\frac{dL(t)}{dt}} = u. \tag{5.9.5}$$

From (5.9.5), it is clear that when the volume of the fracture is kept constant, the velocity ratio increases linearly along the length of the fracture.

The working conditions $\alpha = 1$ and $\alpha = 1/(n+2)$ have velocity ratios that are independent of n, (5.9.3) and (5.9.5). This is clearly shown in Figure 5.28 and implies that for these working conditions, tortuosity does not have any effect on the width averaged fluid velocity.

For $\alpha = 1/[2(n+1)]$, the solution for $f(u)$ is given by (5.7.36) and the derivative of $f(u)$ is

$$\frac{df}{du} = \left(\frac{n}{n+2}\right)^{\frac{1}{n}} (n+1)^{\frac{1-n}{n}} \left(1 - u^{\frac{n+2}{n+1}}\right)^{\frac{1}{n}} u^{-\frac{n}{n+1}} - \left[\frac{n(n+1)}{(n+2)}\right]^{\frac{1-n}{n}} \left(1 - u^{\frac{n+2}{n+1}}\right)^{\frac{1-n}{n}} u^{\frac{2}{n+1}}. \tag{5.9.6}$$

Substituting (5.7.36) and (5.9.6) into (5.9.1) gives the velocity ratio for the limiting fluid extraction working condition:

$$\frac{\overline{v}_x}{\frac{dL(t)}{dt}} = \frac{2(n+1)}{(n+2)} u - \frac{n}{(n+2)} u^{-\frac{1}{n+1}}. \tag{5.9.7}$$

From (5.9.7) it is clear that when the limiting fluid extraction working condition is satisfied, the parameter n and therefore the tortuous nature of the fracture has an effect on the width averaged fluid velocity. This is shown in Figure 5.29.

The velocity ratio curves for both fluid injection and fluid extraction working conditions are drawn in separate Figures for clarity. The velocity ratio curves for the fluid injection working conditions $\alpha = 1$, $\alpha = (n+1)/(n+2)$ and $\alpha = 1/2$ are shown on Figure 5.28 and velocity ratio curves for the fluid extraction working conditions $\alpha = 3/[2(2n+3)]$, $\alpha = 3/(5n+6)$ and $\alpha = 1/[2(n+1)]$ are shown on Figure 5.29. The velocity ratio curves for a fracture with constant volume are shown in Figures 5.28 and 5.29.

For fluid injection, $1/(n+2) < \alpha \leq 1$, equations (5.9.3) and (5.9.5) and Figure 5.28 clearly show that for constant volume and constant speed of propagation working conditions the velocity ratio curves are straight lines. Furthermore, from Figure 5.28 it is clear that the constant rate of fluid injection and the constant pressure working conditions yield velocity ratio curves that increase approximately linearly along the length of the fracture.

This result motivates the investigation of approximate analytical solutions in Section 5.10.

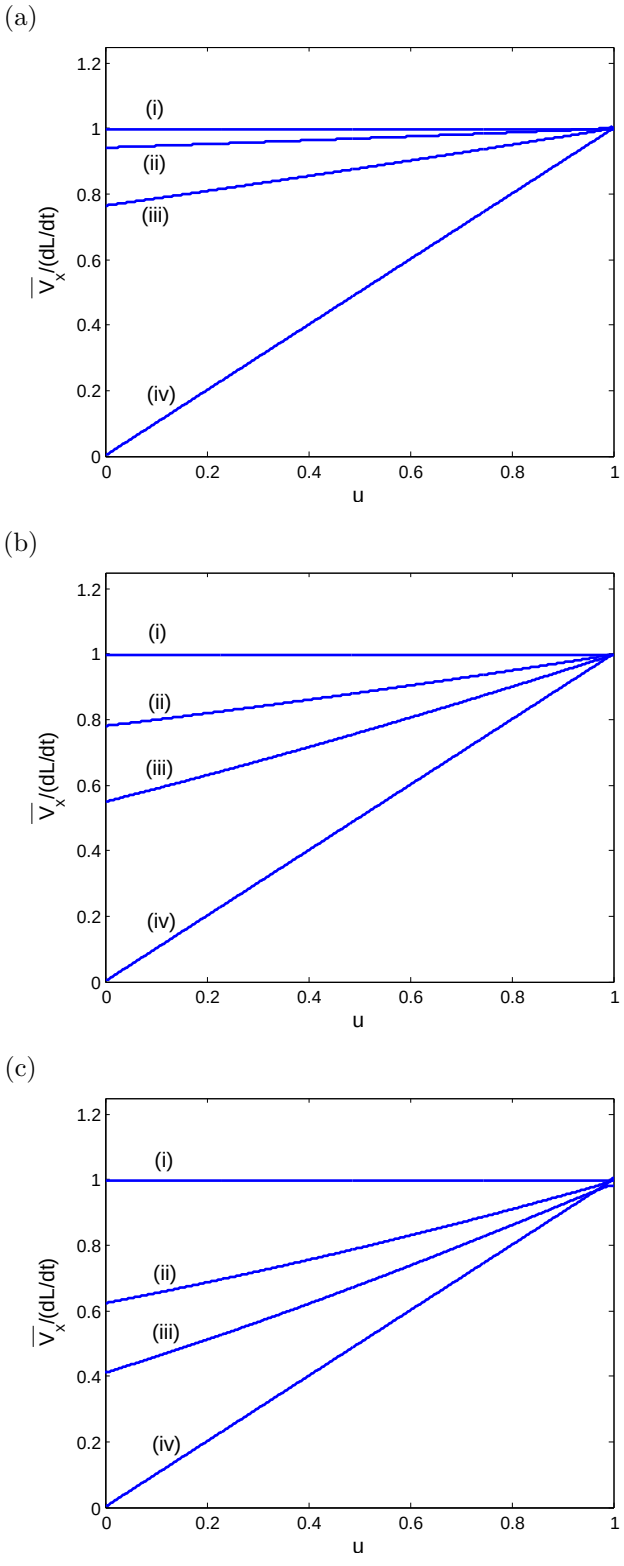

Figure 5.28: Velocity ratios $\overline{v}_x/\frac{dL}{dt}$ plotted against u for working conditions (i) $\alpha = 1$ (constant speed), (ii) $\alpha = (n+1)/(n+2)$ (constant rate of fluid injection), (iii) $\alpha = 1/2$ (constant pressure) and (iv) $\alpha = 1/(n+2)$ (constant volume), and for (a) $n = 3$, (b) $n = 1$, (c) $n = 0.5$.

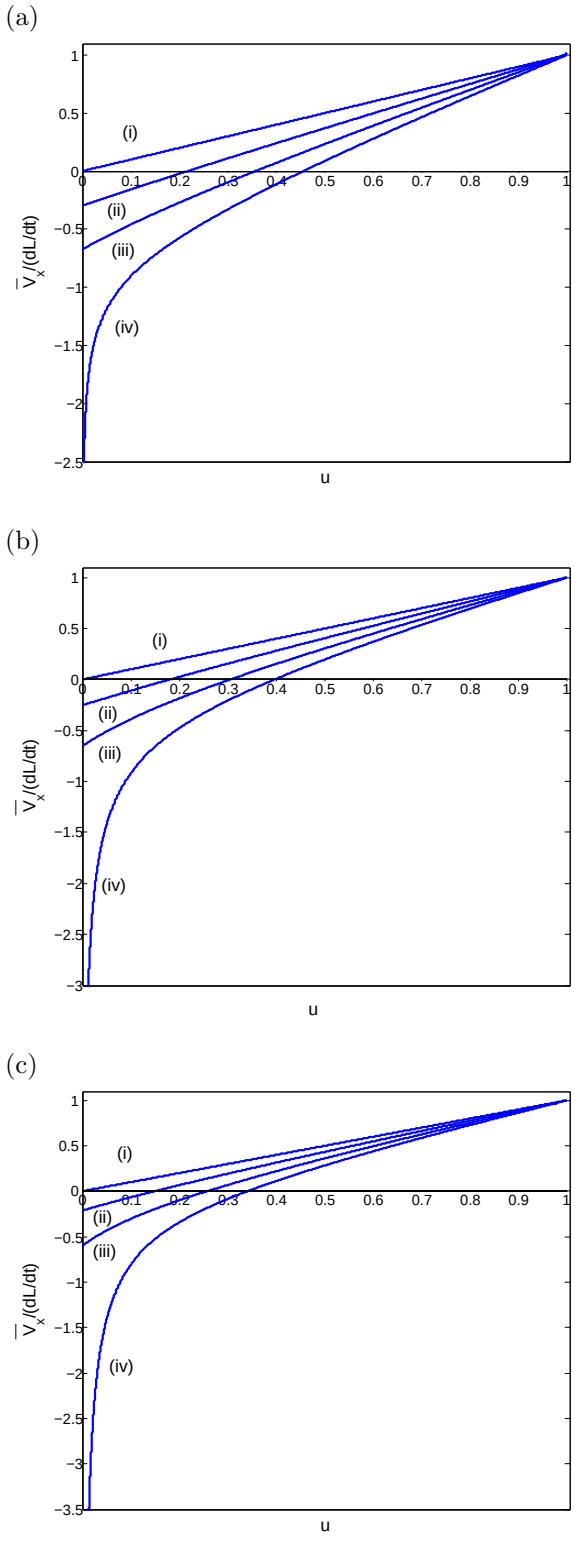

Figure 5.29: Velocity ratios $\overline{v}_x/\frac{dL}{dt}$ plotted against u for working conditions (i) $\alpha = 1/(n+2)$ (constant volume), (ii) $\alpha = 3/[2(2n+3)]$, (iii) $\alpha = 3/(5n+6)$ and (iv) $\alpha = 1/[2(n+1)]$ (limiting solution), and for (a) $n = 3$, (b) $n = 1$, (c) $n = 0.5$.

For fluid extraction, $1/[2(n+1)] \leq \alpha < 1/(n+2)$, Figure 5.29 clearly shows that the width averaged fluid velocity is negative in the neighbourhood of the fracture entry and positive in the neighbourhood of the fracture tip. For the limiting solution of fluid extraction the width averaged fluid velocity is zero at

$$u = \frac{x}{L(t)} = \left[\frac{n}{2(n+1)}\right]^{\frac{n+1}{n+2}}, \tag{5.9.8}$$

which agrees with (5.7.58). Some of the fluid travels torwards the fracture entry while some of the fluid travels towards the fracture tip during the fluid extraction process. This result agrees with the fluid extraction analysis done in Sections 5.7 and 5.8. From Figure 5.29 we see that during the fluid extraction process, fluid close to the fracture tip relaxes further into the fracture with an approximately linear width averaged fluid velocity while fluid close to the fracture entry flows out of the fracture with a nonlinear width averaged velocity. More analysis of the fluid flow behaviour shown in Figure 5.29 will be undertaken in Section 5.11.

5.10 Approximate analytical solutions in the fluid injection region

From equations (5.9.3) and (5.9.5), it is clear that the velocity ratios for a fracture with constant volume and for a fracture propagating with constant speed are straight lines. Figure 5.28 shows that the velocity ratio curves for a fracture propagating with a constant rate of fluid injection at the fracture entry and for a fracture propagating with fluid injected at the fracture entry with a constant pressure increase approximately linearly along the length of the fracture. We therefore make the approximation that the velocity ratio curves for working conditions within the fluid injection region, $1/(n+2) < \alpha < 1$, are straight lines in order to derive approximate analytical solutions. This method was introduced by Fareo [30] who investigated approximate analytical solutions for a power law hydraulic fracture. The velocity ratio, (5.9.1), can therefore be expressed approximately as a linear

curve:

$$\frac{\overline{v_x}}{dL/dt} = mu + c, \tag{5.10.1}$$

where m is the gradient and c is the $\overline{v}_x/\frac{dL}{dt}$-intercept. From Figure 5.28, it is clear that all the velocity ratio curves start at a point (0,A) where the $\overline{v}_x/\frac{dL}{dt}$-intercept, A, depends on the working conditions and end at the same point (1,1). The value of c in (5.10.1), which is the $\overline{v}_x/\frac{dL}{dt}$-intercept, is A and the gradient m is $(1-A)$. Therefore equation (5.10.1) becomes

$$\frac{\overline{v_x}}{dL/dt} = (1-A)u + A. \tag{5.10.2}$$

Now equating (5.10.2) to the velocity ratio equation (5.9.1) gives a variable separable first order ordinary differential equation

$$f^{n-1}(u)\frac{df}{du} = -(1-A)u - A, \tag{5.10.3}$$

which when integrated subject to the boundary condition (5.3.6), $f(1) = 0$, gives

$$f(u) = \left(\frac{n(1+A)}{2}\right)^{\frac{1}{n}}\left[1 + \left(\frac{1-A}{1+A}\right)u\right]^{\frac{1}{n}}(1-u)^{\frac{1}{n}}. \tag{5.10.4}$$

If numerical solutions can be obtained for any working condition within the fluid injection region, then the constant A which is the $\overline{v}_x/\frac{dL}{dt}$-intercept can be obtained by reading it off the $\overline{v}_x/\frac{dL}{dt}$-axis of the graph of the velocity ratio against u. However it is necessary to obtain an analytical expression for A which is independent of the numerical solution and which will apply approximately for $1/(n+2) < \alpha < 1$. From Figure 5.28 we observe that when $n = 3$, A is close to 1 although as n decreases to 1 and then to 0.5, A moves further away from 1. In order to obtain A, we substitute the approximate analytical solution for $f(u)$, (5.10.4), into the second boundary condition (5.3.7). The left hand side of (5.3.7) is calculated by multiplying (5.10.3) by $f(u)$ and evaluating the result at $u = 0$:

$$f^n(0)\frac{df}{du}(0) = -A\left[\frac{n(1+A)}{2}\right]^{\frac{1}{n}}. \tag{5.10.5}$$

The integral on the right hand side of (5.3.7) is evaluated by making an expansion of $f(u)$, (5.10.4), in powers of $(1-A)/(1+A)$:

$$f(u) = \left[\frac{n(1+A)}{2}\right]^{\frac{1}{n}}(1-u)^{\frac{1}{n}}\left[1 + O\left(\frac{1-A}{1+A}\right)\right], \quad \text{as} \quad A \to 1 \tag{5.10.6}$$

and integrating (5.10.6) to obtain

$$\int_0^1 f(u)du = \frac{n}{(n+1)}\left[\frac{n(1+A)}{2}\right]^{\frac{1}{n}}\left[1+O\left(\frac{1-A}{1+A}\right)\right], \quad \text{as} \quad A \to 1. \tag{5.10.7}$$

It therefore follows that the right hand side of (5.3.7) is

$$\frac{1}{n}\left(\frac{1}{\alpha}-(n+2)\right)\int_0^1 f(u)du = \frac{1}{(n+1)}\left(\frac{1}{\alpha}-(n+2)\right)\left[\frac{n(1+A)}{2}\right]^{\frac{1}{n}}\left[1+O\left(\frac{1-A}{1+A}\right)\right], \quad \text{as} \quad A \to 1 \tag{5.10.8}$$

and therefore by equating the left hand side, (5.10.5), and the right hand side, (5.10.8), of (5.3.7) we obtain

$$A = \frac{1}{(n+1)}\left(n+2-\frac{1}{\alpha}\right)\left[1+O\left(\frac{1-A}{1+A}\right)\right], \quad \text{as} \quad A \to 1. \tag{5.10.9}$$

It can be verified that the solution (5.10.6) and the constant (5.10.9) both satisfy the ordinary differential equation (5.3.5) as $A \to 1$.

The approximate analytical solution for the length of the fracture

$$L(t) = \left(1+\frac{2(n+1)\beta^n}{n[(2n+3)\alpha-1]}K_n t\right)^{\alpha} \tag{5.10.10}$$

is obtained by using equations (5.10.6) and (5.10.9) in (5.3.21) and evaluating (5.10.6) at $u = 0$ to obtain $f(0)$ which is equal to f_{max} when fluid is injected into the fracture. Similarly the approximate analytical solution for the half-width of the fracture, (5.3.20), is

$$h(t,x) = \beta\left[1+\frac{2(n+1)\beta^n}{n[(2n+3)\alpha-1]}K_n t\right]^{\frac{2}{n}\left(\alpha-\frac{1}{2}\right)}\left[1+\left(\frac{1-\alpha}{(2n+3)\alpha-1}\right)\frac{x}{L(t)}\right]^{\frac{1}{n}}\left(1-\frac{x}{L(t)}\right)^{\frac{1}{n}}. \tag{5.10.11}$$

It can be verified that the approximate analytical solutions (5.10.10) and (5.10.11) for the length and half-width of the fracture ,respectively, exactly satisfy the exact analytical solutions (5.7.8) and (5.7.10) for constant volume, $\alpha = 1/(n+2)$, and (5.7.20) and (5.7.22)

for constant speed of propagation, $\alpha = 1$. This is because unlike for $1/(n+2) < \alpha < 1$, the working conditions $\alpha = 1/(n+2)$ and $\alpha = 1$ give velocity ratio curves that are exactly straight lines. It therefore follows that for $\alpha = 1/(n+2)$ and $\alpha = 1$ the approximation that the curves in Figure 5.28 are straight lines is exactly satisfied. The $\overline{v}_x/\frac{dL}{dt}$-intercept, A, given by (5.10.9) is $A = 0$ for $\alpha = 1/(n+2)$ and $A = 1$ for $\alpha = 1$ which is exactly the same for the exact analytical solutions given by equations (5.9.3) and (5.9.5). For $\alpha = 1/(n+2)$ $A \to 0$ and therefore the expansion in (5.10.9) as $A \to 1$ is not satisfied. However the integral $\int_0^1 f(u)du$ does not need to be expanded as the remaining factor in (5.10.9) is zero resulting in $A = 0$.

Figure 5.30 shows approximate analytical half-widths plotted with dashed lines (- - -), (5.10.11), and numerical solutions plotted with solid lines (——), (5.3.20), of a partially open fracture, $\beta = 0.5$, with fluid at its entry injected at a constant rate, $\alpha = (n+1)/(n+2)$. From the approximate analytical solution (5.10.11) it is clear that a fracture that is initially partially open with $\alpha = (n+1)/(n+2)$ stays partially open until the scaled transition time

$$K_n t_\tau = \frac{n(2n^2+4n+1)}{2(n+1)(n+2)\beta^n}\left[\left(\frac{1}{\beta}\right)^{n+2} - 1\right], \tag{5.10.12}$$

while from the numerical solution, (5.3.20), a partially open fracture with $\alpha = (n+1)/(n+2)$ exists until the scaled transition time

$$K_n t_\tau = \left(\frac{n+1}{n+2}\right)\left(\frac{f(0)}{\beta}\right)^n\left[\left(\frac{1}{\beta}\right)^{n+2} - 1\right]. \tag{5.10.13}$$

After the scaled transition time (5.10.12) or (5.10.13), the touching asperities at the fluid-rock interface move apart along the length of the fracture forming an open fracture. The scaled transition time, (5.10.12), derived from the approximate analytical solution, (5.10.11), for $n = 3$, 1 and 0.5 is $K_n t_\tau = 576.60$, 8.17 and 1.54, respectively. The scaled transition time, (5.10.13), derived from the numerical solution, (5.3.20), for $n = 3$, 1 and 0.5 is $K_n t_\tau = 577.67$, 8.26 and 1.58, respectively. The percentage error in the approximate analytical solution is 0.19%, 1.09% and 2.53%.

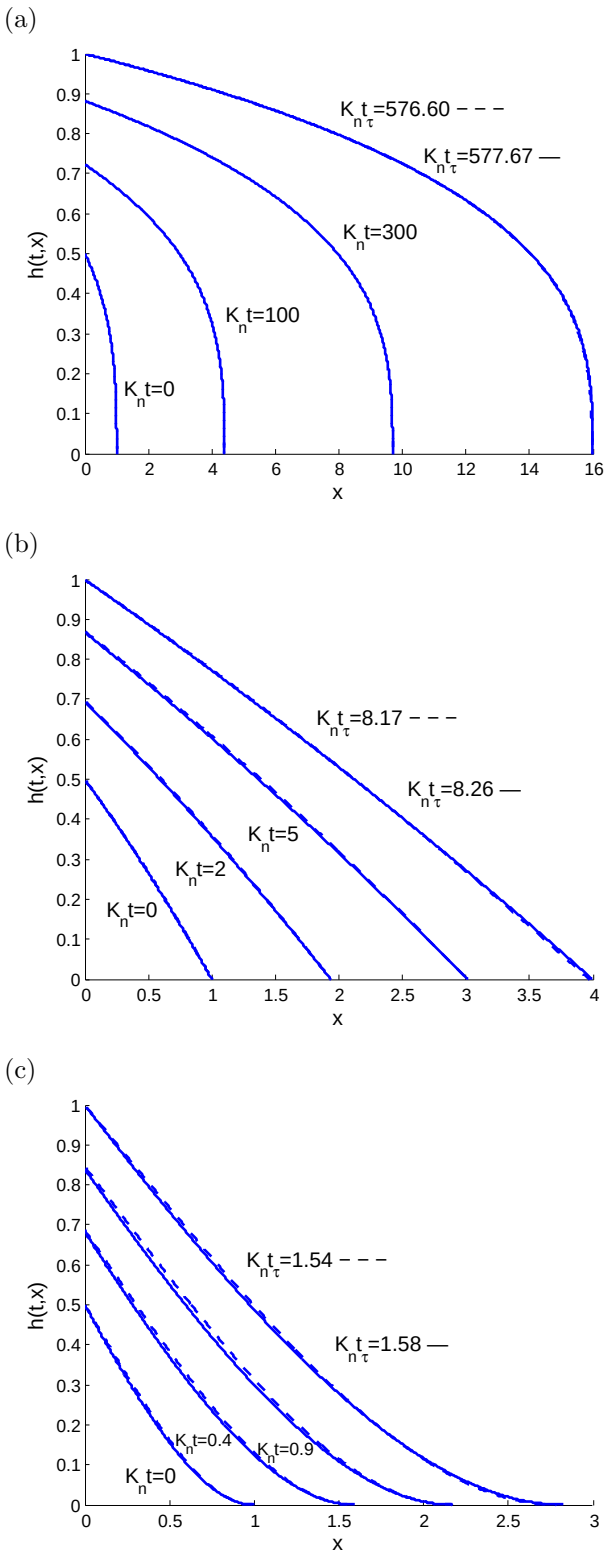

Figure 5.30: Partially open fracture with $\beta = 0.5$ and constant rate of fluid injection at the fracture entry, $\alpha = \frac{n+1}{n+2}$. Comparison of the approximate analytical solution (5.10.11) (- - -) with the numerical solution (5.3.20) (——) for the half-width $h(t, x)$, plotted against x for increasing values of the scaled time $0 \leq K_n t \leq K_n t_\tau$ and for (a) $n = 3$, (b) $n = 1$, (c) $n = 0.5$.

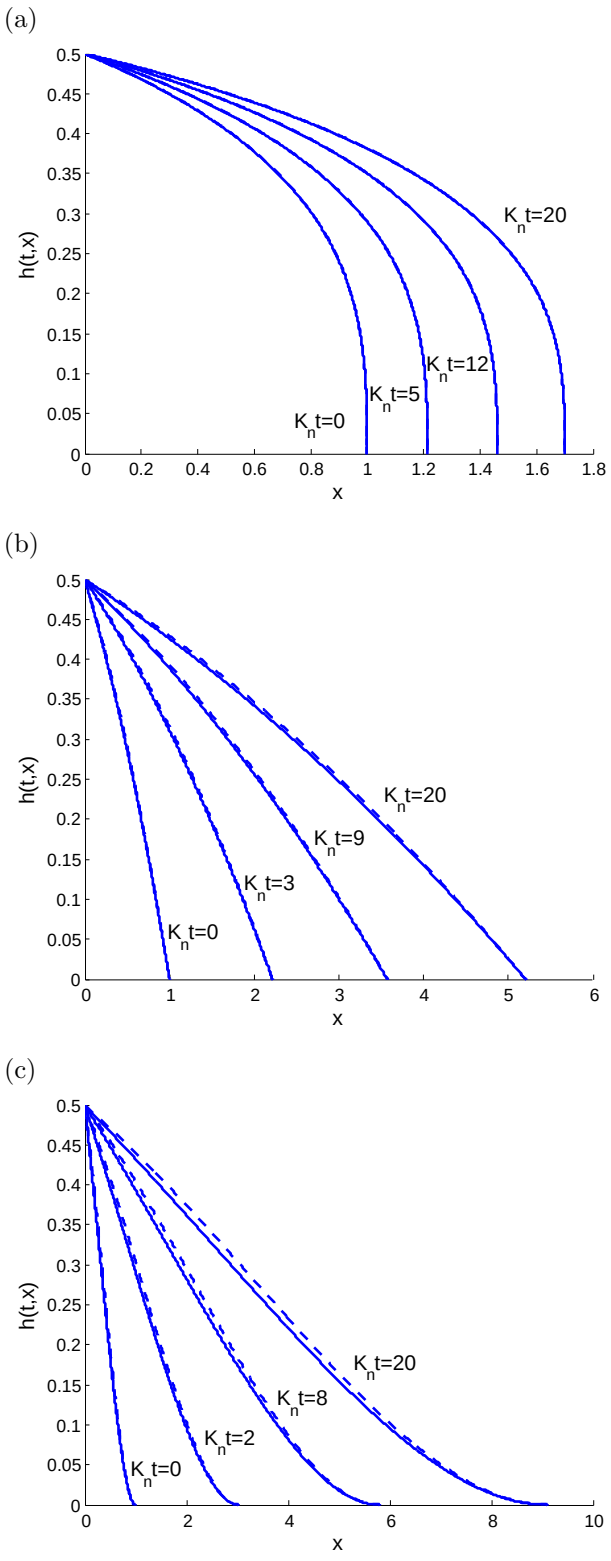

Figure 5.31: Partially open fracture with $\beta = 0.5$ and constant pressure at the fracture entry, $\alpha = \frac{1}{2}$. Comparison of the approximate analytical solution (5.10.11) (- - -) with the numerical solution (5.3.20) (——) for the half-width $h(t, x)$, plotted against x for increasing values of the scaled time $K_n t$ and for (a) $n = 3$, (b) $n = 1$, (c) $n = 0.5$.

Figure 5.31 compares approximate analytical half-width solution (5.10.11), shown by dashed lines (- - -), with the numerical half-width solution (5.3.20), shown by solid lines (——), for a partially open fracture ($\beta = 0.5$) that has fluid injected at its entry with constant pressure, $\alpha = 1/2$. When the fluid pressure at the fracture entry is kept constant, the initially partially open fracture continues to be partially open for all scaled time $K_n t$ as observed in Figure 5.31.

The approximate analytical solution agrees very well with the numerical solution although the accuracy decreases slightly as n and α decrease. The decrease in accuracy is due to the increasing error in (5.10.9). It is also important to recall that when $n = 3$, A is close to 1 and as n decreases to 1 and then to 0.5, A moves further away from 1 while the expression of A given by (5.10.9) applies as $A \to 1$. In order to improve the approximate analytical solution (5.10.6), we consider an extra term in the expansion for A, given in (5.10.9), such that the right hand side of (5.3.7) is

$$\frac{1}{n}\left(\frac{1}{\alpha} - (n+2)\right)\int_0^1 f(u)du =$$
$$\frac{1}{(n+1)}\left(\frac{1}{\alpha} - (n+2)\right)\left[\frac{n(1+A)}{2}\right]^{\frac{1}{n}}\left[1 + \frac{1}{(2n+1)}\left(\frac{1-A}{1+A}\right) + O\left(\left[\frac{1-A}{1+A}\right]^2\right)\right], \text{ as } A \to 1. \tag{5.10.14}$$

It therefore follows from equating (5.10.5) and (5.10.14) that

$$A = \frac{1}{(n+1)}\left(n + 2 - \frac{1}{\alpha}\right)\left[1 + \frac{1}{(2n+1)}\left(\frac{1-A}{1+A}\right) + O\left(\left[\frac{1-A}{1+A}\right]^2\right)\right], \text{ as } A \to 1. \tag{5.10.15}$$

We neglect second order terms in $(1-A)/(1+A)$ in (5.10.15) and rewrite it in iterative form as

$$A_{r+1} = \frac{1}{(n+1)}\left(n + 2 - \frac{1}{\alpha}\right)\left[1 + \frac{1}{(2n+1)}\left(\frac{1-A_r}{1+A_r}\right)\right], \quad r = 0, 1, ..., s. \tag{5.10.16}$$

The constant A will be obtained by iteratively solving equation (5.10.16).

The first iteration of (5.10.16) which occurs when $r = 0$ gives A_1, where A_0 is taken to be the zero order term in (5.10.9). The subsequent iterations are solved using the result of

α	n	Numerical solution for A	Zero order solution for A (5.10.9)	Error % of Numerical A & Zero order soln. for A	First order solution for A (5.10.16)	Error % of Numerical A & First order soln. for A
$\alpha = \frac{n+1}{n+2}$	3	0.9420	0.9375	0.4777	0.9415	0.0496
	1	0.7809	0.7500	3.9570	0.7808	0.0158
	0.5	0.6233	0.5556	10.8615	0.6206	0.4350
$\alpha = \frac{1}{2}$	3	0.7647	0.7500	1.9223	0.7643	0.0506
	1	0.5492	0.5000	8,9585	0.5486	0.1122
	0.5	0.4103	0.3333	18.7668	0.4041	1.5180

Table 5.2: Approximations to the constant A.

A obtained in the previous iteration. The number of iterations, $s+1$, will be determined by how quickly the value of A converges to the numerical value of A, shown in Figure 5.28, and the stopping criteria, which is satisfied when the next iteration gives the same value of A as the previous iteration.

For $\alpha = (n+1)/(n+2)$, the first order solution for A is obtained from (5.10.16) after $s+1 = 14$, 20 and 24 iterations for $n = 3$, 1 and 0.5, respectively. The computational times are 4×10^{-6} seconds for $n = 3$ and 5×10^{-6} seconds for $n = 1$ and $n = 0.5$. For $\alpha = 1/2$, the first order solution for A is obtained from (5.10.16) after $s+1 = 14$, 19 and 21 iterations for $n = 3$, 1 and 0.5, respectively, with computational times 4×10^{-6} seconds for all the specified cases. It is clear that the increasing number of iterations with decreasing parameter n poses no problem as the computational times are negligible.

Table 5.2 shows the error percentage of the numerical solution for A and the zero order solution for A, (5.10.9), and the error percentage of the numerical solution for A and the first order solution for A obtained by iterating (5.10.16). From Table 5.2, columns five and seven, it is clear that the percentage errors decrease significantly when using the first order solution for A, (5.10.16). This implies that the first order solution for A, (5.10.16) gives results that are closer to the numerical solutions than the zero order solution for A, (5.10.9). It follows that using the first order solution for A obtained by

iterating (5.10.16) results in better agreement between the numerical and approximate analytical solutions than that shown in Figures 5.30 and 5.31 and hence results in better approximate analytical solutions.

5.11 Further investigation of fluid extraction

During the fluid extraction process as the fluid in the neighbourhood of the fracture entry flows out of the fracture, fluid in the neighbourhood of the fracture tip relaxes further into the fracture causing the fracture length to continuously increase. This behaviour continues until all the fluid has been extracted from the fracture at time $t \to \infty$. In this Section, we use the velocity ratio graphs, shown in Figure 5.29, to further investigate the process of fluid extraction.

The concept of approximate analytical solutions applied in Section 5.10 to the fluid injection region can also be applied for fluid extraction. However, unlike for fluid injection, the velocity ratio curves for fluid extraction shown in Figure 5.29 slowly diverge from linear-like behaviour as the working conditions decrease from the constant volume condition, $\alpha = 1/(n+2)$, to the limiting condition for fluid extraction, $\alpha = 1/[2(n+1)]$. It therefore follows that although it may be sufficient to make a linear approximation for the velocity ratio curves that are close to the constant volume straight line, which corresponds to $\alpha = 1/(n+2)$, in order to obtain approximate analytical solutions that are accurate, it is definitely not sufficient to do the same for velocity ratios that are close to the limiting fluid extraction curve, which corresponds to $\alpha = 1/[2(n+1)]$. Thus for fluid extraction, a suitable nonlinear curve that best represents the velocity ratio curves, shown in Figure 5.29, would have to be investigated in order to derive an accurate approximate analytical solution.

An important feature in the velocity ratio curves for fluid extraction, shown in Figure 5.29, is that they are negative in the neighbourhood of the fracture entry and positive in the neighbourhood of the fracture tip. Therefore they all have a point at which the mean velocity is zero, $v_x = 0$. We will refer to this point as the "zero point". A negative velocity

ratio simply implies that fluid flows towards the left and out of the fracture at the fracture entry and a positive velocity ratio implies that fluid flows towards the right and further into the fracture causing the fracture length to increase. The "zero points" in Figure 5.29 are the transition points at which the width averaged fluid velocity is instantaneously zero. The velocity ratio is independent of time. This average fluid flow behavior agrees with the fluid extraction analysis done in Section 5.8. For the constant volume solution there is no fluid injection or extraction at the fracture entry and it therefore follows that the corresponding velocity ratio has the zero at $u = 0$ which implies zero fluid velocity at the fracture entry. For working conditions less than the constant volume condition, all zeros are at $u > 0$. For the fluid extraction working conditions $\alpha = 3/[2(2n+3)]$ and $3/(5n+6)$ the zeros can be calculated by equating (5.9.1) to zero to obtain

$$\frac{df}{du} = 0 \tag{5.11.1}$$

and using df/du from numerical results. For the limiting fluid extraction working condition, $\alpha = 1/[2(n+1)]$, the "zero point" can be calculated by equating (5.9.7) to zero to obtain

$$u = \left(\frac{n}{2(n+1)}\right)^{\frac{n+1}{n+2}}. \tag{5.11.2}$$

As expected, it turns out that the zero of the velocity ratio curve for the limiting fluid extraction working condition is u_{max} given by (5.7.39), the point at which the maximum fracture half-width is attained. For the working conditions $\alpha = 3/[2(2n+3)]$ and $\alpha = 3/(5n+6)$ defined within the fluid extraction region, in fact for any working condition within the fluid extraction region, it can be verified that the zeros given by (5.11.1) are the same as the points u_{max} at which the maximum half-widths of the fracture are numerically obtained.

From Figure 5.32, the zeros of the velocity ratio curves in Figure 5.29 are plotted against the increasing parameter n. These curves show the points at which the width averaged fluid velocity changes direction as n increases for the three extraction working conditions considered. For the limiting fluid extraction working condition, $\alpha = 1/[2(n+1)]$, the zero u_{max} is the largest when compared with u_{max} given by the fluid extraction working conditions, $\alpha = 3/[2(2n+3)]$ and $\alpha = 3/(5n+6)$, for any chosen value of n. Thus u_{max}

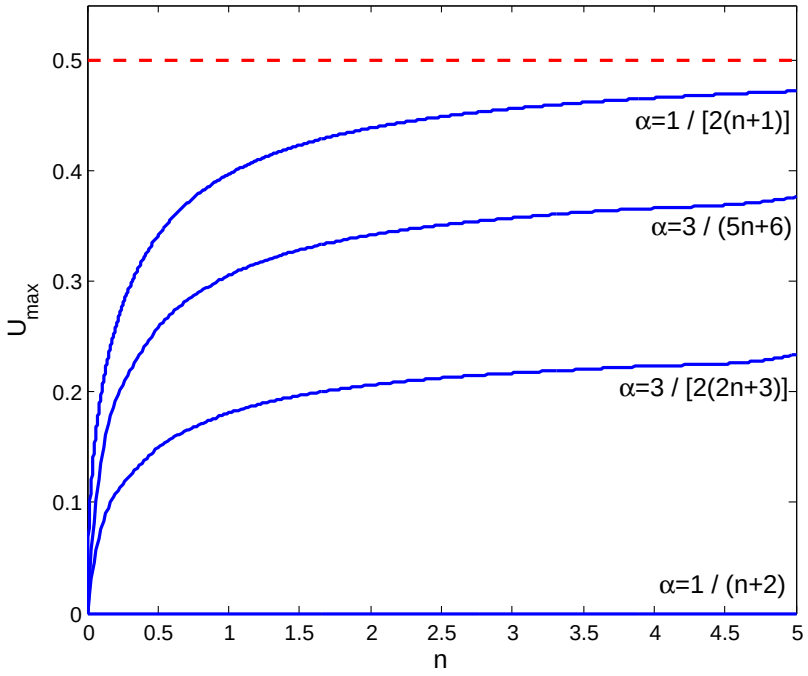

Figure 5.32: Curves of u_{max} plotted against n for specified working conditions.

for the limiting fluid extraction condition is the furthest away from the fracture entry and therefore closest to the fracture tip for all values of $n > 0$. This agrees with, and further explains, the result obtained in Section 5.8 that the limiting fluid extraction condition yields the maximum rate of fluid extraction. Also using (5.11.2),

$$\lim_{n\to\infty} u_{max} = \frac{1}{2}. \tag{5.11.3}$$

We see from Figure 5.32 that u_{max} is an increasing function of n for any given working condition. It therefore follows that the greatest value of u_{max} for all fluid extraction working conditions and for all values of $n > 0$ is $u_{max} = 1/2$. This agrees with the results in Figure 5.32.

From Figure 5.32 we can deduce that the zeros for large fracture arpetures ($n >> 0$) are closer to the fracture tip that those for small tortuous fractures ($0 < n \leq 1$). Instinctively we conjecture that this may lead to more fluid extraction at a time in large fracture apertures than in small tortuous fractures. However proving this through general analysis would be difficult as we cannot compare fracture properties of different values of n due to the unknown and different values of K_n.

5.12 Conclusions

In this Chapter, we analysed the nonlinear diffusion equation of a model linear hydraulic fracture with tortuosity. The model fracture can either be open when the asperities in the actual fracture do not touch each other or partially open when the asperities at the top and bottom surfaces of the actual fracture touch forming contact regions.

Methods of solution considered by different authors [34, 36] for the propagation of a hydraulic fracture and for the propagation of a gravity current, both from a point source and therefore with zero initial length, have not been used in this work. This is because we consider a pre-existing hydraulic fracture with non-zero initial length. The more powerful Lie group analysis methods have been used to obtain a solution to the governing nonlinear diffusion equation (5.1.1). The Lie point symmetry approach has been used to obtain a group invariant solution for the half-width of the fracture $h(t, x)$.

An ordinary differential equation was obtained by substituting the group invariant solution for $h(t, x)$ into the governing partial differential equation (5.1.1). The solution for the length of the fracture, $L(t)$, was derived from analysis of the boundary condition at the fracture tip while the solution for the volume of the fracture, $V(t)$, was used to derive the boundary condition at the fracture entry. All solutions describing properties of the fracture were found to depend on a function $f(u)$ obtained from solving a boundary value problem for the ordinary differential equation. Transformed variables were then used to scale all the governing equations in order to simplify them by reducing the number of parameters in the problem.

In Chapter 4, two conserved vectors for the nonlinear diffusion equation (5.1.1), the elementary and the second conserved vectors, were calculated using three methods. In this Chapter we used the results for these conserved vectors and investigated if they could be associated with the Lie point symmetry generator of the governing partial differential equation (5.1.1). This investigation was motivated by Sjöberg's work on *"Double reduction of PDEs from the association of symmetries with conservation laws with applications"* where she showed through the double reduction theorem and various examples that if a Lie point symmetry generator is associated with a conserved vector for the same partial differ-

ential equation, it may be possible to derive an analytical invariant solution for the partial differential equation [29]. For the elementary conserved vector association was obtained provided the volume of the fracture was kept constant, that is provided $\alpha = 1/(n+2)$. For the second conserved vector association was obtained provided the fluid extraction working condition, $\alpha = 1/[2(n+1)]$, was satisfied. It would remain to later investigate if these two working conditions provided analytical invariant solutions.

Analysis of the invariant solution gave four working conditions at the fracture entry, one of which was already obtained from the elementary conserved vector as the constant volume working condition, $\alpha = 1/(n+2)$. A fifth working condition, $\alpha = 1/[2(n+1)]$, describing fluid extraction and obtained from the association of the second conserved vector with a Lie point symmetry of the governing partial differential equation (5.1.1) was briefly discussed. The remaining three working conditions obtained from this analysis were the case where the rate of fluid injection was kept constant, $\alpha = (n+1)/(n+2)$, the case where the fluid at the fracture entry was pumped into the fracture at a constant pressure, $\alpha = 1/2$, and the case where the fracture propagated at a constant speed, $\alpha = 1$. The latter working condition was acknowledged as a mathematical limit rather than a physical working condition and it can be achieved by slowly increasing the rate of fluid injection from a constant value until the fracture propagates at a constant speed.

An analytical asymptotic solution, valid in the neighbourhood of the fracture tip, of the boundary value problem and therefore of the half-width of the fracture was derived. For Reynolds flow, $n = 3$, Fareo and Mason [14] and Fitt et al [11] obtained a fracture solution with a singularity at the fracture tip. For a fracture with tortuosity, a singularity was obtained when $n > 1$ and therefore the asymptotic solution was used to join with the numerical solution at the fracture tip when $n > 1$.

Three exact analytical solutions were obtained. The first exact analytical solution obtained was that of a fracture with constant volume and therefore a fracture with no fluid injection or extraction at the fracture entry, ($\alpha = 1/(n+2)$). The second exact analytical solution obtained was that of a fracture propagating at constant speed, ($\alpha = 1$). The third exact analytical solution was that of a fracture from which fluid is extracted at the fracture entry. It is of interest that the first and the third exact analytical solutions were obtained

by associating the elementary and second conserved vectors with the Lie point symmetry generator of the governing equation, (5.1.1). These two solutions illustrated the double reduction theorem of Sjöberg. In both cases, the ordinary differential equation, obtained from reducing the partial differential equation with an associated Lie point symmetry, could be integrated once immediately, thus making the second reduction. They could be integrated further and analytical solutions were therefore derived.

All the analytical solutions for $n > 1$ gave a model fracture that had a singularity at the fracture tip while all the analytical solutions for $0 < n \leq 1$ gave a model fracture with a finite spacial gradient at the fracture tip. Given that $n = 3$ corresponds to the Reynolds type of fluid flow, it is clear that a decrease in the parameter n leads to an increase in tortuosity due to the surface roughness. It therefore follows that tortuosity can remove the singularity at the fracture tip of the model fracture provided the tortuosity is sufficiently strong.

There appears to be very little work in the literature on the extraction of fluid from a hydraulic fracture. We therefore investigated in detail the analytical solution corresponding to the fluid extraction working condition, $\alpha = 1/[2(n+1)]$. The analytical solution was closed at the fracture entry, $h(t, 0) = 0$. The reason for the closure was due to the assumption that $h_{min} = 0$ given that $h_{max} >> h_{min}$. However it was clearly discussed by Fitt et al [1] that h_{min} is never zero and the assumption is made for mathematical convenience. It was found that the volume of the fracture is a decreasing function of time and that $V(t) \to 0$ as $t \to \infty$. This steady decrease in volume is due to a non-zero flux of fluid out of the fracture at the fracture entry. It was also found that the spatial gradient of the half-width of the fracture at the fracture entry is positive infinity. Not only does the working condition $\alpha = 1/[2(n+1)]$ correspond to fluid extraction, it also gives the limiting solution for fluid extraction. It therefore follows that the fluid extraction working conditions are defined in the region $1/[2(n+1)] \leq \alpha < 1/(n+2)$ and there are no solutions below the curve $\alpha = 1/[2(n+1)]$. To further investigate the limiting fluid extraction working condition, $\alpha = 1/[2(n+1)]$, we analysed the fluid flux in the fracture. The fluid flux graphs were found to be negative in the neighbourhood of the fracture entry which verified that when $\alpha = 1/[2(n+1)]$ fluid is extracted out of the fracture at the fracture

entry. The same fluid flux curves were found to be positive in the neighbourhood of the fracture tip. This unexpected and interesting result showed that during the fluid extraction process the fluid close to the fracture entry flows out of the fracture, while the fluid close to the fracture tip relaxes further into the fracture. This explained why the length of the fracture grows continuously even during the fluid extraction process. The zero of the fluid flux curves represents the point at which the maximum fracture half-width h_{max} is obtained. The point of zero fluid flux is also the point at which the width averaged fluid velocity vanishes. The point of the maximum half-width is therefore the point at which the width averaged fluid flow changes direction from flowing out of the fracture to flowing into the fracture.

For the fluid injection working conditions, $\alpha = (n+1)/(n+2)$ and $\alpha = 1/2$, and for the fluid extraction working conditions ,$1/[2(n+1)] < \alpha < 1/(n+2)$, exact analytical solutions could not be found. It was therefore necessary to investigate numerical solutions for these working conditions. The method that was used to obtain the invariant solutions numerically for the specified working conditions was that of transforming the boundary value problem into two initial value problems which were solved using the MATLAB ode45 solver. Solving the two initial value problems simultaneously is equivalent to solving the original boundary value problem. This approach of obtaining the numerical solution to the boundary value problem was tested considering the constant volume and the constant speed of propagation working conditions. The numerical method gave solutions which agreed well with the exact analytical solutions for $\alpha = 1$ and $\alpha = 1/(n+2)$. Therefore this numerical method was used for the remaining working conditions, $1/(n+2) < \alpha < 1$ and $1/[2(n+1)] < \alpha < 1/(n+2)$. From the numerical results, it was further verified that tortuosity removes the singularity at the fracture tip of the model fracture when $0 < n \leq 1$.

For both the fluid injection and extraction working conditions, $1/[2(n+1)] \leq \alpha \leq 1$, the length of a partially open fracture, with $\beta = 0.5$, was analysed and plotted against the increasing scaled time $K_n t$ for the values $n = 3$, 1 and 0.5. A significant result that was found from the length graphs is that the more tortuous a fracture is, the less dependent the length of the fracture is on the operating conditions at the fracture entry. This result

was further verified by allowing $n \to 0$, that is, allowing the fracture to be more tortuous. All working conditions in Table 5.1 which are functions of n were found to tend to $\alpha = 1/2$. From this analysis a stronger result was obtained, that all working conditions defined in both the fluid injection and extraction regions yield lengths of partially open fractures that behave like the length of a partially open fracture with fluid injected at the fracture entry at a constant pressure.

For the fluid extraction working conditions , $1/[2(n+1)] < \alpha < 1/(n+2)$, the fluid flux in the fracture was analysed and it was found that, as in the limiting fluid extraction solutions when $\alpha = 1/[2(n+1)]$, during the process of fluid extraction the fluid close to the fracture entry flows out of the fracture while the fluid close to the fracture tip relaxes further into the fracture. We also compared the fluid flux at the fracture entry for different working conditions within the fluid extraction region, $1/[2(n+1)] \leq \alpha < 1/(n+2)$, and found that the limiting fluid extraction condition, $\alpha = 1/[2(n+1)]$, yields the maximum rate of fluid extraction from a fracture.

Given the thin nature of the fracture, it became clear that the width averaged fluid velocity was a more meaningful quantity to investigate than the fluid velocity in the fracture. The ratio of the width averaged fluid velocity and the velocity of propagation of the fracture, $\overline{v}_x/(dL/dt)$, eliminated the diffusion constant that could not be scaled into the time and made it possible to analyse the width averaged fluid velocity. For a fracture with constant volume, the width averaged fluid velocity was found to increase exactly linearly along the length of the fracture while for a fracture propagating with constant speed, the width averaged fluid velocity was found to be constant along the length of the fracture. For all the numerical solutions with working conditions defined within the fluid injection region, the width averaged fluid velocity was found to increase approximately linearly along the length of the fracture. This was a significant result for the fluid injection region because it lead to the derivation of approximate analytical solutions which were first introduced by Fareo [30]. The approximate analytical solutions were found to agree exactly with the analytical solutions for a fracture with constant volume and a fracture propagating with constant speed. The approximate analytical solutions for the remaining working conditions within the fluid injection region were found to agree well with the numerical

solutions. An approximate analytical solution may be useful in practice when an exact analytical solution cannot be obtained and a readily available analytical estimate for the half-width or length of a tortuous fracture is required.

For the fluid extraction region, the width averaged fluid velocity was found to be increasing approximately linearly in the neighbourhood of the fracture tip as fluid relaxes further into the fracture during the fluid extraction process. However in the neighbourhood of the fracture entry the width averaged fluid velocity was found to be increasing nonlinearly along the fracture length as fluid flows out of the fracture during the fluid extraction process. For working conditions closer to the constant volume case in the fluid extraction region, the approximation that the velocity ratio curves are straight lines might be sufficient to give good approximate analytical results. For working conditions close to the limiting fluid extraction case, the approximation that the velocity ratio curves are straight lines would clearly not be sufficient to give good approximate analytical results and a better function to approximate the behaviour of the width averaged fluid velocity would have to be investigated. The velocity ratio curves were negative close to the fracture entry and positive close to the fracture tip and they therefore had zeros. This agreed exactly with the analysis in the earlier Sections of this Chapter, that the zeros are the points at which the maximum half-width is attained and also the points at which the width averaged fluid velocity vanishes and the width averaged fluid flow changes direction. The zeros were plotted against the parameter n. For all working conditions in the fluid extraction region, $1/[2(n+1)] \leq \alpha < 1/(n+2)$, the zeros were closer to the fracture entry than to the fracture tip and for the limiting solution for fluid extraction it was shown that as $n \to 0$ the zero was half-way along the length of the fracture. The fact that the zero point for the limiting condition of fluid extraction, $1/[2(n+1)]$, is the closest to the fracture tip than all other working conditions defined within the fluid extraction region, agrees with the result that the working condition $1/[2(n+1)]$ yields the maximum rate of fluid extraction from the fracture.

Chapter 6

CONSERVATION LAWS FOR THE HYPERBOLIC HYDRAULIC FRACTURE WITH TORTUOSITY

6.1 Introduction

In Chapter 2, we derived the partial differential equation

$$\frac{\partial h}{\partial t} = K_n \frac{\partial}{\partial x}\left(h^n \frac{\partial h}{\partial x} + \phi h^{n-2} \frac{\partial h}{\partial x} \right) \tag{6.1.1}$$

which describes a partially open fracture with contact regions modelled by the hyperbolic crack law, where $\phi > 0$. The diffusion constant K_n is defined by (2.4.85) and the pressure ratio ϕ is defined by (2.4.86). When $\phi = 0$, the hyperbolic model for a hydraulic fracture reduces to a model for a linear hydraulic fracture and the partial differential equation (6.1.1) then describes either an open or a partially open fracture, with K_n defined by (2.4.77) instead of (2.4.85). Since the linear hydraulic fracture was discussed in Chapter 5, in this Chapter we will only consider $\phi > 0$.

In this Chapter we investigate conservation laws for the partial differential equation

(6.1.1) using the direct, the multiplier and the partial Lagrangian methods which were described in detail in Chapter 3. As discussed in Chapter 2, we will always consider parameter values of n that satisfy the condition $n > 0$.

In all calculations of the conservation laws, t, x, h and the partial derivatives of h are treated as independent variables. The subscript notation for partial differentiation will therefore be used. In the subscript notation the partial differential equation (6.1.1) is

$$G = h_t - K_n\Big(nh^{n-1} + \phi(n-2)h^{n-3}\Big)h_x^2 - K_n(h^n + \phi h^{n-2})h_{xx} = 0. \tag{6.1.2}$$

As in Chapter 4, when t and x are regarded as the only independent variables, then the standard notation for partial derivatives will be used.

6.2 Direct method

In order to obtain conserved vectors for the partial differential equation (6.1.2), we consider (3.3.1). The resulting determining equation is

$$\left(\frac{\partial T^1}{\partial t} + \frac{\partial T^1}{\partial h}h_t + \frac{\partial T^1}{\partial h_x}h_{xt} + \frac{\partial T^2}{\partial x} + \frac{\partial T^2}{\partial h}h_x + \frac{\partial T^2}{\partial h_x}h_{xx}\right)\Bigg|_{(6.1.1)} = 0, \tag{6.2.1}$$

where the components of the conserved vector $\mathbf{T}$ are chosen to have the form

$$T^1 = T^1(t, x, h, h_x), \quad T^2 = T^2(t, x, h, h_x). \tag{6.2.2}$$

Substituting h_t, given by (6.1.2), into the determining equation (6.2.1) gives

$$\begin{aligned}&\frac{\partial T^1}{\partial t} + \frac{\partial T^2}{\partial x} + \left(\frac{\partial T^2}{\partial h_x} + K_n(h^n + \phi h^{n-2})\frac{\partial T^1}{\partial h}\right)h_{xx}\\ &+ K_n\Big(nh^{n-1} + \phi(n-2)h^{n-3}\Big)\frac{\partial T^1}{\partial h}h_x^2 + \frac{\partial T^1}{\partial h_x}h_{tx} + \frac{\partial T^2}{\partial h}h_x = 0.\end{aligned} \tag{6.2.3}$$

Now, separating the determining equation (6.2.3) in powers of second order derivatives of h gives the following results:

$$h_{tx} : \frac{\partial T^1}{\partial h_x} = 0, \tag{6.2.4}$$

which implies that

$$T^1 = T^1(t, x, h); \tag{6.2.5}$$

$$h_{xx} : \frac{\partial T^2}{\partial h_x} + K_n(h^n + \phi h^{n-2})\frac{\partial T^1}{\partial h} = 0, \tag{6.2.6}$$

which when integrated with respect to h_x, since equation (6.2.5) holds, gives

$$T^2 = -K_n(h^n + \phi h^{n-2})\frac{\partial T^1}{\partial h}h_x + A(t, x, h) \tag{6.2.7}$$

and the remainder after separating (6.2.3) in powers of second order derivatives of h is

$$Remainder : \frac{\partial T^1}{\partial t} + \frac{\partial T^2}{\partial x} + K_n(nh^{n-1} + \phi(n-2)h^{n-3})\frac{\partial T^1}{\partial h}h_x^2 + \frac{\partial T^2}{\partial h}h_x = 0. \tag{6.2.8}$$

Now, substituting T^2 from equation (6.2.7) into the remainder (6.2.8) gives

$$\frac{\partial T^1}{\partial t} + \frac{\partial A}{\partial x} + \left(\frac{\partial A}{\partial h} - K_n(h^n + \phi h^{n-2})\frac{\partial^2 T^1}{\partial x \partial h}\right)h_x - K_n(h^n + \phi h^{n-2})\frac{\partial^2 T^1}{\partial h^2}h_x^2 = 0. \tag{6.2.9}$$

Since both T^1 and A are independent of h_x, we separate (6.2.9) in powers of h_x to obtain the following results:

$$h_x^2 : \frac{\partial^2 T^1}{\partial h^2} = 0, \tag{6.2.10}$$

which when integrated twice with respect to h gives

$$T^1(t, x, h) = B(t, x)h + C(t, x) \tag{6.2.11}$$

and

$$h_x : \frac{\partial A}{\partial h} - K_n(h^n + \phi h^{n-2})\frac{\partial^2 T^1}{\partial x \partial h} = 0. \tag{6.2.12}$$

Now, from (6.2.12), the value $n = 1$ is a special case. We first consider the general case in which $n > 0$ with $n \neq 1$.

6.2.1 General case: $n > 0$ with $n \neq 1$

Substituting (6.2.11) into (6.2.12) and integrating with respect to h gives

$$A(t, x, h) = K_n\left[\frac{h^{n+1}}{(n+1)} + \phi\frac{h^{n-1}}{(n-1)}\right]\frac{\partial B}{\partial x} + D(t, x). \tag{6.2.13}$$

The remaining terms after separating (6.2.9) in powers of h_x are

$$remainder : \frac{\partial T^1}{\partial t} + \frac{\partial A}{\partial x} = 0. \tag{6.2.14}$$

Substituting (6.2.11) for $T^1(t, x, h)$ and (6.2.13) for $A(t, x, h)$ into the remainder (6.2.14) gives

$$\frac{\partial B}{\partial t}h + \frac{\partial C}{\partial t} + K_n\left[\frac{h^{n+1}}{(n+1)} + \phi\frac{h^{n-1}}{(n-1)}\right]\frac{\partial^2 B}{\partial x^2} + \frac{\partial D}{\partial x} = 0. \tag{6.2.15}$$

We separate (6.2.15) in powers of h. It can be verified that $n = 2$ is not a special case as it leads to the same conserved vectors obtained when $n > 0$ and $n \neq 2$. Thus separating (6.2.15) in powers of h, with $n \neq 1$, gives the following results:

$$h : \frac{\partial B}{\partial t} = 0, \tag{6.2.16}$$

which implies that

$$B = B(x); \tag{6.2.17}$$

$$h^{n-1} : \frac{d^2 B}{dx^2} = 0, \tag{6.2.18}$$

which when integrated twice with respect to x gives

$$B = ax + b, \tag{6.2.19}$$

where a and b are constants. No new information is obtained when separating (6.2.15) by h^{n+1}. The remaining terms are

$$\frac{\partial C}{\partial t} + \frac{\partial D}{\partial x} = 0. \tag{6.2.20}$$

Now, substituting (6.2.13) for A and (6.2.19) for B into T^1, (6.2.11), and T^2, (6.2.7), gives the following results:

$$T^1 = (ax + b)h + C(t, x), \tag{6.2.21}$$

$$T^2 = -K_n\left((h^n + \phi h^{n-2})(ax + b)h_x - \left[\frac{h^{n+1}}{(n+1)} + \phi\frac{h^{n-1}}{(n-1)}\right]a\right) + D(t, x). \tag{6.2.22}$$

Now $T^1 = C(t, x)$ and $T^2 = D(t, x)$ are components of a trivial conserved vector because, from (6.2.20), the conservation law equation (3.3.1) is identically satisfied without imposing the PDE (6.1.2). Therefore we take

$$C(t, x) = 0, \quad D(t, x) = 0. \tag{6.2.23}$$

Thus (6.2.21) and (6.2.22), when written in canonical form ($a = 0, b = 1$ and $a = 1, b = 0$), give the elementary conserved vector

$$\begin{aligned}\mathbf{T_{(1)}} &= (T^1, T^2) \\ &= \left(h, -K_n(h^n + \phi h^{n-2})h_x\right)\end{aligned} \tag{6.2.24}$$

and the second conserved vector

$$\begin{aligned}\mathbf{T_{(2)}} &= (T^1, T^2) \\ &= \left(xh, -K_n\left[(h^n + \phi h^{n-2})xh_x - \frac{h^{n+1}}{(n+1)} - \phi\frac{h^{n-1}}{(n-1)}\right]\right).\end{aligned} \tag{6.2.25}$$

6.2.2 Special case: $n = 1$

All equations defined before (6.2.12) are also applicable for the $n = 1$ case. Substituting $n = 1$ and (6.2.11) for T^1 into (6.2.12) gives

$$\frac{\partial A}{\partial h} - K_1\left(h + \frac{\phi}{h}\right)\frac{\partial B}{\partial x} = 0. \tag{6.2.26}$$

Integrating (6.2.26) with respect to h gives

$$A(t, x, h) = K_1\left(\frac{h^2}{2} + \phi ln(h)\right)\frac{\partial B}{\partial x} + D(t, x). \tag{6.2.27}$$

For $n = 1$ the remaining terms after separating (6.2.9) in powers of h_x are still given by (6.2.14):

$$remainder : \frac{\partial T^1}{\partial t} + \frac{\partial A}{\partial x} = 0. \tag{6.2.28}$$

Substituting (6.2.11) for T^1 and (6.2.27) for A into (6.2.28) gives

$$h\frac{\partial B}{\partial t} + \frac{K_1}{2}h^2\frac{\partial^2 B}{\partial x^2} + K_1\phi ln(h)\frac{\partial^2 B}{\partial x^2} + \frac{\partial C}{\partial t} + \frac{\partial D}{\partial x} = 0. \tag{6.2.29}$$

Differentiating (6.2.29) with respect to h gives

$$h\frac{\partial B}{\partial t} + K_1h^2\frac{\partial^2 B}{\partial x^2} + K_1\phi\frac{\partial^2 B}{\partial x^2} = 0. \tag{6.2.30}$$

Since B is independent of h, we separate (6.2.30) by powers of h and find:

$$h : \frac{\partial B}{\partial t} = 0, \tag{6.2.31}$$

which implies that $B = B(x)$ and

$$h^2 : \frac{d^2B}{dx^2} = 0, \tag{6.2.32}$$

which when integrated twice with respect to x gives

$$B = ax + b. \tag{6.2.33}$$

The remainder in (6.2.30) also gives (6.2.32). Substituting (6.2.33) into (6.2.29) gives (6.2.20). With the same argument made for the general case, we choose $C = 0$ and $D = 0$. Therefore for the special case $n = 1$, from equations (6.2.11) and (6.2.33), the elementary conserved vector is

$$\mathbf{T_{(1)}} = \left(h, -K_1\left[h + \frac{\phi}{h}\right]h_x\right) \tag{6.2.34}$$

and, from equations (6.2.7) and (6.2.27), the second conserved vector is

$$\mathbf{T_{(2)}} = \left(xh, -K_1\left[\left(h + \frac{\phi}{h}\right)xh_x - \frac{h^2}{2} - \phi ln(h)\right]\right). \tag{6.2.35}$$

Notice that when $n = 1$, (6.2.24) reduces to (6.2.34) but (6.2.25) does not reduce to (6.2.35). It follows that the special case $n = 1$ arises from the fact that when $n = 1$ the second component of the second conserved (6.2.25) breaks down.

6.3 Multipliers method

We consider a multiplier of the form

$$\Lambda = \Lambda(t, x, h) \tag{6.3.1}$$

which, for the partial differential equation (6.1.2), satisfies the condition

$$\Lambda(t,x,h)\left[h_t - K_n\left(nh^{n-1} + \phi(n-2)h^{n-3}\right)h_x^2 - K_n(h^n + \phi h^{n-2})h_{xx}\right] = D_1T^1 + D_2T^2, \tag{6.3.2}$$

where D_1 and D_2 are the total derivatives given by equations (3.2.7) and (3.2.8). Applying the Euler operator E_h, (3.3.5), to equation (6.3.2) annihilates the divergence expression

on the right-hand side of (6.3.2) and gives the determining equation

$$E_h\Lambda(t,x,h)\left[h_t - K_n\left(nh^{n-1} + \phi(n-2)h^{n-3}\right)h_x^2 - K_n(h^n + \phi h^{n-2})h_{xx}\right] = 0. \quad (6.3.3)$$

Expanding equation (6.3.3) and simplifying the result gives

$$\begin{aligned}
&\left(\frac{\partial\Lambda}{\partial t} + K_n(h^n + \phi h^{n-2})\frac{\partial^2\Lambda}{\partial x^2}\right) + 2K_n(h^n + \phi h^{n-2})\frac{\partial^2\Lambda}{\partial x\partial h}h_x \\
&+ K_n\left((nh^{n-1} + \phi(n-2)h^{n-3})\frac{\partial\Lambda}{\partial h} + (h^n + \phi h^{n-2})\frac{\partial^2\Lambda}{\partial h^2}\right)h_x^2 \\
&+ 2K_n(h^n + \phi h^{n-2})\frac{\partial\Lambda}{\partial h}h_{xx} = 0. \quad (6.3.4)
\end{aligned}$$

Separating equation (6.3.4) in powers of the derivatives of h gives the following results:

$$h_{xx} : \frac{\partial\Lambda}{\partial h} = 0, \quad (6.3.5)$$

which implies that

$$\Lambda = \Lambda(t,x); \quad (6.3.6)$$

separating (6.3.4) in powers of h_x and h_x^2 gives no new information and the remainder after separating (6.3.4) in powers of derivatives of h is

$$\frac{\partial\Lambda}{\partial t} + K_n(h^n + \phi h^{n-2})\frac{\partial^2\Lambda}{\partial x^2} = 0. \quad (6.3.7)$$

Since equation (6.3.6) holds, separating (6.3.7) in powers of h gives the following results:

$$h^0 : \frac{\partial\Lambda}{\partial t} = 0, \quad (6.3.8)$$

which implies that

$$\Lambda = \Lambda(x); \quad (6.3.9)$$

$$h^n : \frac{d^2\Lambda}{dx^2} = 0, \quad (6.3.10)$$

which when integrated with respect to x gives

$$\Lambda = ax + b, \quad (6.3.11)$$

where a and b are constants. Separating (6.3.7) by h^{n-2} gives no new information. Note that in (6.3.7), $n = 2$ is not a special case because we can separate first by h^n.

Now so far, $h(t,x)$ is (6.3.2) is arbitrary. We now suppose that $h(t,x)$ is a solution of the PDE (6.1.2). Then (3.3.1) is satisfied and we know that

$$(ax+b)\left[h_t - K_n\left(nh^{n-1}+\phi(n-2)h^{n-3}\right)h_x^2 - K_n(h^n+\phi h^{n-2})h_{xx}\right] = 0, \tag{6.3.12}$$

can be expressed as a linear combination of conservation laws. When written in canonical form ($a=0$ and $b=1$ or $a=1$ and $b=0$), (6.3.12) gives

$$h_t - K_n\left(nh^{n-1}+\phi(n-2)h^{n-3}\right)h_x^2 - K_n(h^n+\phi h^{n-2})h_{xx} = 0, \tag{6.3.13}$$

$$x\left[h_t - K_n\left(nh^{n-1}+\phi(n-2)h^{n-3}\right)h_x^2 - K_n(h^n+\phi h^{n-2})h_{xx}\right] = 0. \tag{6.3.14}$$

By performing elementary operations, both equation (6.3.13) and (6.3.14) can be expressed in the form

$$D_1T^1 + D_2T^2 = 0. \tag{6.3.15}$$

The first term of equation (6.3.13) can be expressed as

$$h_t = D_1(h), \tag{6.3.16}$$

which implies that

$$T^1 = h \tag{6.3.17}$$

and the second and third terms of equation (6.3.13) can be expressed as

$$-K_n\left[\left(nh^{n-1}+\phi(n-2)h^{n-3}\right)h_x^2+(h^n+\phi h^{n-2})h_{xx}\right] = D_2\left[-K_n(h^n+\phi h^{n-2})h_x\right], \tag{6.3.18}$$

which implies that

$$T^2 = -K_n(h^n+\phi h^{n-2})h_x. \tag{6.3.19}$$

Equations (6.3.17) and (6.3.19) are the components of the elementary conserved vector

$$\begin{aligned}\mathbf{T_{(1)}} &= (T^1,T^2)\\ &= \left(h, -K_n(h^n+\phi h^{n-2})h_x\right).\end{aligned} \tag{6.3.20}$$

The first term of (6.3.14) can be written as

$$xh_t = D_1(xh), \tag{6.3.21}$$

which implies that

$$T^1 = xh \tag{6.3.22}$$

and the second and third terms of (6.3.14) can be written as

$$\begin{aligned} -K_n\bigg[x\bigg(nh^{n-1}+\phi(n-2)h^{n-3}\bigg)h_x^2 + x(h^n+\phi h^{n-2})h_{xx}\bigg] \\ = D_2\bigg(- K_n\bigg[(h^n+\phi h^{n-2})xh_x - \frac{h^{n+1}}{(n+1)} - \phi\frac{h^{n-1}}{(n-1)}\bigg]\bigg), \end{aligned} \tag{6.3.23}$$

which implies that

$$T^2 = -K_n\bigg((h^n+\phi h^{n-2})xh_x - \frac{h^{n+1}}{(n+1)} - \phi\frac{h^{n-1}}{(n-1)}\bigg). \tag{6.3.24}$$

Equations (6.3.22) and (6.3.24) are the components of the second conserved vector

$$\begin{aligned} \mathbf{T}_{(\mathbf{2})} &= (T^1, T^2) \\ &= \bigg(xh, -K_n\bigg[(h^n+\phi h^{n-2})xh_x - \frac{h^{n+1}}{(n+1)} - \phi\frac{h^{n-1}}{(n-1)}\bigg]\bigg). \end{aligned} \tag{6.3.25}$$

It is clear that the conserved vectors for the partial differential equation (6.1.2) derived by the multiplier method, (6.3.20) and (6.3.25), are the same as the conserved vectors for the PDE derived by the direct method, (6.2.24) and (6.2.25). When $n = 1$, it is clear from (6.3.25) that the second component of the second conserved vector breaks down. Therefore we investigate the special case $n = 1$.

6.3.1 Special case: n=1

It can be verified that the multiplier Λ, (6.3.11), is also applicable for $n = 1$. Now, substituting $n = 1$ and (6.3.11) for Λ into (6.3.12) gives

$$(ax+b)\bigg[h_t - K_1\bigg(1-\frac{\phi}{h^2}\bigg)h_x^2 - K_1\bigg(h+\frac{\phi}{h}\bigg)h_{xx}\bigg] = 0. \tag{6.3.26}$$

Firstly, for $a = 0$ and $b = 1$ we obtain

$$h_t - K_1\bigg(1-\frac{\phi}{h^2}\bigg)h_x^2 - K_1\bigg(h+\frac{\phi}{h}\bigg)h_{xx} = 0. \tag{6.3.27}$$

By elementary manipulations, from (6.3.27),

$$h_t = D_1(t) \tag{6.3.28}$$

and

$$-K_1\left(1-\frac{\phi}{h^2}\right)h_x^2 - K_1\left(h+\frac{\phi}{h}\right)h_{xx} = D_2\left(-K_1\left[h+\frac{\phi}{h}\right]h_x\right). \tag{6.3.29}$$

Therefore the elementary conserved vector is

$$\mathbf{T}_{(\mathbf{1})} = \left(h, -K_1\left[h+\frac{\phi}{h}\right]h_x\right). \tag{6.3.30}$$

Similarly for $a = 1$ and $b = 0$, it can be verified that (6.3.26) gives the second conserved vector

$$\mathbf{T}_{(\mathbf{2})} = \left(xh, -K_1\left[\left(h+\frac{\phi}{h}\right)xh_x - \frac{h^2}{2} - \phi ln(h)\right]\right). \tag{6.3.31}$$

We observe that even for the special case $n = 1$, the conserved vectors for the partial differential equation (6.1.2) derived by the multiplier method, (6.3.30) and (6.3.31), are the same as the conserved vectors for the PDE derived by the direct method, (6.2.34) and (6.2.35).

6.4 Partial Lagrangian method

In order to derive conserved vectors for the partial differential equation (6.1.2) using the partial Lagrangian method, we consider the partial Lagrangian

$$L = \frac{K_n}{2}(h^n + \phi h^{n-2})h_x^2, \tag{6.4.1}$$

of equation (6.1.2). Now, applying the Euler operator E_h, (3.3.5), to the partial Lagrangian (6.4.1) and evaluating the result on the partial differential equation (6.1.2) gives

$$E_h\left(\frac{K_n}{2}(h^n + \phi h^{n-2})h_x^2\right)\Big|_{(6.1.2)} = \frac{K_n}{2}\left(nh^{n-1} + \phi(n-2)h^{n-3}\right)h_x^2 - h_t. \tag{6.4.2}$$

Equation (6.4.2) will be used later when deriving the partial Noether symmetry generator

$$X = \xi^1(t,x,h)\frac{\partial}{\partial t} + \xi^2(t,x,h)\frac{\partial}{\partial x} + \eta(t,x,h)\frac{\partial}{\partial h}, \tag{6.4.3}$$

of the partial differential equation (6.1.2) which will be used to derive conserved vectors.

We consider the determining equation

$$X^{[1]}L + L(D_1\xi^1 + D_2\xi^2) = D_1B^1 + D_2B^2 + (\eta - \xi^1 h_t - \xi^2 h_x)\Big(E_h L\Big|_{(6.1.1)}\Big), \qquad (6.4.4)$$

for the partial Noether symmetry generator, where D_1 and D_2 are the total derivatives given by (3.2.7) and (3.2.8), respectively, $\Big(E_h L\Big|_{(6.1.1)}\Big)$ is given by equation (6.4.2) and B^1 and B^2 are the gauge functions. We will consider gauge functions of the form

$$B^1 = B^1(t, x, h), \quad B^2 = B^2(t, x, h). \qquad (6.4.5)$$

The operator

$$X^{[1]} = X + \zeta_2 \frac{\partial}{\partial h_x}, \qquad (6.4.6)$$

used in (6.4.4) is the first prolongation of the partial Noether operator (6.4.3) where ζ_2 is defined by equation (3.2.5). Expanding equation (6.4.4) gives

$$\begin{aligned}
&K_n\Big(h^n + \phi h^{n-2}\Big)\left(\frac{\partial \eta}{\partial h} + \frac{1}{2}\frac{\partial \xi^1}{\partial t} - \frac{1}{2}\frac{\partial \xi^2}{\partial x}\right)h_x^2 + \left(K_n(h^n + \phi h^{n-2})\frac{\partial \eta}{\partial x} - \frac{\partial B^2}{\partial h}\right)h_x \\
&- \frac{K_n}{2}\left((h^n + \phi h^{n-2})\frac{\partial \xi^1}{\partial h} - \Big[nh^{n-1} + \phi(n-2)h^{n-3}\Big]\xi^1\right)h_x^2 h_t + \left(\eta - \frac{\partial B^1}{\partial h}\right)h_t \\
&- \frac{K_n}{2}\left((h^n + \phi h^{n-2})\frac{\partial \xi^2}{\partial h} - \Big[nh^{n-1} + \phi(n-2)h^{n-3}\Big]\xi^2\right)h_x^3 - \xi^1 h_t^2 \\
&- \left(K_n(h^n + \phi h^{n-2})\frac{\partial \xi^1}{\partial x} + \xi^2\right)h_x h_t - \left(\frac{\partial B^1}{\partial t} + \frac{\partial B^2}{\partial x}\right) = 0. \qquad (6.4.7)
\end{aligned}$$

Separating equation (6.4.7) by h_t^2 and $h_x h_t$ gives

$$h_t^2 : \xi^1 = 0, \qquad (6.4.8)$$

and

$$h_x h_t : K_n(h^n + \phi h^{n-2})\frac{\partial \xi^1}{\partial x} + \xi^2 = 0, \qquad (6.4.9)$$

which reduces to

$$\xi^2 = 0, \qquad (6.4.10)$$

given that equation (6.4.8) is satisfied. Separating (6.4.7) by $h_x^2 h_t$ and h_x^3 gives no new information while separating (6.4.7) by the remaining powers of h_x and h_t gives the following

results:

$$h_x^2 : \frac{\partial \eta}{\partial h} = 0, \tag{6.4.11}$$

which implies that

$$\eta = \eta(t, x); \tag{6.4.12}$$

$$h_x : K_n(h^n + \phi h^{n-2})\frac{\partial \eta}{\partial x} - \frac{\partial B^2}{\partial h} = 0. \tag{6.4.13}$$

Integrated (6.4.13) with respect to h, gives different results for $n = 1$ and $n \neq 1$. Therefore we take $n = 1$ as a specilal case. We first consider the general case of $n > 0$ with $n \neq 1$.

6.4.1 General case: $n > 0$ and $n \neq 1$

Now, integrating (6.4.13) with respect to h, since equation (6.4.12) holds, gives

$$B^2(t, x, h) = K_n\left[\frac{h^{n+1}}{(n+1)} + \phi\frac{h^{n-1}}{(n-1)}\right]\frac{\partial \eta}{\partial x} + M(t, x); \tag{6.4.14}$$

separating (6.4.7) by h_t gives

$$h_t : \eta - \frac{\partial B^1}{\partial h} = 0, \tag{6.4.15}$$

which when integrated with respect to h, since equation (6.4.12) holds, gives

$$B^1(t, x, h) = h\eta(t, x) + N(t, x) \tag{6.4.16}$$

and the remaining terms after separating (6.4.7) in powers and products of derivatives of h:

$$Remainder : \frac{\partial B^1}{\partial t} + \frac{\partial B^2}{\partial x} = 0. \tag{6.4.17}$$

Now, substituting B^1, given by (6.4.16), and B^2, given by (6.4.14), into the remainder (6.4.17) yields

$$\frac{\partial N}{\partial t} + h\frac{\partial \eta}{\partial t} + K_n\left[\frac{h^{n+1}}{(n+1)} + \phi\frac{h^{n-1}}{(n-1)}\right]\frac{\partial^2 \eta}{\partial x^2} + \frac{\partial M}{\partial x} = 0, \tag{6.4.18}$$

which when separated in powers of h gives the following results:

$$h : \frac{\partial \eta}{\partial t} = 0, \tag{6.4.19}$$

which implies that

$$\eta = \eta(x) \tag{6.4.20}$$

and

$$h^{n+1} : \frac{d^2\eta}{dx^2} = 0, \tag{6.4.21}$$

which when integrated with respect to x twice gives

$$\eta = ax + b, \tag{6.4.22}$$

where a and b are constants. Separating (6.4.18) by h^{n-1} gives again (6.4.21) and the remainder after separating (6.4.18) in powers of h is

$$\frac{\partial N}{\partial t} + \frac{\partial M}{\partial x} = 0. \tag{6.4.23}$$

From equation (6.4.22), it is clear that the gauge functions (6.4.14) and (6.4.16) reduce to

$$B^1 = (ax + b)h + N(t, x), \tag{6.4.24}$$

$$B^2 = K_n \left[\frac{h^{n+1}}{(n+1)} + \phi \frac{h^{n-1}}{(n-1)} \right] a + M(t, x), \tag{6.4.25}$$

where $M(t, x)$ and $N(t, x)$ satisfy (6.4.23). Now, from (3.3.13) and (3.3.14) the conserved vectors corresponding to the partial Noether symmetries of a partial differential equation are

$$T^1 = B^1 - \xi^1 L - (\eta - \xi^1 h_t - \xi^2 h_x) \frac{\partial L}{\partial h_t}, \tag{6.4.26}$$

$$T^2 = B^2 - \xi^2 L - (\eta - \xi^1 h_t - \xi^2 h_x) \frac{\partial L}{\partial h_x}. \tag{6.4.27}$$

Substituting the partial Lagrangian (6.4.1), the partial Noether symmetries (6.4.3) and the gauge functions (6.4.24) and (6.4.25) into equations (6.4.26) and (6.4.27) gives

$$T^1 = (ax + b)h + N(t, x), \tag{6.4.28}$$

$$T^2 = K_n \left[\frac{h^{n+1}}{(n+1)} + \phi \frac{h^{n-1}}{(n-1)} \right] a - (ax + b) K_n (h^n + \phi h^{n-2}) h_x + M(t, x), \tag{6.4.29}$$

where $M(t, x)$ and $N(t, x)$ satisfy (6.4.23). Now $T^1 = N(t, x)$ and $T^2 = M(t, x)$ are components of a trivial conserved vector because the conservation law equation (3.3.1) is identically satisfied by (6.4.23), without imposing the PDE (6.1.2). Therefore we take

$$N(t, x) = 0, \quad M(t, x) = 0. \tag{6.4.30}$$

When written in canonical form ($a = 0$ and $b = 1$ or $a = 1$ and $b = 0$), equations (6.4.28) and (6.4.29) give, respectively, the elementary conserved vector

$$\begin{aligned}\mathbf{T_{(1)}} &= (T^1, T^2) \\ &= \left(h, -K_n(h^n + \phi h^{n-2})h_x\right)\end{aligned} \tag{6.4.31}$$

and the second conserved vector

$$\begin{aligned}\mathbf{T_{(2)}} &= (T^1, T^2) \\ &= \left(xh, -K_n\left[(h^n + \phi h^{n-2})xh_x - \frac{h^{n+1}}{(n+1)} - \phi\frac{h^{n-1}}{(n-1)}\right]\right).\end{aligned} \tag{6.4.32}$$

We find that the elementary conserved vector, (6.4.31), and the second conserved vector, (6.4.32), derived by the partial Lagrangian method with gauge functions of the form (6.4.5) are the same as the conserved vectors derived by the direct and the multiplier methods. Furthermore we notice that the partial Lagrangian method with this form of gauge functions does not give any other conserved vectors besides the conserved vectors, (6.4.31) and (6.4.32), already derived by the direct method and the multiplier method.

6.4.2 Special case: n=1

All equations prior (6.4.13) are also applicable for $n = 1$. Therefore

$$\xi^1 = 0, \quad \xi^2 = 0, \quad \eta = \eta(t, x). \tag{6.4.33}$$

Also, B^1 is defined by (6.4.16). Substituting $n = 1$ into (6.4.13) gives

$$K_1\left(h + \frac{\phi}{h}\right)\frac{\partial \eta}{\partial x} - \frac{\partial B^2}{\partial h} = 0, \tag{6.4.34}$$

which when differentiated with respect to h gives

$$B^2(t, x, h) = K_1\left(\frac{h^2}{2} + \phi ln(h)\right)\frac{\partial \eta}{\partial x} + M(t, x). \tag{6.4.35}$$

Now substituting (6.4.16) for B^1 and (6.4.35) for B^2 into the remainder (6.4.17) gives

$$h\frac{\partial \eta}{\partial t} + K_1\left(\frac{h^2}{2} + \phi ln(h)\right)\frac{\partial^2 \eta}{\partial x^2} + \frac{\partial N}{\partial t} + \frac{\partial M}{\partial x} = 0. \tag{6.4.36}$$

It can be verified that differentiating (6.4.36) and separating the result with respect to h gives equation (6.4.22) for η, which reduces (6.4.36) to (6.4.23). Therefore using the same argument as in the general case, we choose $M = 0$ and $N = 0$. By (6.4.26) and (6.4.27), it can be verified that the elementary conserved vector is

$$\mathbf{T}_{(\mathbf{1})} = \left(h, -K_1\left[h + \frac{\phi}{h}\right]h_x\right). \tag{6.4.37}$$

and the second conserved vector is

$$\mathbf{T}_{(\mathbf{2})} = \left(xh, -K_1\left[\left(h + \frac{\phi}{h}\right)xh_x - \frac{h^2}{2} - \phi ln(h)\right]\right). \tag{6.4.38}$$

which agree with the results obtained from the direct and the multiplier methods for $n = 1$.

6.5 Generation of new conserved vectors from known conserved vectors

The method of generating conserved vectors from known conserved vectors that was introduced by Kara and Mahomed [42] will now be used to investigate if the governing partial differential equation (6.1.2) admits any other conserved vector besides the elementary conserved vector, (6.4.31), and the second conserved vector, (6.4.32), already derived using the direct, the multiplier and the partial Lagrangian methods in Sections 6.2, 6.3 and 6.4. The components [42],

$$T^1_* = X(T^1) + T^1 D_2(\xi^2) - T^2 D_2(\xi^1), \tag{6.5.1}$$

$$T^2_* = X(T^2) + T^2 D_1(\xi^1) - T^1 D_1(\xi^2), \tag{6.5.2}$$

can either give new conserved vectors of the governing PDE or only a linear combination of the known conserved vectors or give zero. The Lie point symmetry X is prolonged to as many derivatives as required.

It is shown in Appendix B that the Lie point symmetry generator for the partial differential equation (6.1.2) is

$$X = (c_1 + c_2 t)\frac{\partial}{\partial t} + \left(c_3 + \frac{c_2}{2}x\right)\frac{\partial}{\partial x}, \tag{6.5.3}$$

where c_1, c_2 and c_3 are constants. Using (3.2.5) for ζ_2, the first prolongation of X, the formula of which is given by (3.3.12), is

$$X^{[1]} = (c_1 + c_2 t)\frac{\partial}{\partial t} + \Big(c_3 + \frac{c_2}{2}x\Big)\frac{\partial}{\partial x} - \frac{c_2}{2}h_x\frac{\partial}{\partial h_x}, \tag{6.5.4}$$

where ζ_1 will not be required to calculate $\mathbf{T}_*$. First, we investigate using the elementary conserved vector, (6.4.31), to generate a conserved vector. Using equations (6.5.1) to (6.5.4), it can be verified that

$$T^1_* = \frac{c_2}{2}T^1_{(1)}, \quad T^2_* = \frac{c_2}{2}T^2_{(1)}, \tag{6.5.5}$$

which implies that

$$\mathbf{T}^*_{(1)} = \frac{c_2}{2}\mathbf{T}_{(1)}. \tag{6.5.6}$$

Similarly, for the second conserved vector (6.4.32),

$$T^1_* = c_3 T^1_{(1)} + c_2 T^1_{(2)}, \quad T^2_* = c_3 T^2_{(1)} + c_2 T^2_{(2)}, \tag{6.5.7}$$

which implies that

$$\mathbf{T}^*_{(2)} = c_3\mathbf{T}_{(1)} + c_2\mathbf{T}_{(2)}. \tag{6.5.8}$$

From equations (6.5.6) and (6.5.8), it is clear that the generated conserved vectors are not new conserved vectors since $\mathbf{T}^*_{(1)}$ is a scalar multiple of the elementary conserved vector, (6.4.31), and $\mathbf{T}^*_{(2)}$ is a linear combination of the elementary conserved vector, (6.4.31), and the second conserved vector, (6.4.32).

It can be verified that the conserved vector generated from the second conserved vector of the special case ($n = 1$), (6.4.38), satisfies (6.5.8). The conserved vector generated from the elementary conserved vector of the special case ($n = 1$), (6.4.37), clearly satisfies (6.5.6) by setting $n = 1$ in the elementary conserved vector of the general case ($n > 0$ and $n \neq 1$).

6.6 Conclusions

In this Chapter we derived conserved vectors for the partial differential equation (6.1.1). We first applied the direct method and then used the multiplier and the partial Lagrangian

methods in order to determine if more conserved vectors besides the ones derived by the direct method could be found. The three methods yielded the same two conserved vectors, namely: the elementary conserved vector, (6.4.31), and the second conserved vector, (6.4.32).

We then investigated the method of Kara and Mahomed [42] of generating new conserved vectors from known conserved vectors and the Lie point symmetry of the partial differential equation. We found that the generated conserved vectors were not new conserved vectors for the partial differential equation (6.1.1) but were either a scaling multiple of the elementary conserved vector or a linear combination of the elementary conserved vector and the second conserved vector.

Our analysis indicated that $n = 1$ and $n = 2$ are special cases for the derivation of the conservation laws for the partial differential equation (6.1.1), however we did not investigate these special cases. We only considered the general case of $n > 0$ with $n \neq 1$ and $n \neq 2$.

Chapter 7

HYPERBOLIC HYDRAULIC FRACTURE WITH TORTUOSITY

7.1 Introduction

In Chapter 2, a two-dimensional symmetric model representing a partially open fracture with contact regions modelled by the hyperbolic crack law was developed. The partial differential equation for the half-width of the model fracture is

$$\frac{\partial h}{\partial t} = K_n \frac{\partial}{\partial x}\left(h^n \frac{\partial h}{\partial x} + \phi h^{n-2} \frac{\partial h}{\partial x} \right), \tag{7.1.1}$$

where the diffusion constant is

$$K_n = \frac{a_n h_{max}^{n-3}}{3}\left(\frac{1}{1 - \frac{\sigma_{zz}^{(\infty)}}{\Lambda h_{max}}} \right), \tag{7.1.2}$$

the parameter ϕ is given by

$$\phi = -\frac{k}{\Lambda h_{max}} = \frac{\text{Pressure due to the asperities}}{\text{Pressure due to the fluid inside the fracture}} > 0, \tag{7.1.3}$$

a_n is an experimentally determined constant and h_{max} is the maximum half-width of the fracture. The investigation of a tortuous partially open fracture with contact regions

modelled by the hyperbolic crack law is motivated by Fitt et al. [1] who state that the hyperbolic crack law is generally considered as a more realistic model that describes the existence of contact regions in a partially open fracture.

In Section 7.2, we will use the Lie point symmetry approach to derive the group invariant solution for the length, volume and half-width of the model fracture. All properties of the fracture, such as the length and volume of the fracture, and quantities analysing fluid flow in the fracture, such as equations of fluid flux and the width averaged fluid velocity, depend on an unknown function. This unknown function can be obtained by reducing the governing PDE (7.1.1) to an ODE, using the group invariant solution for the half-width of the fracture, and by solving the ODE subject to two boundary conditions, one at the fracture tip and the other at the fracture entry.

Section 7.3 considers the scaling of the governing equations that describe the properties and fluid flow in a partially open fracture with contact regions modelled by the hyperbolic crack law. This reduces the number of parameters in the problem.

The association of a Lie point symmetry of the partial differential equation (7.1.1) with the conserved vectors for (7.1.1) derived in Chapter 6, will be investigated in Section 7.4. If association is satisfied, then we will be able to investigate whether analytical solutions of the problem can be derived with the aid of Sjöberg's double reduction theorem [29].

We will investigate operating conditions at the fracture entry admitted by a partially open fracture with contact regions modelled by the hyperbolic crack law in Section 7.5. Analytical solutions corresponding to the working conditions which are obtained will be instestigated.

In Section 7.6 the asymptotic solution of the problem is derived at the fracture tip and in the ε-neighbourhood of the fracture tip, where $\varepsilon << 1$. This asymptotic solution will be necessary in any numerical solution found to have a singularity at the fracture tip. It will also determine the fracture tip behaviour we should expect in the numerical solution for different values of the parameter n.

In Section 7.7 we will obtain the numerical solution of the hyperbolic hydraulic fracture for various values of n while Section 7.8 will focus on the analysis of the width averaged fluid velocity in the fracture. The thin nature of the fracture makes the latter quantity

more meaningful to describe the fluid flow in the fracture than the fluid velocity. In Section 7.9, we will investigate approximate analytical solutions and compare them with the numerical solutions.

Section 7.10 will summarise the work done in this Chapter and briefly discuss important results obtained.

7.2 Group invariant solution

The group invariant solution $h = \Psi(t, x)$ satisfies

$$X(h - \Psi(t, x))\Big|_{h=\Psi} = 0 \tag{7.2.1}$$

where

$$X = \Big(c_1 + c_2 t\Big)\frac{\partial}{\partial t} + \Big(c_3 + \frac{c_2}{2}x\Big)\frac{\partial}{\partial x}, \tag{7.2.2}$$

with constants c_1, c_2 and c_3, is the Lie point symmetry of (7.1.1) derived in Appendix B, which is valid for all $\phi > 0$ and $0 < n < \infty$. Expanding (7.2.1) gives the first order linear partial differential equation

$$\Big(c_1 + c_2 t\Big)\frac{\partial \Psi}{\partial t} + \Big(c_3 + \frac{c_2}{2}x\Big)\frac{\partial \Psi}{\partial x} = 0. \tag{7.2.3}$$

The differential equations of the characteristic curves of (7.2.3) are

$$\frac{dt}{(c_1 + c_2 t)} = \frac{dx}{\Big(c_3 + \frac{c_2}{2}x\Big)} = \frac{d\Psi}{0}. \tag{7.2.4}$$

We consider the general case in which $c_2 \neq 0$. The first terms and the last term in (7.2.4) give

$$\frac{2\frac{c_3}{c_2} + x}{\Big(\frac{c_1}{c_2} + t\Big)^{\frac{1}{2}}} = a_1, \quad \Psi = a_2, \tag{7.2.5}$$

where a_1 and a_2 are constants. The general solution of (7.2.3) is

$$a_2 = F(a_1), \tag{7.2.6}$$

where F is an arbitrary function. Since $h = \Psi(t, x)$, the group invariant solution for the half-width of the fracture is

$$h(t, x) = F(\xi), \tag{7.2.7}$$

where the similarity variable is

$$\xi = \frac{2\frac{c_3}{c_2} + x}{\left(\frac{c_1}{c_2} + t\right)^{\frac{1}{2}}}. \tag{7.2.8}$$

We now express the problem in terms of the group invariant solution. The partial derivatives of the similarity variable (7.2.8) with respect to t and x are

$$\frac{\partial \xi}{\partial t} = -\frac{\xi}{2\left(\frac{c_1}{c_2} + t\right)}, \quad \frac{\partial \xi}{\partial x} = \frac{1}{\left(\frac{c_1}{c_2} + t\right)^{\frac{1}{2}}}. \tag{7.2.9}$$

Subsituting the group invariant solution (7.2.7), with the aid of (7.2.9), into the governing partial differential equation (7.1.1) reduces the PDE to an ordinary differential equation

$$2K_n \frac{d}{d\xi}\left(F^n(\xi)\frac{dF}{d\xi} + \phi F^{n-2}(\xi)\frac{dF}{d\xi}\right) + \frac{d}{d\xi}\left(\xi F(\xi)\right) - F(\xi) = 0. \tag{7.2.10}$$

The ODE (7.2.10) does not depend on c_3. We choose $c_3 = 0$ which makes $\xi = 0$ when $x = 0$ and reduces the similarity variable (7.2.8) to

$$\xi = \frac{x}{\left(\frac{c_1}{c_2} + t\right)^{\frac{1}{2}}}. \tag{7.2.11}$$

We now consider the boundary condition at the fracture tip which also gives an expression for $L(t)$. The boundary condition at the fracture tip,

$$h(t, L(t)) = 0, \tag{7.2.12}$$

in terms of the group invariant solution is

$$F(A(t)) = 0, \tag{7.2.13}$$

where

$$A(t) = \frac{L(t)}{\left(\frac{c_1}{c_2} + t\right)^{\frac{1}{2}}}. \tag{7.2.14}$$

Differentiating (7.2.13) with respect to $'t'$ gives

$$\frac{dF}{dA}\frac{dA}{dt} = 0. \tag{7.2.15}$$

But in general,

$$\frac{dF}{dA} \neq 0, \tag{7.2.16}$$

and therefore

$$\frac{dA}{dt} = 0. \tag{7.2.17}$$

Thus

$$A(t) = \frac{L(t)}{\left(\frac{c_1}{c_2} + t\right)^{\frac{1}{2}}} = k, \tag{7.2.18}$$

where k is a constant. It follows that

$$L(t) = k\left(\frac{c_1}{c_2} + t\right)^{\frac{1}{2}}. \tag{7.2.19}$$

But since the characteristic length of the fracture was chosen to be the dimensional initial length of the fracture, it follows that

$$L(0) = k\left(\frac{c_1}{c_2}\right)^{\frac{1}{2}} = 1. \tag{7.2.20}$$

and therefore

$$L(t) = \left(1 + \frac{c_2}{c_1}t\right)^{\frac{1}{2}} \tag{7.2.21}$$

and the boundary condition at the fracture tip, (7.2.13), becomes

$$F\left(\left[\frac{c_2}{c_1}\right]^{\frac{1}{2}}\right) = 0. \tag{7.2.22}$$

The second boundary condition, (2.4.84), is

$$-2K_n\left(h^n(t,0)\frac{\partial h}{\partial x}(t,0) + \phi h^{n-2}(t,0)\frac{\partial h}{\partial x}(t,0)\right) = \frac{dV}{dt}, \tag{7.2.23}$$

where the dimensionless volume of the fracture, (2.4.76), is

$$V(t) = 2\int_0^{L(t)} h(t,x)dx. \tag{7.2.24}$$

The volume of the fracture (7.2.24) re-expressed in terms of the group invariant solution (7.2.7) is

$$V(t) = 2\Big(\frac{c_1}{c_2}\Big)^{\frac{1}{2}} L(t) \int_0^{\left(\frac{c_2}{c_1}\right)^{\frac{1}{2}}} F(\xi) d\xi \tag{7.2.25}$$

and therefore

$$\frac{dV}{dt} = \Big(\frac{c_2}{c_1}\Big)^{\frac{1}{2}} \frac{1}{L(t)} \int_0^{\left(\frac{c_2}{c_1}\right)^{\frac{1}{2}}} F(\xi) d\xi. \tag{7.2.26}$$

Using (7.2.7) also to express the left hand side of (7.2.23) in terms of the group invariant solution, the second boundary condition becomes

$$-2K_n\Big(F^n(0) + \phi F^{n-2}(0)\Big)\frac{dF}{d\xi}(0) = \int_0^{\left(\frac{c_2}{c_1}\right)^{\frac{1}{2}}} F(\xi) d\xi. \tag{7.2.27}$$

The zero flux condition at the fracture tip given by (2.4.90) reduces to

$$\left(F^n\Big(\Big[\frac{c_2}{c_1}\Big]^{\frac{1}{2}}\Big) + \phi F^{n-2}\Big(\Big[\frac{c_2}{c_1}\Big]^{\frac{1}{2}}\Big)\right)\frac{dF}{d\xi}\Big(\Big[\frac{c_2}{c_1}\Big]^{\frac{1}{2}}\Big) = 0 \tag{7.2.28}$$

when expressed in terms of the group invariant solution. Similarly, expressing the volume flux of fluid per unit breadth

$$Q(t,x) = -2K_n\left(h^n\frac{\partial h}{\partial x} + \phi h^{n-2}\frac{\partial h}{\partial x}\right) \tag{7.2.29}$$

and the width averaged fluid velocity

$$\overline{v}_x(t,x) = -K_n\left(h^{n-1}\frac{\partial h}{\partial x} + \phi h^{n-3}\frac{\partial h}{\partial x}\right), \tag{7.2.30}$$

both derived in (2.4.87) and (2.4.88) respectively, in terms of the group invariant solution (7.2.7) gives

$$Q(t,x) = -\frac{2K_n}{L(t)}\Big(\frac{c_2}{c_1}\Big)^{\frac{1}{2}}\Big(F^n(\xi) + \phi F^{n-2}(\xi)\Big)\frac{dF}{d\xi}, \tag{7.2.31}$$

$$\overline{v}_x(t,x) = -\frac{K_n}{L(t)}\Big(\frac{c_2}{c_1}\Big)^{\frac{1}{2}}\Big(F^{n-1}(\xi) + \phi F^{n-3}(\xi)\Big)\frac{dF}{d\xi}. \tag{7.2.32}$$

7.3 Scaling of the governing equations

In this Section, we introduce the transformation of variables

$$u = \frac{x}{L(t)}, \quad \xi = \left(\frac{c_2}{c_1}\right)^{\frac{1}{2}} u, \quad F(\xi) = Bf(u), \quad 0 \leq u \leq 1, \tag{7.3.1}$$

where B is a constant that will be determined later, in order to reduce the number of parameters and therefore simplify the boundary value problem.

Firstly, applying the transformation of variables (7.3.1) to the ordinary differential equation (7.2.10) gives

$$\frac{2K_n B^n c_1}{c_2} \frac{d}{du}\left(f^n(u)\frac{df}{du} + \frac{\phi}{B^2} f^{n-2}(u)\frac{df}{du} \right) + \frac{d}{du}\Big(uf(u) \Big) - f(u) = 0. \tag{7.3.2}$$

We choose

$$\frac{2K_n B^n c_1}{c_2} = 1. \tag{7.3.3}$$

It follows that

$$B = \left(\frac{1}{2K_n}\frac{c_2}{c_1}\right)^{\frac{1}{n}}. \tag{7.3.4}$$

Using (7.3.1) and (7.3.4) to scale the remaining equations, it can be verified that the problem is to solve the ordinary differential equation

$$\frac{d}{du}\left(f^n(u)\frac{df}{du} + \frac{\phi}{\left[\frac{1}{2K_n}\frac{c_2}{c_1}\right]^{\frac{2}{n}}} f^{n-2}(u)\frac{df}{du} \right) + \frac{d}{du}\Big(uf(u) \Big) - f(u) = 0, \tag{7.3.5}$$

subject to the boundary conditions

$$f(1) = 0, \tag{7.3.6}$$

$$\left(f^n(0) + \frac{\phi}{\left[\frac{1}{2K_n}\frac{c_2}{c_1}\right]^{\frac{2}{n}}} f^{n-2}(0) \right) \frac{df}{du}(0) = -\int_0^1 f(u)du. \tag{7.3.7}$$

The length, volume and half-width of the fracture are

$$L(t) = \left(1 + \frac{c_2}{c_1}t\right)^{\frac{1}{2}}, \tag{7.3.8}$$

$$V(t) = 2\Big[\frac{1}{2K_n}\frac{c_2}{c_1}\Big]^{\frac{1}{n}} L(t) \int_0^1 f(u)du, \tag{7.3.9}$$

$$h(t,x) = \Big[\frac{1}{2K_n}\frac{c_2}{c_1}\Big]^{\frac{1}{n}} f(u), \tag{7.3.10}$$

while the volume flux of fluid per unit breadth and the width averaged fluid velocity in the fracture are

$$Q(t,x) = -\frac{2K_n}{L(t)}\left[\frac{1}{2K_n}\frac{c_2}{c_1}\right]^{\frac{n+1}{n}}\left(f^n(u) + \frac{\phi}{\left[\frac{1}{2K_n}\frac{c_2}{c_1}\right]^{\frac{2}{n}}}f^{n-2}(u)\right)\frac{df}{du}, \tag{7.3.11}$$

$$\overline{v}_x(t,x) = -\frac{1}{2L(t)}\left(\frac{c_2}{c_1}\right)\left(f^{n-1}(u) + \frac{\phi}{\left[\frac{1}{2K_n}\frac{c_2}{c_1}\right]^{\frac{2}{n}}}f^{n-3}(u)\right)\frac{df}{du}. \tag{7.3.12}$$

The solution at the fracture tip must satisfy the zero flux condition,

$$\left(f^n(1) + \frac{\phi}{\left[\frac{1}{2K_n}\frac{c_2}{c_1}\right]^{\frac{2}{n}}}f^{n-2}(1)\right)\frac{df}{du}(1) = 0. \tag{7.3.13}$$

In Section 2.4, we chose the characteristic half-width of the fracture, H, to be the maximum half-width of the fracture, h_{max}. It therefore follows that the dimensionless half-width of the fracture satisfies

$$h^*(t^*,x^*) = \frac{h(t,x)}{H} = \frac{h(t,x)}{h_{max}}. \tag{7.3.14}$$

We define

$$\beta = h^*(0,x_{max}) = \frac{h(0,x_{max})}{h_{max}}, \tag{7.3.15}$$

where x_{max} is the point along the length of the fracture at which the maximum half-width at $t = 0$ is attained. In a partially open fracture $h_{min} \leq h(t,x) < h_{max}$, where we make the approximation that the minimum half-width of the fracture is zero ($h_{min} = 0$), and therefore the range of β is $0 \leq \beta < 1$. In an open fracture $h \geq h_{max}$ and therefore the range of β is $\beta \geq 1$. In this Chapter we only consider analysis of a partially open fracture, $\phi > 0$, and therefore we will only consider the range $0 \leq \beta < 1$.

Note that equations (7.3.8) to (7.3.13) are dimensionless although the dimensionless notation (*) is suppressed. Imposing (7.3.15) on (7.3.10) at $t = 0$ gives

$$\beta = h(0,x_{max}) = \left[\frac{1}{2K_n}\frac{c_2}{c_1}\right]^{\frac{1}{n}} f(u_{max}), \tag{7.3.16}$$

where at $t = 0$, $u_{max} = x_{max}$ since $L(0) = 1$. Thus

$$\frac{c_2}{c_1} = 2K_n\left(\frac{\beta}{f(u_{max})}\right)^n. \tag{7.3.17}$$

It will be shown later that $u_{max} = 0$ and therefore $f(u_{max}) = f(0)$. Substituting (7.3.17), with $u_{max} = 0$, into the governing equations (7.3.5) to (7.3.13) gives

$$\frac{d}{du}\left(f^n(u)\frac{df}{du} + \phi\Big(\frac{f(0)}{\beta}\Big)^2 f^{n-2}(u)\frac{df}{du}\right) + \frac{d}{du}\Big(uf(u)\Big) - f(u) = 0, \tag{7.3.18}$$

$$f(1) = 0, \tag{7.3.19}$$

$$f^n(0)\frac{df}{du}(0) = -\frac{1}{(1+\frac{\phi}{\beta^2})}\int_0^1 f(u)du, \tag{7.3.20}$$

where

$$L(t) = \left(1 + 2\Big(\frac{\beta}{f(0)}\Big)^n K_n t\right)^{\frac{1}{2}}, \tag{7.3.21}$$

$$V(t) = 2\beta L(t)\int_0^1 \frac{f(u)}{f(0)}du, \tag{7.3.22}$$

$$h(t,x) = \beta\frac{f(u)}{f(0)}, \tag{7.3.23}$$

and

$$Q(t,x) = -\frac{2K_n}{L(t)}\Big(\frac{\beta}{f(0)}\Big)^{n+1}\left(f^n(u) + \phi\Big[\frac{f(0)}{\beta}\Big]^2 f^{n-2}(u)\right)\frac{df}{du}, \tag{7.3.24}$$

$$\overline{v}_x(t,x) = -\frac{K_n}{L(t)}\Big(\frac{\beta}{f(0)}\Big)^{n}\left(f^{n-1}(u) + \phi\Big[\frac{f(0)}{\beta}\Big]^2 f^{n-3}(u)\right)\frac{df}{du}, \tag{7.3.25}$$

$$\frac{c_2}{c_1} = 2K_n\Big(\frac{\beta}{f(0)}\Big)^n. \tag{7.3.26}$$

The zero flux condition (7.3.13) that must be satisfied at the fracture tip therefore reduces to

$$\left[f^n(1) + \Big(\frac{\phi f^2(0)}{\beta^2}\Big)f^{n-2}(1)\right]\frac{df}{du}(1) = 0. \tag{7.3.27}$$

The pressure ratio ϕ in the governing equations (7.3.18) to (7.3.27) is given by (7.1.3). The diffusion constant K_n can be obtained experimentally, for example when $n = 3$, $a_3 = 1$ [1] and therefore

$$K_3 = \frac{1}{3}\left(\frac{1}{1 - \frac{\sigma_{zz}^{(\infty)}}{\Lambda h_{max}}}\right). \tag{7.3.28}$$

However, we would like to keep the analysis general and not case specific, therefore when plotting solutions we will scale K_n into the time. We consider a partially open fracture ($\phi > 0$) and therefore we will use parameter values that satisfy $0 \leq \beta < 1$. The maximum function value $f(u_{max}) = f(0)$ will be obtained by simply solving the boundary value problem (7.3.18) to (7.3.20) and determining the maximum of the solution $f(u)$ by finding where $df/du = 0$. Unlike the ODE (5.3.5) for the linear crack law, there is no arbitrary parameter α in the ODE (7.3.18) which could be chosen to specify the working condition at the fracture entry. We will show later that for the hyperbolic hydraulic fracture there is only one working condition which is already imposed on the equations (7.3.18) to (7.3.26).

7.4 Asymptotic solution at the fracture tip

In this Section we investigate the asymptotic solution, $f(u)$, of the ODE (7.3.18) at the fracture tip. We will then be able to derive the asymptotic solution for the half-width of the fracture, $h(t, x)$, at the fracture tip. The asymptotic solution will allow us to characterize the behaviour at the fracture tip of the half-width for different values of the parameter n. We consider $\phi > 0$. The asymptotic solution when $\phi = 0$ was derived in Section 5.6 of Chapter 5 for a linear hydraulic fracture. We look for an asymptotic solution of (7.3.18) of the form

$$f(u) \sim A(1-u)^p, \quad \text{as} \quad u \to 1, \tag{7.4.1}$$

where the constants A and $p > 0$ will have to be determined later. It is necessary for the solution (7.4.1) to satisfy the first boundary condition (7.3.19) and it does for $p > 0$. The solution (7.4.1) does not satisfy the second boundary condition (7.3.20) but it is not expected to satisfy this boundary condition. The derivative of (7.4.1) will also be needed

in our calculation, therefore it is necessary to differentiate (7.4.1) to obtain

$$\frac{df}{du} = -Ap(1-u)^{p-1}. \tag{7.4.2}$$

Substituting (7.4.1), with the aid of (7.4.2), into the ordinary differential equation (7.3.18) and dividing the result by Ap gives

$$A^n[(n+1)p-1](1-u)^{(n+1)p-2}+\phi\left(\frac{f(0)}{\beta}\right)^2 A^{n-2}[(n-1)p-1](1-u)^{(n-1)p-2}+$$
$$(1-u)^p-(1-u)^{p-1}=0. \tag{7.4.3}$$

We did not use (7.4.1) to approximate the initial condition $f(0)$ in the ordinary differential equation (7.3.18) because (7.4.1) is not a good approximation at $u=0$.

Suppose first that $n \neq 2$. For $p > 2$, the second term in (7.4.3) is larger than the first term as $u \to 1$. The two dominant terms as $u \to 1$ are therefore the second and fourth terms. We balance the two dominant terms. Equating exponents and coefficients of the second and fourth terms of equation (7.4.3) gives, for $n \neq 2$,

$$p = \frac{1}{(n-2)}, \quad A = \left[(n-2)\frac{\beta^2}{\phi f^2(0)}\right]^{\frac{1}{(n-2)}}. \tag{7.4.4}$$

The remaining first and third terms in (7.4.3) vanish as $u \to 1$ provided $2 < n < 5$. From (7.4.1) and (7.4.4), it therefore follows that the asymptotic solution is

$$f(u) \sim \left[(n-2)\frac{\beta^2}{\phi f^2(0)}\right]^{\frac{1}{(n-2)}}(1-u)^{\frac{1}{(n-2)}}, \quad \text{as} \quad u \to 1, \tag{7.4.5}$$

provided $2 < n < 5$. We now check the zero flux condition at the fracture tip (7.3.27). Using (7.4.5), we have

$$\left[f^n(u)+\Big(\frac{\phi f^2(0)}{\beta^2}\Big)f^{n-2}(u)\right]\frac{df}{du}(u) \sim -\frac{A^{n-1}}{(n-2)}\left[A^2(1-u)^{\frac{3}{n-2}}+\phi\Big(\frac{f(0)}{\beta}\Big)^2(1-u)^{\frac{1}{n-2}}\right],$$
$$\text{as} \quad u \to 1. \tag{7.4.6}$$

On letting $u \to 1$ we see that (7.3.27) is satisfied since $n > 2$.

Consider now $n = 2$. When $n = 2$, equation (7.4.3) becomes

$$A^2(3p-1)(1-u)^{2p}+\phi\left(\frac{f(0)}{\beta}\right)^2(p-1)+(1-u)^2-(1-u)=0. \tag{7.4.7}$$

We take the limit of (7.4.7) as $u \to 1$. Then

$$\phi\left(\frac{f(0)}{\beta}\right)^2 (p-1) = 0 \tag{7.4.8}$$

and therefore $p = 1$. Equation (7.4.7) then becomes

$$(2A^2+1)(1-u)^2 - (1-u) = 0. \tag{7.4.9}$$

Differentiating (7.4.9) by u and letting $u \to 1$ gives $1 = 0$ which is not satisfied. We therefore conclude that there is no asymptotic solution as $u \to 1$ for $n = 2$.

Since the asymptotic solution as $u \to 1$ of the ODE (7.3.18) exists only for $2 < n < 5$, we conclude that the solution of the problem exists only for $2 < n < 5$.

Consider now the spatial gradient of the half-width of the fracture as $x \to L(t)$ for $2 < n < 5$. The half-width of the fracture (7.3.23) with $f(u)$ given by (7.4.5) is

$$h(t,x) \sim \beta\left[(n-2)\frac{\beta^2}{\phi f^n(0)}\right]^{\frac{1}{(n-2)}}\left(1-\frac{x}{L(t)}\right)^{\frac{1}{(n-2)}}, \quad \text{as} \quad x \to L(t) \tag{7.4.10}$$

and

$$\frac{\partial h}{\partial x}(t,x) \sim -\frac{\beta}{L(t)}(n-2)^{\frac{3-n}{n-2}}\left[\frac{\beta^2}{\phi f^n(0)}\right]^{\frac{1}{(n-2)}}\left(1-\frac{x}{L(t)}\right)^{\frac{3-n}{(n-2)}}, \quad \text{as} \quad x \to L(t). \tag{7.4.11}$$

It therefore follows that

$$\frac{\partial h}{\partial x}(t,L(t)) \sim \begin{cases} -\infty, & 3 < n < 5, \\ -\frac{1}{\phi L(t)}\left(\frac{\beta}{f(0)}\right)^3, & n = 3, \\ 0, & 2 < n < 3. \end{cases} \tag{7.4.12}$$

Equation (7.4.12) shows the different fracture tip behaviour for different values of the parameter n. It is clear from (7.4.12) that there is a singularity at the fracture tip due to the negative infinity spatial gradient of the half-width at the fracture tip when $3 < n < 5$. The singularity is removed for $2 < n \leq 3$ with the spatial gradient of the half-width at the fracture tip being finite and non-zero for $n = 3$ and zero for $2 < n < 3$.

In the subsequent Sections, we will investigate analytical and numerical solutions which are both expected to agree with the asymptotic solution at the fracture tip and in the

$\varepsilon-$neightbourhood of the fracture tip, where $\varepsilon << 1$. The numerical solution will be matched to the asymptotic solution when there is a singularity at the fracture tip for $3 < n < 5$.

7.5 Association of Lie point symmetries with conserved vectors

In this Section we investigate if the Lie point symmetry (7.2.2) of the governing partial differential equation (7.1.1) can be associated with the conserved vectors (6.4.31) and (6.4.32) of (7.1.1), which were derived in Chapter 6, for some values of the constants c_1, c_2 and c_3. If the condition for association is satisfied, then the double reduction theorem of Sjöberg will apply which may lead to an analytical solution.

For the general case of $n > 0$ and $n \neq 1$, the conserved vectors for (7.1.1) which were found in Chapter 6 are

$$\mathbf{T_{(1)}} = (T^1, T^2) = \left(h, -K_n(h^n + \phi h^{n-2})h_x\right), \tag{7.5.1}$$

and

$$\mathbf{T_{(2)}} = (T^1, T^2) = \left(xh, -K_n\left[(h^n + \phi h^{n-2})xh_x - \frac{h^{n+1}}{(n+1)} - \phi\frac{h^{n-1}}{(n-1)}\right]\right). \tag{7.5.2}$$

The Lie point symmetry generator of (7.1.1),

$$X = \left(c_1 + c_2 t\right)\frac{\partial}{\partial t} + \left(c_3 + \frac{c_2}{2}x\right)\frac{\partial}{\partial x}, \tag{7.5.3}$$

is associated with (7.5.1) or (7.5.2) provided $\mathbf{T}^* = \mathbf{0}$, that is if [41, 42]

$$T^*_{(i)} = X(T^i) + T^i D_k(\xi^k) - T^k D_k(\xi^i) = 0, \quad i = 1, 2, \tag{7.5.4}$$

where $D_1 = D_t$, given by (3.2.7), and $D_2 = D_x$, given by (3.2.8), are the total derivatives defined in Chapter 3.

Consider first the elementary conserved vector (7.5.1). Then

$$\mathbf{T^*_{(1)}} = \frac{c_2}{2}\mathbf{T_{(1)}} = \mathbf{0} \tag{7.5.5}$$

provided $c_2 = 0$, a condition that is satisfied for all values of c_3. From (7.5.3), the associated Lie point symmetry is

$$X = c_1 \frac{\partial}{\partial t} + c_3 \frac{\partial}{\partial x}. \tag{7.5.6}$$

However, in Section 7.2 of this Chapter, we considered $c_3 = 0$, and therefore (7.5.6) reduces to

$$X = c_1 \frac{\partial}{\partial t}. \tag{7.5.7}$$

But setting $c_2 = 0$ gives a trivial group invariant solution of the half-width of the fracture, $h(t, x) = 0$. Association of the Lie point symmetry (7.5.3) with the elementary conserved vector (7.5.1) gives a trivial solution. This trivial solution is not of interest in this thesis because we consider fractures that are propagating with increasing time t and therefore we are interested in $c_2 > 0$.

Consider next the second conserved vector (7.5.2). Then

$$\mathbf{T}^*_{(\mathbf{2})} = c_3 \mathbf{T}_{(\mathbf{1})} + c_2 \mathbf{T}_{(\mathbf{2})} = \mathbf{0} \tag{7.5.8}$$

provided both conditions $c_2 = 0$ and $c_3 = 0$ are satisfied. From (7.5.3) the associated Lie point symmetry is (7.5.7). Since $c_2 = 0$, the association of the Lie point symmetry (7.5.3) with the second conserved vector (7.5.2) again gives the trivial solution $h(t, x) = 0$.

The association of the Lie point symmetry of the PDE with the conserved vectors for the PDE did not lead to non-trivial solutions as it did for the linear crack law. It is possible to obtain analytical solutions that are not generated by a Lie point symmetry associated with a conserved vector. For example, for the linear crack law an analytical solution was derived for a hydraulic fracture propagating at constant speed.

In the next Section we will investigate the physical significance of the working condition at the fracture entry for the invariant solution derived in Section 7.3.

7.6 Operating conditions at the fracture entry

From (7.3.23) at the fracture entry, $x = 0$,

$$h(t, 0) = \beta. \tag{7.6.1}$$

The half-width at the fracture entry therefore remains constant as the fracture evolves with increasing time t. But from (2.4.89) for a partially open fracture with contact regions modelled by the hyperbolic crack law and the PKN approximation, we have at the fracture entry

$$p(t,0) = \left(\frac{1-\frac{\phi}{h^2(t,0)}}{1-\frac{\sigma_{zz}^{(\infty)}}{\Lambda h_{max}}}\right)h(t,0) - \left(\frac{k+\sigma_{zz}^{(\infty)}}{\Lambda h_{max}-\sigma_{zz}^{(\infty)}}\right) \tag{7.6.2}$$

and therefore $p(t,0)$ is constant for $t \geq 0$. Therefore the working condition at the fracture entry is that of fluid injected into the fracture at the fracture entry with a constant pressure. Unlike the linear crack law for which there is a range of working conditions, for the hyperbolic fracture there is only one working condition at the fracture entry.

Since there is fluid inflow at the fracture entry of the hyperbolic hydraulic fracture, it follows that $\overline{v}_x(t,x) > 0$ for $0 \leq x < L(t)$ $(0 \leq u < 1)$ and therefore from (7.3.25), $(df/du) < 0$ for $0 \leq u < 1$. Thus $f(u)$ is a monotonically decreasing function of u and therefore $f(u)$ attains its maximum value at $u = 0$. Thus $u_{max} = 0$ which is the value of u_{max} used in the invariant solution (7.3.18) to (7.3.26) for the hyperbolic fracture.

Consider now comparison with the model of the linear hydraulic fracture. From (5.3.20), with $f_{max} = f(0)$,

$$h(t,0) = \beta\left[1+\frac{1}{\alpha}\left(\frac{\beta}{f(0)}\right)^n K_n t\right]^{\frac{2}{n}\left(\alpha-\frac{1}{2}\right)}, \tag{7.6.3}$$

where $\alpha = c_4/c_2$ and therefore $h(t,0)$ is constant provided $\alpha = 1/2$. But from (2.4.80),

$$p(t,0) = \left(\frac{1-\frac{\sigma_R}{\Lambda h_{max}}}{1-\frac{\sigma_{zz}^{(\infty)}}{\Lambda h_{max}}}\right)h(t,0) + \left(\frac{\sigma_R-\sigma_{zz}^{(\infty)}}{\Lambda h_{max}-\sigma_{zz}^{(\infty)}}\right) \tag{7.6.4}$$

and therefore $p(t,0)$ is constant at the fracture entry provided $\alpha = 1/2$, that is $2c_4 = c_2$. The Lie point symmetry (5.2.1), for the PDE of the linear hydraulic fracture with tortuosity, (5.1.1), is

$$X = (c_1+c_2t)\frac{\partial}{\partial t} + (c_3+c_4x)\frac{\partial}{\partial x} + \frac{1}{n}(2c_4-c_2)h\frac{\partial}{\partial h}, \tag{7.6.5}$$

where c_1, c_2, c_3 and c_4 are constants. But when $\alpha = 1/2$, it reduces to

$$X = \Big(c_1+c_2t\Big)\frac{\partial}{\partial t} + \left(c_3+\frac{c_2}{2}x\right)\frac{\partial}{\partial x}, \tag{7.6.6}$$

which is the same as the Lie point symmetry (7.5.3) for the PDE of the hyperbolic hydraulic fracture.

7.7 Numerical solution of the boundary value problem

We found that the hyperbolic hydraulic fracture, defined by equations (7.3.18) to (7.3.26), assumes only one working condition, that of fluid injection at the fracture entry with constant pressure. Since we cannot integrate the ordinary differential equation (7.3.18) in order to obtain an analytical solution, we investigate a numerical solution for the boundary value problem (7.3.18) to (7.3.20). This will give a numerical result for the group invariant solution for the length, (7.3.21), volume, (7.3.22), and half-width of the fracture, (7.3.23).

7.7.1 Transformation of the BVP to two IVPs

The method of transforming a boundary value problem into a pair of initial value problems, which when solved together yields a solution to the original boundary value problem, will be used in this Chapter. It was also used in Chapter 5 for solving a model of the linear hydraulic fracture with tortuosity, [49]. It was shown that this method of solution can be used provided there exists a non-trivial scaling transformation that leaves the ordinary differential equation from the BVP invariant, [50].

Consider a scaling transformation of the form

$$\overline{u} = \lambda^a u, \quad \overline{f} = \lambda^b f, \tag{7.7.1}$$

where a and b are constants to be determined. Substituting (7.7.1) into the ordinary differential equation (7.3.18) gives

$$\lambda^{2a-bn}\frac{d}{d\overline{u}}\left(\overline{f}^n\frac{d\overline{f}}{d\overline{u}} + \frac{\phi\overline{f}^2(0)}{\beta^2}\overline{f}^{n-2}\frac{d\overline{f}}{d\overline{u}}\right) + \frac{d}{d\overline{u}}(\overline{u}\overline{f}) - \overline{f} = 0. \tag{7.7.2}$$

From (7.7.2), it is clear that the ordinary differential equation (7.3.18) is invariant under the transformation (7.7.1) provided

$$b = \frac{2}{n}a. \tag{7.7.3}$$

Letting $a = 1$ (which is equivalent to redefining λ^a as λ) simplifies (7.7.3) to

$$b = \frac{2}{n} \tag{7.7.4}$$

and therefore reduces (7.7.1) to

$$\overline{u} = \lambda u, \quad \overline{f} = \lambda^{\frac{2}{n}} f. \tag{7.7.5}$$

Since the non-trivial scaling transformation (7.7.5) leaves the ordinary differential equation (7.3.18) invariant, it follows that the boundary value problem (7.3.18) to (7.3.20) can be transformed, using (7.7.5), into a pair of initial value problems. Lie group analysis can also be used to obtain the scaling transformation (7.7.5), although not discussed in this Chapter, [14].

We substitute the scaling transformation (7.7.5) into the boundary value problem (7.3.18) to (7.3.20) and choose $\overline{f}(0) = 1$. Then

$$f(0) = \lambda^{\frac{2}{n}} \tag{7.7.6}$$

where the parameter λ is obtained from the boundary condition $f(1) = 0$ and the transformation (7.7.5) which gives $\overline{f}(\lambda) = 0$. The first initial value problem is

Initial value problem I (IVP I)

$$\frac{d}{d\overline{u}}\left(\overline{f}^n \frac{d\overline{f}}{d\overline{u}} + \frac{\phi}{\beta^2}\overline{f}^{n-2}\frac{d\overline{f}}{d\overline{u}}\right) + \frac{d}{d\overline{u}}(\overline{u}\overline{f}) - \overline{f} = 0, \tag{7.7.7}$$

$$\overline{f}(0) = 1, \tag{7.7.8}$$

$$\frac{d\overline{f}}{d\overline{u}}(0) = -\left(\frac{1}{1+\frac{\phi}{\beta^2}}\right)\int_0^{\lambda} \overline{f}(\overline{u})d\overline{u}, \tag{7.7.9}$$

where $0 \leq \overline{u} \leq \lambda$ and λ satisfies

$$\overline{f}(\lambda) = 0. \tag{7.7.10}$$

Solving the first initial value problem, (7.7.7) to (7.7.10), gives the value of the parameter λ which will be required in the second initial value problem. Substituting the tranformation (7.7.5) into the first initial value problem, (7.7.7) to (7.7.9), gives the second initial value problem

$$\frac{d}{du}\left(f^n\frac{df}{du}+\frac{\phi}{\lambda^{\frac{4}{n}}\beta^2}f^{n-2}\frac{df}{du}\right)+\frac{d}{du}(uf)-f=0, \tag{7.7.11}$$

$$f(0)=\lambda^{-\frac{2}{n}}, \tag{7.7.12}$$

$$\frac{df}{du}(0)=-\left(\frac{\lambda^2}{1+\frac{\phi}{\beta^2}}\right)\int_0^1 f(u)du, \tag{7.7.13}$$

The boundary condition at the fracture tip, $f(1)=0$, is identically satisfied because it was used to derive condition (7.7.10) for λ which is used in IVP II. Since the second initial condition (7.7.13) is complicated because of the integral sign, we use an alternative expression for the second initial condition obtained by differentiating f with respect to u in the transformation of variables (7.7.5) and evaluating the result at $u=0$. Instead of solving the second initial value problem (7.7.11) to (7.7.13), we equivalently solve the second initial value problem

Initial value problem II (IVP II)

$$\frac{d}{du}\left(f^n\frac{df}{du}+\frac{\phi}{\lambda^{\frac{4}{n}}\beta^2}f^{n-2}\frac{df}{du}\right)+\frac{d}{du}(uf)-f=0, \tag{7.7.14}$$

$$f(0)=\lambda^{-\frac{2}{n}}, \tag{7.7.15}$$

$$\frac{df}{du}(0)=\lambda^{\frac{n-2}{n}}\frac{d\overline{f}}{d\overline{u}}(0), \tag{7.7.16}$$

where $0\le u\le 1$ and λ and $\frac{d\overline{f}}{d\overline{u}}(0)$ are attained from IVP I.

The derivative $\frac{d\overline{f}}{d\overline{u}}(0)$ in (7.7.16) is obtained from solving the first initial value problem. Solving the two initial value problems, (7.7.7) to (7.7.10) and (7.7.14) to (7.7.16), is the same as solving the original boundary value problem, (7.3.18) to (7.3.20).

The unknown initial value $f(0)$ which occured in the ODE (7.3.18) for the BVP does not occur in the ODEs (7.7.7) and (7.7.14) for IVP I and IVP II. This is because in IVP I we chose the initial condition $\overline{f}(0) = 1$ and in IVP II it followed from the transformation (7.7.5) that $f(0) = \lambda^{-\frac{2}{n}}$. This result for $f(0)$ is also used to calculate the properties of the fracture, (7.3.21) to (7.3.26).

The IVP I is solved using both the MATLAB ode45 solver, which uses the Runga Kutta scheme of order 4 and 5 with adaptive stepsize, and the backward shooting method. The solution $\overline{f}(\overline{u})$, obtained from (7.7.7), is shot from the $\overline{u}-$axis, satisfying the condition (7.7.10), to the $\overline{f}-$axis iteratively until the initial conditions (7.7.8) and (7.7.9) with tolerance of order 10^{-10} are satisfied. In the first iteration the initial estimates for both λ and the spatial derivative $\frac{d\overline{f}}{d\overline{u}}$ at the point $(\lambda, 0)$ from which the solution $\overline{f}$ is shot, to the $\overline{f}-$axis, are required. The estimate for λ used in Chapter 5 for the constant pressure solution of a linear hydraulic fracture will be used in this Chapter as a base estimate until a suitable initial estimate for λ is obtained. The derivative of the asymptotic solution, (7.4.7), in the barred variables, (7.7.5),

$$\frac{d\overline{f}}{d\overline{u}} = -\lambda^{\frac{1}{n-2}}(n-2)^{\frac{3-n}{n-2}}\left(\frac{\beta^2}{\phi}\right)^{\frac{1}{n-2}}(\lambda - u)^{\frac{3-n}{n-2}}, \tag{7.7.17}$$

will be used as the initial estimate of the slope at the root λ. For subsequent iterations both the value of λ and the corresponding spatial derivative at the root λ generated from the previous iteration will be used to obtain the solution $\overline{f}(\overline{u})$ in the current iteration. After solving the IVP I, (7.7.7) to (7.7.10), in order to obtain the solution $\overline{f}(\overline{u})$, we will use the corresponding obtained values of λ and the initial condition $\frac{d\overline{f}}{d\overline{u}}(0)$, both achieved after convergence of the solution $\overline{f}(\overline{u})$, to solve the the IVP II, (7.7.14) to (7.7.16).

The IVP II is solved using the MATLAB ode45 solver with the parameter λ given by the IVP I and the initial condition $\frac{d\overline{f}}{d\overline{u}}(0)$ in (7.7.16) also given by the IVP I. Although an analytical solution could not be obtained for the hyperbolic hydraulic fracture, an approximate analytical solution will be derived in Section 7.9 which be compared with the numerical solution.

7.7.2 Discussion of the numerical solution

In Section 7.5, we found that the hyperbolic hydraulic fracture with tortuosity admits only one working condition which is fluid injection at the fracture entry with constant pressure. In Subsection 7.7.1 we discussed the method of solution that will be used to solve this problem. A range of values of the parameter ϕ will be chosen in the IVP I and IVP II. We first choose $\phi = 1$ and plot the half-width of a partially open fracture, with $\beta = 0.5$, for increasing scaled time $K_n t$ and for $n = 4$, 3 and 2.5, in Figure 7.1. We consider numerical solutions satisfying the parameter range $2 < n < 5$ as directed by the asymptotic solution. It is clear from Figure 7.1 that for $3 < n < 5$ lubrication theory breaks down at the fracture tip because of the negative infinity spatial gradient of the half-width at the fracture tip. Lubrication theory is satisfied for $2 < n \leq 3$ because the spatial gradient of the half-width at the fracture tip is finite and non-zero when $n = 3$ and vanishes when $2 < n < 3$. This behaviour at the fracture tip is consistent with the asymptotic solution of the hyperbolic fracture at the fracture tip derived in equation (7.4.12). From (7.3.10), $h(t, 0) = \beta$ for all $t \geq 0$ which is clearly shown in Figure 7.1. Since $h(t, 0)$ is constant the pressure at the fracture entry $p(t, x)$ is also constant by (7.6.2) which defines the working condition for the hyperbolic fracture.

We now investigate the effect of the increasing parameter ϕ on the length of the fracture. In Figure 7.2, the half-width of the fracture is plotted against x at the scaled time $K_n t = 20$ and for different parameter values of $\phi = 0$, 0.1, 0.5 and 1. The length of a partially open hyperbolic hydraulic fracture increases as the parameter ϕ increases. This is shown in Figure 7.2 and more clearly in Figure 7.3.

The hyperbolic crack law is generally considered to be a more realistic crack law that describes the presence of contact regions, [1]. It is interesting to note that all the working conditions dependent on the parameter n for the linear hydraulic partially open fracture discussed in Chapter 5, reduce to the constant pressure working condition as tortuosity increases and therefore as $n \to 0$ in Chapter 5. The partially open hyperbolic hydraulic fracture with tortuosity in this Chapter admits only the constant pressure working condition. We investigate comparison of the constant pressure solution obtained in Chapter 5 for the partially open linear hydraulic fracture with the constant pressure solution of the partially open hyperbolic hydraulic fracture in order to understand the differences of the two crack laws.

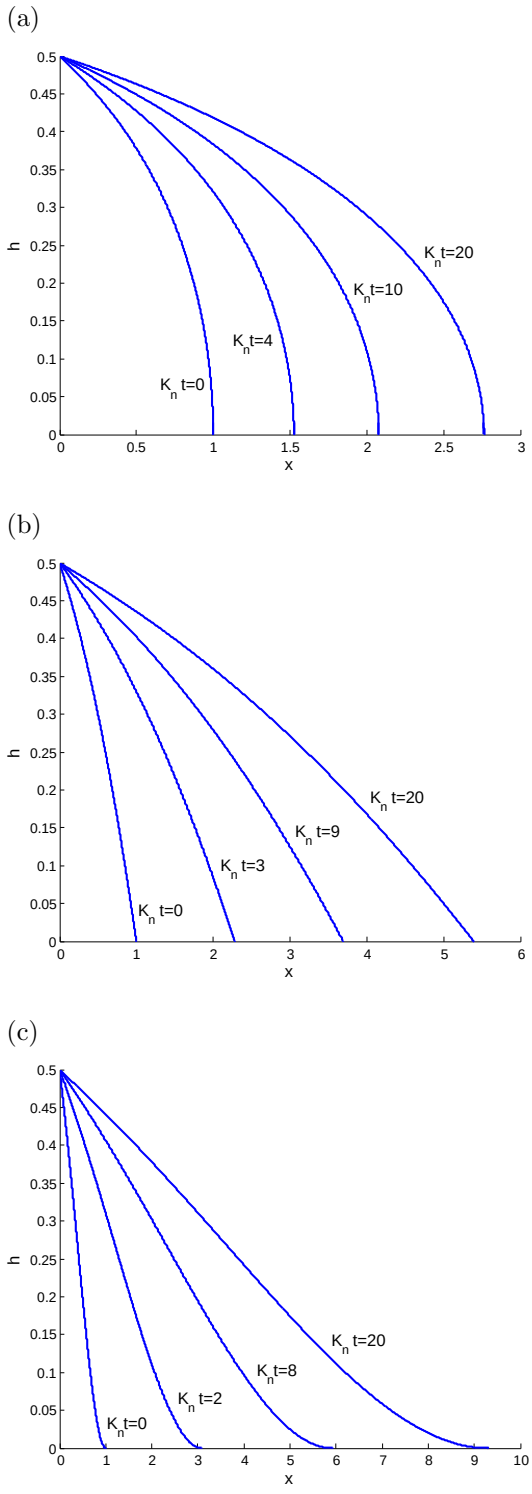

Figure 7.1: Partially open fracture, $\beta = 0.5$, propagating with fluid injected at the fracture entry at a constant pressure. The numerical solution (7.3.23) for the half-width $h(t, x)$ plotted against x for increasing values of the scaled time $K_n t$ and for (a) $n = 4$, (b) $n = 3$, (c) $n = 2.5$.

To do this, their scaled times, $K_n t$, must be the same. Firstly, from Chapter 2 the characteristic time

$$T = \frac{\mu L_o^2}{h_{max}^2(\Lambda h_{max} - \sigma_{zz}^{(\infty)})} \tag{7.7.18}$$

applies to both the linear and the hyperbolic hydraulic fractures and therefore their dimensionless times t in $K_n t$ are the same. It therefore remains to consider the diffusion constants K_n of the linear and the hyperbolic hydraulic fractures. The diffusion constant for a linear hydraulic fracture given in (5.1.2) is

$$K_n^L = \frac{a_n h_{max}^{n-3}}{3}\left(\frac{1 - \frac{\sigma_R}{\Lambda h_{max}}}{1 - \frac{\sigma_{zz}^{(\infty)}}{\Lambda h_{max}}}\right) \tag{7.7.19}$$

and the diffusion constant for a hyperbolic hydraulic fracture given in (7.1.2) is

$$K_n^H = \frac{a_n h_{max}^{n-3}}{3}\left(\frac{1}{1 - \frac{\sigma_{zz}^{(\infty)}}{\Lambda h_{max}}}\right), \tag{7.7.20}$$

where the superscripts L and H in (7.7.19) and (7.7.20) distinguish the two diffusion constants. The diffusion constants, (7.7.19) and (7.7.20), are not the same. We consider the ratio

$$\frac{K_n^L}{K_n^H} = \left(1 - \frac{\sigma_R}{\Lambda h_{max}}\right) > 1, \quad \sigma_R < 0. \tag{7.7.21}$$

However, (7.7.21) is not sufficient to provide general conclusive results about the difference in the properties of the two models resulting from the linear and the hyperbolic crack laws. Therefore further investigation, though not provided in this thesis, is necessary in order to compare the linear and the hyperbolic hydraulic fractures.

We found that the numerical solutions for the hyperbolic hydraulic fracture, when $\phi = 0$ and $K_n^L = K_n^H$, overlap the numerical solutions for the linear hydraulic fracture with fluid injected at the fracture entry at a constant pressure, as shown in Figure 7.2. This is a good numerical check for the hyperbolic hydraulic fracture given that it has no analytical solutions to test the numerical scheme. The results show that the numerical scheme used to solve the hyperbolic crack law model is correct at least for $\phi = 0$. Note that in Figures 7.2 and 7.3 we cannot compare properties of the linear hydraulic fracture, $\phi = 0$, and of the hyperbolic hydraulic fracture, $\phi > 0$, because they have the same scaled time and therefore $K_n^L/K_n^H = 1$ which does not satisfy the condition (7.7.21).

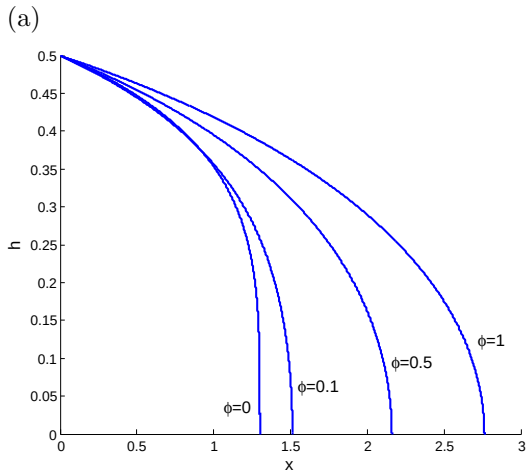

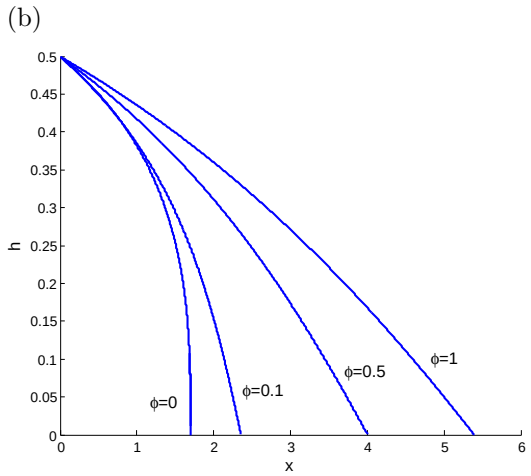

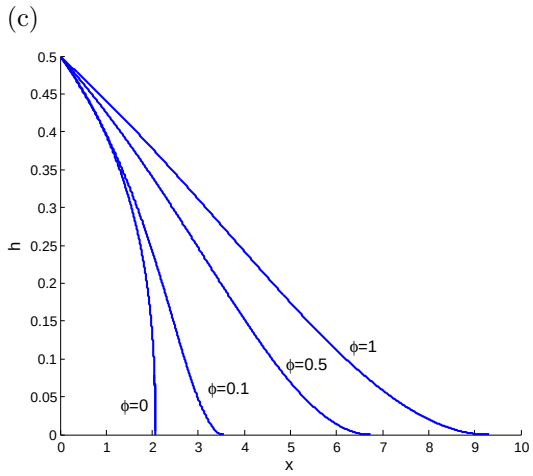

Figure 7.2: Partially open fracture, $\beta = 0.5$, propagating with fluid injected at the fracture entry at a constant pressure. The numerical solution (7.3.23) for the half-width $h(t, x)$ plotted against x for $K_n^H = K_n^L t = 20$ and for (a) $n = 4$, (b) $n = 3$, (c) $n = 2.5$. The linear fracture, $\phi = 0$ and the hyperbolic fracture, $\phi = 0.1$, 0.5 and 1.

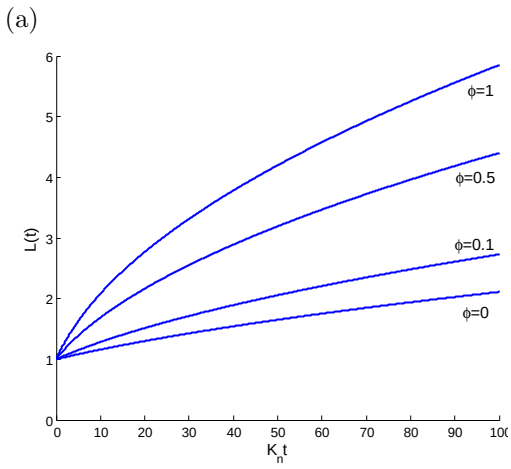

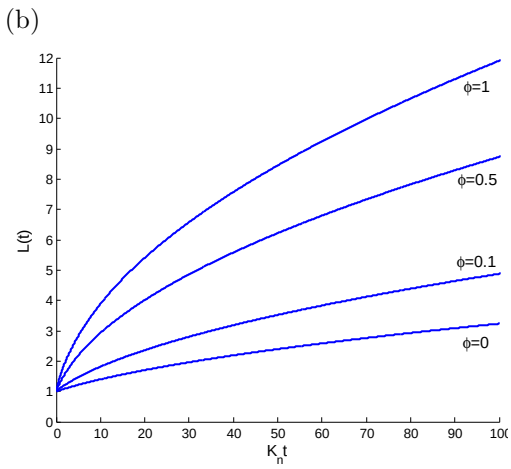

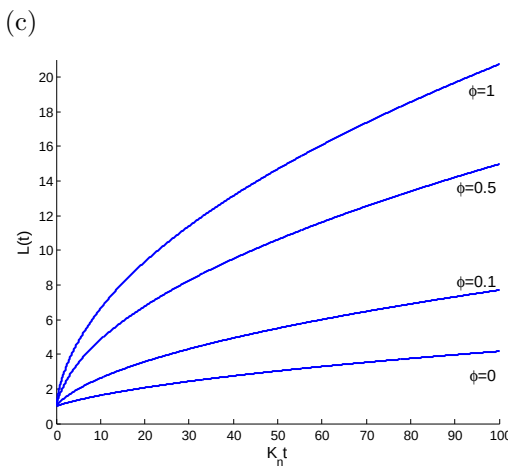

Figure 7.3: Lengths of the linear, $\phi = 0$, and hyperbolic, $\phi = 0.1$, 0.5 and 1, partially open fractures, $\beta = 0.5$, plotted against the increasing values of the scaled time $K_n^L t$, (7.7.19), and for fluid injected at the fracture entry at a constant pressure where (a) $n = 4$, (b) $n = 3$, (c) $n = 2.5$.

7.8 Width averaged fluid velocity

In this Section, we investigate the width averaged fluid velocity in a fracture that has contact regions modelled by the hyperbolic crack law. The width averaged fluid velocity given by equation (7.3.25):

$$\overline{v}_x(t,x) = -\frac{K_n}{L(t)}\Big(\frac{\beta}{f(0)}\Big)^n\left(f^{n-1}(u) + \phi\Big[\frac{f(0)}{\beta}\Big]^2 f^{n-3}(u)\right)\frac{df}{du}, \tag{7.8.1}$$

is a more meaningful measure of the fluid behaviour in a thin fracture with tortuosity than the fluid velocity. Although the parameters in the diffusion constant K_n can be obtained through experiments, they are not readily available. Also we want to keep the results general and not applicable to specific fractures by specifying K_n. We therefore consider the velocity ratio $\overline{v}_x(t,x)/\frac{dL}{dt}$ in which the speed of propagation of the fracture

$$\frac{dL}{dt} = \Big(\frac{\beta}{f(0)}\Big)^n \frac{K_n}{L(t)}, \tag{7.8.2}$$

is obtained by differentiang the length of the fracture, (7.3.21), with respect to time $'t'$. From (7.8.1) and (7.8.2) we find that

$$\frac{\overline{v}_x(t,x)}{dL/dt} = -\left(f^{n-1} + \frac{\phi f^2(0)}{\beta^2} f^{n-3}\right)\frac{df}{du}. \tag{7.8.3}$$

The function $f(u)$ and the function value $f(0)$ are obtained by solving the boundary value problem (7.3.18) to (7.3.20) numerically. The parameter range $0 < \beta < 1$ is chosen since we are analysing a partially open fracture and the parameter ϕ is chosen in the range $0 \leq \phi \leq 1$.

In Figure 7.4 the velocity ratio (7.8.3) is plotted against u for chosen parameter values $\phi = 0$, 0.1 and 1 and $\beta = 0.5$. We recall that the case $\phi = 0$ corresponds to a tortuous hydraulic fracture with contact regions modelled by the linear crack law and with fluid injected at the fracture entry at a constant pressure. The graphs in Figure 7.4 show that the velocity ratio increases approximately linearly along the length of the fracture. The approximation for $\phi = 0$ is good for the values $n = 4, 3$ and 2.5 considered. For $\phi = 0.1$ and $\phi = 1$, the approximation is still good for $n = 3$ but the velocity ratio curve departs from a straight line graph as n decreases which describes an increase in tortuosity. The graphs

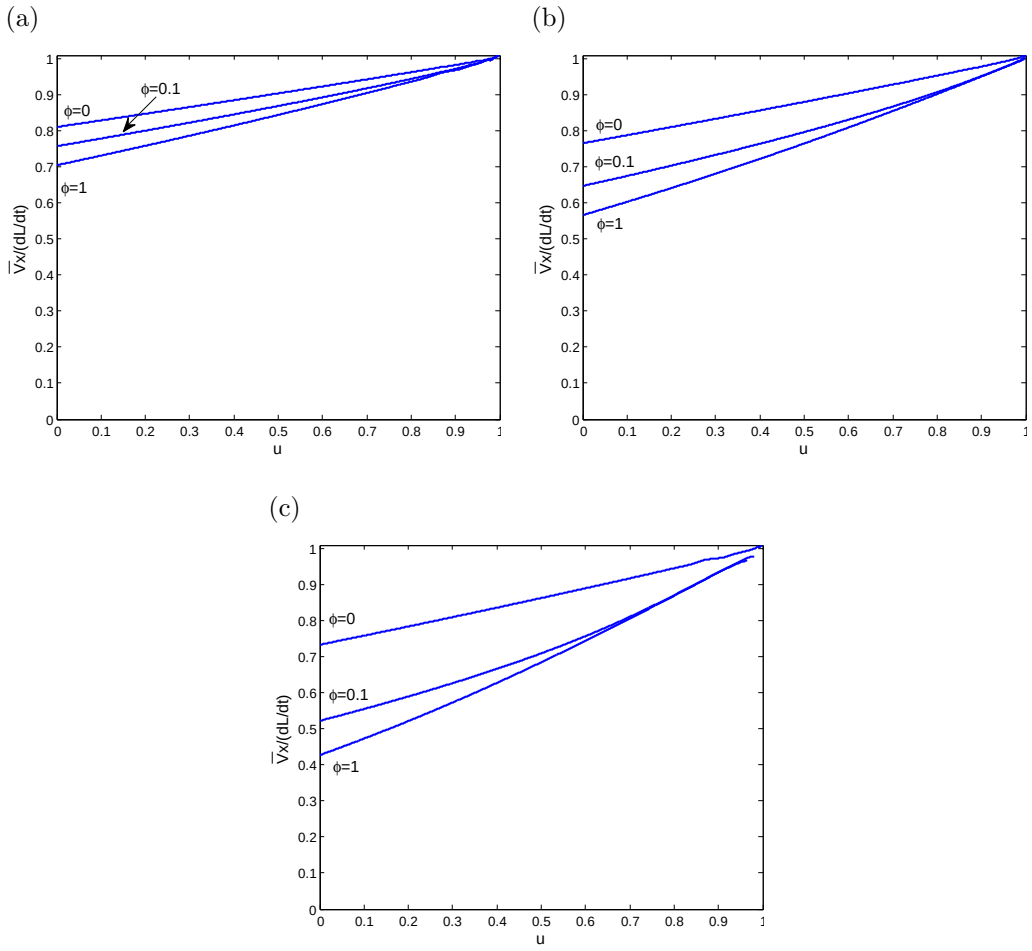

Figure 7.4: Partially open fracture, $\beta = 0.5$, propagating with fluid injected at the fracture entry at a constant pressure. The numerical solution (7.8.3) for the velocity ratio $\overline{v}_x(t,x)/\frac{dL}{dt}$ plotted against u for the linear fracture, $\phi = 0$, and the hyperbolic fracture, $\phi = 0.1$ and 1, where (a) $n = 4$, (b) $n = 3$, (c) $n = 2.5$.

show that the increase in fluid velocity along the fracture, becomes steeper as ϕ increases and the hyperbolic fracture departs further from the linear fracture. The velocity ratio also becomes steeper and the graphs are more spread out, showing that the differences are greater, as n decreases and the flow becomes more tortuous.

7.9 Approximate analytical solution

Due to the approximately linear behaviour of the velocity ratio curves along the length of the fracture, found in Figure 7.4, we make the approximation that the velocity ratio curves are exactly linear in order to investigate approximate analytical solutions as investigated for the linear crack law model in Chapter 5. This implies that we assume that the velocity ratio $\frac{\overline{v}_x}{dL/dt}$ plotted against u takes the form of a straight line

$$\frac{\overline{v}_x}{dL/dt} = mu + c, \tag{7.9.4}$$

where the constants c and m are the $\frac{\overline{v}_x}{dL/dt}-$intercept and the gradient respectively. From Figure 7.4 it is clear that the velocity ratio curves start on the $\frac{\overline{v}_x}{dL/dt}$-axis at the point $(0, A)$ and end at the point $(1, 1)$, where $c = A$. It follows that the gradient m is $(1 - A)$. Now, substituting (7.8.3) for the velocity ratio into (7.9.4) gives the variables separable ordinary differential equation

$$(1 - A)u + A = -\left(f^{n-1} + \frac{\phi f^2(0)}{\beta^2} f^{n-3}\right)\frac{df}{du}, \tag{7.9.5}$$

which, when integrated subject to the boundary condition at the fracture tip $f(1) = 0$ for $n \neq 2$, reduces to

$$\frac{f^n}{n} + \frac{\phi}{(n-2)}\Big(\frac{f(0)}{\beta}\Big)^2 f^{n-2} = -\frac{(1-A)}{2}u^2 - Au + \frac{(A+1)}{2}. \tag{7.9.6}$$

By evaluating the solution (7.9.6) at $u = 0$, we obtain

$$f(0) = \left(\frac{A+1}{2}\right)^{\frac{1}{n}} \left[\frac{n(n-2)\beta^2}{(n-2)\beta^2 + \phi n}\right]^{\frac{1}{n}} \tag{7.9.7}$$

The constant A can be read off the $\frac{\overline{v}_x}{dL/dt}-$axis in Figure 7.4. An approximate analytical derivation of A will be considered later in this Section.

Equation (7.9.6) can be written in polynomial form as

$$f^n + pf^{n-2} = q, \tag{7.9.8}$$

where

$$p = \frac{\phi n f^2(0)}{\beta^2(n-2)}, \quad q = \frac{(A+1)n}{2}\left[1 + \left(\frac{1-A}{1+A}\right)u\right](1-u). \tag{7.9.9}$$

Since we consider solutions only in the range $2 < n < 5$ as directed by the asymptotic solution (7.4.5), we first investigate analytical solutions of the polynomial (7.9.8) for the cubic, $n = 3$, and the quartic, $n = 4$, cases.

For the cubic case (7.9.8) reduces to the depressed form

$$f^3 + pf = q. \tag{7.9.10}$$

The discriminant of the cubic equation (7.9.10) is

$$\Delta = -4p^3 - 27q^2 < 0 \tag{7.9.11}$$

since $p > 0$ (because $n > 2$) and also $q > 0$. It therefore follows that (7.9.10) has one real root and two complex conjugate roots. In order to find the real root, we use Cardano's method (1501 - 1576) and consider a solution of the form

$$f(u) = a - b \tag{7.9.12}$$

where $a = a(u)$ and $b = b(u)$ must satisfy equations

$$3ab = p, \quad a^3 - b^3 = q, \tag{7.9.13}$$

which have been derived geometrically and using the binomial theorem in literature. Thus

$$a = \frac{p}{3b}, \tag{7.9.14}$$

which when substituted into the second equation in (7.9.13) gives a sixth order polynomial equation that can be reduced to a quadratic equation

$$z^2 + qz - \frac{p^3}{27} = 0 \tag{7.9.15}$$

using the transformation $z = b^3$. Thus

$$b = \left(\frac{-q \pm \sqrt{q^2 + 4(p^3/27)}}{2} \right)^{\frac{1}{3}}. \tag{7.9.16}$$

Substituting (7.9.14) and (7.9.16) into (7.9.12) gives three solutions to the cubic equation (7.9.10). They are one real solution,

$$f(u) = \left(\frac{9q + \sqrt{3}\sqrt{27q^2 + 4p^3}}{18} \right)^{\frac{1}{3}} - \left(\frac{2}{3(9q + \sqrt{3}\sqrt{27q^2 + 4p^3})} \right)^{\frac{1}{3}} p, \tag{7.9.17}$$

and two complex conjugate solutions which have no application in this work. For $n = 3$, the approximate analytical solution of the length and half-width of the fracture can be obtained by substituting (7.9.7) for $f(0)$ and (7.9.17) into equations (7.3.21) and (7.3.23) respectively.

For the quartic case, the polynomial (7.9.8) reduces to

$$f^4 + pf^2 = q, \tag{7.9.18}$$

which is a bi-quadratic equation, where p and q are given by (7.9.9). Let

$$z = f^2, \tag{7.9.19}$$

which reduces (7.9.18) to a quadratic equation

$$z^2 + px - q = 0. \tag{7.9.20}$$

Solving (7.9.20) and using (7.9.19) gives the approximate analytical solution

$$f(u) = \sqrt{\frac{-p + \sqrt{p^2 + 4q}}{2}}, \tag{7.9.21}$$

which is real and positive. Solving (7.9.20) also yields the conjugate of (7.9.21) which gives the bottom half of the symmetric fracture and two other complex conjugate solutions which have no application in this work. For $n = 4$, the approximate analytical solution of the length and half-width of the fracture can be obtained by substituting (7.9.7) for $f(0)$ and (7.9.21) into equations (7.3.21) and (7.3.23) respectively.

For fractional values of n in the range $2 < n < 5$, we cannot use classical methods that were used for the cases $n = 3$ and $n = 4$ to solve the polynomial equation (7.9.8) analytically. The approximate analytical solution (7.9.6) is implicit and therefore needs to be solved further for $f(u)$. An iterative solution can be derived. It follows from (7.9.6) that

$$f(u) = \left[\frac{[(A+1) - 2Au - (1-A)u^2]\beta^2 n(n-2)f^2(u)}{2[\beta^2(n-2)f^2(u) + \phi n f^2(0)]}\right]^{\frac{1}{n}}, \tag{7.9.22}$$

which can be solved for $f(u)$ through iterating until convergence of the function $f(u)$ is achieved. The solution (7.9.22) can be written as

$$f_{i+1} = \left[\frac{[(A+1) - 2Au - (1-A)u^2]\beta^2 n(n-2)f_i^2}{2[\beta^2(n-2)f_i^2 + \phi n f^2(0)]}\right]^{\frac{1}{n}}, \quad i = 0, 1, 2, ...s, \tag{7.9.23}$$

where $s+1$ denotes the number of iterations for convergence to be achieved. Firstly, an initial estimate is made for the function f_0, then a solution f_1 is obtained. For all the subsequent iterations, the solution is substituted on the right-hand side of (7.9.23) until convergence of the function $f(u)$ is reached and the $i+1^{st}$ iteration is the same as the i^{th} iteration.

Now, although the constant A can be read from the $\frac{\overline{v}_x(t,x)}{dL/dt}-$intercept of the velocity ratio curves obtained numerically, we also need to be able to calculate the value of A in a way that is independent of the numerical solution. In order to obtain the value of A, we use the second boundary condition (7.3.20) at the fracture entry. Multipying (7.9.5) by $f(u)$ and evaluating the result at $u=0$, with the aid of (7.9.7) for $f(0)$, gives the left-hand side of the boundary condition (7.3.20):

$$f^n(0)\frac{df}{du}(0) = -\frac{Af(0)}{\left(1+\frac{\phi}{\beta^2}\right)} = -\frac{A}{\left(1+\frac{\phi}{\beta^2}\right)}\left(\frac{A+1}{2}\right)^{\frac{1}{n}}\left[\frac{n(n-2)\beta^2}{\beta^2(n-2)+\phi n}\right]^{\frac{1}{n}}. \tag{7.9.24}$$

The right-hand side of the boundary condition (7.3.20) is obtained by evaluating $\int_0^1 f(u)$ using (7.9.7) for $f(0)$ and (7.9.22):

$$\begin{aligned}
&-\frac{1}{\left(1+\frac{\phi}{\beta^2}\right)}\int_0^1 f(u)du = \\
&-\frac{1}{\left(1+\frac{\phi}{\beta^2}\right)}\left(\frac{A+1}{2}\right)^{\frac{1}{n}}\left[2^{\frac{1}{n}}\beta^2 n(n-2)[\beta^2(n-2)+\phi n]^{\frac{2}{n}}\right]^{\frac{1}{n}}\int_0^1\left[1+\left(\frac{1-A}{1+A}\right)u\right]^{\frac{1}{n}}(1-u)^{\frac{1}{n}}\times \\
&\left(\frac{f^2(u)}{2^{\frac{2}{n}}\beta^2(n-2)[\beta^2(n-2)+\phi n]^{\frac{2}{n}}f^2(u)+\phi n(A+1)^{\frac{2}{n}}[n(n-2)\beta^2]^{\frac{2}{n}}}\right)^{\frac{1}{n}}du.
\end{aligned} \tag{7.9.25}$$

From Figure 7.4, we see that for $n \neq 4$, $1-A$ is small although it increases as n decreases and ϕ increases. We make the approximation that

$$\left[1+\left(\frac{1-A}{1+A}\right)u\right]^{\frac{1}{n}} \approx 1. \tag{7.9.26}$$

Substituting (7.9.24) and (7.9.25), where (7.9.26) is satisfied, into the boundary condition (7.3.20) at the fracture entry gives

ϕ	n	Numerical value of A	Approx. analytical value of A, Eqn (7.9.28)	Error % of numerical A & approx. analytical A
0.1	4	0.7575	0.7455	1.5842
	3	0.6471	0.6311	2.4726
	2.5	0.5221	0.5026	3.7349
1	4	0.7047	0.6921	1.7880
	3	0.5662	0.5498	2.8965
	2.5	0.4271	0.4103	3.9335

Table 7.1: Comparison of numerical and approximnate analytical estimates of A.

$$A = \left[2^{\frac{1}{n}}\beta^2 n(n-2)[\beta^2(n-2)+\phi n]^{\frac{2}{n}}\right]^{\frac{1}{n}} \int_0^1 (1-u)^{\frac{1}{n}} \times \left(\frac{f^2(u)}{2^{\frac{2}{n}}\beta^2(n-2)[\beta^2(n-2)+\phi n]^{\frac{2}{n}} f^2(u) + \phi n(A+1)^{\frac{2}{n}}[n(n-2)\beta^2]^{\frac{2}{n}}}\right)^{\frac{1}{n}} du. \quad (7.9.27)$$

In order to obtain the constant A, we will need an initial estimate for A and $f(u)$ on the right-hand side of (7.9.27) and iterate with updated values of A and $f(u)$ until convergence is reached. Equation (7.9.27) can be written in iterative form as

$$A_{i+1} = \left[2^{\frac{1}{n}}\beta^2 n(n-2)[\beta^2(n-2)+\phi n]^{\frac{2}{n}}\right]^{\frac{1}{n}} \int_0^1 (1-u)^{\frac{1}{n}} \times \left(\frac{f_i^2}{2^{\frac{2}{n}}\beta^2(n-2)[\beta^2(n-2)+\phi n]^{\frac{2}{n}} f_i^2 + \phi n(A_i+1)^{\frac{2}{n}}[n(n-2)\beta^2]^{\frac{2}{n}}}\right)^{\frac{1}{n}} du, \quad i = 0, 1, 2, ...s, \quad (7.9.28)$$

where $s+1$ is the number of iterations necessary to achieve convergence. While initial estimates for the scalar constant A_0 and the vector f_0 are necessary, in subsequent iterations the values of A and f obtained in the previous iteration will be used to obtain values of A and f in the next iterations. Convergence of the constant A is reached when $A_{i+1} = A_i$. The solution $f(u)$, (7.9.23), and the constant A, (7.9.28), are iteratively solved together as they depend on each other.

Table 7.1 compares the values of A obtained numerically with the approximate

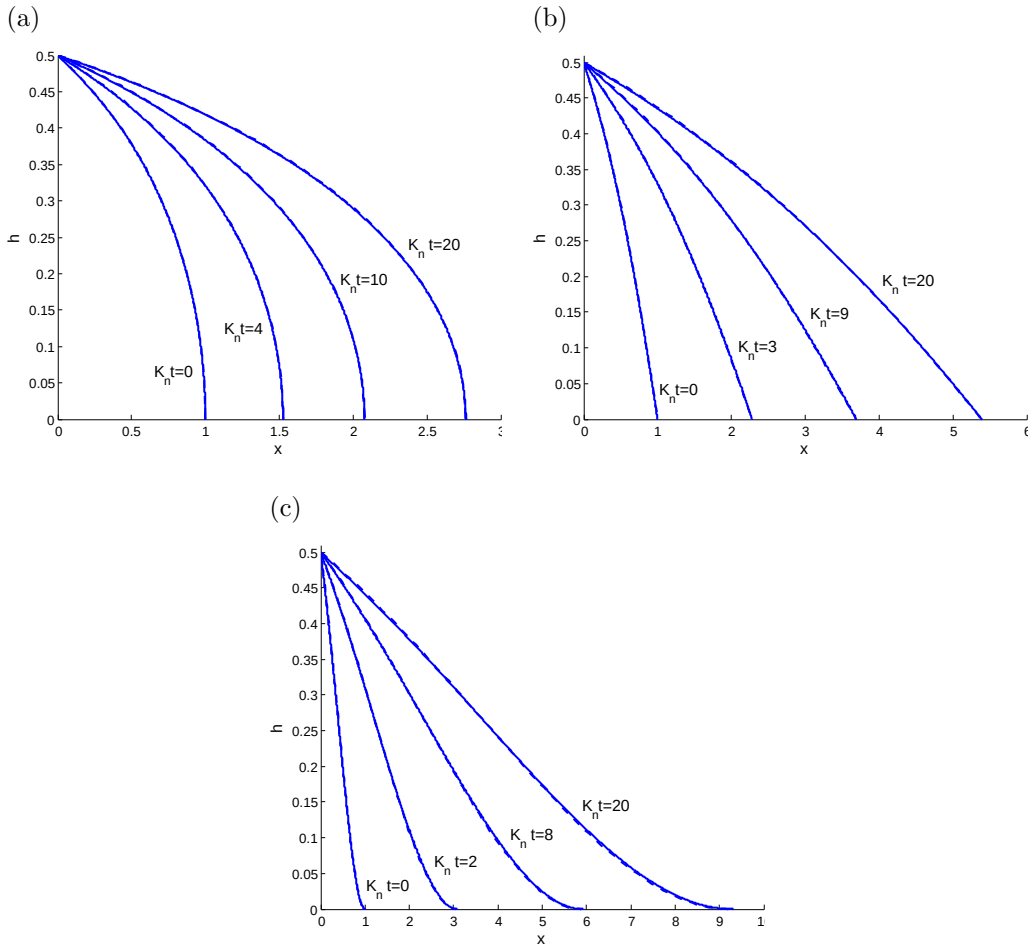

Figure 7.5: Comparison of the numerical (——) and approximate analytical (– – –) solutions of the half-width of the partially open hyperbolic fracture, $\beta = 0.5$, for increasing values of the scaled time $K_n t$, and for $\phi = 1$ where (a) $n = 4$, (b) $n = 3$, (c) $n = 2.5$.

analytical solution. The fifth column of Table 7.1 shows that the percentage error between the numerical and approximate analytical values of A is less than 4% for the chosen values of n and ϕ.

In Figure 7.5 a comparison is made of the numerical solution and the approximate analytical solution for a partially open fracture for $n = 4$, $n = 3$ and, with the iterative solution, for $n = 2.5$. The graphs overlap indicating that the approximation is good. The accuracy decreases slightly as n decreases corresponding to an increase in tortuosity. This is consistent with Figure 7.4 from which we see that the velocity ratio curves depart more from the straight line as n decreases.

7.10 Conclusions

In this chapter we investigated a tortuous hydraulic fracture with contact regions defined by the hyperbolic crack law.

As was done for a tortuous hydraulic fracture with contact regions modelled by the linear crack law in Chapter 5, we used Lie group analysis to solve the problem of a tortuous hyperbolic hydraulic fracture. We derived the Lie point symmetries of the governing partial differential equation for a hyperbolic hydraulic fracture with tortuosity which lead to the derivation of the similarity solution for the half-width of the hyperbolic hydraulic fracture. Equations for the length and volume of the fracture were also derived. The fluid flow in the hyperbolic hydraulic fracture was analysed using the equations for the fluid flux and the width averaged fluid velocity. The governing partial differential equation was reduced to an ordinary differential equation using the group invariant solution for the half-width and the boundary conditions were derived. There were no arbitrary parameters in the governing equations and boundary conditions. This is because, unlike for the linear fracture, the invariant solution for the hyperbolic fracture admits only one working condition at the fracture entry.

The association of the Lie point symmetry of the partial differential equation for the hyperbolic fracture with the conserved vectors for the PDE was investigated. This analysis was motivated by the double reduction theorem of Sjöberg who showed that reduction of the PDE by an associated Lie point symmetry may lead to an analytical solution of the PDE. Unfortunately, we found that for the range of values of n of interest the Lie point symmetry of the PDE was not associated with any conserved vector for the PDE describing a tortuous fracture propagating with increasing time t. The conservation laws of the PDE did not identify any working condition at the fracture entry that could lead to an analytical solution.

The working condition at the fracture entry was determined by the invariant solution. It was found that the half-width at the fracture entry is constant for all time and therefore by the PKN approximation the working condition is injection of fluid at constant pressure at the fracture entry. The Lie point symmetry generator for the hyperbolic fracture was

the same as that for the linear fracture with the constant pressure working condition at the fracture entry. For both the linear and the hyperbolic fractures the problem could not be solved analytically for this working condition and numerical methods had to be used.

The asymptotic solution for the half-width in the neighbourhood of the fracture tip was very useful. This solution was used to join the numerical solution with an analytical asymptotic solution in an ε-neighbourhood of the fracture tip where $\varepsilon << 1$, for solutions that had singular fracture tips. It also gave the range of the parameter n for which the invariant solution for the hyperbolic fracture exists. Unlike the linear fracture, this range is finite, $2 < n < 5$. The asymptotic solution determined the behaviour of the solution at the fracture tip. Although the range of n is small, the spatial gradient of the half-width at the fracture tip can be zero, finite or negative infinity, as for the linear fracture.

The method that was used to obtain the numerical solution for the hyperbolic hydraulic fracture was that of transforming a BVP into two IVPs and solving the IVPs. The invariant solution for the half-width, length and volume of the fracture was obtained numerically. Although the unknown initial value $f(0)$ occured in the ODE for the BVP, it did not occur in the ODEs for the IVPs. This was because the initial value $\overline{f}(0)$ could be chosen in the first IVP and $f(0)$ in the second IVP was related to $\overline{f}(0)$ by a simple transformation. This greatly simplified the numerical solution. The IVPs were solved using the MATLAB ode45 solver while the first IVP was solved also using a backward shooting method. The limit $\phi = 0$ reduced the hyperbolic crack model to the linear crack model with fluid injected at the fracture entry at constant pressure and with a diffusion constant of the linear hydraulic fracture. Since we had tested the numerical solutions for constant pressure for the linear hydraulic fracture in Chapter 5, these solutions could be used to test the numerical scheme developed for solving the hyperbolic model, at least for $\phi = 0$. Given that we could not derive analytical solutions that could be used for testing the numerical scheme for the hyperbolic model, these numerical solutions for the linear crack model served as an important benchmark for the numerical scheme used to solve the hyperbolic hydraulic fracture model.

While the advantage of the hyperbolic hydraulic fracture model is that it produces results that are closer to practical situations, its disadvantage is that it allows analysis

for only one working condition, that of fluid injection at the fracture entry at constant pressure. The advantage of the linear hydraulic fracture model is that it admits multiple working conditions that allow analysis of different cases of fluid injection or extraction at the fracture entry.

We analysed the velocity ratio of the width averaged fluid velocity and the propagation speed of the fracture. For all values of the parameter $2 < n < 5$ and the range $0 \leq \phi \leq 1$ considered, we found that the velocity ratios increase approximately linearly along the length of the fracture. As n decreased and ϕ increased the linear approximation was less valid. The approximately linear behaviour of the velocity ratios lead to the derivation of the approximate analytical solutions.

We approximated the velocity ratio curves as straight lines given their approximate linear behaviour. This allowed us to derive approximate analytical solutions. These solutions are essential for the hyperbolic hydraulic fracture model since it does not have any analytical solutions. We obtained a polynomial in $f(u)$, which was derived from the governing BVP. We solved the polynomial equation analytically for the special cases, $n = 3$ and $n = 4$. For the remaining parameter values in the range $2 < n < 5$ we iterated the polynomial until convergence of $f(u)$ was reached. The approximate analytical solutions were found to agree well with the numerical solutions.

Chapter 8

CONCLUSIONS

In this work we investigated a tortuous hydraulic fracture with rough upper and lower surfaces and, if present, with contact regions. We found that a hydraulic fracture can either be open, when the fluid pressure due to the fluid inside the fracture is sufficient to support the normal stresses exerted by the surrounding rock, or partially open, when the fluid pressure due to the fluid inside the fracture is insufficient to support the normal stresses exerted by the surrounding rock leading to the formation of contact regions that assist to support the normal stresses.

In Chapter 2, in order to model the hydraulic fracture, we replaced the actual tortuous fracture, with or without contact regions, by a symmetric two-dimensional model in which the effects of tortuosity and contact regions were incorporated. We first considered the classical Reynolds flow law that describes fluid flow in a thin, fairly rough to smooth surfaced fracture. However, given that the fracture we investigated in this work could have very rough surfaces, we modified the Reynolds cubic flow law by using a general flow law that considers surface roughness of any form [1]. We then used the Perkins-Kern-Nordgren (PKN) approximation in which the normal stress at the crack walls is proportional to the half-width of the symmetric model fracture. For an open fracture the effective stress, which is defined as the sum of the fluid pressure and the normal stress at the fluid-rock interface, must vanish while for a partially open fracture the effective stress must be neg-

ative. The linear and hyperbolic crack laws satisfy the negative effective stress condition and mathematically describe different ways in which contact regions can occur. Two governing partial differential equations subject to the corresponding boundary conditions were derived for a tortuous hydraulic fracture with contact regions modelled by the linear and hyperbolic crack laws respectively. The model for a partially open linear hydraulic fracture was found to also describe an open fracture provided a different diffusion constant relevant to an open fracture was used.

Instead of using the methods that have been developed in literature for a fracture or gravity current propagating from a line source, we decided to use the more powerful Lie group analysis in order to be able to solve the problem of the pre-existing hydraulic fracture with non-zero initial length. In Chapter 3, we discussed the background and process of solving partial differential equations using the Lie point symmetry approach. By the double reduction theorem of Sjöberg, if a Lie point symmetry of a PDE is associated with a conserved vector of the same PDE, then the partial differential equation can be reduced to an ordinary differential equation which can be integrated at least once. Sjöberg further showed that for some special cases, the resulting ordinary differential equation can be integrated completely to give an analytical solution. This motivated our investigation of conservation laws for the governing partial differential equations. We used three methods to derive conserved vectors for the governing PDES: the direct, the multiplier and the partial Lagrangian methods. The main reason for using more than one method to derive conserved vectors was to investigate if other methods could identify more conserved vectors.

In Chapters 4 and 6, we derived conserved vectors of the governing partial differential equation describing a linear hydraulic fracture and a hyperbolic hydraulic fracture respectively using the three methods. For each partial differential equation, we obtained two conserved vectors, the elementary and a second conserved vector. Also, the hyperbolic hydraulic fracture identified a special case of $n = 1$ that gave two more conserved vectors. We took a step further in Chapters 4 and 6 by using the method of generating other conserved vectors from known conserved vectors and the Lie point symmetry of the partial differential equation. However using this method also did not yield any new conserved

vectors for the linear and the hyperbolic hydraulic fractures.

For a linear hydraulic fracture, we derived the group invariant solution for the half-width, volume and length of the fracture using the Lie point symmetry approach. We also derived the fluid-flux and the width averaged fluid velocity which would be used in later analyses. Computation of the asymptotic solution in the neighbourhood of the fracture tip gave different fracture tip behaviour for different values of n. For parameter values $n > 1$, we found a singularity at the fracture tip while tortuosity, $0 < n \leq 1$, was found to remove the singularity at the fracture tip. We investigated association of the Lie point symmetries of the PDE for the linear hydraulic fracture with the conserved vectors of the PDE. We found that the Lie point symmetry generator is associated with the elementary conserved vector provided the constant volume working condition, $\alpha = 1/(n+2)$, is satisfied, that is provided there is no fluid injection or extraction at the fracture entry. We also found that the Lie point symmetry generator is associated with the second conserved vector provided the fluid extraction working condition, $\alpha = 1/[2(n+1)]$, is satisfied. Since association of Lie point symmetries with conserved vectors was satisfied, it was guaranteed that for the working conditions $\alpha = 1/(n+2)$ and $\alpha = 1/[2(n+1)]$, the partial differential equation could be reduced to an ordinary differential equation which could be integrated at least once. We further investigated the governing equations for the working conditions $\alpha = 1/(n+2)$ and $\alpha = 1/[2(n+1)]$ and found that the resulting ordinary differential equations could be integrated completely to give analytical solutions. While constant volume solutions have been discussed in the literature, we have not found discussions on fluid extraction in the literature.

By analysing the group invariant solutions for the physical properties of the fracture, we were able to deduce operating conditions for a fracture propagating with fluid injected at the fracture entry at constant pressure, $\alpha = 1/2$, for a fracture propagating with fluid injected at the fracture entry at a constant rate, $\alpha = (n+1)/(n+2)$, and for a fracture propagating at a constant speed, $\alpha = 1$. The constant speed working condition gave an analytical solution. From this analysis, it became clear that the working conditions can be classified into three categories: the fluid extraction region, $1/[2(n+1)] \leq \alpha < 1/(n+2)$, in which there is one analytical solution, for $\alpha = 1/[2(n+1)]$; the constant volume working

condition that admits one analytical solution, for $\alpha = 1/(n+2)$, and the fluid injection region, $1/(n+2) < \alpha \leq 1$, in which there is one analytical solution, for $\alpha = 1$. All other solutions in the described regions were obtained numerically. The numerical method used to solve the governing equations for different values of α was that of transforming the governing boundary value problem into two initial value problems which when solved together give a solution to the original boundary value problem. The two initial value problems were solved with MATLAB ode45 solver that uses the Runga Kutta method of order 4 and 5 with adaptive stepsize. All analytical and numerical solutions were found to agree with the asymptotic solution in the ε-neighbourhood of the fracture tip, where $\varepsilon << 1$.

For fluid injection, we analysed a solution of a fracture propagating at a constant speed, $\alpha = 1$, a fracture propagating with fluid injected at the fracture entry at a constant rate, $\alpha = (n+1)/(n+2)$, and a fracture propagating with fluid injected at the fracture entry at a constant pressure, $\alpha = 1/2$. All solutions of fluid injection were found to have a negative slope at the fracture entry. As expected for the case $\alpha = 1/2$, we found that the length of the fracture increases as the half-width at the fracture entry stays the same as the fracture propagates for increasing scaled time $K_n t$. This result occurs due to the direct proportionality relation that the half-width of the fracture has with the fluid pressure in the fracture due to the PKN approximation. For the constant pressure working condition, $\alpha = 1/2$, we found that an initially open fracture stays open for all scaled times $K_n t$ and an initially partially open fracture stays partially open for all scaled time $K_n t$. For working conditions $\alpha > 1/2$, we found that the half-width of the fracture would steadily increase with increasing scaled time $K_n t$. This implies that for the specified working conditions, an initially open fracture stays open for all scaled times $K_n t$ while an initially partially open fracture later becomes an open fracture after a calculated scaled time $K_n t_\tau$, where t_τ in this context is the time of transition from a partially open fracture to an open fracture. For working conditions $0 < \alpha < 1/2$, we found that the half-width of the fracture would steadily decrease with increasing scaled times $K_n t$. This implies that for the specified working conditions, an initially partially open fracture stays partially open for all scaled times $K_n t$ while an initially open fracture later becomes a partially open fracture after a calculated scaled time $K_n t_\tau$, where t_τ is the time of transition from an open fracture to a

partially open fracture. A significant result that was obtained is that the more tortuous the fracture, as the parameter n tends to zero, the more the length of the fracture becomes less dependent on the operating conditions at the fracture entry. This result was found to also be applicable to all discussed working conditions including the fluid extraction working conditions. It therefore follows that for a very tortuous fracture, the operating conditions have a negligible effect on the length of the fracture. The width averaged fluid velocity of the fracture propagating with constant speed was found to be constant along the length of the fracture and equal to the speed of propagation of the fracture. The width averaged fluid velocities corresponding to all the remaining fluid injection working conditions were found to increase approximately linearly along the length of the fracture. This result lead to the derivation of approximate analytical solutions which were found to agree exactly with the analytical solution for $\alpha = 1$ and very well with the numerical results of all the remaining working conditions of fluid injection.

For a hydraulic fracture with constant volume, the half-width of the fracture was found to have a zero slope at the fracture entry. The working condition for this fracture was identified by the elementary conserved vector and verified by analysing the group invariant solution of the volume of the fracture. The width averaged fluid velocity of the constant volume solution was found to increase exactly linearly along the length of the fracture, from zero at the frature entry to the propagation speed of the fracture at the fracture tip. The derived approximate analytical solution was found to agree exactly with the analytical solution of a hydraulic fracture with constant volume.

For fluid extraction, we first analysed the analytical solution for the working condition $\alpha = 1/[2(n+1)]$ that was identified by the second conserved vector of the governing partial differential equation for the linear hydraulic fracture. An important feature we observed from the analytical solution is that at the fracture entry, the half-width of the fracture is zero for all scaled time $K_n t$. This implies that the fracture entry is closed. This results from the simplification we applied in the modelling process where we approximated the minimum half-width of the fracture to be zero, $h_{min} = 0$, since the minimum half-width of the fracture is much smaller in magnitude than the maximum half-width of the fracture, $h_{min} << h_{max}$, although in real applications h_{min} is never zero [1]. Although the fracture

entry was found to be closed, we found that the volume of the fracture steadily decreased and the length of the fracture continued to grow as the scaled time $K_n t$ increased. This implies that at the fracture entry where the minimum fracture half-width is achieved, fluid flows out of the fracture. This fluid extraction behaviour at the fracture entry was verified by analysis of the fluid flux equation. We therefore concluded that the simplification in the modelling process that $h_{min} = 0$ does not alter the properties of the fracture because even when the half-width of the fracture was found to be zero at the fracture entry, the fluid extraction behaviour at the fracture entry was still observed. Analysis of the fluid flux in the fracture gave a significant and unexpected result that during the fluid extraction process, as the fluid adjacent to the fracture entry flows out of the fracture, the fluid in the neighboughood of the fracture tip relaxes further into the fracture causing the fracture length to continuously grow. Analysis of the width averaged fluid velocity verified the process of fluid extraction and showed that there is a cross-section that is a transition between fluid flowing towards the fracture entry to be extracted from the fracture and fluid flowing towards the fracture tip causing the fracture length to grow. Furthermore during the fluid extraction process we observed that the velocity of the fluid leaving the fracture behaves nonlinearly along the length of the fracture while the velocity of the fluid travelling towards the fracture tip increases linearly along the length of the fracture. Further work that was not considered in this thesis regarding fluid extraction would be to investigate the nonlinearity in fluid velocity resulting from fluid leaving the fracture in order to derive approximate analytical solutions. Solutions of the remaining working conditions defined within the fluid extraction region, $1/[2(n+1)] < \alpha < 1/(n+2)$, were obtaining using the numerical method. A feature that was observed in all fluid extraction solutions is that the slope of the half-width of the fracture at the fracture entry is positive and finite for $1/[2(n+1)] < \alpha < 1/(n+2)$ and positive and infinite for $\alpha = 1/[2(n+1)]$. The working condition $\alpha = 1/[2(n+1)]$ gives the limiting solution for fluid extraction from a fracture. Another significant result on fluid extraction was that the analytical solution for the working condition $\alpha = 1/[2(n+1)]$ gave maximum fluid flux out of the fracture and therefore the maximum volume rate of fluid out of the fracture since the surrounding rock mass is impermeable. Furthermore, we found that the volume of the fracture for all

working conditions defined within the fluid extraction region tends to zero as $K_n t \to \infty$. The length of the fracture continuously grows with increasing scaled time $K_n t$ and tends to ∞ as $K_n t \to \infty$. This may be a useful result in the oil or gas industry where the fluid remaining in the fracture after the oil or gas has been extracted will always leave the fracture resulting in no long term contamination issues.

For a hyperbolic hydraulic fracture, we also used the Lie point symmetry approach to derive the group invariant solution of the half-width, volume and length of the fracture. We first derived the asymptotic solution for the half-width of the fracture in the ε-neighbourhood of the fracture tip which gave the result that the invariant solution of the hyperbolic hydraulic fracture is defined in the parameter range $2 < n < 5$. We also found that while the lubrication approximation breaks down due to the singularity of the spacial gradient of the half-width of the fracture at the fracture tip when $n > 3$, it is satisfied for $2 < n \leq 3$ because the spatial gradient of the half-width at the fracture tip is finite and non-zero for $n = 3$ and vanishes for $2 < n < 3$. Unlike the PDE for the linear hydraulic fracture, the PDE for the hyperbolic hydraulic fracture does not contain an arbitrary parameter determined by the working conditions at the fracture entry. The half-width of the hyperbolic fracture at the fracture entry remains constant as the fracture evolves and from the PKN approximation this implies that the fluid pressure remains constant at the fracture entry. The hyperbolic fracture therefore admits only one working condition of fluid injection at the fracture entry with constant pressure. The Lie point symmetry of the PDE for the hyperbolic hydraulic fracture is the same as the Lie point symmetry of the PDE for the linear hydraulic fracture for the constant pressure working condition. For $2 < n < 5$, we investigated the association of the Lie point symmetry of the partial differential equation describing a hyperbolic hydraulic fracture with the conserved vectors of the PDE derived in Chapter 6 and found that both the elementary and second conserved vectors did not identify any working condition. The hyperbolic hydraulic fracture was solved numerically by the same method as used for the linear hydraulic fracture. The motivation to investigate the hyperbolic hydraulic fracture is that it is generally considered to be a more realistic model that describes the presence of contact regions due to touching asperities [1]. This is supported by the fact that when the linear hydraulic fracture is very

tortuous, that is as $n \to 0$, then all solutions of the physical properties of the fracture for various working conditions behave as solutions of a linear hydraulic fracture with fluid injected at the fracture entry with constant pressure, the one working condition admitted by the hyperbolic hydraulic fracture.

The advantage of using the model describing the linear hydraulic fracture is that the invariant solution describes various working conditions at the fracture entry for fluid injection and also for fluid extraction. The advantage of the model describing the hyperbolic hydraulic fracture is that it gives the most realistic working condition of constant pressure. However the group invariant solution does not give information about fluid extraction which is an important application in industry. In both models the approximate analytical solutions are useful but especially in the hyperbolic fracture model for which no exact analytical solution was derived.

Futher work could involve relaxing the assumption that the rock surrounding the fracture is impermeable and therefore considering a tortuous hydraulic fracture, with contact regions caused by touching asperities, that propagates in a permeable rock mass.

Appendix A

Lie point symmetries of the PDE for the linear hydraulic fracture

In this Appendix, we outline the derivation of the Lie point symmetries of the nonlinear diffusion equation

$$F = h_t - K_n n h^{n-1} h_x^2 - K_n h^n h_{xx} = 0, \tag{A.0.1}$$

where K_n is the diffusion constant and the subscripts t and x denote partial differentiation. The Lie point symmetry generator

$$X = \xi^1(t,x,h)\frac{\partial}{\partial t} + \xi^2(t,x,h)\frac{\partial}{\partial x} + \eta(t,x,h)\frac{\partial}{\partial h} \tag{A.0.2}$$

satisfies the invariance condition

$$X^{[2]} F\Big|_{F=0} = 0, \tag{A.0.3}$$

where

$$X^{[2]} = X + \zeta_1 \frac{\partial}{\partial h_t} + \zeta_2 \frac{\partial}{\partial h_x} + \zeta_{22} \frac{\partial}{\partial h_{xx}}, \tag{A.0.4}$$

$$\zeta_i = D_i(\eta) - h_k D_i(\xi^k), \quad i = 1,2, \tag{A.0.5}$$

$$\zeta_{ij} = D_j(\zeta_i) - h_{ik} D_j(\xi^k), \quad i,j = 1,2. \tag{A.0.6}$$

There is a summation over the repeated index k from 1 to 2 and

$$D_1 = D_t = \frac{\partial}{\partial t} + h_t \frac{\partial}{\partial h} + h_{tt} \frac{\partial}{\partial h_t} + h_{xt} \frac{\partial}{\partial h_x} ..., \tag{A.0.7}$$

$$D_2 = D_x = \frac{\partial}{\partial x} + h_x \frac{\partial}{\partial h} + h_{tx} \frac{\partial}{\partial h_t} + h_{xx} \frac{\partial}{\partial h_x} ..., \tag{A.0.8}$$

are the total derivatives. Expanding the determining equation (A.0.3) gives

$$\begin{aligned}
&\Bigg[\left(2K_n h^n \frac{\partial^2 \xi^2}{\partial x \partial h} - K_n h^n \frac{\partial^2 \eta}{\partial h^2} - 2K_n n h^{n-1} \frac{\partial \eta}{\partial h} - K_n n(n-1) h^{n-2} \eta + 2K_n n h^{n-1} \frac{\partial \xi^2}{\partial x} \right) h_x^2 \\
&+ \left(K_n h^n \frac{\partial^2 \xi^2}{\partial x^2} - 2K_n h^n \frac{\partial^2 \eta}{\partial x \partial h} - 2K_n n h^{n-1} \frac{\partial \eta}{\partial x} - \frac{\partial \xi^2}{\partial t} \right) h_x \\
&+ \left(2K_n n h^{n-1} \frac{\partial \xi^1}{\partial x} - \frac{\partial \xi^2}{\partial h} + 2K_n h^n \frac{\partial^2 \xi^1}{\partial x \partial h} \right) h_x h_t \\
&+ \left(2K_n h^n \frac{\partial \xi^2}{\partial x} - K_n h^n \frac{\partial \eta}{\partial h} - K_n n h^{n-1} \eta \right) h_{xx} \\
&+ \left(2K_n n h^{n-1} \frac{\partial \xi^1}{\partial h} + K_n h^n \frac{\partial^2 \xi^1}{\partial h^2} \right) h_x^2 h_t \\
&+ \left(2K_n n h^{n-1} \frac{\partial \xi^2}{\partial h} + K_n h^n \frac{\partial^2 \xi^2}{\partial h^2} \right) h_x^3 \\
&+ \left(\frac{\partial \eta}{\partial h} - \frac{\partial \xi^1}{\partial t} + K_n h^n \frac{\partial^2 \xi^1}{\partial x^2} \right) h_t \\
&+ 2K_n h^n \frac{\partial \xi^1}{\partial x} h_{tx} \\
&+ 2K_n h^n \frac{\partial \xi^1}{\partial h} h_x h_{tx} \\
&+ K_n h^n \frac{\partial \xi^1}{\partial h} h_t h_{xx} \\
&+ 3K_n h^n \frac{\partial \xi^2}{\partial h} h_x h_{xx} \\
&+ \frac{\partial \eta}{\partial t} - K_n h^n \frac{\partial^2 \eta}{\partial x^2} \\
&- \frac{\partial \xi^1}{\partial h} h_t^2 \Bigg] \Bigg|_{F=0} = 0.
\end{aligned} \tag{A.0.9}$$

Equation (A.0.1) can be re-expressed as

$$h_{xx} = \frac{h_t - K_n n h^{n-1} h_x^2}{K_n h^n} \tag{A.0.10}$$

which when substituted into (A.0.9) gives

$$\begin{aligned}
&\left(2K_n h^n \frac{\partial^2 \xi^2}{\partial x \partial h} - K_n h^n \frac{\partial^2 \eta}{\partial h^2} - K_n n h^{n-1} \frac{\partial \eta}{\partial h} + K_n n h^{n-2} \eta\right) h_x^2 \\
&+ \left(K_n h^n \frac{\partial^2 \xi^2}{\partial x^2} - 2K_n h^n \frac{\partial^2 \eta}{\partial x \partial h} - 2K_n n h^{n-1} \frac{\partial \eta}{\partial x} - \frac{\partial \xi^2}{\partial t}\right) h_x \\
&+ \left(2K_n n h^{n-1} \frac{\partial \xi^1}{\partial x} + 2\frac{\partial \xi^2}{\partial h} + 2K_n h^n \frac{\partial^2 \xi^1}{\partial x \partial h}\right) h_x h_t \\
&+ \left(K_n h^n \frac{\partial^2 \xi^1}{\partial x^2} - \frac{\partial \xi^1}{\partial t} - \frac{n}{h}\eta + 2\frac{\partial \xi^2}{\partial x}\right) h_t \\
&+ \left(K_n n h^{n-1} \frac{\partial \xi^1}{\partial h} + K_n h^n \frac{\partial^2 \xi^1}{\partial h^2}\right) h_x^2 h_t \\
&+ \left(K_n h^n \frac{\partial^2 \xi^2}{\partial h^2} - K_n n h^{n-1} \frac{\partial \xi^2}{\partial h}\right) h_x^3 \\
&+ 2K_n h^n \frac{\partial \xi^1}{\partial x} h_{tx} \\
&+ 2K_n h^n \frac{\partial \xi^1}{\partial h} h_x h_{tx} \\
&+ \frac{\partial \eta}{\partial t} - K_n h^n \frac{\partial^2 \eta}{\partial x^2} \\
&= 0. \qquad \text{(A.0.11)}
\end{aligned}$$

Now separating equation (A.0.11) with respect $h_x h_{tx}$, h_{tx} and $h_x h_t$ gives

$$h_x h_{tx} : \frac{\partial \xi^1}{\partial h} = 0, \qquad \text{(A.0.12)}$$

which implies that

$$\xi^1 = \xi^1(t, x); \qquad \text{(A.0.13)}$$

$$h_{tx} : \frac{\partial \xi^1}{\partial x} = 0, \qquad \text{(A.0.14)}$$

which implies that

$$\xi^1 = \xi^1(t) \qquad \text{(A.0.15)}$$

and

$$h_x h_t : 2K_n n h^{n-1} \frac{\partial \xi^1}{\partial x} + 2K_n h^n \frac{\partial^2 \xi^1}{\partial x \partial h} + 2\frac{\partial \xi^2}{\partial h} = 0, \qquad \text{(A.0.16)}$$

that, from using equation (A.0.15), reduces to

$$\frac{\partial \xi^2}{\partial h} = 0, \qquad \text{(A.0.17)}$$

which implies that

$$\xi^2 = \xi^2(t, x). \tag{A.0.18}$$

Separating equation (A.0.11) by $h_x^2 h_t$ and h_x^3 does not give any new information. Separating (A.0.11) by h_t and h_x gives

$$h_t : \eta - \frac{h}{n}\left(K_n h^n \frac{\partial^2 \xi^1}{\partial x^2} + 2\frac{\partial \xi^2}{\partial x} - \frac{\partial \xi^1}{\partial t}\right) = 0, \tag{A.0.19}$$

which when simplified by equation (A.0.15) gives

$$\eta = \frac{h}{n}\left(2\frac{\partial \xi^2}{\partial x} - \frac{d\xi^1}{dt}\right) \tag{A.0.20}$$

and

$$h_x : K_n h^n \frac{\partial^2 \xi^2}{\partial x^2} - 2K_n h^n \frac{\partial^2 \eta}{\partial x \partial h} - 2K_n n h^{n-1} \frac{\partial \eta}{\partial x} - \frac{\partial \xi^2}{\partial t} = 0, \tag{A.0.21}$$

which when simplified using (A.0.18) and (A.0.20) gives

$$\left(\frac{3n+4}{n}\right) K_n h^n \frac{\partial^2 \xi^2}{\partial x^2} + \frac{\partial \xi^2}{\partial t} = 0. \tag{A.0.22}$$

Since ξ^2 is independent of h we can separate (A.0.22) in powers of h. Also $n > 0$. Thus

$$h^0 : \frac{\partial \xi^2}{\partial t} = 0, \tag{A.0.23}$$

which implies that

$$\xi^2 = \xi^2(x) \tag{A.0.24}$$

and

$$h^n : \frac{d^2 \xi^2}{dx^2} = 0, \tag{A.0.25}$$

which implies that

$$\xi^2 = c_3 + c_4 x, \tag{A.0.26}$$

where c_3 and c_4 are constants. Separating (A.0.11) by h_x^2 gives an equation that is identically satisfied. The remainder is

$$\frac{\partial \eta}{\partial t} - K_n h^n \frac{\partial^2 \eta}{\partial x^2} = 0, \tag{A.0.27}$$

which when simplified using (A.0.20) and (A.0.26) reduces to

$$\frac{d^2\xi^1}{dt^2} = 0. \tag{A.0.28}$$

Integration of (A.0.28) with respect to t gives

$$\xi^1 = c_1 + c_2 t, \tag{A.0.29}$$

where c_1 and c_2 are constants. It follows from equations (A.0.20), (A.0.26) and (A.0.29) that

$$\xi^1(t) = c_1 + c_2 t, \quad \xi^2(x) = c_3 + c_4 x, \quad \eta(h) = \frac{1}{n}(2c_4 - c_2)h \tag{A.0.30}$$

and therefore the Lie point symmetry of the PDE (A.0.1) for the linear hydraulic fracture is

$$X = (c_1 + c_2 t)\frac{\partial}{\partial t} + (c_3 + c_4 x)\frac{\partial}{\partial x} + \frac{1}{n}(2c_4 - c_2)h\frac{\partial}{\partial h}. \tag{A.0.31}$$

Appendix B

Lie point symmetries of the PDE for the hyperbolic hydraulic fracture

We now derive the Lie point symmetries of the partial differential equation

$$F = h_t - K_n(nh^{n-1} + \phi(n-2)h^{n-3})h_x^2 - K_n(h^n + \phi h^{n-2})h_{xx} = 0 \tag{B.0.1}$$

for the half-width of a hyperbolic hydraulic fracture, where K_n is the diffusion constant given by (7.1.2) and ϕ is the constant given by (7.1.3). We consider $\phi > 0$ because $\phi = 0$ describes the linear crack law. We also consider $0 < n < \infty$. The subscripts t and x denote partial differentiation with respect to t and x respectively.

The Lie point symmetry generator

$$X = \xi^1(t,x,h)\frac{\partial}{\partial t} + \xi^2(t,x,h)\frac{\partial}{\partial x} + \eta(t,x,h)\frac{\partial}{\partial h} \tag{B.0.2}$$

satisfies the invariance condition

$$X^{[2]}F\Big|_{F=0} = 0 \tag{B.0.3}$$

where $X^{[2]}$ is the second prolongation of the generator (B.0.2) given by equation (A.0.4). Expanding the determining equation (B.0.3) gives

$$
\begin{aligned}
&\Bigg(\Bigg[2K_n(nh^{n-1}+\phi(n-2)h^{n-3})\left(\frac{\partial\xi^2}{\partial x}-\frac{\partial\eta}{\partial h}\right)-K_n(h^n+\phi h^{n-2})\left(\frac{\partial^2\eta}{\partial h^2}-2\frac{\partial^2\xi^2}{\partial x\partial h}\right)\\
&\qquad -K_n(n(n-1)h^{n-2}+\phi(n-2)(n-3)h^{n-4})\eta\Bigg]h_x^2\\
&+\left[K_n(h^n+\phi h^{n-2})\left(\frac{\partial^2\xi^2}{\partial x^2}-2\frac{\partial^2\eta}{\partial x\partial h}\right)-2K_n(nh^{n-1}+\phi(n-2)h^{n-3})\frac{\partial\eta}{\partial x}-\frac{\partial\xi^2}{\partial t}\right]h_x\\
&+\left[K_n(h^n+\phi h^{n-2})\left(2\frac{\partial\xi^2}{\partial x}-\frac{\partial\eta}{\partial h}\right)-K_n(nh^{n-1}+\phi(n-2)h^{n-3})\eta\right]h_{xx}\\
&+\left[2K_n(nh^{n-1}+\phi(n-2)h^{n-3})\frac{\partial\xi^1}{\partial x}+2K_n(h^n+\phi h^{n-2})\frac{\partial^2\xi^1}{\partial x\partial h}-\frac{\partial\xi^2}{\partial h}\right]h_xh_t\\
&+\left[2K_n(nh^{n-1}+\phi(n-2)h^{n-3})\frac{\partial\xi^1}{\partial h}+K_n(h^n+\phi h^{n-2})\frac{\partial^2\xi^1}{\partial h^2}\right]h_x^2h_t\\
&+\left[2K_n(nh^{n-1}+\phi(n-2)h^{n-3})\frac{\partial\xi^2}{\partial h}+K_n(h^n+\phi h^{n-2})\frac{\partial^2\xi^2}{\partial h^2}\right]h_x^3\\
&+\left[K_n(h^n+\phi h^{n-2})\frac{\partial^2\xi^1}{\partial x^2}+\frac{\partial\eta}{\partial h}-\frac{\partial\xi^1}{\partial t}\right]h_t\\
&+3K_n(h^n+\phi h^{n-2})\frac{\partial\xi^2}{\partial h}h_xh_{xx}\\
&+K_n(h^n+\phi h^{n-2})\frac{\partial\xi^1}{\partial h}h_th_{xx}\\
&+2K_n(h^n+\phi h^{n-2})\frac{\partial\xi^1}{\partial h}h_xh_{tx}\\
&+2K_n(h^n+\phi h^{n-2})\frac{\partial\xi^1}{\partial x}h_{tx}\\
&-\frac{\partial\xi^1}{\partial h}h_t^2\\
&+\frac{\partial\eta}{\partial t}-K_n(h^n+\phi h^{n-2})\frac{\partial^2\eta}{\partial x^2}\Bigg)\Bigg|_{F=0}=0.
\end{aligned}
\tag{B.0.4}
$$

Equation (B.0.1) can be re-expressed as

$$
h_{xx}=\frac{h_t-K_n(nh^{n-1}+\phi(n-2)h^{n-3})h_x^2}{K_n(h^n+\phi h^{n-2})},
\tag{B.0.5}
$$

which when substituted into equation (B.0.4) gives

$$\begin{aligned}
&\left[\left(\frac{(nh^{n-1}+\phi(n-2)h^{n-3})^2}{(h^n+\phi h^{n-2})}-K_n(n(n-1)h^{n-2}+\phi(n-2)(n-3)h^{n-4})\right)\eta\right.\\
&\qquad\left.-K_n(nh^{n-1}+\phi(n-2)h^{n-3})\frac{\partial\eta}{\partial h}-K_n(h^n+\phi h^{n-2})\left(\frac{\partial^2\eta}{\partial h^2}-2\frac{\partial^2\xi^2}{\partial x\partial h}\right)\right]h_x^2\\
&+\left[K_n(h^n+\phi h^{n-2})\left(\frac{\partial^2\xi^2}{\partial x^2}-2\frac{\partial^2\eta}{\partial x\partial h}\right)-2K_n(nh^{n-1}+\phi(n-2)h^{n-3})\frac{\partial\eta}{\partial x}-\frac{\partial\xi^2}{\partial t}\right]h_x\\
&+\left[K_n(h^n+\phi h^{n-2})\frac{\partial^2\xi^1}{\partial x^2}-\left(\frac{nh^{n-1}+\phi(n-2)h^{n-3}}{h^n+\phi h^{n-2}}\right)\eta-\frac{\partial\xi^1}{\partial t}+2\frac{\partial\xi^2}{\partial x}\right]h_t\\
&+\left[2K_n(nh^{n-1}+\phi(n-2)h^{n-3})\frac{\partial\xi^1}{\partial x}+2K_n(h^n+\phi h^{n-2})\frac{\partial^2\xi^1}{\partial x\partial h}-2\frac{\partial\xi^2}{\partial h}\right]h_xh_t\\
&+\left[K_n(nh^{n-1}+\phi(n-2)h^{n-3})\frac{\partial\xi^1}{\partial h}+K_n(h^n+\phi h^{n-2})\frac{\partial^2\xi^1}{\partial h^2}\right]h_x^2h_t\\
&+\left[K_n(h^n+\phi h^{n-2})\frac{\partial^2\xi^2}{\partial h^2}-K_n(nh^{n-1}+\phi(n-2)h^{n-3})\frac{\partial\xi^2}{\partial h}\right]h_x^3\\
&+2K_n(h^n+\phi h^{n-2})\frac{\partial\xi^1}{\partial h}h_xh_{tx}\\
&+2K_n(h^n+\phi h^{n-2})\frac{\partial\xi^1}{\partial x}h_{tx}\\
&+\frac{\partial\eta}{\partial t}-K_n(h^n+\phi h^{n-2})\frac{\partial^2\eta}{\partial x^2}=0. \qquad \text{(B.0.6)}
\end{aligned}$$

Now, since ξ^1, ξ^2 and η are independent of the partial derivatives of h, we separate (B.0.6) in powers and products of partial derivatives of h. Firstly, separating (B.0.6) by h_xh_{tx}, h_{tx} and h_xh_t gives

$$h_xh_{tx}:\frac{\partial\xi^1}{\partial h}=0, \qquad \text{(B.0.7)}$$

which implies that

$$\xi^1=\xi^1(t,x); \qquad \text{(B.0.8)}$$

$$h_{tx}:\frac{\partial\xi^1}{\partial x}=0, \qquad \text{(B.0.9)}$$

which implies that

$$\xi^1=\xi^1(t) \qquad \text{(B.0.10)}$$

and

$$h_x h_t : 2K_n(nh^{n-1} + \phi(n-2)h^{n-3})\frac{\partial \xi^1}{\partial x} + 2K_n(h^n + \phi h^{n-2})\frac{\partial^2 \xi^1}{\partial x \partial h} - 2\frac{\partial \xi^2}{\partial h} = 0, \quad \text{(B.0.11)}$$

that, by equation (B.0.10), reduces to

$$\frac{\partial \xi^2}{\partial h} = 0, \quad \text{(B.0.12)}$$

which implies that

$$\xi^2 = \xi^2(t, x). \quad \text{(B.0.13)}$$

Separating (B.0.6) by $h_x^2 h_t$ and h_x^3 does not give any information about ξ^1, ξ^2 and η. Separating (B.0.6) by h_t, with (B.0.10) satisfied, gives an equation for η:

$$\eta = \left[\frac{h^n + \phi h^{n-2}}{nh^{n-1} + \phi(n-2)h^{n-3}}\right]\left(2\frac{\partial \xi^2}{\partial x} - \frac{d\xi^1}{dt}\right). \quad \text{(B.0.14)}$$

Separating (B.0.6) by h_x^2 and using (B.0.13) gives

$$h_x^2 : \left(\frac{(nh^{n-1} + \phi(n-2)h^{n-3})^2}{(h^n + \phi h^{n-2})} - K_n\left[n(n-1)h^{n-2} + \phi(n-2)(n-3)h^{n-4}\right]\right)\eta$$
$$- K_n\left[nh^{n-1} + \phi(n-2)h^{n-3}\right]\frac{\partial \eta}{\partial h} - K_n(h^n + \phi h^{n-2})\frac{\partial^2 \eta}{\partial h^2} = 0. \quad \text{(B.0.15)}$$

Substituting η, given by (B.0.14), into (B.0.15) and simplifying the result using MATHEMATICA gives

$$\frac{h^{n-3}}{[nh^2 + (n-2)\phi]^3}G(h; n, \phi) = 0, \quad \text{(B.0.16)}$$

where

$$G(h; n, \phi) =$$
$$\left[(K_n - 1)n^4 h^8 + 4n\left[K_n - (K_n - 1)n^2(n-2)\right]h^6\phi + 2\left[3(n-2)^2 n^2(K_n - 1) - 4K_n(n-3)\right]h^4\phi^2\right.$$
$$\left. + 4(n-2)\left[K_n(n-3)(1 + n(n-1)) - (n-2)^2 n\right]h^2\phi^3 + (K_n - 1)(n-2)^4\phi^4\right]\left(\frac{d\xi^1}{dt} - 2\frac{\partial \xi^2}{\partial x}\right). \quad \text{(B.0.17)}$$

It is clear that equation (B.0.16) is satisfied provided

$$G(h; n, \phi) = 0. \quad \text{(B.0.18)}$$

Since ϕ is a constant and both ξ^1 and ξ^2 are independent of h, it follows that we may separate (B.0.18) by powers of h. Separating (B.0.18) by h^8 gives

$$h^8 : (K_n - 1)n^4\left(\frac{d\xi^1}{dt} - 2\frac{\partial\xi^2}{\partial x}\right) = 0. \tag{B.0.19}$$

But we are considering $n > 0$. Thus if $K_n \neq 1$ then

$$\frac{d\xi^1}{dt} - 2\frac{\partial\xi^2}{\partial x} = 0. \tag{B.0.20}$$

In order to show that (B.0.20) is also satisfied when $K_n = 1$, we substitute $K_n = 1$ into (B.0.17) and therefore (B.0.18) reduces to

$$G(h; n, 1) = \left(4nh^6\phi - 8(n-3)h^4\phi^2 - 12(n-2)h^2\phi^3\right)\left[\frac{d\xi^1}{dt} - 2\frac{\partial\xi^2}{\partial x}\right] = 0. \tag{B.0.21}$$

Separating (B.0.21) by h^6 gives

$$h^6 : 4n\phi\left[\frac{d\xi^1}{dt} - 2\frac{\partial\xi^2}{\partial x}\right] = 0 \tag{B.0.22}$$

and since $n > 0$ and $\phi > 0$, it follows that equation (B.0.20) is again satisfied. Thus (B.0.20) is satisfied for all values of $K_n > 0$ and therefore by (B.0.14),

$$\eta = 0. \tag{B.0.23}$$

Separating (B.0.6) by h_x with $\eta = 0$ gives

$$h_x : K_n(h^n + \phi h^{n-2})\frac{\partial^2\xi^2}{\partial x^2} - \frac{\partial\xi^2}{\partial t} = 0. \tag{B.0.24}$$

Since ξ^2 is independent of h, we can separate (B.0.24) by powers of h. If we separate first by h^n then we do not need to treat $n = 2$ as a special case:

$$h^n : \frac{\partial^2\xi^2}{\partial x^2} = 0, \tag{B.0.25}$$

and (B.0.24) reduces to

$$\frac{\partial\xi^2}{\partial t} = 0, \tag{B.0.26}$$

which implies that

$$\xi^2 = \xi^2(x). \tag{B.0.27}$$

From (B.0.27), it follows that integrating equation (B.0.25) twice with respect to x gives

$$\xi^2 = c_3 + c_4 x, \tag{B.0.28}$$

where c_3 and c_4 are constants. Since $\xi^1 = \xi^1(t)$, given by (B.0.10), and $\xi^2 = \xi^2(x)$, given by (B.0.27), it follows from (B.0.20) that

$$\frac{d\xi^1}{dt} = c_2, \quad \text{and} \quad 2\frac{d\xi^2}{dx} = c_2, \tag{B.0.29}$$

where c_2 is a constant. Solving for ξ^1 by integrating the first equation in (B.0.29) with respect to t gives

$$\xi^1 = c_1 + c_2 t, \tag{B.0.30}$$

where c_1 is a constant. Solving for ξ^2 by integrating the second equation in (B.0.29) with respect to x gives

$$\xi^2 = c_3 + \frac{1}{2}c_2 x \tag{B.0.31}$$

and from (B.0.28), it is clear that $c_4 = \frac{1}{2}c_2$. After separating (B.0.6) by powers and products of the derivatives of h, the remaining terms are

$$Remainder : \frac{\partial \eta}{\partial t} - K_n(h^n + \phi h^{n-2})\frac{\partial^2 \eta}{\partial x^2} = 0. \tag{B.0.32}$$

Equation (B.0.32) is identically satisfied since $\eta = 0$.

Therefore from equations (B.0.23), (B.0.30) and (B.0.31), it is clear that the Lie point symmetry of the partial differential equation (B.0.1) for the hyperbolic hydraulic fracture, with $\phi > 0$ and all $n > 0$, is

$$X = (c_1 + c_2 t)\frac{\partial}{\partial t} + \Big(c_3 + \frac{c_2}{2}x\Big)\frac{\partial}{\partial x}. \tag{B.0.33}$$

Bibliography

[1] A. D. Fitt, A. D. Kelly and C. P. Please, Crack propagation models for rock fracture in a geothermal energy reservoir, *SIAM J. Appl. Math.* **55** (1995) 1592-1608.

[2] S. Emerman, D. L. Turcotte and D. A. Spence, Transport of magma and hydrothermal solutions by laminar and turbulent fluid fracture, *Phys. Earth Planet. Int.* **36** (1986) 276-284.

[3] J. Weertman, Velocity at which liquid-filled cracks move in the Earth's crust or in glaciers, *J. Geophys. Res.* **76** (1971) 8544-8553.

[4] D. T. Secor and D. D. Pollard, On the stability of open hydraulic fractures in the Earth's crust, *Geophys. Res. Lett.* **2** (1975) 510-513.

[5] D. A. Spence and D. L. Turcotte, Magma-driven propagation of cracks, *J. Geophys. Res.* **90** (1985) 575-580.

[6] D. A. Spence, P. Sharp and D. L. Turcotte, Buoyancy-driven crack propagation: a mechanism for magma migration, *J. Fluid Mech.* **174** (1987) 135-153.

[7] J. Geertsma and F. de Klerk, A rapid method of predicting width and extent of hydraulic induced fractures, *J. Pet. Technol.* **246** (1969) 1571-1581.

[8] J. Geertsma and R. Haafkens, A comparison of the theories for predicting width and extent of vertical hydraulically induced fractures, *J. Energy Res. Tech.* **101** (1979) 8-19.

[9] A. M. Jaffe, How shale gas is going to rock the world: huge discoveries of gas promise to shake up the energy markets and geopolitics; and that's just for starters, *Wall Str. J.* (2010) 10.

[10] A. D. Fitt, N. D. Fowkes, D. P. Mason, T. G. Myers, E. A. Moss and J. Cheng, Fracturing rock with ultra high pressure water, *Proceedings in the Mathematics in Industry Study Group, University of the Witwatersrand, Johannesburg*, 2004, pp. 33-49.

[11] A. D. Fitt, D. P. Mason and E. A. Moss, Group invariant solution for a pre-existing fluid driven fracture in impermeable rock, *Z. Angew. Math. Phys. (ZAMP)* **58** (2007) 1049-1067.

[12] A. G. Fareo, Group invariant solutions for a pre-existing fluid-driven fracture in permeable rock (MSc Dissertation), University of the Witwatersrand, Johannesburg, South Africa, 23 February 2008.

[13] H. O. Weeren, Waste disposal by shale fracturing at ORNL, *Nucl. Eng. Des.* **44** (1977) 291-300.

[14] A. G. Fareo and D. P. Mason, A group invariant solution for a pre-existing fluid driven fracture in permeable rock, *Nonlinear Anal.: Real World Appl.* **12** (2011) 767-779.

[15] S. Khristianovic and Y. Zheltov, Formation of vertical fractures by means of highly viscous fluids, *In: 4th World Pet. Congr*, Rome, (1955) 579-586.

[16] T. Perkins and L. Kern, Widths of hydraulic fractures, *J. Pet. Technol.* **222** (1961) 937-949.

[17] R. Nordgren, Propagation of vertical hydraulic fractures, *J. Pet. Technol.* **253** (1972) 306-314.

[18] A. A. Savitski and E. Detournay, Propagation of a penny-shaped fluid-driven fracture in an impermeable rock: asymptotic solutions, *Int. J. Solids Struct.* **39** (2002) 6311-6337.

[19] S. Ge, A governing equation for fluid flow in rough fractures, *Water Resour. Res.* **33** (1997) 53-61.

[20] A. P. Oron and B. Berkowitz, Flow in rock fractures: The local cubic law assumption re-examined, *Water Resour. Res.* **34** (1998) 2811-2825.

[21] J. Qian, Z. Chen, H. Zhan and H. Guan, Experimental study of the effect of roughness and Reynolds number on fluid flow in rough-walled single fractures: a check of local cubic law, *Hydrol. Process.* **25** (2011) 614-622.

[22] P. A. Witherspoon, J. S. Y. Wang, K. Iwai and J. E. Gale, Validity of cubic law for fluid flow in a deformable rock fracture, *Water Resour. Res.* **16** (1980) 1016-1024.

[23] N. G. W. Cook, Natural joints in rock: mechanical, hydraulic and seismic behaviour and properties under normal stress, *Int. J. Rock Mech. Min. Sci. Geomech. Abstr.* **29** (1992) 198-223.

[24] J. I. Adachi and A. P. Peirce, Asymptotic analysis of an elasticity equation for a finger-like hydraulic fracture, *J. Elast.* **90** (2008) 43-69.

[25] R. J. Pine and P. A. Cundall, Applications of the fluid-rock interaction programme (FRIP) to the modelling of hot dry geothermal energy systems, *Proc. Int. S Fundamentals*, September 1985, pp 293-302.

[26] R. E. Goodman, The mechanical properties of joints, *Proc. 3rd Congr ISRM, Denver,* **1A**, 1947, pp. 127-140.

[27] S. Bandis, A. C. Lumsden and N.R. Barton, Fundamentals of rock joint deformation, *Int. J. Rock Mech. Min. Sci. Geomech. Abstr.* **20** , 1983, pp. 249-268.

[28] H. Murphy, Z. Dash and G. Zyvoloski, A. White and M. Wing, Fluid flow in deformable rock joints: Part 1,Memorandum ESS-4-85-84, *Los Alamos National Lab, Los Alamos, NM,* 1985.

[29] A. Sjöberg, Double reduction of PDEs from the association of symmetries with conservation laws with applications, *Appl. Math. Comput.* **184** (2007) 608-616.

[30] A. G. Fareo, Group invariant solutions for a pre-existing fracture driven by a non-Newtonian fluid in permeable and impermeable rock (PhD Thesis) University of the Witwatersrand, Johannesburg, South Africa, 5 November 2012.

[31] D. P. Mason and M. R. R. Kgatle, Propagation of a linear hydraulic fracture with tortuosity, *Int. J. Nonlinear Mech.* **61** (2014) 39-53.

[32] D. J. Acheson, Elementary Fluid Dynamics, *Clarendon Press, Oxford*, 1990, 238-251.

[33] R. P. Gillepsie, *Integration*, Oliver and Boyd, Edinburgh , 1959, pp. 113-116.

[34] D. A. Spence and P. Sharp, Self-similar solutions for elastohydrodynamic cavity flow, *Proc. R. Soc. Land A* **400** (1985) 289-313.

[35] J. R. King and M. Bowen, Moving boundary problems and non-uniqueness for thin film equations, *European J. Appl. Math.* **12** (2001) 321-356.

[36] H. E. Huppert, The propagation of two-dimensional and axisymmetric viscous gravity currents over a rigid horizontal surface, *J. Fluid Mech.* **121** (1982) 43-58.

[37] M. Anthonyrajah, D. P .Mason and A. G. Fareo, Propagation of a pre-existing turbulent fluid fracture, *Int. J. Nonlinear Mech.* **54** (2013) 105-114.

[38] A. G. Fareo and D. P. Mason, Group invariant solution for a pre-existing fracture driven by a power-law fluid in impermeable rock, *Commun. Nonlinear Sci. Numer. Simul.* **18** (2013) 32983316.

[39] N. H. Ibragimov and R. L. Anderson, One-parameter transformation groups, in: N. H. Ibragimov (Ed.), CRC Handbook of Lie Group Analysis of Differential Equations. Symmetries, Exact Solutions and Conservation Laws, vol. 1, CRC Press, Boca Raton, 1994, pp. 7-14.

[40] R. Naz, F. M. Mahomed and D. P. Mason, Comparison of different approaches to conservation laws for some partial differential equations in fluid mechanics, *Appl. Math. Comput.* **205** (2008) 212-230.

[41] A. H. Kara and F. M. Mahomed, Relationship between symmetries and conservation laws, *Int. J. Theor. Phys.* **39** (2000) 23-40.

[42] A. H. Kara and F. M. Mahomed, A basis of conservation laws for partial differential equations, *J. Nonlinear Math. Phy.* **9** (2002) 60-72.

[43] P. S. Laplace (English translation, Celestrial Mechanics, New York, 1966), 1798.

[44] M. Anthonyrajah and D. P. Mason, Conservation laws and invariant solutions in the Fanno model for turbulent compressible flow, *Math. Comput. Applic.* **15** (2010) 529-542.

[45] R. Naz, D. P. Mason and F. M. Mahomed, Conservation laws and conserved quantities for laminar two-dimensional and radial jets, *Nonlinear Anal.: Real*, (2008) doi:10.1016/j.nonrwa.2008.07.003.

[46] E. Noether, Invariante Variationsprobleme, Nacr. Konig. Gesell. Wissen., *Gottingen, Math.-Phys. Kl. Heft* 2 (1918) 235257 (English translation in Transport Theory and Statistical Physiscs 1 (3) (1971) 186207).

[47] A. H. Kara and F. M. Mahomed, Noether-type symmetries and conservation laws via partial Lagragians, *Nonlinear Dynam.* **45** (2006) 367383.

[48] S. Goldtein, Modern Developments in Fluid Dynamics, vol. 1, Oxford University Press, 1957, London.

[49] M. S. Klamkin, On the transformation of a class of boundary value problems into initial value problems for ordinary differential equations, *SIAM Review* **4**, 1962, 4347.

[50] W. F. Ames, Applications of group theory in computation - a survey, in: N. H. Ibragimov, (Ed.), CRC Handbook of Lie Group Analysis of Differential Equations, CRC Press, Boca Raton, vol. 1. Symmetries, Exact Solutions and Conservation Laws, 1994, pp. 350355.

[51] T. Y. Na, Transforming boundary conditions into initial conditions for ordinary differential equations, *SIAM Rev.* **9**, 1967, 204-210

[52] T. Y. Na, Further extensions on transforming from boundary value to initial value problems, *SIAM Rev.* **10**, 1968, 8587.

[53] M. S. Klamkin, Transformation of boundary value problems, *J. Math. Anal Applic.* **32** (1970) 308-330.

[54] J. R. Dormand and P. J. Prince, A family of embedded Runge-Kutta formulae, *J. Comp. Appl. Math.* **6** (1980) 19-26.